# Exploring the Orthogonal Dynamic Covalent Imine and Disulfide Bonds in Polymer Systems

***Michael Edward Bracchi***

A thesis submitted for the degree of *Doctor of Philosophy in Chemistry*

School of Chemistry

Newcastle University

August 2017

**ABSTRACT OF THE DISSERTATION**

Exploring the Orthogonal Dynamic Covalent Imine and Disulfide Bonds in Polymer Systems

*Michael Edward Bracchi*

In the field of supramolecular systems chemistry the desire of researchers to endow functional macromolecular systems with *orthogonal* stimuli-responsiveness has fueled interest in the incorporation of multiple orthogonal dynamic covalent chemistries within a single chemical system. Dynamic covalent chemistry involves reversible bond forming processes which can be harnessed in the development of dynamic supramolecular systems providing a mechanism for structural reconfiguration of system components in response to external stimuli. Despite the inspiring gamut of recently brandished studies, there is a still a call on the resourcefulness of chemists to expand the capacity for the introduction of multi-faceted, orthogonal, stimuli-responsive behaviors. Herein, a critical analysis of recently reported landmark studies has been undertaken wherein the utility of orthogonal dynamic covalent bonding motifs in functional systems is highlighted. Furthering the concepts of orthogonality with respect to dynamic covalent chemistry presented therein, a small molecule 'model system' was developed with which the orthogonality of imine and disulfide dynamic covalent bonds was demonstrated by its operation. A key focus of this preliminary work was the orthogonal *bond forming* and *bond breaking* processes of imine and disulfide dynamic covalent bonds. Upon the establishment of conditions necessary to exploit the orthogonal utility of imine and disulfide bonds, the incorporation of aldehydes, amines and thiols within acrylamide-based copolymers as pendant functional groups was achieved. These pre-formed functional polymer building blocks were shown to undergo stimuli-responsive intermolecular cross-linking in aqueous media yielding disulfide or imine cross-linked nanoparticles or hydrogels. The scope and utility of imine and disulfide bonds in the formation of these nanostructured materials is compared and contrasted. It is reasoned that expanding understanding and availability of dynamic covalent bonding motifs will facilitate evolution of systems of greater sophistication capable of embodying increasingly information-rich processes.

# ACKNOWLEDGEMENTS

First and foremost, I cannot overstate my appreciation for the unwavering support and encouragement I have received from my PhD supervisor Dr David A Fulton. His extensive understanding of chemistry, and remarkable enthusiasm for research has nurtured a stimulating and challenging research environment at Newcastle and I am truly grateful to have been granted the opportunity to flourish within it as an early career researcher. Reflecting on how much I've developed as a scientist and considering how far I've come, it cannot be emphasized enough how important a good relationship with a supervisor who is concerned not only with 'results' but with the wholesome development of their students, I am truly lucky to have been granted such an opportunity.

During my years in the Fulton group, I have had the genuine pleasure of working close to an extremely talented, motivated and conscientious group of peers. I'd therefore like to extend my gratitude to Dr Clare Mahon, Dr Chris McGurk, Dr Gema Dura, Dr Luke Ian Dixon, Dr Antonio Ruiz-Sanchez, Patrick Higgs and Milene Dalmina, Dr Dan Coleman all of whom embody a genuine passion for chemical research and whose support has proved invaluable. I have been unendingly inspired by their creativity and insightfulness and I am forever indebted to them for their invaluable support, and mostly, I'm grateful for their friendship. I would also like to express my gratitude to those working in the Chemical Nanoscience Laboratory outside of the Fulton group, including Dr Colette Whitfield, Dr Sam Bhatt, Dr Scott Watson, Dr David Smith, Dr Johnny Pate, Dr Osama El-Zubir, Sam Lunn, Rachel Little, Tom Bamford, Shams Ali, Glenn Lamming, Steve Nomor, Mansur Yahaya, Hector Oyem, Lamia Al-Mahamad.

I owe my absolute deepest gratitude to my parents Kevin and Susan Bracchi (and my brother Matthew!) for their relentless support and encouragement, they have always backed me through difficult times and put up with me in the foulest of moods, I will never forget the role they have played in my educational development. I'd also like to thank my amazing girlfriend Taylor Beck, her support and encouragement has never wavered throughout my studies.

Finally, I am forever indebted to Newcastle University. I have spent eight years within this remarkable institution and the quality of my experience in the School of Chemistry cannot be overstated, a truly stimulating, invaluable and rewarding experience.

# TABLE OF ABBREVIATIONS

| | |
|---|---|
| RAFT | Reversible additions-fragmentation chain transfer |
| DCB | Dynamic covalent bond |
| TCEP | Tris(2-carboxyethyl)phosphine |
| DTT | Dithiothreitol |
| PEG | Polyethylene glycol |
| SOSIP | Self-organizing surface-initiated polymerization |
| MeOH | Methanol |
| DMF | Dimethyl formamide |
| µL | Microliter |
| 2D EXSY | 2-Dimensional exchange spectroscopy |
| DMAc | Dimethylacrylamide |
| DDMAT | 2-(Dodecylthiocarbonothioylthio)-2-methylpropionic acid |
| GPC | Gel permeation chromatography |
| CTA | Chain transfer agent |
| PDI | Polydispersity index |
| DLS | Dynamic light scattering |
| PFPA | Pentafluorophenyl acrylate |
| AIBN | 2,2’-Azobis(2-methylpropionitrile) |
| Da | Dalton |
| EDC | 1-Ethyl-3-(3-dimethylaminopropyl)carbodiimide |
| DDQ | 2,3-Dichloro-5,6-dicyano-1,4-benzoquinone |
| TFA | Trifluoroacetic acid |
| THF | Tetrahydrofuran |
| DCM | Dichloromethane |
| IPN | Interpenetrating network |

# TABLE OF CONTENTS

# LIST OF FIGURES

**Chapter 1:** ***The utility of orthogonal dynamic covalent bonds in systems chemistry***

polymer scaffold with pendant *ortho*-substituted boronic acids whose corresponding hydrogel contracts in response to the presence of glucose on account of the formation of intermolecular cross-links between polymeric system components. In both cases, pH-sensitivity was observed on account of the pH-dependant formation of hydroxyboronate anion – a precursor in the formation of boronic esters with glucose.

*Figure 1.7* Boronic acid bearing bullvalene **37** capable of recognizing a range of bio-relevant polyol compounds. When bound to a polyol analyte, structural isomerization of bullvalene chemosensor **37** yielded, a particular isomer distribution influenced by the structural and electronic nature of the analyte. Analysis usng $^{13}C$ NMR spectroscopy produced barcodes specific to each compound measured.

*Figure 1.8* (a) Three-component system consisting of *(S)*-BINOL, 2-formylphenyl boronic acid **38** and a range of racemic primary amines. Using $^{1}H$ NMR spectroscopic analysis, straightforward determination of the enantiopurity of a range of chiral primary amines was achieved. (b) Three-component chiral derivatizing system consisting of 2-formylphenyl boronic acid **38**, enantiopure α-methylbenzylamine and a range of 1,2-, 1,3- and 1,4-diols. Determination of diol enantiopurity was achieved using $^{1}H$ NMR spectroscopic analysis.

*Figure 1.9* Disulfide and hydrazone containing macrocycle **39** was observed to undergo disulfide *or* hydrazone exchange depending on whether the system was placed under basic *or* acidic conditions, respectively, affording macrocycle library 1 *or* macrocycle library 2, respectively. It was demonstrated that disulfide scavenger **40** and hydrazone scavenger **41** engaged in component exchange with dual-functional macrocycle **39** under basic *or* acidic conditions, respectively. In the presence of both disulfide **40** and hydrazone **41**, disulfide exchange *or* hydrazone exchange occurred exclusively under basic *or* acidic conditions, respectively demonstrating true orthogonality between disulfide and hydrazone bonding motifs.

*Figure 1.10* Molecular walker system wherein a 21-atom molecular walker (purple) was demonstrated to traverse a 'four-platform' molecular track by the reversible formation and breaking of dynamic covalent imine and disulfide bonds. (a) Walker position **I** wherein both hydrazone and disulfide bonds are fixed to the track. (b) Decreasing the system pH encourages reversible breaking of the hydrazone bond present and thermodynamic re-equilibration about the disulfide pivot foot. (c) Walker position **III**, wherein a 'forward-step' is achieved through a passing-leg gait mechanism and driven by the formation of a new hydrazone bond. (d) Increasing the system's pH facilitated reversible breaking of the disulfide bond present in walker position **II** and displacement of the placeholder disulfide moieity by thiol-disulfide interchange.

*Figure 1.11* Dual-adaptive, self-healing hydrogel **44** formed through condensation of trialdehyde **43** and disulfide-based dihydrazide linker **42**. It was

# LIST OF TABLES

**Chapter 3:** ***Dynamic covalent imine and disulfide cross-linked nanoparticles***



**Chapter 4:** ***Dynamic covalent imine and disulfide cross-linked nanoparticles***

# LIST OF SCHEMES

**Chapter 1:** ***The utility of orthogonal dynamic covalent bonds in systems chemistry***



**Chapter 2:** ***Orthogonal utility of dynamic covalent imine and disulfide bonds in a small molecule '4-Node' model network***

**Chapter 3:** ***Dynamic covalent imine and disulfide cross-linked nanoparticles***



**Chapter 4:** ***Dynamic covalent imine and disulfide cross-linked nanoparticles***

# Chapter 1

## *The Utility of Orthogonal Dynamic Covalent Bonds in Systems Chemistry*

# Table of Contents

## 1.1 Abstract

*Systems chemistry is centered on the principal that, in Nature, the output of any functioning chemical network is greater than merely the sum of its parts. Finely tuned, complex chemical systems pervade the natural world wherein orchestrated system-level phenomena play a key role in the existence and evolution of life. The broadening ability of chemists to 'pre-programme' structurally well-defined functional molecules and macromolecules with stimuli-responsive properties has led the way for the design and implementation of a range of functional synthetic systems impressive in their sophistication. Whilst systems chemistry remains firmly in its infancy, researchers encroach ever closer towards being able to effectively probe the chemistry of systems within a wholly-synthetic, well-characterized chemical framework. Recent developments within the fields of systems chemistry and supramolecular systems chemistry are outlined herein.*

## 1.2 Introduction

The natural world is spectacular in its complexity. By way of illustration, eukaryotic cells are internally comprised of vastly dynamic, complex biochemical networks and are themselves part of larger-scale biological networks[1] (e.g. neuronal, signalling and metabolic networks) whose functions contribute to physiological systems that are ultimately able to support complex living and even conscious organismal life. The naturally-occurring molecular and macromolecular entities that constitute our physical being cannot tell the whole story of how we function as animate life forms. Consider that the 'output' of a biological system is more than simply the sum of its component parts working in isolation. Analogously, the comprehensive mapping of each part of an automobile, albeit resulting usefully in a catalogue of its internal components, does not adequately explain how it attains its function. A dynamic, system level understanding of many orchestrated processes acting in relation to one another is required to properly understand the machine and its function.

Exploration into biological systems reveals an increasingly prominent need for system level understanding. Developing structural knowledge of cellular components remains vastly important and therefore a focus of biochemists past and present, however, questions regarding cellular internal system dynamics remain largely unanswered. For example, the development of inter-connective relationships between proteins leading to the formation of

pathways that can support metabolism is not fully understood. With respect to such phenomena, understanding how the functioning biological system in question is related to interactions between the individual molecular and macromolecular components which comprise it, remains an essential step towards fully understanding such systems. Upon developing a more clear understanding of system-level phenomena one could envisage modelling system network structures, potentially identifying basic network motifs which are prevalent and reoccurring in the natural world. Furthermore, will sufficient understanding eventually empower us to design and engineer biomimetic systems? Tackling such questions has long been the goal of systems biology,[2] however, top-down investigation into the immense complexity of biological systems poses appreciable challenges when it comes to the deconvolution of individual processes relating to a particular system function. Recently developed high-throughput data acquisition techniques[3] have facilitated the growing interest in systems biology, although data sets are often unmanageably vast and specific interactions between system components lack good characterization, rendering the development of effective computational models extremely difficult. Performing *in vivo* experiments to probe biological system function also has limitations insofar as invasive measurements and manipulations can result in undesirable perturbations in system function, often leading to cell or organism death.

### 1.3 Systems Chemistry

Systems chemistry[4] poses a 'bottom-up' strategy in the investigation of complex chemical systems by encouraging synthetic design of complex chemical systems in which molecular components and the interactions between them are well characterized. Thus, investigation into system-level phenomena can proceed without encumbering uncertainties in large intractable data sets. Biological systems naturally embody adaptability and responsiveness through the abilities of their components to 'communicate' with each other and it is ultimately the dynamics of a complex chemical system which gives rise to its emergent properties. Biological systems employ a range of molecular- and macromolecular-level processes in order to give rise to dynamic characteristics and emergent properties. Examples of these processes include the controlled and directed forming or breaking of covalent/non-covalent bonds, changes in the stereochemical configuration of molecular system components and adjustment of component concentration gradients through component exchange within complex

libraries. The challenge of implementing the same sort of dynamic attributes in unnatural systems giving rise to emergent properties poses a great synthetic challenge and lies at the heart of furthering our capabilities in the field of systems chemistry.

The design of complex chemical systems with emergent properties has recurred interest in the concept of orthogonality in chemistry. The capabilities of researchers to incorporate orthogonal processes into a single chemical framework, thereby introducing complexity, seems an obvious prerequisite in the journey towards attaining synthetic, 'smart' systems which embody function. Certainly, the power and ubiquity of orthogonality in Nature should not be overlooked biological systems – where from the chaos of astonishing chemical complexity emerges powerful, reproducible functionality. The ideas of chemical orthogonality were first crystallised by Merrifield *et al*[5] in 1977 with the orthogonal protection of amino acids as a strategy for their selective functionalization. In the decades that followed, supramolecular chemistry harnessed orthogonality in the development of controlled processes of the macroscale, wherein, orthogonality signifies that the operation of two or more orthogonal processes can be independently controlled depending on conditions in the absence of inter-process 'cross-talk'. Michael Schmittel recently summarized advances in the application of chemical orthogonality in discreet self-assembly processes in an excellent review.[6]

**1.4 Supramolecular Systems Chemistry**

Progress in systems chemistry in recent years has largely centered around the utilization of small molecules, with the largest contributions emerging from the realms of dynamic combinatorial chemistry.[7] Despite the ubiquitous involvement of biomacromolecules in natural systems, their utilization in supramolecular systems chemistry is still largely unexplored, and the development of supramolecular systems which are dynamic in the macromolecular regime remains a major goal. It should be acknowledged that many systems have been reported wherein self-assembly of small molecules has led to formation of complex structures on the nanoscale, however, systems in which pre-formed empirical building blocks are themselves supramolecular in nature are far less common. More often than not, synthetic supramolecular systems are dynamic in their nature on account of reversible, labile non-covalent interconnections between macromolecular species. These interactions are able to re-shuffle and re-organise over time driving structural evolution of systems on the nanoscale

towards thermodynamic minimum energy states, and this feature has resulted in a vast array of impressive supramolecular architectures[8] whose sophisticated complexity is often unobtainable by classical synthetic techniques. It remains an important challenge in supramolecular chemistry to be able to pre-programme dynamic character and functionality with greater control by better understanding interactions between supramolecular system components.

A key driver in the launch of supramolecular systems chemistry has been the rapid expansion in the supramolecular chemist's tool-kit, equipping researchers with remarkable scope for designing and creating structurally well-defined, highly functional macromolecular building blocks. In particular, the development of controlled living radical polymerization techniques,[9] namely, reversible addition-fragmentation chain transfer (RAFT) polymerization,[10] has proved extremely useful in the experimentally-straightforward preparation of functional polymeric building blocks with high levels of molecular precision. The extensive versatility of RAFT polymerization towards a wide range of experimental conditions permits the copolymerization of a broad range of functional vinylic monomers producing end-functionalized,[11] pendant-functionalized,[12] block copolymers,[13] polymer brushes[14] and more. Access to structurally well-defined, functional polymeric species has seeded interest in their subsequent aggregation in efforts to construct larger architectures in a controlled manner. By understanding the interactions which drive the formation of larger architectures and then go on to impart dynamic character on account their lability, researchers have yielded many supramolecular systems whose integrity rely on the presence of non-covalent interactions within their structures including hydrogen bonding,[15] halogen bonding[16] and ionic interaction.[17]

### 1.5 Dynamic Covalent Chemistry

The utility of non-covalent interactions has proven extremely useful in supramolecular chemistry in the formation of complex architectures,[18] however, it is often difficult to control the formation and breaking of such interactions. This deficiency gives rise to limitations when attempting to develop supramolecular systems capable of discreet structural rearrangement phenomena in response to specific environmental stimuli. An extremely attractive route to programmable, controlled self-assembly of preformed polymeric building blocks into complex supramolecular systems is the utility of dynamic covalent chemistry. Many dynamic covalent

bonds (DCBs) have been investigated in recent decades in the context of adaptable, 'smart' macromolecular systems including, but not limited to, disulfide,[19] boronic acid,[20] hydrazone[21] and imine bonds.[22] These five bonds represent by the far the

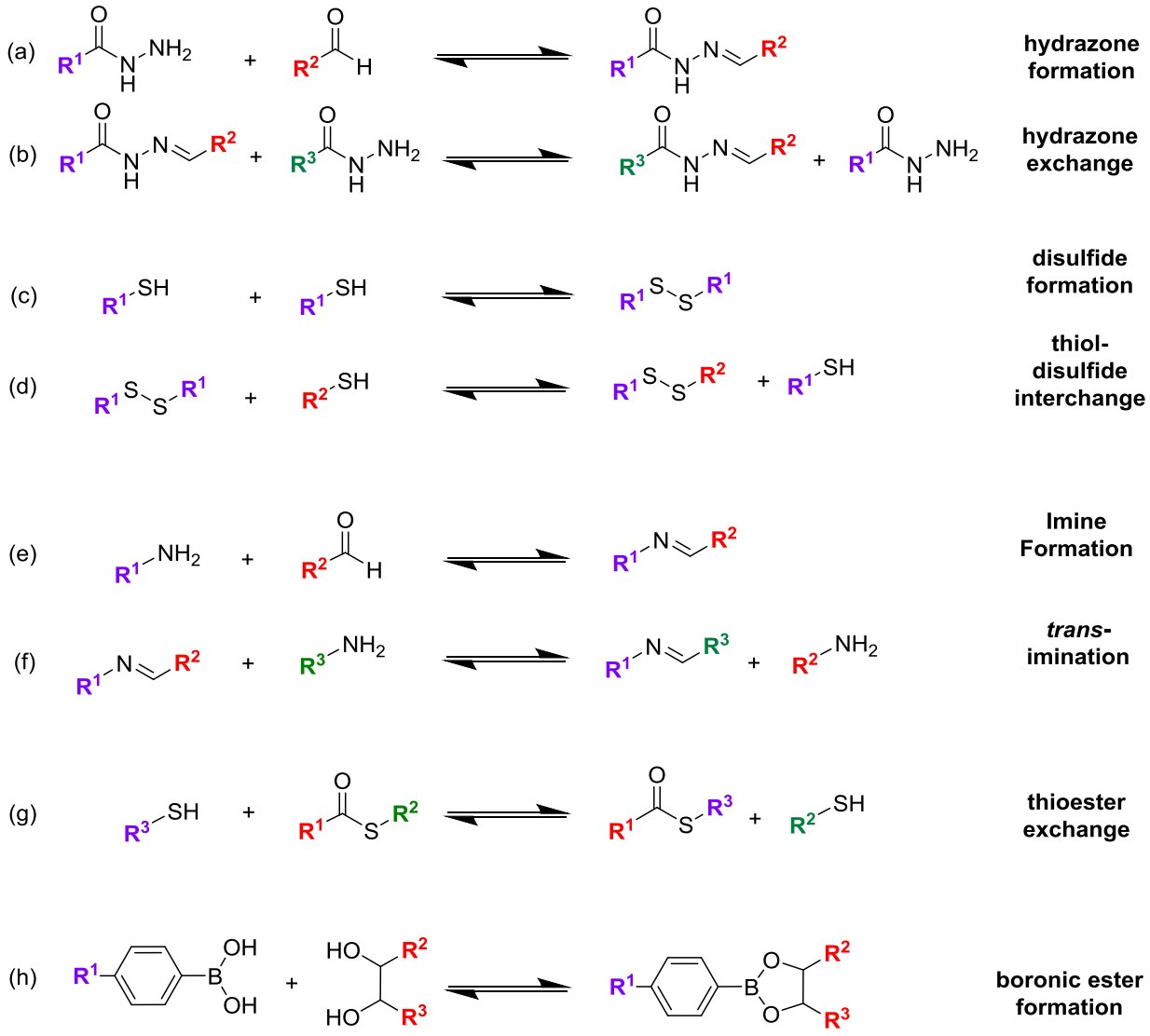


Scheme 1.1 Summary of the five major dynamic covalent bonds utilized in functional systems. (a) Hydrazone formation between a hydrazide and a carbonyl. (b) Hydrazone exchange occurs at acidic and neutral pH between a hydrazone and a hydrazide. (c) Oxidative coupling of thiols to form a disulfide bond. (d) Thiol-disulfide interchange between a disulfide and a thiol, usually catalyzed by base. (e) Imine formation occurs under alkali conditions by condensation of an aldehyde with a primary amine. Imine hydrolysis occurs at acidic pH. (f) *Trans*-amination imine exchange between an imine and an amine. (g) Thioester exchange between a thiol and a disulfide occurs under basic conditions. (h) Boronic ester formation occurs at high pH between a boronic acid and a 1,2, 1,3- or 1,4 diol. Boronic ester hydrolysis occurs under acidic conditions.

most utilised DCBs to date, yet, there is an extensive range of DCBs appearing less frequently whose prevalence will surely increase in coming years such as oximes[23] and hemithioacetals[24] and dithianes.[25] DCBs have attracted huge attention on account of their ability to adopt characteristics of both non-covalent bonds, breaking and forming reversibly under certain conditions, and covalent bonds, retaining their integrity and robustness under different conditions. The dynamic hydrazone bond, for example, can readily undergo component exchange in acidic media, but at alkali pH, its capacity for component exchange is diminished. In the realm of supramolecular chemistry, this presents a useful opportunity for stimuli-responsive structural reorganization of macromolecular entities whose architecture depends on the degree and nature of dynamic covalent bonds within it. The capacity for dynamic covalent bonds to 're-shuffle' within achemical system through thermodynamic re-equilibration provides an 'error-checking' mechanism, contrasting more traditional kinetically controlled self-assembly processes in which the resulting macromolecular species, once assembled, remains more or less structurally fixed. The re-equilibration qualities imparted to a system by incorporation of DCBs is reminiscent of dynamic characteristics observed in naturally occurring systems. Indeed, many examples of exchange processes involving dynamic covalent bonds can be observed in natural systems such as thiol-disulfide interchange processes in protein folding[26] and the exquisite utility of imine bonds in the biochemistry of vision.[27]

The following section aims to briefly summarise the recent development in the utility of DCBs in supramolecular systems chemistry.

### 1.5.1 *Dynamic covalent disulfides in systems chemistry*

The dynamic covalent disulfide bond has been well studied[18b] and remains the most utilised motif on account of its widespread existence in natural systems, playing a key role in the tertiary and quaternary structure of proteins through formation of inter- and intramolecular disulfide bonds between cysteine amino acid residues.[26] Disulfide bond formation occurs by oxidative coupling of thiols (Scheme 1.2a) and is a redox-sensitive process. Once formed,

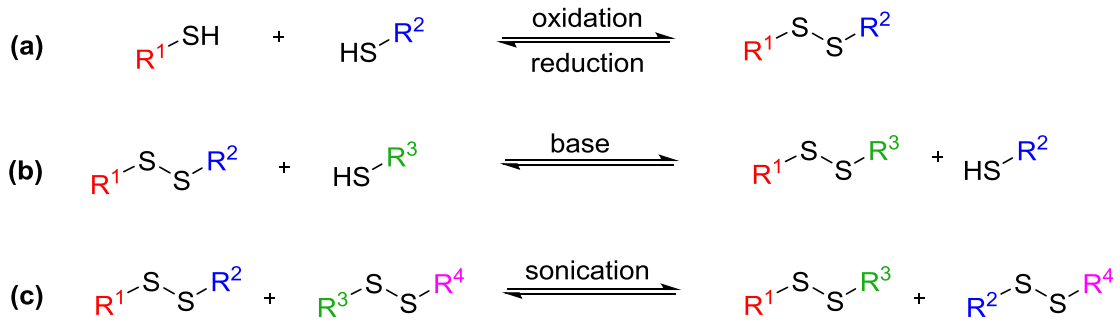


Scheme 1.2 (a) oxidation of thiols to form a disulfide bond. (b) Base catalyzed thiol-disulfide interchange. (c) Sonication induced disulfide bond metathesis.

a sufficiently reducing environment will then facilitate cleavage of the disulfide bonds recovering the original thiol reaction partners.[28] The use of chemical oxidising agents in the formation of disulfides, such as hydrogen peroxide[28] and iodine[29] are commonplace along with atmospheric oxygen in aqueous conditions. In the reduction of disulfide moieties many organic reducing agents have been frequently employed in the reduction of disulfides, the most common of which include tris(2-carboxyethyl)phosphine (TCEP)[30] and dithiothreitol (DTT). Disulfide reduction by electrochemical[31] and photochemical[32] methodologies have also been exploited. Component exchange in dynamic covalent disulfides is known to occur in a range of solvents[33] by a thiol-disulfide interchange mechanism (Scheme 1.2b), typically catalysed by a small amount of reducing agent and base although several other methods have been used to induce exchange behaviour including by photoirradiation[34] and, in a remarkably interesting study by von Delius *et* al[35] where sonic agitation was shown to induce disulfide metathesis exchange (Scheme 1.2c). This versatile and reliable exchange behaviour, coupled with the bio-relevancy of the disulfide bonding motif, has cemented its position in the system chemist's roster for utility in the introduction of function into complex chemical systems.

One of the earliest applications of dynamic covalent disulfide chemistry in systems chemistry was provided by the groups of Sanders[36] (Figure 1.1a) in 2002 by demonstrating the effectiveness of dynamic combinatorial chemistry to identify and amplify best-binding macrocyclic disulfide-based receptors for a pair of contrasting guests. The macrocyclic species were initially formed by oxidative coupling of aromatic dithiols **1** - **3** affording a library of interconverting disulfide-based macrocycles (**4** and **5**) under thermodynamic control. Upon the introduction of molecular guests, the disulfide macrocycle library underwent thermodynamic re-equilibration leading to the amplification of disulfide macrocyclic species

which were capable of forming host-guest complexes. The addition of 2-methylisoquinolinium iodide (**6**) or morphine derivative **7** led to amplification of macrocycles **8** and **9** respectively. The observed amplification phenomena is unquestionably reliant on system dynamics

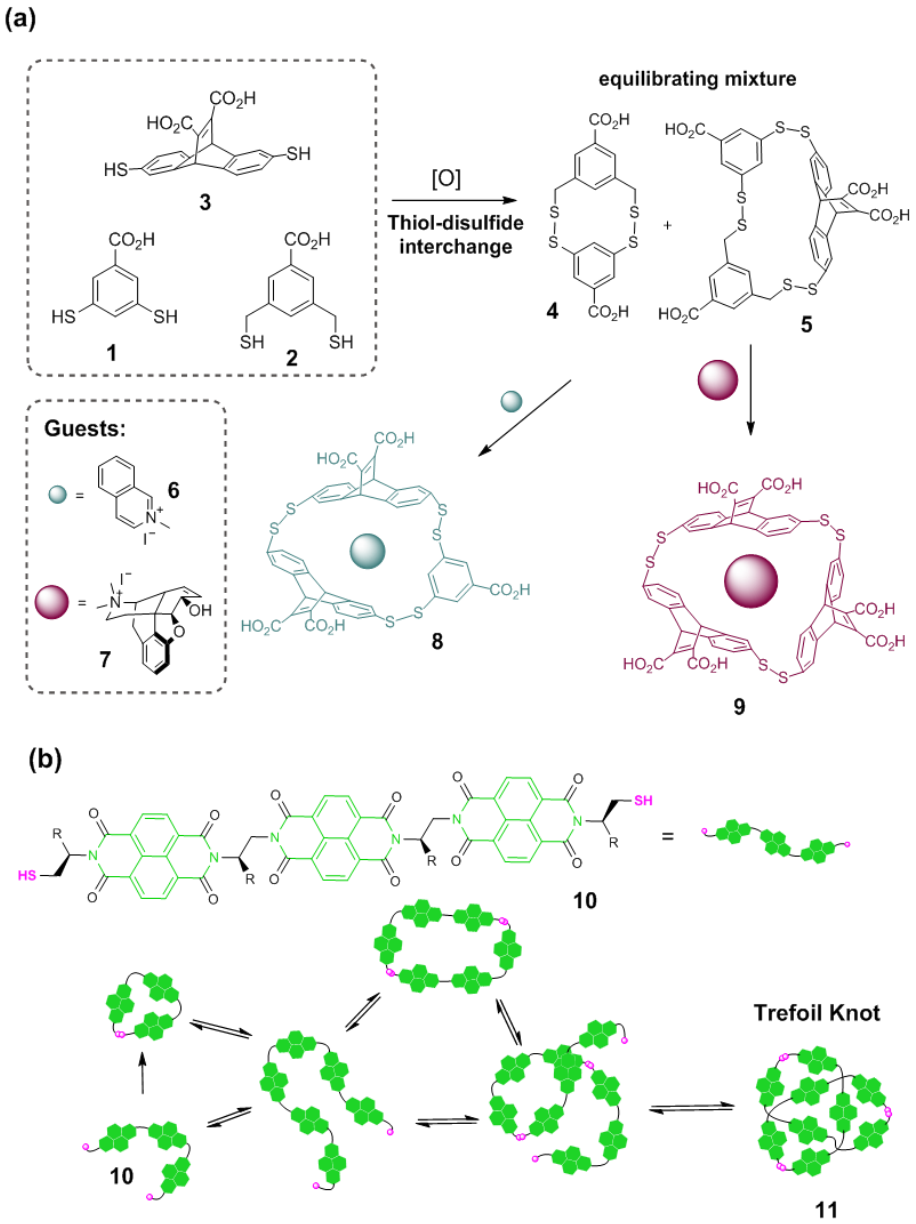


Figure 1.1 (a) Thermodynamic equilibrated Dynamic combinatorial library established from a set of aromatic dithiols in the absence of a molecular guest. This library was capable of undergoing thermodynamic re-equilibration in the presence of molecular guests to amplify certain best binding macrocyclic hosts.[18b] (b) Preparation of a molecular trefoil knot (**11**) formed from three napthalenediimide dithiol building block **10** by a thiol-disulfide interchange mechanism and stabilized by the hydrophobic effect.[37]

imparted by dynamic covalent disulfide chemistry highlighting the utility of disulfide-based dynamic combinatorial libraries in the identification of best-binding macrocyclic hosts for specific molecular guests.

More recently, Sanders *et al* has shown[37] the power of dynamic covalent disulfide chemistry in the near-quantitative formation of a molecular trefoil knot (Figure 1.1b). The trefoil knot (named after the clover or trefoil plant), was prepared by the careful intertwining of three napthalendiimide based oligomeric building blocks (**10**) terminated with thiol moieties in a process driven largely by the hydrophobic affect. Oxidation of thiol end-groups led to the formation of a range of disulfide-linked architectures. A number of dynamic combinatorial libraries were established under different conditions, notably, different ionic strengths and concentrations of napthalenediimide-based **10**, allowing the elucidation of a mechanism for knot formation. The dynamic character associated with the disulfide bond provides an 'error-checking' safety net, driving the product distribution past kinetically favoured disulfide-based linear architectures towards the more ordered and more thermodynamically stable trefoil knot (**11**). Without the capacity for facile structural rearrangement imparted by the reversible nature of the dynamic covalent disulfide bond, structural evolution of the trefoil knot would require fast-forming oligomers of **10** to undergo slow, energetically unfavorable processes of unfolding, exposing the hydrophobic plane of napthalendiimide sub-units to the polar environment. The utility of dynamic covalent disulfide chemistry in the meticulous formation of the trefoil knot elegantly represents an important step towards developing models that aid understanding of bio-relevant processes within a wholly synthetic framework, as well as being a fantastic example of supramolecular synthesis.

A study by Otto *et al* further demonstrates[38] the utility of dynamic disulfide bonds in a stunning example (Figure 1.2b) of supramolecular systems chemistry wherein dithiol-bearing oligopeptide building block **12** undergoes oxidative coupling to yield a library of macrocycles. Macrocycles **13** and **14** were able to stack to form fibrous nanostructures (Figure 1.2a) that are stabilized by the formation of β-sheets extending outwards from the stacked macrocyclic-core and were formed by complimentary orientation of alternating hydrophobic-hydrophilic amino acid units of the oligopeptide building block, **12**. These two self-replicating nanostructures were in direct competition with each other as they emerged from the same chemical environment, competing for the same dithiol building block, **12**. Remarkably, it was demonstrated that the when a mechanical agitation was applied (shaking or stirring), the nature of agitation was key in influencing which nanostructure dominated with respect to the

kinetics of growth. Several astute control experiments were performed enabling the elucidation of a seeded-growth mechanism through which self-assembly is believed to occur. This work highlights how, within a fully characterized synthetic framework, system level phenomena can be studied with respect to the impact of competing, self-replicating nanostructure growth on the product distribution in a dynamic

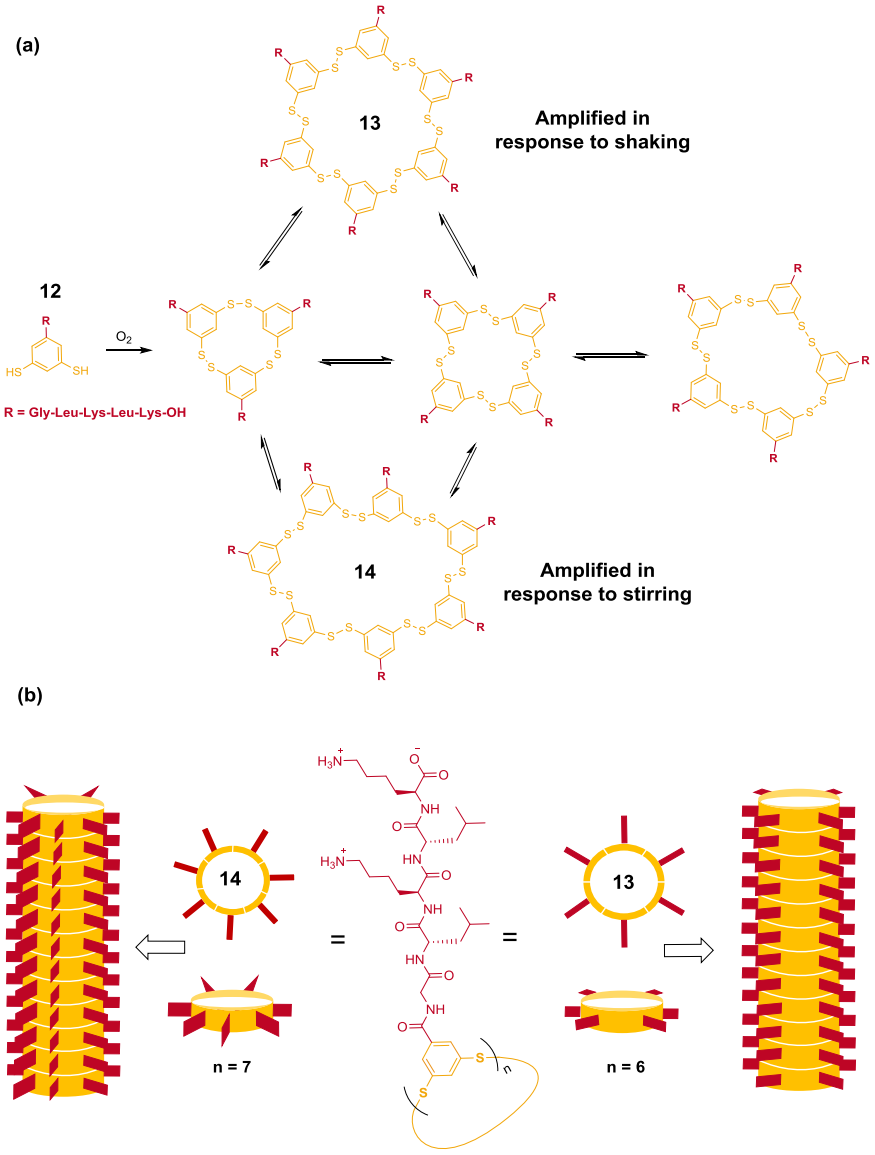


Figure 1.2 (a) Nano-structuring of disulfide hexameric and heptameric disulfide macrocycles **13** and **14** affording a peripheral β-sheet stabilized stacked nanostructure.[36, 38a] (b) Library of exchanging disulfide macrocycles formed from building block **12** amplification of hexameric and heptameric disulfide macrocycles **13** and **14** was driven by their capacity to form long nanostructures.

library of exchanging disulfide macrocycles. Importantly, this work is an example of a dynamic complex chemical system operating far from equilibrium control and demonstrates that it is possible to yield kinetic products from a dynamic mixture within which all interactions are reversible. It must be the case that, in the evolution of life, kinetic control began to dominate processes of self-assembly as is the case in the natural world around us. In a later study, Otto *et al* were able to demonstrate[39] that macrocycles **13** and **14**, after forming the described stacked nanostructure, went on to form hydrogels upon photoirradiation.

Taken together these studies demonstrate the usefulness of the dynamic covalent disulfide bond in the development of complex chemical systems exhibiting dynamic character giving rise to emergent properties, highlighting the utility of disulfide bonds in both molecular and supramolecular systems chemistry.

### 1.5.2 *Dynamic covalent imines in systems chemistry*

The chemistry of the dynamic covalent imine bond and its implementation in complex chemical systems has been well studied.[22, 40] In aqueous solution, imine condensation occurs at high pH between amine and aldehyde reaction partners (Scheme 1.3a) and imine hydrolysis occurs in response to a reduction in pH.[41] Furthermore, imine bonds undergo component exchange behaviour via transamination (Scheme 1.3b).

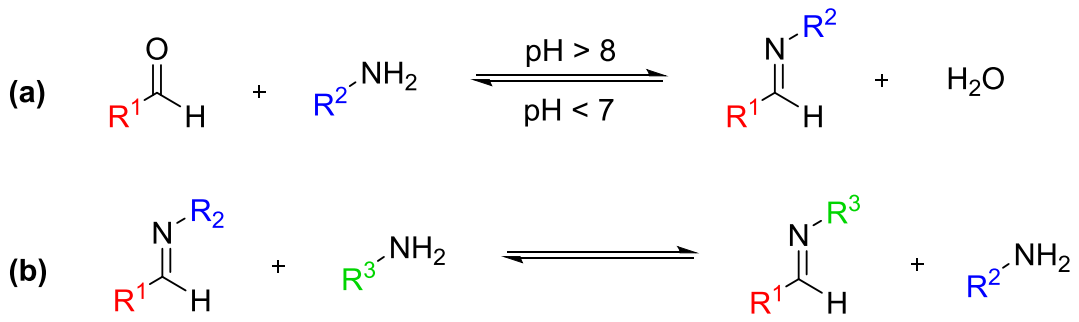


Scheme 1.3 (a) Imine condensation between amine and aldehyde reaction partners. (b) Trans-amination imine exchange wherein nucleophilic attack of a primary amine yields a new imine proceeding through a tetrahedral intermediate.

These possibilities have led to the dynamic covalent imine bonding motif being extensively employed to impart pH-sensitivity to functional chemical systems. It was realized in an extensively thorough study[41] performed by Lehn *et al* that it was possible to tune the relative

stability of imine products by adjusting the structural and electronic nature of the aldehyde reaction partner, providing a means by which to influence the pH range over which imine condensation and hydrolysis occurs.

The Lüning group have utilized[42] dynamic covalent imine chemistry to identify a sensor for $CaCl_2$ by preparing a two-phase dynamic combinatorial library which facilitated the transport of $CaCl_2$ across a bulk solvent membrane (Figure 1.3). A macrocyclic $CaCl_2$ carrier was amplified as the $CaCl_2$ selected its own carrier from a thermodynamically

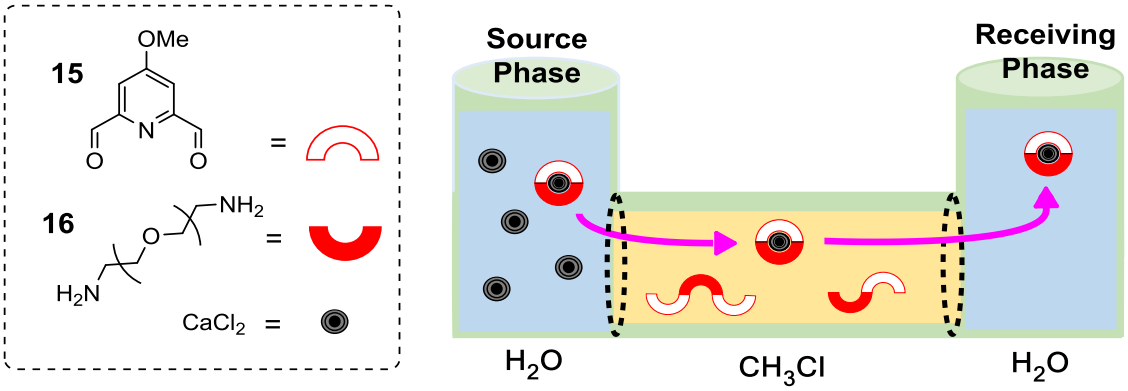


Figure 1.3 Transport of $Ca^{2+}$ ions from a source aqueous phase to a receiving aqueous phase through a 2-membrane channel facilitated by *in situ* amplification of a $Ca^{2+}$ carrier macrocycle formed between dialdehyde **15** and diamine **16** and selected from a range of possible imine-based oligomers. No $Ca^{2+}$ transport was observed in the absence of dialdehyde **15** and imine **16**.[42]

equilibrating mixture of imines formed between building blocks **15** and **16**. After one week, the $^1H$ NMR spectrum of the "receiving" phase displayed signals corresponding to macrocycle carrier. Importantly, $CaCl_2$ ions dissolved in the "source" phase do not cross the bulk liquid membranes into the "receiving" phase in the presence of *only* **15** or **16** as evidenced by mass spectrometry. This example demonstrates the potential for dynamic covalent imine chemistry in environmental chemistry, conceptually providing a means of cleaning heavy metal contaminated water by application of an appropriate dynamic combinatorial library. The dynamic nature in the distribution of possible imine products is implicit in endowing the system with its function of cross-phase calcium ion transportation.

The power of dynamic covalent imine chemistry in the formation of complex architectures was demonstrated[43] (Figure 1.4a) in a study by the group of Stoddart wherein,

amine- and aldehyde-functional building blocks **17** and **18** were utilized in the formation of a borromean ring by a transition-metal templation strategy. A borromean ring is a nanostructure consisting of three mechanically interlocked molecular rings which cannot be separated without breaking one of the rings. The formation of this architecturally complex structure was reliant on the capacity for thermodynamic equilibration on account

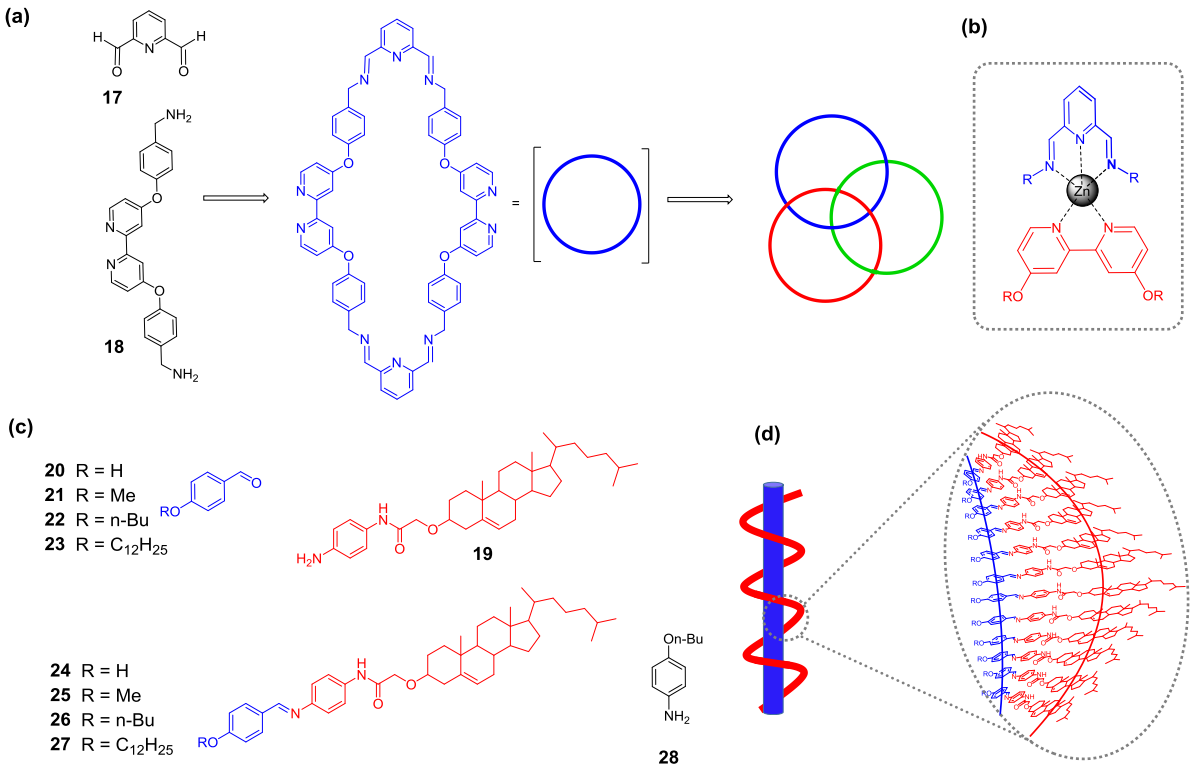


Figure 1.4 (a) Transition-metal templated formation of a molecular borromean rings from building blocks **17** and **18**.[43] (b) Six zinc-complexation sites existed within the furnished borromean rings structure, each consisting of a five-coordinate zinc(II) complex involving binding of *exo*-bipyridyl and *endo*-diiminopyridyl ligand moieties intrinsic to the imine-based macrocycle. (c) Dynamic imine library formed by condensation of aniline-appended cholesterol **19** and a range of aromatic aldehydes **20** – **23**. The gelation capacity of imines **25** – **27** facilitated their amplification relative to non-gelating imines.[44] (d) Schematic representation of the nanostructuring of cholesteric imines affording pseudo-helical nanofibrous structures.

of the dynamic character afforded by reversible and exchanging imine bonds, which impart the high levels of error-correction into the chemical system necessary to ensure formation of the interlocked structure. Additionally, the reversible metal-ligand interactions (Figure 1.4b)

are essential in guiding controlled aggregation of the imine building blocks. This study highlights the utility of dynamic covalent bonds in conjunction with non-covalent metal-ligand interactions, affording robust, nanoscale organic frameworks aided by the geometrical precision and guiding influence of coordination chemistry.

A study by Li *et al* reported[44a] gelation-driven amplification in a range of cholesteric imines whose structures are displayed in Figure 1.4c. It was demonstrated that aniline-appended cholesterol (**19**) did not undergo gelation in any tested solvent, however, when subjected to condensation with aldehydes **20** - **23** gelation was observed with most of the resulting imines (**25 - 27**) as they were capable of forming pseudo-helical nanofibers (Figure 1.4d), stabilized by the stacking of aromatic rings and hydrophobic regions
of the cholesterol moieties. By conducting several competition studies it was observed that when **19**, **21** - **23** and non-cholesteric amine **28** were combined under a range of concentrations, enrichment of cholesteric imines occurred in the gel-phase, driven by the their tendency to self-assemble to form nanofibers. It was shown by careful control experiments that unreacted aldehyde and amine reaction did not affect critical gelation concentration prior to imine formation. The system's capacity for gelation-driven amplification highlights a potential novel strategy for the identification of best-gelling species from a dynamic mixture of potential candidates in a similar way to the identification of best-binding species in host-guest systems from equilibrating dynamic combinatorial libraries in solution.

Very recently, the group of Lehn, reported[45] an extremely interesting dynamic imine based system (Figure 1.5) which, when dissolved in an evaporating solvent droplet, underwent self-sorting exchange behavior in response to non-equilibrium conditions within the evaporating droplet. It is well understood that evaporation of solvent from a deposited droplet occurs from its periphery, driving capillary flow of solvent from the center of the droplet outwards[46]. Solutes dissolved within the droplet are thus displaced by the
resulting flow forcing them towards its periphery. Providing the solutes exhibit suitably low solubilities, they are deposited in a two-dimensional, circular "coffee stain" pattern. This phenomena has been explored in the interest of gaining temporal and spatial control in deposition of small molecules in ink-jet printing and its success depends on many factors relating to the adaptability of the dissolved molecular network to the non-equilibrium conditions which arise upon evaporation. In this work, initially, a two imine system was established by dissolving amines **29** and **30** and aldehyde **31** in a droplet of acetonitrile initially forming a mixture of imine **33** and **34**. After droplet deposition, evaporation led to

amplification of imine **33**, driven by its favored precipitation compared with imine **34** arising on account of **33** exhibiting a lower solubility in acetonitrile than **34**. Complete droplet evaporation led to full deposition of imines in the solid-state, yielding a deposition pattern which was investigated using fluorescence spectroscopy.

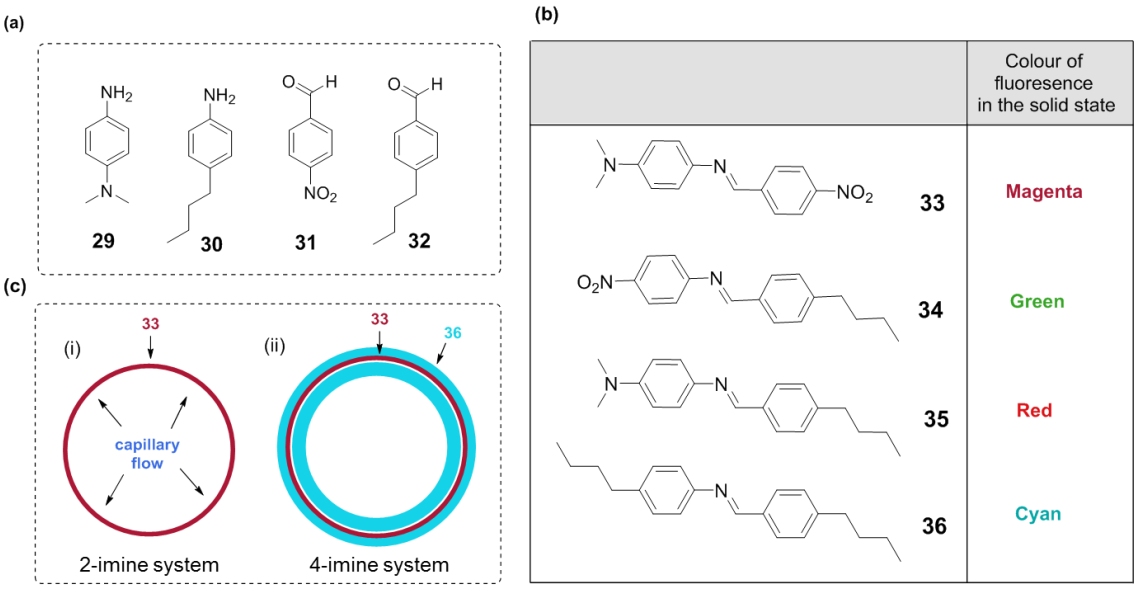


Figure 1.5 (a) Structure of amine and aldehyde system components studied by Lehn *et al*.[45] (b) Library of exchanging imines (**33** – **36**) formed from building blocks **29** - **32** facilitating straightforward analysis of their observed deposition patterns. (c) Schematic representation of 'coffee-stain' precipitation effect after complete droplet evaporation in: (i) two imine library, (ii) four imine library.

Imine **34** was not observed at all, however, imine **33** was deposited in a near-perfect "coffee-stain" pattern (Figure 1.5c). This observation indicates that the molecular network dynamics imparted by dynamic covalent imine chemistry facilitated the complete depletion of imine **34**, entirely consuming aldehyde **31** and amine **29** in the formation of imine **33**. A four imine system consisting of all amine and aldehyde precursors (**29 - 32**) was then set up affording an equilibrating mixture of imines **33 - 36.** Firstly, amplification of imine **33** occurred on account of it exhibiting the lowest solubility of all four imines (**33 – 36**) yielding the previously observed "coffee stain" pattern. This precipitation event forced the system to re-organize on account of the depletion of amine **29** and aldehyde **31** in the formation of imine **33**. The remaining amine (**30**) and aldehyde (**32**) components condensed to form imine **36** which was deposited in two bold rings, formed inside and outside of the deposited imine, **33** (Figure 1.5c). The

observed spatial resolution between imines **33** and **36** in the solid-state indicated successful adaptation of the four imine library in response to the non-equilibrium conditions created during evaporation. Furthermore, a degree of temporal resolution had been achieved when considering that imine **33** had deposited before imine **36**.

Taken together these studies draw attention to the extensive dynamic nature of the imine bond. The wide variety of readily available amine and aldehyde building blocks has favoured the imine bond as an ideal candidate when there is need to in the introduce function into many broadly contrasting chemical systems with a range of outputs.

### 1.5.3 *Dynamic covalent boronic esters in systems chemistry*

Boronic esters, are formed reversibly between reaction of boronic acids and 1,2- or 1,3-diols, have been extensively studied[18b, 47] and utilized to introduce function in chemical systems.[20] Boronic acids exhibit Lewis acidity on account of boron's empty *p*-orbital, and thus, under aqueous conditions, boronic acids are in equilibrium with their corresponding hydroxyboronate anions (Scheme 1.4). There is great scope in the synthesis of boronic acids to modify

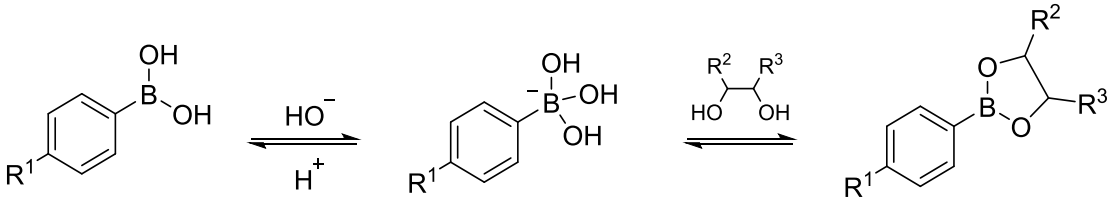


Scheme 1.4 Formation of hydroxyboronate anion from a boronic acid followed by condensation with a 1,2-diol to affording a dynamic covalent boronic ester.

acid $pK_a$ with, reported values ranging from 4.0 - 10.5.[20] This flexibility has empowered researchers with the ability to tune the reactivity of boronic acids towards the formation of boronic esters with a wide range of bio-relevant polyols, such as carbohydrates[48] and glycoproteins,[49] as well as synthetic polymers[50] in the preparation of boronic ester cross-linked materials.[18c, 51]

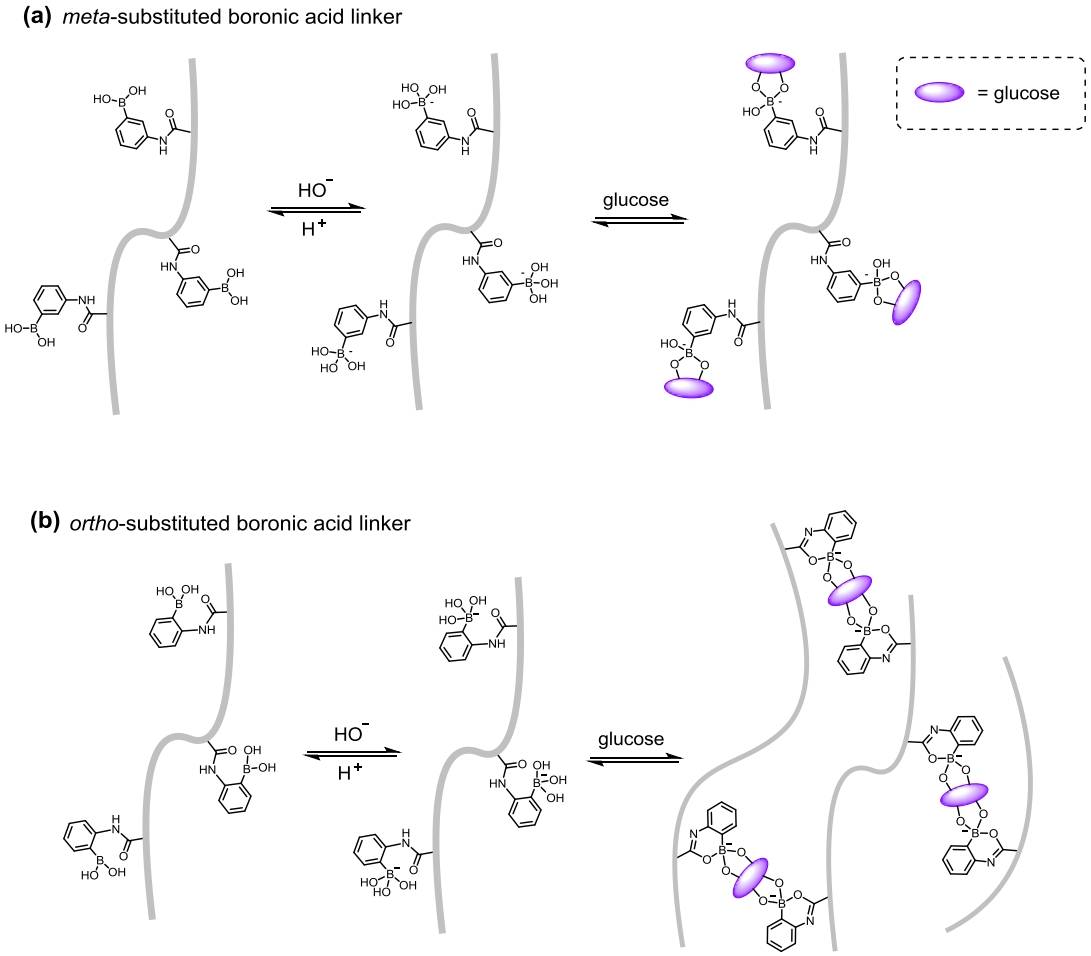


Figure 1.6 (a) NIPAM-based Polymer scaffold with pendant *meta*-substituted boronic acids. The hydrogel expands in response to glucose.[52] (b) NIPAM-based polymer scaffold with pendant *ortho*-substituted boronic acids whose corresponding hydrogel contracts in response to the presence of glucose on account of the formation of intermolecular cross-links between polymeric system components. In both cases, pH-sensitivity was observed on account of the pH-dependant formation of hydroxyboronate anion – a precursor in the formation of boronic esters with glucose.

In a series of studies by Zhang and coworkers,[52b] *N*-isopropylacrylamide was copolymerised with acrylic and methylene bis-acrylamide affording a cross-linked microgel which was subsequently modified with 2-aminophenyl boronic acid[52a, 52c] and 3-aminophenyl boronic ester[52d] to form polymeric cross-linked microgels exhibiting free boronic ester functional groups. It was shown that the microgel containing *meta*-substituted boronic acid underwent expansion (Figure 1.6a) when soaked in a solution of glucose whereas in the case of ortho-substituted boronic acid a contraction was observed under the same conditions. This marked contrast in behaviour is attributed to the capacity of the *ortho*-substituted boronic

acid to form a 2:1 complex with glucose as the carbonyl oxygen is able to stabilize a tetrahedral geometry at the boron atom (Figure 1.6b). This interaction drives hydrogel contraction on account of an increased number of cross-links relative to the *meta*-substituted boronic acid containing hydrogel for whom the same stabilizating interaction cannot occur. Thus, in the *meta*-substituted boronic acid containing hydrogel, a 1:1 glucose:boronic acid complex dominates and no contraction is observed. The interaction of boronic acids and glucose has attracted much attention in the interest of developing technologies to more effectively tackle self-regulated insulin delivery in response to changing blood glucose levels. Zhang *et al* have since expanded these ideas to incorporate the encapsulation and controlled release of insulin,[53] an early step towards a microgel-based implant technology for the treatment of type-1 diabetes.

The group of Bode[54] has recently reported the utility of dynamic boronic ester in a polyol sensor array based on a "shape-shifting" bullvalene core decorated with two boronic acid moieties (Figure 1.7). Functionalized bullvalene is capable of undergoing Cope rearrangements,[55] producing hundreds or even thousands of interconverting

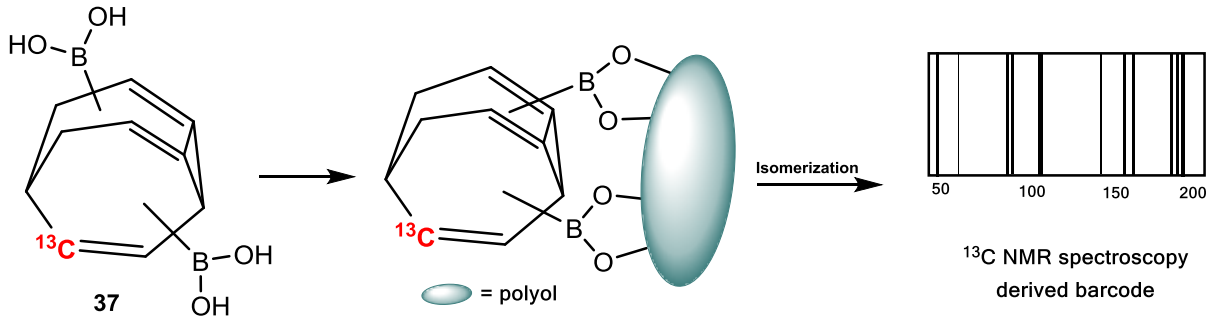


Figure 1.7 Boronic acid bearing bullvalene **37** capable of recognizing a range of bio-relevant polyol compounds. When bound to a polyol analyte, structural isomerization of bullvalene chemosensor **37** yielded, a particular isomer distribution influenced by the structural and electronic nature of the analyte. Analysis usng $^{13}C$ NMR spectroscopy produced barcodes specific to each compound measured.[54]

structural isomers. $^{13}C$ labelled chemosensor **37** was exposed to a range polyols including carbohydrates, flavanols, sucrose and sailic acids which formed boronic esters reversibly with **37** causing the equilibrium of the bullvalene rearrangement process to shift. $^{13}C$ NMR spectroscopy was performed on the resulting dynamic libraries of bullvalene-based boronic

esters. Depending on which analyte was bound to **37**, a particular fingerprint peak pattern was observed which acted as a "barcode", aiding the facile identification of analytes when cross-referenced with a previously collated catalogue of "barcodes". As a negative control the authors developed a structurally analogous, non-dynamic boronic acid sensor, whose fixed bullvalene core could not undergo shape-shifting as a result of Cope rearrangement. The non-dynamic backbone of the static chemosensor rendered its binding capacity extensively diminished, binding only some of the poly analytes in comparison to dynamic chemosensor **37** and the generation of "barcode" spectra was not achieved. This work highlights a powerful combination of two dynamic attributes: the ability of boronic acids to form esters reversibly with a wide range of biologically important polyols, and the extensive rearrangement chemistry of the bullvalene moiety, which together afford an effective sensor based on a single molecule.

The capacity of boronic esters to bind sialic acids was exploited[56] by Wang *et al* in a dual-responsive cell capture surface functionalised with boronic acids. The authors employed a radical polymerisation strategy to grow boronic acid functional polymers from a shaped silicon nanowire surface. The functional surface was capable of interconverting between cell-adhesive and cell-repulsive states in the presence of glucose at pH 6.8 and pH 7.8, respectively. At pH 7.8, removal of the glucose stimulus re-induced the cell-adhesive state on account of the higher binding constant of sialic acid compared with glucose. By reversibly switching conditions between pH 6.8/0 mM glucose and pH 7.8/70 mM glucose, the authors have shown the surface to undergo 5-cycles of cell-binding and cell-release events with high cell viability (95%). This example of an AND logic gate cell binding surface represents an innovative implementation of dynamic covalent boronic esters, capable of undergoing component exchange between cell-bound sialic acids and free glucose, expanding the field of smart, cell-specific binding surface technologies.

The group of Kiser have harnessed[57] the pH-sensitivity of the dynamic boronic ester bond in the preparation of a HIV barrier gel. The target gel would be sufficiently densely cross-linked to prevent diffusive transmission of HIV virions between seminal fluid and cervicovaginal mucosa during heterosexual intercourse, however, the application of extensively cross-linked gel-materials can give rise to problems regarding tissue bio-distribution. It was therefore necessary develop a gel with viscous flow properties at low pH, which was capable of undergoing changes in its mechanical properties at physiological pH when applied to the vaginal cavity. It is known that gels formed between salicylhydroxamic

acid and boronic acids exhibit relatively weak mechanical properties when formed in acidic conditions and much stronger mechanical properties in basic conditions[58]. This difference in mechanical properties arises on account of the position of equilibrium shifting towards the formation of hydroxyboronate anion at higher pH, thus favouring the formation of boronic esters with salicylhydroxamate. Grafting these two complimentary functionalities on acrylamido-copolymers provided a route for the authors to develop boronic ester cross-linked gels capable of changing their cross-link densities dramatically over a relatively narrow pH range of pH 4.8 - 7.4. The dynamic, pH-senstivie nature of the boronic ester facilitates the gels *in-situ* structural modification, potentially providing a point-of-contact technology for the prevention of male-to-female HIV-1 transmission.

### 1.5.4 *Orthogonal dynamic covalent bonds in systems chemistry*

The first examples of orthogonal dynamic covalent bonds confined to a single functional system was reported by the groups of James and Bull. The described 3-component Systems (Figure 1.8), exhibited the capacity to form dynamic boronic ester and imine bonds and was

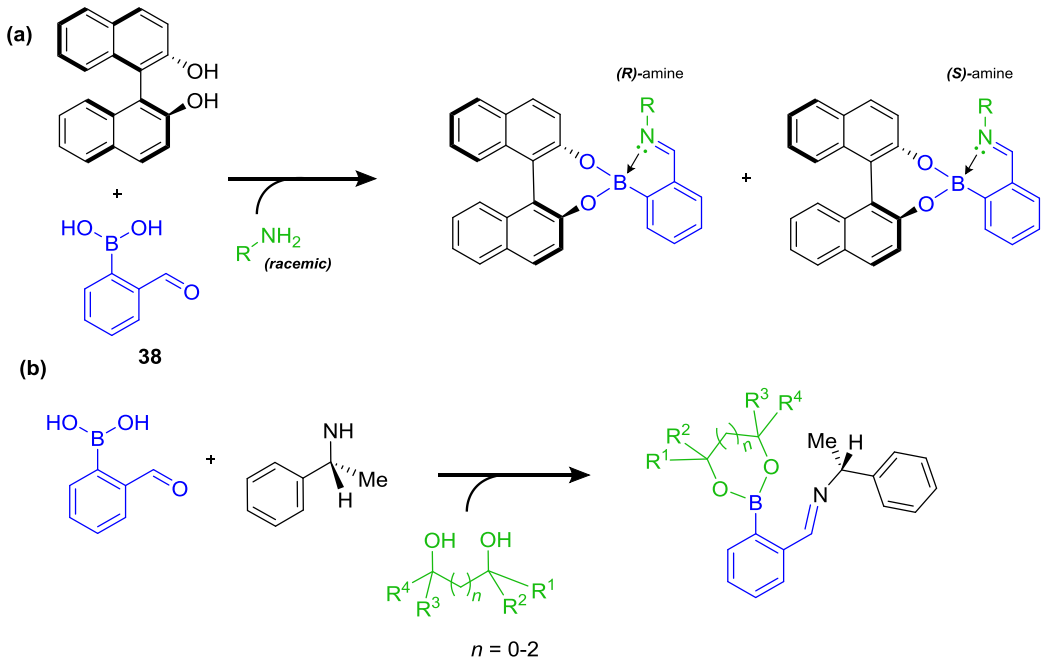


Figure 1.8 (a) Three-component system consisting of *(S)*-BINOL, 2-formylphenyl boronic acid **38** and a range of racemic primary amines.[59] Using $^{1}$H NMR spectroscopic analysis, straightforward determination of the enantiopurity of a range of chiral primary amines was achieved. (b) Three-component chiral derivatizing system consisting of 2-formylphenyl boronic acid **38**, enantiopure α-methylbenzylamine and a range of 1,2-, 1,3- and 1,4-diols. Determination of diol enantiopurity was achieved using $^{1}$H NMR spectroscopic analysis.[60]

capable of determining the enantiopurity of a range of chiral primary amines[59] (Figure 1.8a) and chiral 1,2-, 1,3- and 1,4-diols[60] (Figure 1.8b) using $^{1}$H NMR spectroscopic analysis. This seminal work seeded immediate interest in the introduction of multiple, orthogonal dynamic covalent bonds within supramolecular systems, wherein dynamic covalent chemistry had already demonstrated great promise. This drive has led to the meticulous design and

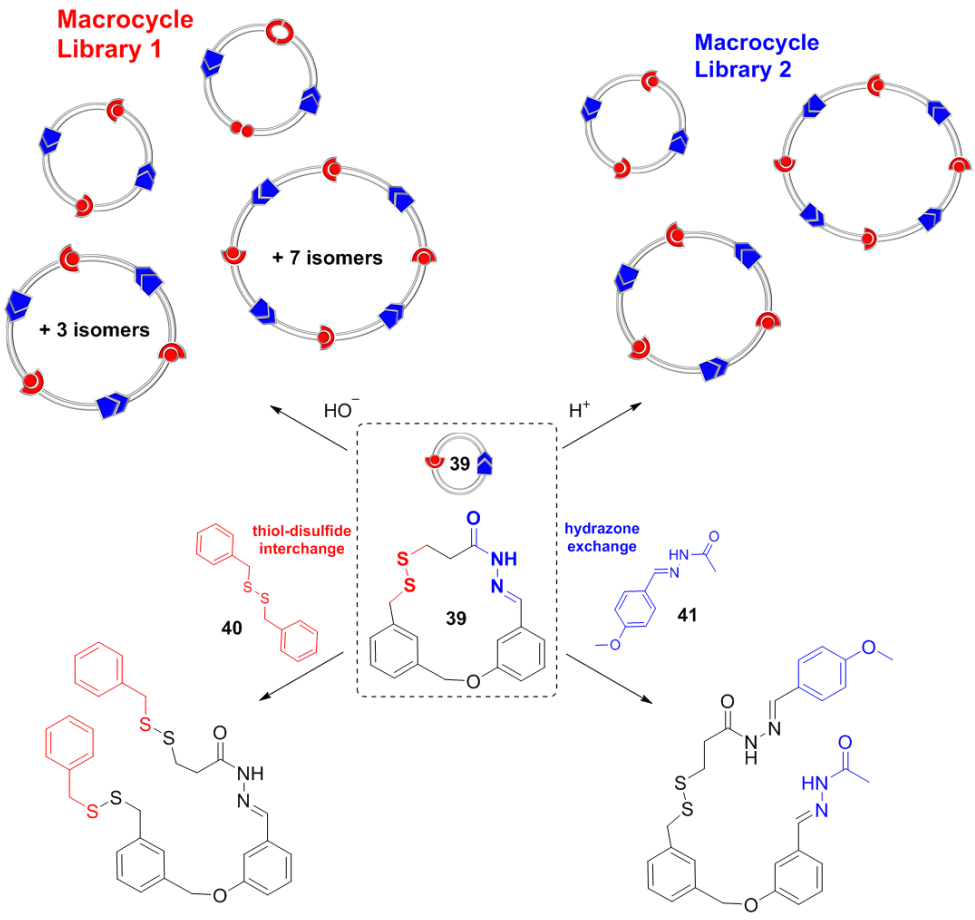


Figure 1.9 Disulfide and hydrazone containing macrocycle **39** was observed to undergo disulfide *or* hydrazone exchange depending on whether the system was placed under basic *or* acidic conditions, respectively, affording macrocycle library 1 *or* macrocycle library 2, respectively. It was demonstrated that disulfide scavenger **40** and hydrazone scavenger **41** engaged in component exchange with dual-functional macrocycle **39** under basic *or* acidic conditions, respectively. In the presence of both disulfide **40** and hydrazone **41**, disulfide exchange *or* hydrazone exchange occurred exclusively under basic *or* acidic conditions, respectively demonstrating true orthogonality between disulfide and hydrazone bonding motifs.[61]

preparation of complex nanoscale architectures in early studies by Nitschke *et al*[62] and Matile,[63] the latter of whom has recently produced an inspiring landmark review detailing advances in the utility of orthogonal dynamic covalent bonds in functional systems.[64] Encouraged by well-known studies performed independently by Otto and Furlan *et al*[65] in which libraries of dual-stimuli disulfide and hydrazone macrocycles were studied, the group of Leigh developed[61] a similar disulfide- and hydrazone-based
macrocyclic system (Figure 1.9). The orthogonality of the imine and disulfide bonds in macrocyle **39** was probed in three key experiments. Firstly, the orthogonal formation of hydrazone and disulfide bonds was demonstrated by operation of the system under basic
and acidic conditions. Analysis of the resulting macrocycle mixtures using $^{1}$H NMR spectroscopy and mass spectrometry revealed two contrasting macrocycle libraries afforded by either hydrazone or disulfide exchange which proceeded under acidic or basic conditions, respectively. Many more macrocyclic isomers were detected in macrocycle library 1 compared with macrocycle 2 on account of the capacity for the system to exhibit three structural variants of disulfide bond, whereas only a single type of hydrazone bond was possible. Next, by introducing hydrazone scavenger **41** *or* disulfide scavenger **40** and interconverting between acidic and basic conditions, it was shown that cleavage of macrocycle **39** occurred at the hydrazone or disulfide linkage *only* when the system was under acidic or basic conditions, respectively. Finally, it was shown that both disulfide and hydrazone bonds exhibited orthogonality when the system was operated in the presence of hydrazone scavenger **41** *and* disulfide scavenger **40**. As expected, disulfide exchange occurred only under basic conditions whereas hydrazone exchange occurred only under acidic conditions, and there was no observed cross-reactivity. These observations demonstrated that hydrazone and disulfide exchange chemistries between macrocycle **39** and hydrazone or disulfide scavengers, **41** and **40**, occur independently of each other and exhibit true orthogonality.

Leigh *et al* proceeded to expand their hydrazone and disulfide based system culminating in a stunning and extremely well-renowned example of orthogonal dynamic covalent chemistry in functional systems wherein a molecular walker system was prepared (Figure 1.10).[66] This remarkable molecular machine consisted of a 21-atom molecular walker unit attached to a 'four-platform' track. The molecular walker was capable of taking steps along the molecular track with a passing-leg gait driven by switching between acidic and basic conditions. One 'leg' of the molecular walker was terminated with a hydrazide functional group, the other a thiol group, and this arrangement allowed binding of the

walker's feet to complimentary footholds on the molecular track by the formation of hydrazone and disulfide bonds, respectively. Starting at position **I** (Figure 1.10a), when the system was placed under acidic conditions, the disulfide 'foot' remained kinetically fixed and bound to the track, whereas, the walker's hydrazone foot was able to reversibly exchange with the nearest aryl 'platform' along the molecular track. These conditions brought about thermodynamic re-equilibration about the pivot foot (Figure 1.10b) (the foot which was still attached to the track) achieving directionally un-biased movement of the walker back and

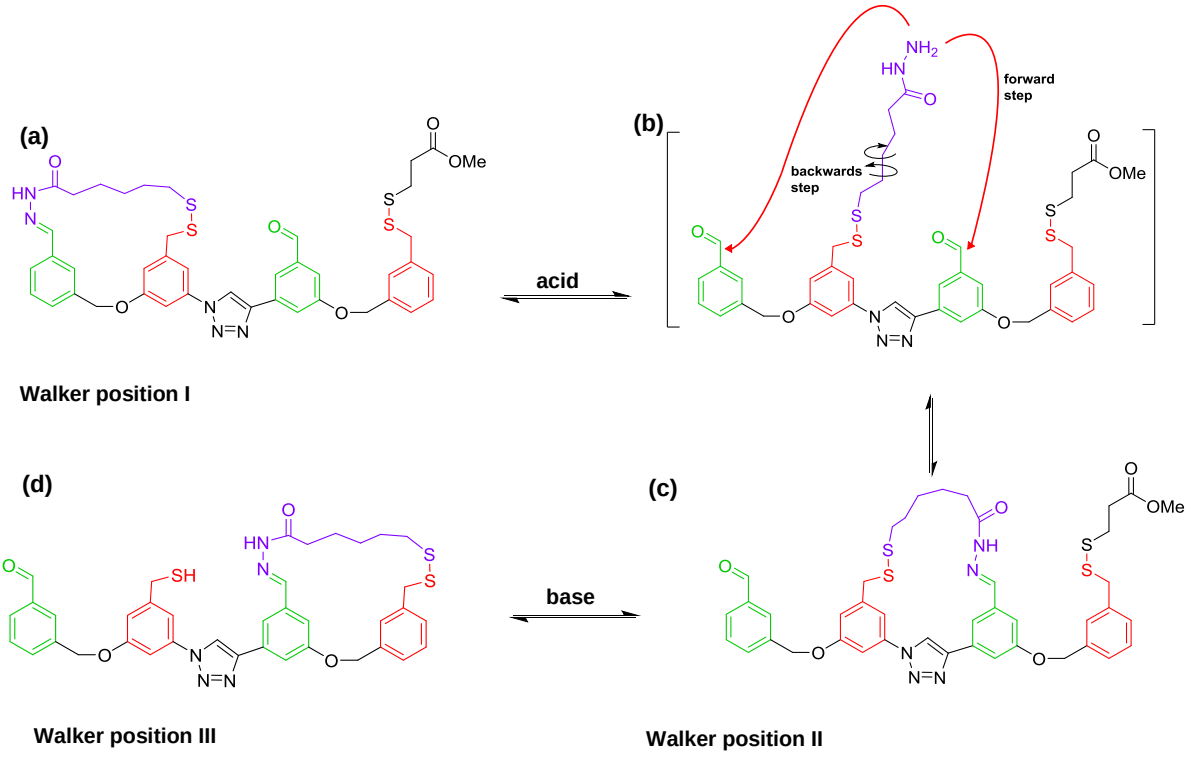


Figure 1.10 Molecular walker system wherein a 21-atom molecular walker (purple) was demonstrated to traverse a 'four-platform' molecular track by the reversible formation and breaking of dynamic covalent imine and disulfide bonds. (a) Walker position **I** wherein both hydrazone and disulfide bonds are fixed to the track. (b) Decreasing the system pH encourages reversible breaking of the hydrazone bond present and thermodynamic re-equilibration about the disulfide pivot foot. (c) Walker position **III**, wherein a 'forward-step' is achieved through a passing-leg gait mechanism and driven by the formation of a new hydrazone bond. (d) Increasing the system's pH facilitated reversible breaking of the disulfide bond present in walker position **II** and displacement of the placeholder disulfide moieity by thiol-disulfide interchange.[66]

forth along the hypothetical track. This re-equilibration caused the system to interconvert between positions **I** and **II** (Figure 1.10c). Under basic conditions, the walker's hydrazone foot remained bound to its complimentary foothold, however, the disulfide foot was free to reversibly exchange with the placeholder disulfide group along the molecular track facilitating interconversion between positions **II** and **III** (Figure 1.10d). The authors then replaced the base-catalyzed disulfide exchange mechanism with a two-step redox process operating under kinetic control, allowing directionally biased walking on account of a Brownian ratchet mechanism, driving a net migration of the molecular walker to position **III** in preference to position **II** on account of the newly introduced kinetic driving force. Leigh *et al* further expanded[67] this molecular walker system by the incorporation of a light-sensitive alkene in place of the triazole moieity, thereby affording a system with a much greater uni-directionality on account of a well-timed light-induced *cis*- to *trans*-isomerization of the molecular track, favouring a 'forward-step' over the reverse process.

Orthogonal dynamic covalent chemistry has shown promise in the preparation of multi-adaptive self-healing materials capable of changing their mechanical properties in response to two or more orthogonal stumuli. An embodiment of these ideas was presented in a study by Chen, Liu and Deng[68] in which dynamic covalent disulfide and hydrazone bonds were implemented in a macroscopic hydrogel by condensation of disulfide-containing *bis*-hydrazide linker **42** with PEG-based trialdehyde **43** (Figure 1.11)**.** The resulting dual-adaptive hydrogel **44** was capable, when cut into two halves, of undergoing self-healing, recovering its original shape under acidic and neutral conditions *via* hydrazone exchange and basic conditions *via* thiol-disulfide interchange conditions. It was demonstrated that, once cut a second time along the initial cut, the material healed again in exactly the same way. The hydrogel's sol-gel transition was induced by manipulation of either redox conditions or pH. Very recently, a similar system composed of orthogonal dynamic oxime and boronic

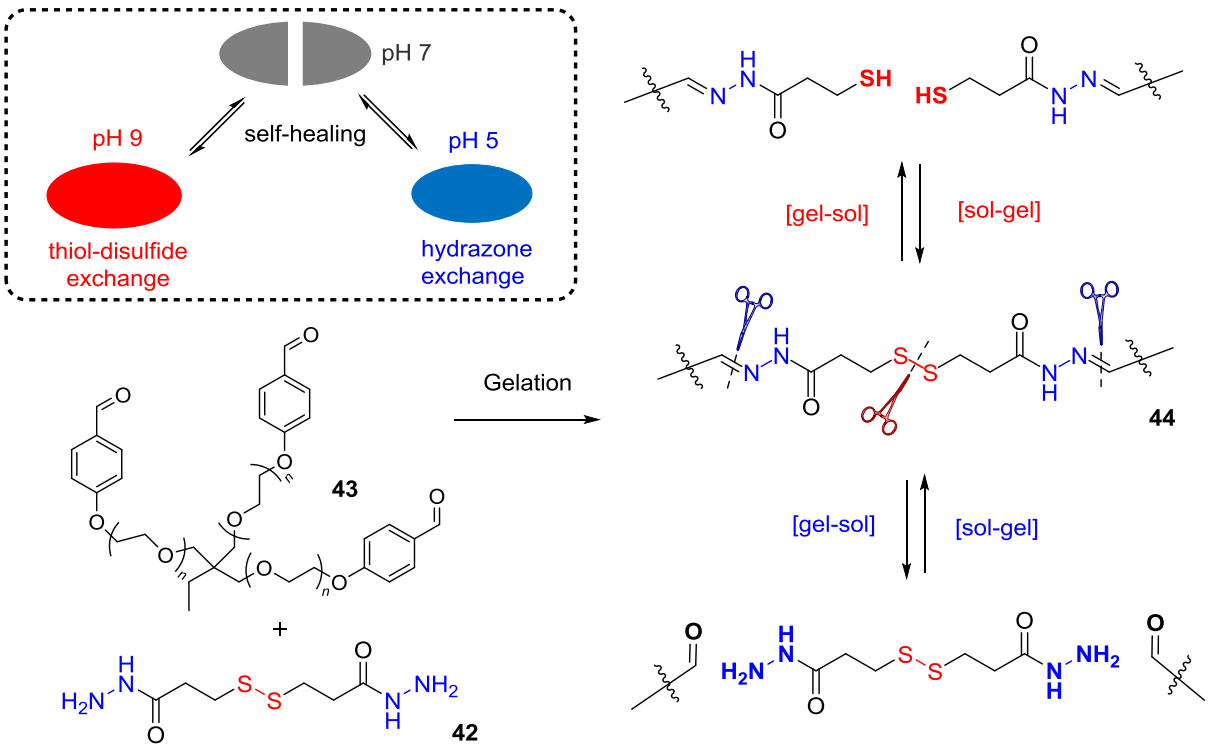


Figure 1.11 Dual-adaptive, self-healing hydrogel **44** formed through condensation of trialdehyde **43** and disulfide-based dihydrazide linker **42**. It was demonstrated that hydrogel **44** was capable of self-healing, when mechanically cut, in acidic and neutral conditions on account of hydrazone exchange and basic conditions on account of disulfide exchange (as displayed in the inset). Two discreet sol-gel transitions were observed arising from the capability of the dual-functional system to undergo gelation by a hydrazone exchange mechanism under neutral and acidic pH and by a disulfide exchange mechanism under basic conditions.[68]

ester bonds was reported[23]. Such systems hold promise in contributing towards the development of 'smart' soft materials with potential applications in tissue engineering, biomedical devices and drug delivery.

Orthogonal dynamic covalent bonds have been employed by the groups of Sakai and Matile[69] in self-organizing surface initiated polymerization (SOSIP) – a method of constructing highly ordered surface-bound nanostructures for application in surface photochemistry.[70] Initiator **45** (Figure 1.12) was bound to an indium tin oxide surface using its phosphate anchors and then extended with building block **46** using thiol-disulfide interchange, affording surface-bound poly-disulfide **47** whose structure was stabilized by hydrophobic interactions of the napthalenediimide sub-units. The peripheral

hydrazone units of architecture **47** were cleaved with hydroxylamine yielding discreet, hydrazide-rich channels within the surface macrostructure which were subsequently post-functionalized with a range of napthalendiimide-based aldehydes affording a range of double channel photosystems. The authors proceeded to demonstrate 'stack-exchange' wherein several aldehydes were aggregated to a pre-formed surface architecture using hydrazone exchange chemistry affording a variety of well-ordered multicomponent surface structures.

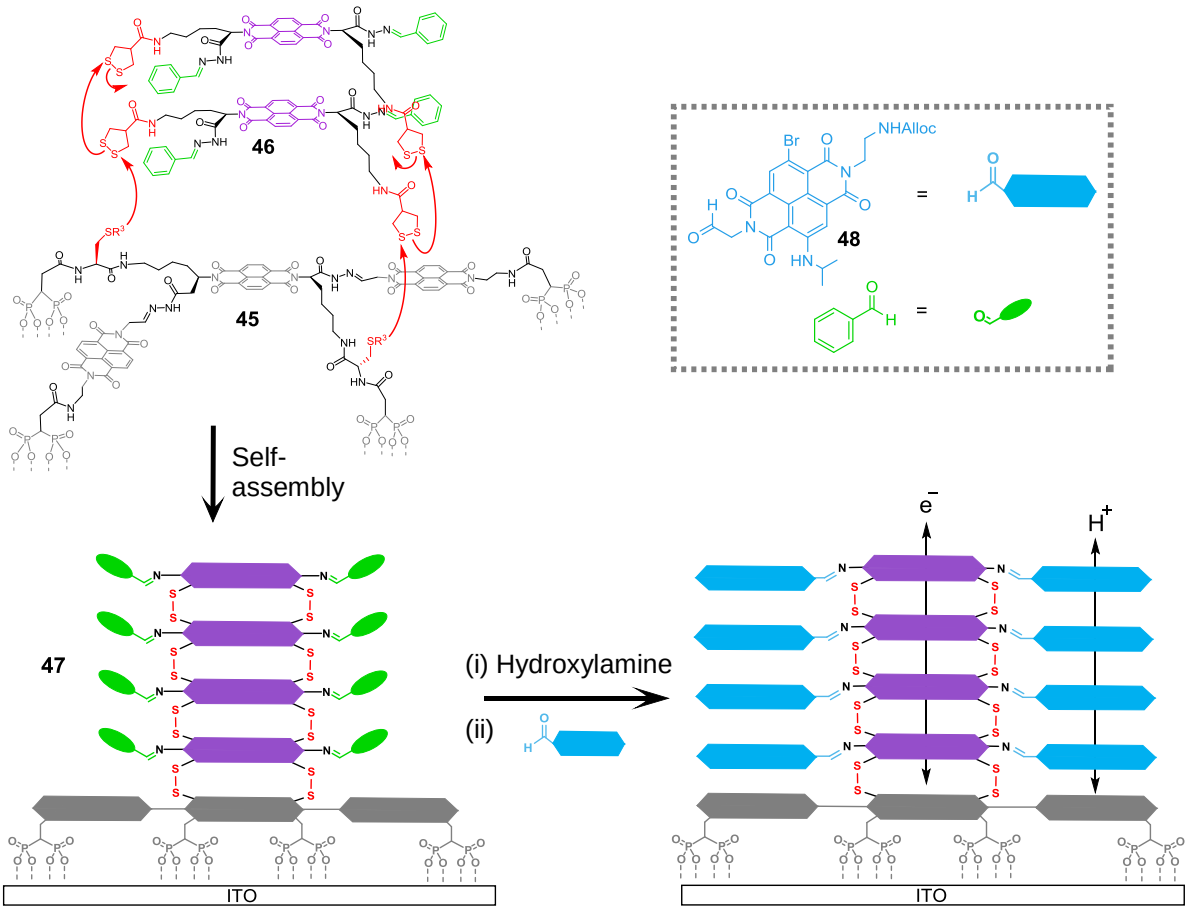


Figure 1.12 Surface bound initiator **47**, self-assembled by sequential layering of disulfide **46** by thiol-disulfide interchange, consisted of a stacked napthalenediimide core bound to an indium tin oxide surface by phosphate anchor 'moieties'. Cleavage of its peripherial hydrazones moieities using hydroxylamine yielded hydrazide-rich channels which were subsequently post-functionalized with a range of napthalendiimide based aldehydes.[69-70]

Recent advances in the development of SOSIP technologies has seen orthogonal dynamic covalent chemistry utilized in the formation of triple-channel photosystems[71] which employ boronic esters in conjuction with hydrazones and disulfides. The production of these

extremely highly ordered structures is fairly straight-forward with the advent of orthogonal dynamic covalent chemistry. Additionally, the extensive range of building blocks with suitable functional groups and the capability of remarkable structural control on the nanoscale render dynamic covalent chemistry a hugely powerful tool in the development of multicomponent surface architectures of high sophistication.

Very recently, Anslyn and coworkers furnished a proof-of-principle study[72] wherein four orthogonal DCBs were operated simultaneously using $^1$H NMR spectroscopy exchange studies. By careful deconvolution of $^1$H NMR spectra corresponding to

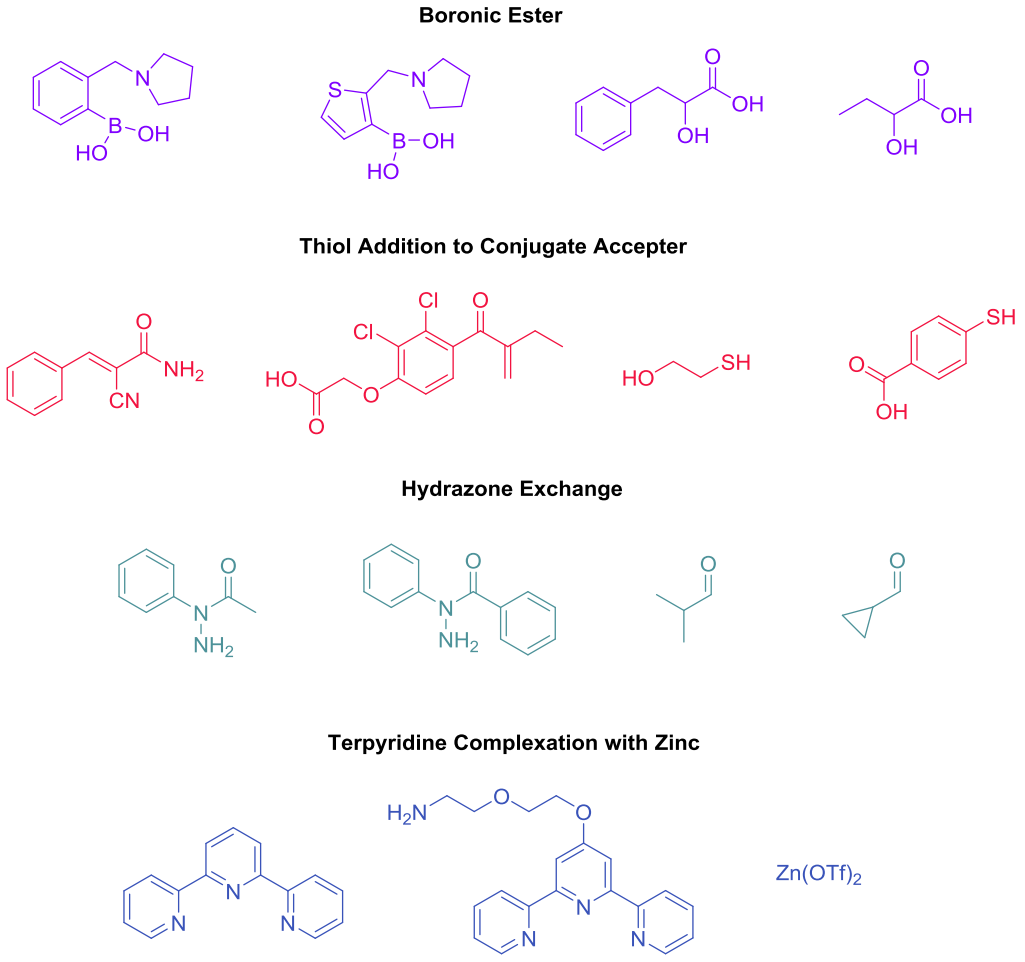


Figure 1.13 Exchanging system components capable of forming the four studied dynamic covalent chemistries: boronic ester formation, thiol additions to a conjugate acceptor, hydrazone exchange and terpyridine complexation with zinc. All four exchange reactions were demonstrated to occur orthogonal by semiquantative $^1$H NMR spectroscopic analysis.[72]

equilibrating mixtures containing all four dynamic covalent bonding motifs (boronic esters, hydrazone, thiol addition and zinc-complexation of terpyridines) semiquantative analysis was

performed confirming the independence of each reaction pathway *in-situ*. Although this work is some way from finding utility in functional systems, it speaks volumes of the desire for chemists to increase their ability to create complex functional systems with multi-faceted stimuli-responsiveness using orthogonal dynamic covalent bonds.

## 1.6 Conclusion

The fields of systems chemistry and supramolecular systems chemistry are undoubtedly in their infancy, however, the last decade has seen the birth of an array of functional systems extensive in their variety. An already well-established appreciation for the capacity for dynamic covalent chemistry to impart dynamic characteristics in complex chemical systems has paved the way for the development of systems with emergent properties where the output is more than merely the sum of its parts. The studies presented in this Chapter collectively represent a venture beyond the traditional realms of synthetic chemistry, towards understanding system-level phenomena in orchestrated processes on the molecular and macromolecular level, the kind of which are ubiquitously observed in Nature. Whilst a great deal of inspiring work has been reported, there still remains a call on the resourcefulness of chemists to evolve systems with greater sophistication capable of embodying increasingly information-rich processes. Specifically, *orthogonal* dynamic covalent chemistry provides a robust, yet dynamic, means of invoking multi-faceted stimuli-responsiveness to chemical systems. The ever-growing ability of chemists to pre-programme molecular and supramolecular systems with orthogonality endowing them with the ability to process information by responding to their environment takes us closer to emulating the very essence of life.

# Chapter 2

## *The Utility of Orthogonal Dynamic Covalent Bonds in Systems Chemistry*

# Table of Contents

## 2.1 Abstract

*Water soluble aldehyde, amine and thiol compounds were prepared and utilized to demonstrate orthogonal bond-breaking and forming of dynamic covalent disulfide and imine bonds in aqueous solution. Considering only situations in which imine and disulfide DCBs are in either ''broken'' or ''formed'' states there are four distinct scenarios which can be mapped onto a 4-node network. $^1$H NMR Spectroscopy and mass spectrometry was used to characterize each node of the'4-node network' and the order in which the system traverses through the 4 system 'nodes' (**A – D**) was demonstrated to be dependent upon which one of two orthogonal stimuli was applied at any node. Through judicious choice of reaction partners and conditions, it is possible to cleave and reform selectively these bonds in the presence of each other in the absence of unwanted competing processes.*

## 2.2 Introduction

The design and study of functional systems of molecules is an area of interest within the growing field of systems chemistry.[4, 73] A key aim of researchers within the field of systems chemistry is to more effectively increase the complexity of functional systems by broadening the rapidly growing tool-kit of methodologies available to them as synthetic chemists. An molecules[74] and responsive materials,[23, 68] and to continue this development there is a clear need for well-understood orthogonal interactions.[64]

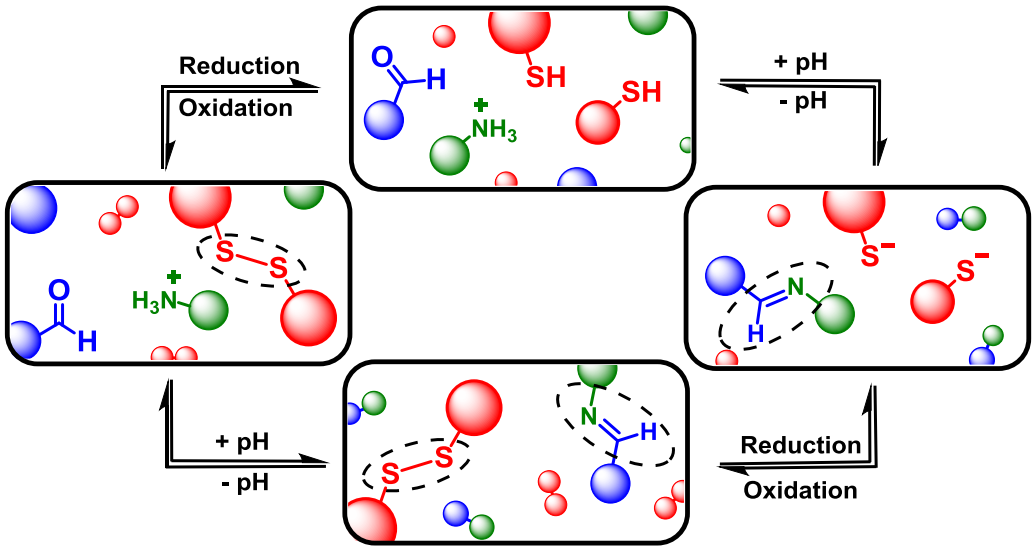


Figure 2.1 Considering only situations in which imine and disulfide DCBs are in either ''broken'' or ''formed'' states, there are four distinct scenarios which can be mapped onto a four-node network.[75]

Chemical bonds which can reversibly break and reform in response to stimuli are well-known[18a, 18b] in chemistry, and these so-called ‘‘dynamic covalent bonds’’ (DCBs) can be utilized as ‘‘modules’’[76] to introduce stimuli-responsiveness into functional systems.[6, 64, 72, 77] Of particular interest at Newcastle are reversible imine[12a, 22, 78] and disulfide[33, 36, 61, 65a, 79] bonds. Imine bonds are formed from the condensation of amines and carbonyls, and the position of the equilibrium is pH dependent, with work by Lehn *et al* demonstrating[41] that the position of the imine equilibrium can be shifted from almost complete imine to starting materials over about three pH units. Redox-sensitive disulfide bonds can be reduced to their corresponding thiols in the presence of a reducing stimulus, and re-oxidized to form the disulfide. Since pH and redox can be controlled independent of each other it should be possible to selectively cleave and reform one of these bonds in the presence of the other, and thus these bonds can be considered to be orthogonal. Assuming complete orthogonality, and considering only situations in which DCBs are in either ‘‘broken’’ or ‘‘formed’’ states, there are four distinct scenarios (Figure 2.1). It is convenient to map these states onto a four-node network where each node represents one of four possible scenarios regarding whether the disulfide and imine bonds are ‘‘broken’’ or ‘‘formed’’ and the vertices display the orthogonal stimuli required to drive the bond forming and breaking processes. The condition for orthogonality is that it is possible to successfully navigate between all nodes through the application of appropriate orthogonal stimuli with no undesired reactions occurring between the molecules in the mixture *i.e.* alternative combinations of the reaction partners are not detectable by $^{1}$H NMR spectroscopy. In particular, the reaction between thiols and aldehydes to form hemithioacetals was identified as a potential competing process, and our investigation showed that careful choice of reaction partners is necessary to avoid this problem. $^{1}$H NMR Spectroscopy was chosen to analyse the system at each node because it allowed *in-situ* monitoring of changes in chemical shifts of key, diagnostic signals corresponding to protons in the model compounds. This allowed us to quantify the extent of bond breaking/bond forming processes between nodes.

## 2.3 Results and discussion

### 2.3.1 *Synthesis of model system components*

As a redox-sensitive DCB, the disulfide **3** (Scheme 2.1a) was chosen as its quaternary ammonium groups impart water solubility. Reversible interconversion of this species with thiol **4** is achievable upon application of suitable reducing and oxidising agents. Imine **8** was chosen as a pH-sensitive DCB (Figure 2.1b), which by modulation of pH can be reversibly interconverted into its water-soluble components amine **7** and aldehyde **6**. The equilibrium of imine formation is shifted to form almost exclusively imine **8** at pH 12.0, whereas the components amine **7** and aldehyde **6** reaction are favored at pH 6.5.

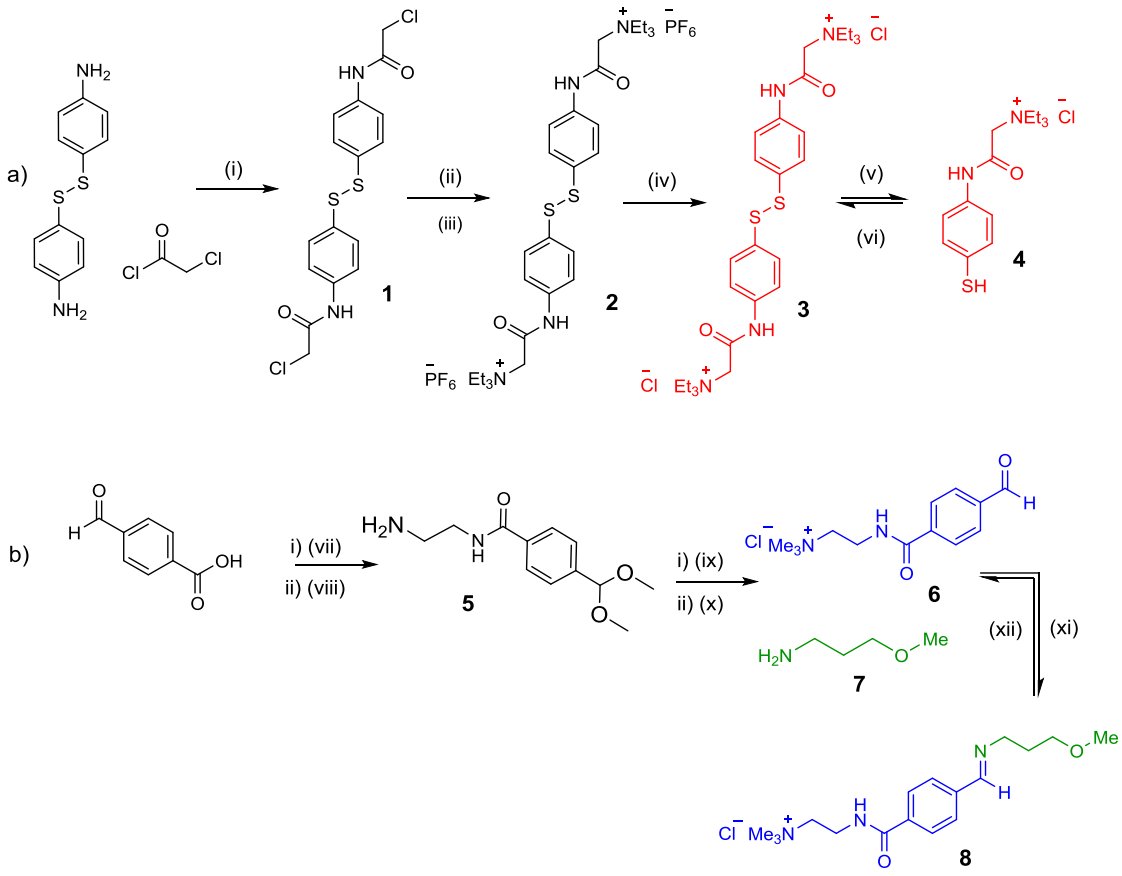


Scheme 2.1 a) Synthesis of disulfide **3** and its interconversion with thiol **4** b) Synthesis of aldehyde **6** and condensation with amine **7** to form imine **8**. (i) $Et_3N$, $CH_2Cl_2$, 30 °C 18 h. (ii) $Et_3N$, MeOH, 60 °C, 72 h. (iii) $NH_4PF_6$, MeOH, 60 °C, 16 h,. (iv) Amberlite® IRA-410, MeOH, 40 °C, 18 h, 36 % (v) DTT, $H_2O$, 25 °C, 3 h. (vi) $H_2O_2$, $H_2O$, 25 °C, 2 h. (vii) $CH(OCH_3)_3$ MeOH, $H_2SO_4$, 48 h. (viii) Ethylenediamine, 130 °C, 18 h, 36 %. (ix) MeI, $K_2CO_3$, MeOH, 8 h, 55 °C. (x) HCl, acetone:$H_2O$ (1:1, v/v), 2 h, 69 %. (xi) NaOH, $H_2O$. (xii) HCl, $H_2O$.

Disulfide **3** was prepared (Figure 2.1a) starting from 4-aminophenyl disulfide, which was acylated with chloroacetyl chloride to afford **1**. Reaction with excess triethylamine followed by refluxing overnight in a saturated solution of $NH_4PF_6$ in MeOH afforded disulfide **2,** which was isolated by precipitation in $H_2O$ and then collected by filtration. Disulfide **2** was refluxed in MeOH in the presence of trimethylammonium-functionalized Amberlite (chloride form) to furnish water-soluble target disulfide **3**. The transformation of disulfide **3** into thiol **4** was achieved using organic reducing agent dithiothreitol (DTT) in aqueous solution, and reconversion of thiol **4** to disulfide **3** was accomplished in the presence of 1 M $H_2O_2$. Aldehyde **6** was prepared (Figure 2.1b) by refluxing 4-carboxybenzaldehyde with trimethylorthoformate to afford methyl 4-(dimethoxymethyl)benzoate (**5**). The reaction of **5** with excess ethylenediamine followed by methylation with iodomethane and subsequent acetal hydrolysis in HCl furnished water soluble aldehyde **6**. Adjusting the pH of an aqueous solution of **6** and commercially-available amine **7** to pH 12.0 with aliquots (5 µL) of 1 M NaOH lead to their condensation, affording imine **8**. The reconversion of imine **8** to aldehyde **6** and amine **7** was achieved by lowering the pH of its solution to pH 6.5 with addition of aliquots of 1 M HCl.

### 2.3.2 *Operation of a pH-redox sensitive '4-node network'*

The four-node network (Figure 2.2) can in principle be explored starting at any node, and then traversing the network in either a clockwise or anticlockwise direction. In the interest of experimental simplicity, node **A** was selected as a starting position from which one clockwise cycle was performed. Thus, a solution of disulfide **3**, amine **7** and aldehyde **6** in $D_2O$ (15 mM of each of these three species) at pH 6.5 was prepared and analyzed by $^1H$ NMR spectroscopy (Figure 2.3a). The presence of aldehyde **6** was confirmed by a singlet at δ = 9.9 ppm and a pair of aromatic doublets at δ = 7.7–8.0 ppm. Signals at δ = 7.4 ppm indicates the presence of the aromatic disulfide **3**, indicating disulfide **3** is stable at pH 6.5 and the absence of a signal at δ = 8.4 ppm suggests that there is no unwanted imine formation at this pH. Closer examination of this spectrum does reveal a second pair of doublets of extremely low intensity between δ = 7.5–7.7 ppm and a singlet at δ = 6.0 ppm suggesting the presence of a

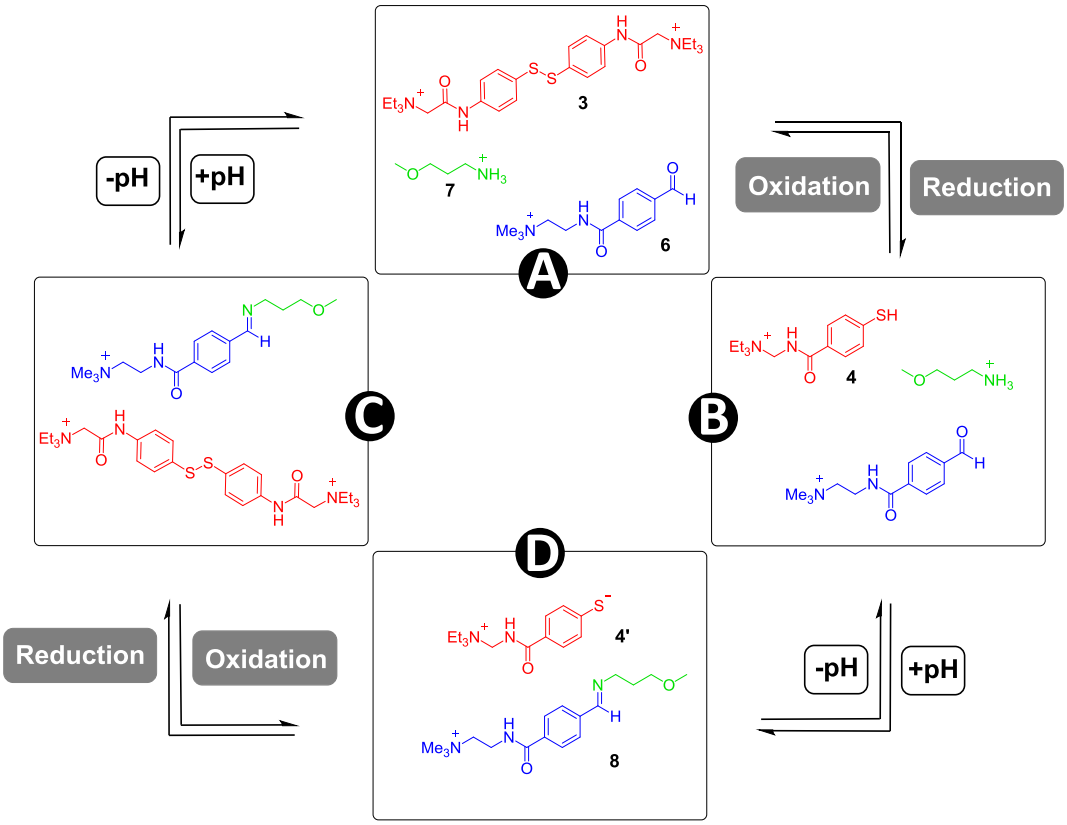


Figure 2.2 pH-Redox sensitive '*4-node network*'.

small amount of hydrate (Figure 2.4a). At pH 6.5 the hydrate of **6** exists merely as a ''spectating'' species in low concentration and does not influence the orthogonality of the imine and disulfide bonds. An aliquot (10 µl) of the solution corresponding to node **A** was diluted in $H_2O$ (10 ml) and analysed by electrospray mass spectrometry (Figure 2.3b). The mass spectrum revealed two signals with m/z ratios corresponding to disulfide **3** and aldehyde **6** at 266.14 and 235.14, respectively. The signal corresponding to disulfide **3** displays spacing of ≈ 0.5 m/z between isotope peaks which is characteristic of a doubly charged ion. Amine **7** was not visible on account of its molecular weight being lower than the cut-off threshold for the instrument. To drive the transition from node **A** to node **B**, a reductive stimulus was applied through the addition of a slight excess of the organic reductant DTT. Analysis by $^1$H NMR spectroscopy (Figure 2.3c) reveals the appearance of a broad multiplet at δ = 7.8 ppm associated with thiol **4** and the disappearance of the pair of doublets at δ = 7.3–7.5 ppm associated with disulfide **3**. Furthermore, signals corresponding to amine **7** (not shown) remain unchanged between nodes **A** to **B**, indicating no unwanted processes occur involving **7**. Analysis by mass spectrometry (Figure 2.3d)

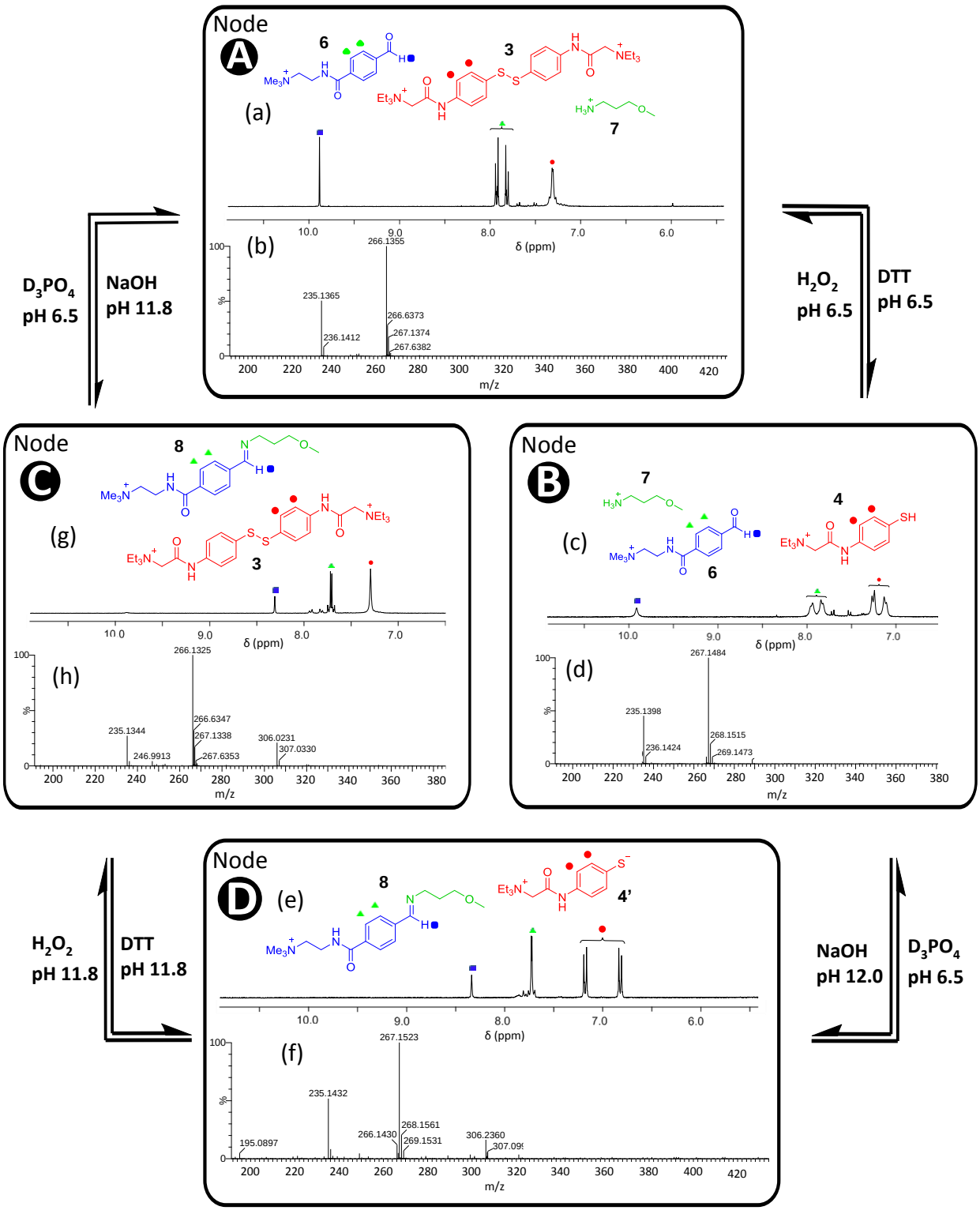


Figure 2.3 Partial $^{1}H$ NMR spectroscopy (300 MHz, $D_2O$) and electrospray mass spectrometry characterization of '*4-node network*' nodes **A** – **D**. In node **A**, the disulfide bond is ''formed'' and the imine ''broken''. In node B both the disulfide and imine bonds are ''broken''. In node **C** both the disulfide and imine bonds are ''formed'', and in node **D** the disulfide bond is ''broken'' the imine ''formed''. It is possible to successfully navigate between all nodes through the application of the appropriate orthogonal stimuli.

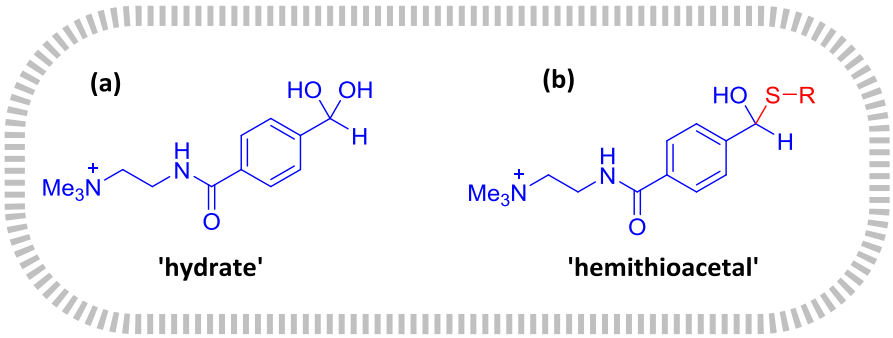


Figure 2.4 Structures of (a) the hydrate of aldehyde **6** and (b) hemithioacetal afforded by the reaction of a thiol with aldehyde **6**.

revealed signals with m/z ratios corresponding to thiol **4** and aldehyde **6** at 267.15 and 235.14, respectively. With respect to the signal corresponding to thiol **4**, spacing of ≈ 1 m/z indicates a singly charged species. These observations indicate the successful and complete reduction of disulfide **3** into thiol **4**. The chemical shifts of the signals corresponding to aldehyde **6** remain unchanged suggesting no significant formation of unwanted hemithioacetal (Figure 2.4b) formation has occurred through reaction of thiol **4** with aldehyde **6**. The signals are however broader and less intense, suggesting the possibility of a chemical exchange phenomena involving thiol and aldehyde which will be discussed later.

The transition from node **B** to node **D** was driven by raising the solution pH, serving as a stimulus to favour the condensation of **6** with **7** to form imine **8**. Analysis by $^{1}$H NMR spectroscopy revealed (Figure 2.3e) the disappearance of the aldehyde proton signal at δ = 9.9 ppm and emergence of a new singlet at δ = 8.4 ppm corresponding to imine proton in **8**. This change was accompanied by the appearance of a new pair of aromatic doublets at δ = 6.8–7.2 ppm corresponding to the aromatic protons of imine **8** and the disappearance of the aromatic protons associated with aldehyde **6**. Integration analysis of the signals corresponding to the aromatic protons and aldehyde protons in aldehyde **6** was compared between node **A** and node **B**. The same integral ratio was observed (within 5 %) between the signals aldehyde and aromatic protons at 1:4. These observations suggest near-quantitative formation of imine **8** from aldehyde **6** and amine **7** at pH 12.0 without the formation of any unwanted side-products. In particular, there is no evidence for the formation of unwanted hemithioacetal as observed by the absence of a singlet at δ = 6.1–6.2 ppm. Deprotonation of thiol **4** was evidenced by a change in the signals corresponding to its aromatic protons, the chemical shift of the aromatic signals in **4'** was between δ = 6.7–7.2 ppm. It is also worthwhile to note that

at pH 12 aldehyde **6** is not susceptible to hydrate formation, as evidenced by the lack of a signal at δ = 6.0–6.1 ppm. The mass spectrum of the system at node **D** (Figure 2.3f) revealed peaks corresponding to thiol **4** and imine **8**, as expected, at m/z ratios 267.15 and 306.24, respectively. A third signal at m/z ≈ 235.14 corresponds to aldehyde **6** which is afforded on account of significant hydrolysis of imine **8** upon dilution to a suitable concentration for analysis.

The transition from node **D** to node **C** was completed by slow addition of 1 M $H_2O_2$ to drive the oxidation of the thiolate **4'** whilst maintaining pH at 11.8. The resulting $^1$H NMR spectrum (Figure 2.3g) displays a pair of aromatic doublets at δ = 7.3 ppm corresponding to aromatic protons in **4** and the disappearance of the pair of doublets corresponding to the thiolate **4'**. A singlet corresponding to the imine proton at δ = 8.4 ppm of **8** accompanied by the characteristic pair of aromatic doublets at δ = 7.6 ppm suggests the imine bond has been successfully retained. The presence of low-intensity doublets at δ = 8.0 ppm suggest the presence of a very small fraction of unreacted aldehyde **6**. Mass spectrometry of node **C** (Figure 2.3h) displayed peaks at m/z = 266.13 and 306.02 evidencing the presence of disulfide **3** and imine **8**, respectively. A peak corresponding to aldehyde **6** at m/z = 235.13 was observed which had resulted from hydrolysis of imine **6** after dilution for analysis. These observations indicate that successful oxidation of thiol **4** to form stable disulfide **3** at pH 11.8 in the presence of imine **8**. These experiments taken together demonstrate one successful clockwise cycle of the '*4-node* network' in which imine and disulfide bonds are broken and formed orthogonally.

To ensure the complete reversibility of every step within the network, an anti-clockwise cycle starting at node **A** was performed and analysed at each node by $^1$H NMR spectroscopy (Figure 2.5)**.** At node **A**, signals corresponding to disulfide **3** and aldehyde **6** are present in the expanded $^1$H NMR spectrum (Figure 2.5a). The aromatic doublets **a** and **b** appear slightly at slightly different chemical shifts compared with Figure 2.3a, this may be on account of slightly different pH or amounts of material. In the transition from node **A** to node **C** the successful condensation of aldehyde **6** and amine **7** is evidenced by the appearance of new signals corresponding to imine **8** (Figure 2.5c). The chemical shift of signals corresponding to the aromatic protons **a** and **b** changes slightly on account of a change in hydrogen bonding about the amide bond caused by the significant change in pH. These observations suggest imine **8** has been formed in the presence of aldehyde **6** and amine **7** in the absence of unwanted side reactivity. In the transition from node **C** to node **D** (Figure 2.5d), reduction of

disulfide **3** by DTT to form thiolate **4'** is reflected in the disappearance of the aromatic proton signals **a** and **b** and the emergence of two new signals **k** and **l** corresponding to the aromatic protons in **4'**. Importantly, signals corresponding to imine **8** (**h**, **i** and **j**) remain unchanged, aside from a small amount of aldehyde **6** formed as a result of hydrolysis of imine **8** on account of a slight reduction in pH, suggesting that reduction of disulfide

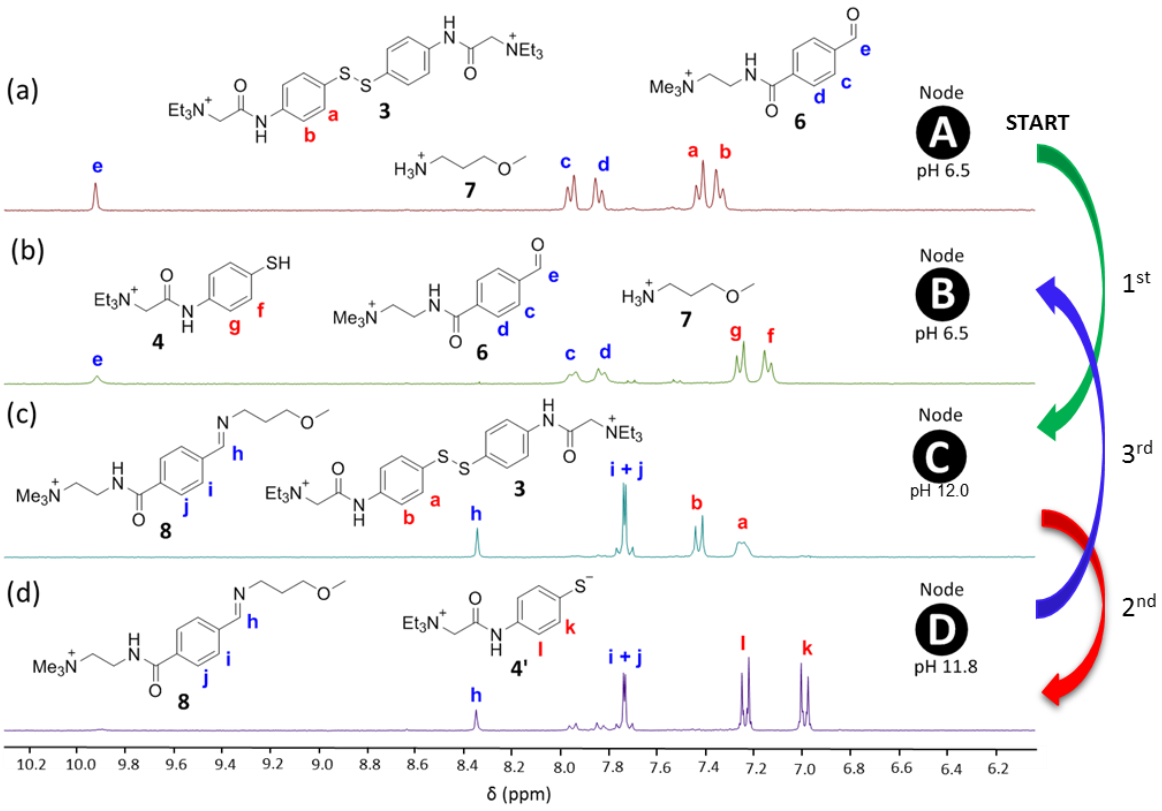


Figure 2.5 $^{1}$H NMR Spectroscopy (300 MHz, $D_2O$) analysis of '*4-node* network' traversed anticlockwise starting at node **A**.

**3** by DTT at pH 11.8 is successfully achieved in the presence of imine **8** with only a small amount of aldehyde hydrolysis on account of a reduction in pH. In the transition from node **D** to node **B** (Figure 2.5b), lowering the pH of the mixture from pH 11.8 to pH 6.5 resulted in the re-emergence of signals corresponding to protons in aldehyde **6** (**c**, **d** and **e**) and the disappearance of signals corresponding to imine **8** (**h**, **i** and **j**) suggesting hydrolysis of imine **8** to yield aldehyde **6** and amine **7**. Protonation of thiolate **4'** is evidenced by a new pair of aromatic doublets corresponding to the aromatic protons in thiol **4** (**f** and **g**). In this transition imine **8** is hydrolysed while, other than protonation, thiol **4** remains chemically unchanged. In the transition from node **B** to node **A** oxidative coupling of thiol **4** to form disulfide **3** by $H_2O_2$ at pH 6.5 is indicated by disappearance of the aromatic proton signals **g** and **f** in a new

spectrum (not shown) and re-emergence of signals **a** and **b** corresponding to disulfide **3**. During this oxidative transformation, signals corresponding to protons in aldehyde **6** (**c**, **d** and **e**) remain unchanged suggesting the absence of competing chemical processes. These spectra demonstrate orthogonal control over the breaking and forming of disulfide and imine dynamic covalent bonding motifs when traversing the '*4-node* network' in an anticlockwise fashion.

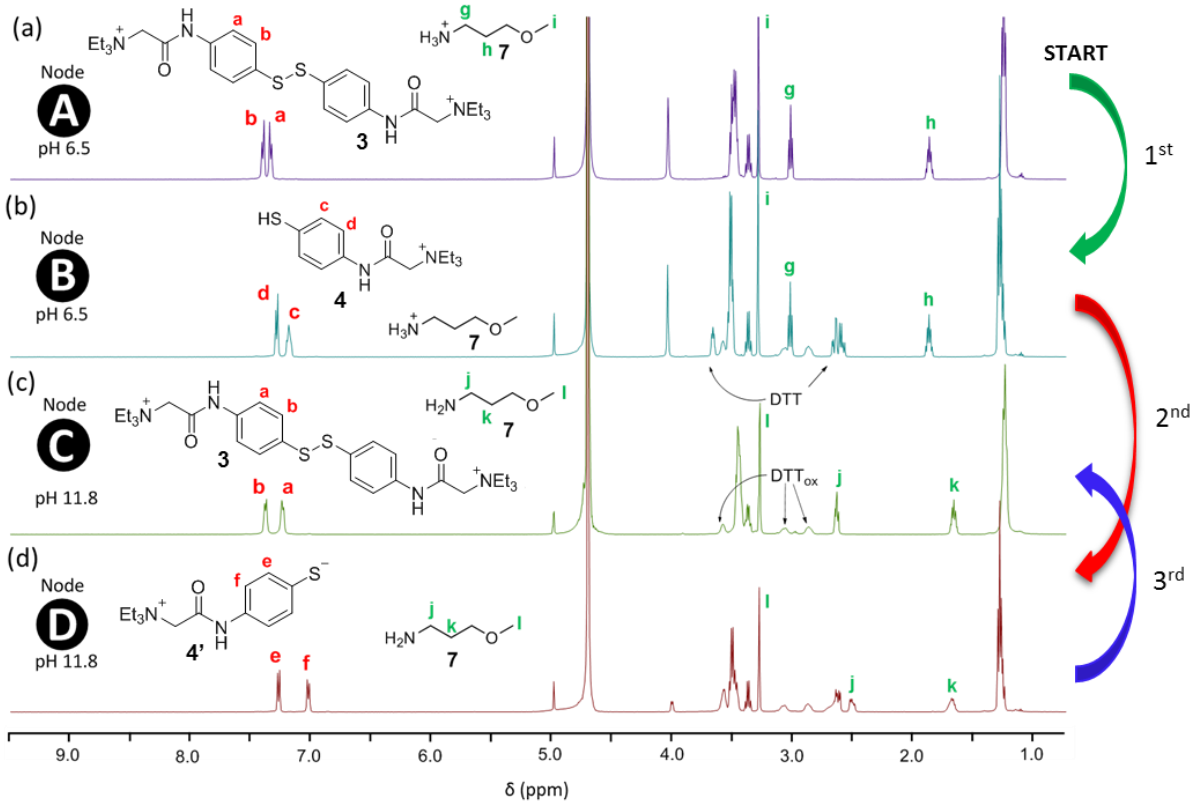


Figure 2.6 $^{1}$H NMR Spectroscopy (300 MHz, $D_2O$) analysis of '*4-node* network' traversed clockwise starting at node **A** in the absence of aldehyde **6**.

To investigate the potential for competing side reactivity between the disulfide/thiol component and amine **7**, a control experiment was performed in which one clockwise cycle of the '*4-node* network' was performed, starting at node **A**, in the absence of aldehyde **6**. $^{1}$H NMR Spectroscopy analysis was used (Figure 2.6) to investigate the system at each node. In the transition between node **A** and node **B**, disulfide **3** is quantitatively reduced to form thiol **4** with a small excess of DTT in presence of amine **7** at pH 6.5, with $^{1}$H NMR confirming the absence of unwanted competing processes (Figure 2.6b). Between node **B** and node **D** (Figure 2.6d), increasing the pH from 6.5 to 11.8 results in deprotonation of thiol **4** to form thiolate **4'**. Amine **7** is deprotonated as evidenced by a new set of signals (**j**, **k** and **l**), the changes in the chemical shift of the signals corresponding to protons in **7** upon ammonium deprotonation

are consistent with literature values. It is worth noting that there is a singlet at δ = 4.0 corresponding to the -C*H*$_2$- in disulfide **3** and thiol **4**, this likely undergoes exchange at high pH, at or above it's p$K_a$, with deuterium. This is why this singlet does not appear or appears to a with a smaller integral at higher pH (node **C** and node **D**). In the transition from node **D** to node **C** (Figure 2.6c) thiolate **4'** is oxidatively coupled with itself to form disulfide **3** in the presence of amine **7** whilst avoiding unwanted processes. In the transition between node **C** and node **A** the pH of the mixture was reduced from pH 11.8 to pH 6.5, amine **7** is protonated as indicated by the re-emergence of signals corresponding to **7** in its protonated form (**g**, **h** and **i**) in a new spectrum (not shown). These control experiments indicate that interconversion between disulfide **3** and thiol **4** or thiolate **4'** proceeds as expected in the absence of aldehyde **6** without competing side processes involving amine **7**.

To probe the possibility of side reactivity involving the thiol/disulfide component and aldehyde **6,** a second control experiment was undertaken in which $^1$H NMR spectroscopy was utilized (Figure 2.7) to follow a clockwise cycle of the '*4-node* network', starting at node **A**, in the absence of amine **7.** Signals **c**, **d** and **e**, which correspond to protons in aldehyde **6**, remain

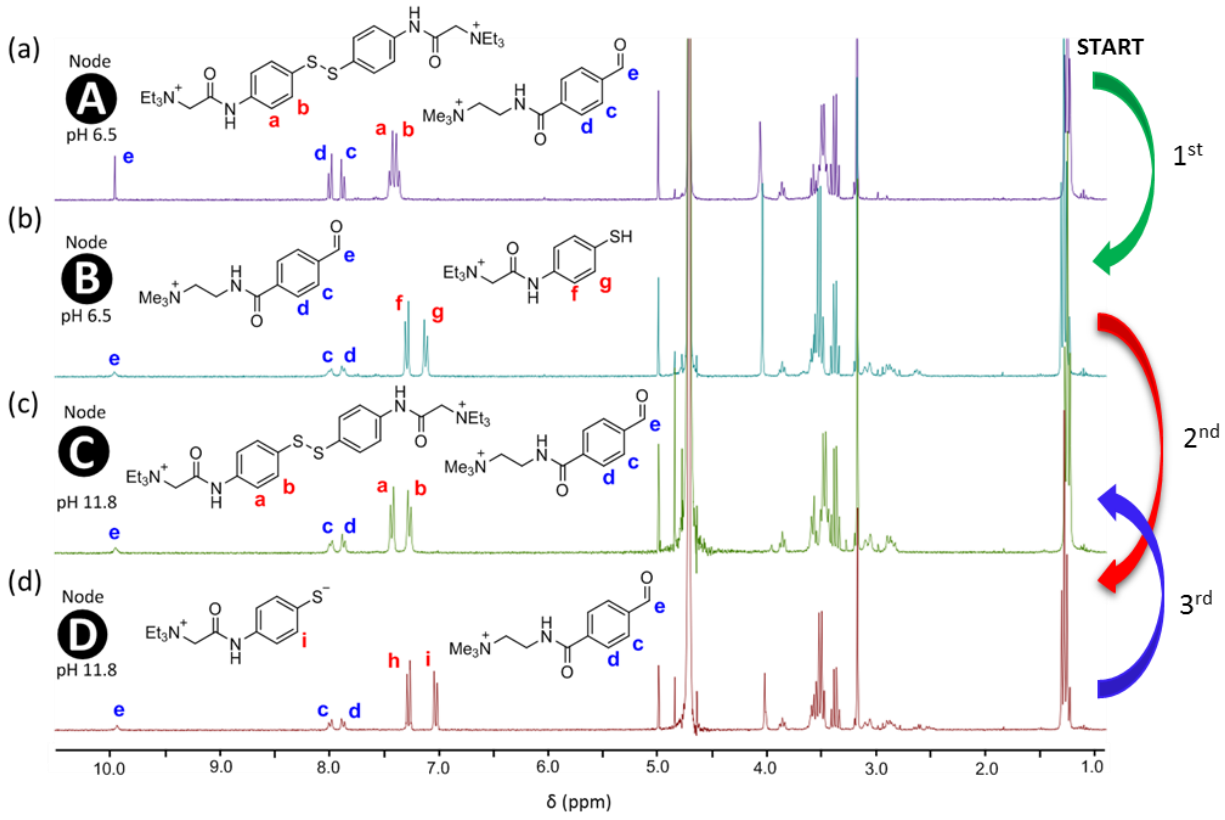


Figure 2.7 $^1$H NMR Spectroscopy (300 MHz, $D_2O$) analysis of '*4-node* network' traversed clockwise starting at node **A** in the absence of amine **7**.

unchanged throughout each node transition aside from line broadening whose origin is elaborated later in this chapter. Between nodes, the expected changes in signals corresponding to the thiol/disulfide component are observed. In the transition from node **A** to node **B** (Figure 2.7b), disulfide **3** is reduced quantitatively by DTT to form thiol **4** which proceeds in the absence of undesired side reactivity in the presence of aldehyde **3**. In the transition from node **B** to node **D** (Figure 2.7d), increasing the pH from 6.5 to 11.8 results in deprotonation of thiol **4** forming thiolate **4'**, there is no change in signals **c**, **d** and **e**, suggesting there are no competing processes involving aldehyde **6**. During the transition from node **D** to node **C** (Figure 2.7c)**,** successful oxidative coupling of thiolate **4'** with $H_2O_2$ proceeds without a change to signals **c**, **d** and **e**. Taken together these control experiments indicate that interconversion between disulfide **3**, thiol **4** and thiolate **4'** proceeds as expected without undesired side reactivity in the absence of amine **7**.

Taken together a set of conditions has been established which, when applied to a mixture of disulfide **3**, aldehyde **6** and amine **7**, allow orthogonal control over bond-breaking and bond-forming processes with respect to imine and disulfide DCBs.

### 2.3.3 *System limitations*

To investigate the origin of line broadening observed in some of the $^1$H NMR spectra presented in this chapter, $^1$H 2D EXSY NMR spectroscopy was performed on a 1:1 mixture of thiol **4** and disulfide **3** (Figure 2.8). The EXSY spectrum displays two sets of cross peaks ***(i)*** and ***(ii)*** indicating chemical exchange between aromatic protons **a** & **c** and **b** & **d**, respectively. This observation suggests thiol-disulfide interchange between disulfide **3** and thiol **4** occurs on the NMR timescale in $D_2O$ at pH 6.5. It is worth noting that there is no significant line broadening with respect to signals corresponding to imine **8**. Broadening of signals associated with aldehyde **6** suggest a second chemical exchange process occurring in parallel to thiol/disulphide interchange. To investigate this hypothesis, firstly, thiol **4** was afforded by reduction of disulfide **3** with triphenylphosphine and purified by extraction. $^1$H NMR spectroscopy performed (Figure 2.9) on an equimolar aqueous solution of aldehyde **6** and thiol **4** at pH 6.5 revealed significant line broadening was observed with respect to signals in

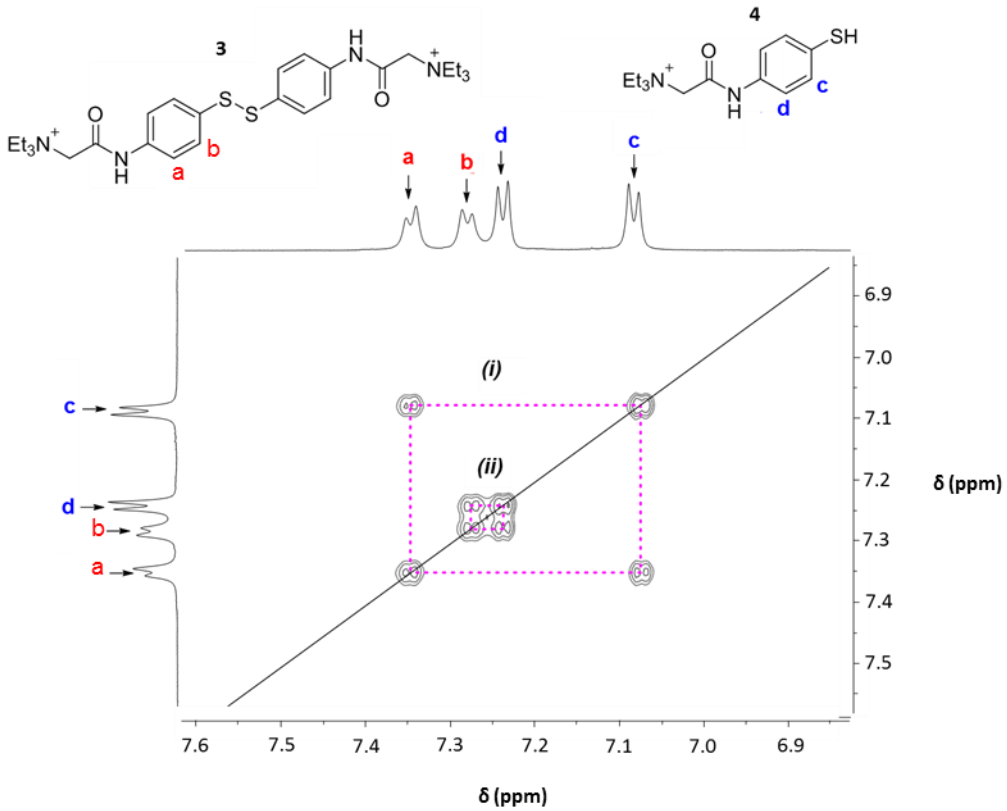


Figure 2.8 2D EXSY $^{1}$H NMR spectrum (700 MHz, $D_2O$, pH 6.5) at 100 ms mixing time of the expanded 'aromatic region' of a 1:1 mixture of disulfide **3** and thiol **4** (30 mM total concentration). A 1D spectrum of disulfide **3** and thiol **4** in $D_2O$ (pH 6.5) is shown on the vertical and horizontal projections.

the expanded spectrum corresponding to both aldehyde **6** (**c**, **d** and **e**) and thiol **4** (**a** and **b**). It was reasoned that this line broadening arises on account of chemical exchange involving reaction of aldehyde **6** and thiol **4** to form traces of hemithioacetal at pH 6.5, and this process is slow on the NMR timescale.

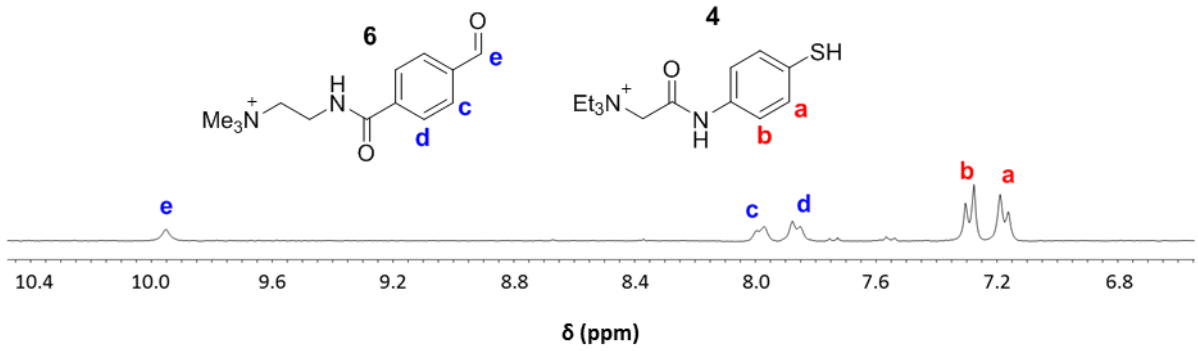


Figure 2.9 $^{1}$H NMR (300 MHz, $D_2O$) spectrum of a 1:1 mixture of thiol **4** and aldehyde **6** at pH 6.5.

Alternative reaction partners investigated by us failed to deliver orthogonality. When electron-rich aldehydes such as 4-hydroxybenzaldehyde were used, it was found that there is very little reaction with amine **7** to form imine at pH 12.0. The chosen electron-deficient aromatic aldehyde **6** appears to be both relatively resistant to hydrate formation and is capable of forming imines near-quantitatively at pH 12.0. A series of alkyl thiols were also investigated as substitutes for thiol **4**. At pH 6.5 in $D_2O$ these thiols engaged in nucleophilic attack at aldehyde **6**, with further $^1H$ NMR spectroscopic studies providing evidence for the

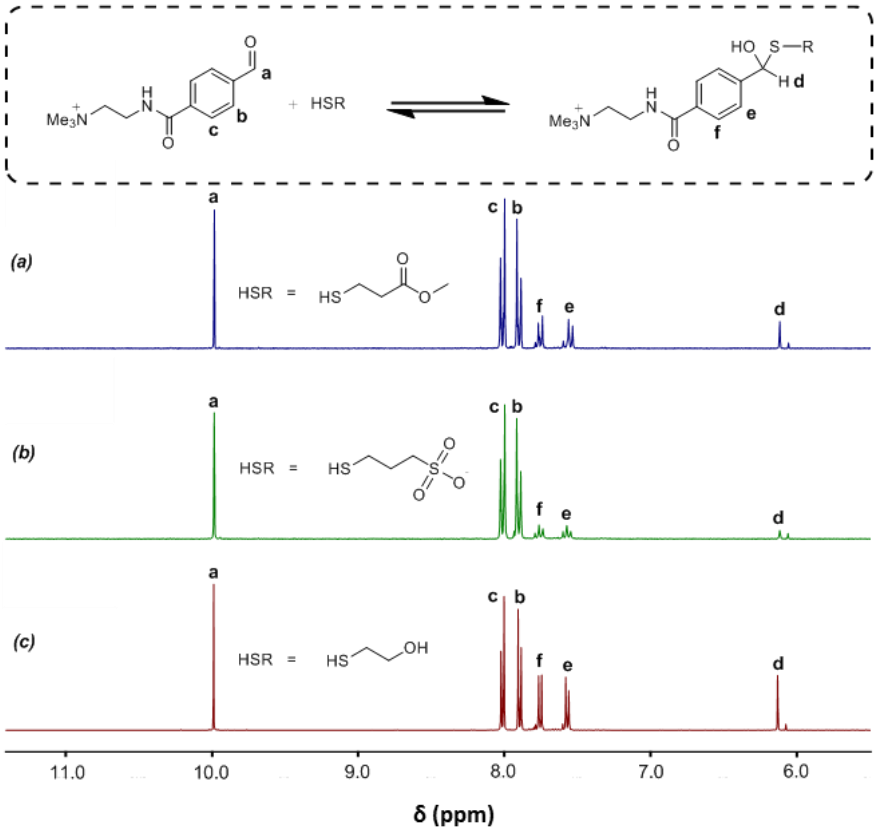


Figure 2.10 $^1H$ NMR spectra (300 MHz, $D_2O$) demonstrating formation of hemithioacetal at pH 6.5. Aldehyde **6** and RSH present in 15 mM concentration (30 mM total). RSH = (a) 2-mercaptoethyl acetate, (b) sodium 3-mercapto-1-propanesulfonate, (c) 2-mercaptoethanol. The low intensity signlet observed just upfield of the diagnostic hemithioacetal signal at δ = 6.2 ppm indicates the presence of expected hydrate formed by reaction of aldehyde with water.

formation of unwanted hemithioacetals (Figure 2.10). There is a small set of aromatic doublets (slightly obscured by the hemithioacetal aromatic doublets) and a low intensity singlet (δ = 6.1

ppm) which correspond to a small amount of hydrate in all cases (a – c). The chemical shift of the signals corresponding to this hydrate is consistent with all $^{1}$H NMR experiments performed using aldehyde **6**. The propensity to form hemithioacetals with electron-deficient aldehydes rules alkyl thiols out as potential thiol-disulfide system components. The chosen aromatic thiol **4** does not form hemithioacetal to a siginificant extent with aldehyde **6**, probably on account of aromatic thiols being poorer nucleophiles than alkyl thiols and thus less likely to form hemithioacetals. It is demonstrated that the molecular structure of aldehyde and thiol/disulfide system components must be carefully considered if this system is to be conducive to orthogonal bond-forming and bond-breaking processes of imine and disulfide dynamic covalent bonds in the absence of 'cross-talk'.

### 2.3 Conclusion

Novel water soluble species were prepared which exhibit the capacity to form imine and disulfide DCB's. The implementation of these model compounds in a '*4-node* network' allowed us to explore the orthogonal nature of the bond-forming and bond-breaking processes of imine and disulfide DCBs. By studying a range of structural variants of the chemical components incorporated in the system it is demonstrated that electron deficient aromatic aldehydes are essential for quantitative imine formation and that aromatic thiols are necessary to minimize the potential for the formation of hemithioacetal between thiol and eletron-deficient aldehydes. The work reported highlights the importance of carefully testing orthogonal systems through the application of well- considered models, and that careful choice of reaction partners is important to ensure the absence of any unwanted competing processes. Upon establishing a set of conditions under which bond-forming and bond-breaking processes of imine and disulfide DCBs we are now applying this knowledge to develop multi-stimuli responsive polymer materials which employ imine and disulfide chemistries as orthogonal dynamic covalent cross-linking methodologies. Thus, facilitating the controlled self-assembly of preformed functional polymer building blocks pertaining to the development of smart materials.

## 2.5 Experimental

All chemicals were purchased from Sigma-Aldrich or Alfa Aesar and were used without further purification. *N,N*-Dimethylacrylamide was purified by vacuum distillation at 60 $^{o}$C. Dimethylamine was purchased from Alfa Aesar as a 2.0 M solution in THF. AIBN was recrystallized in MeOH. $^{1}$H NMR, $^{19}$F NMR and $^{13}$C NMR spectroscopy analysis was performed using a Bruker Avance 300 spectrometer at 300, 282 and 75 MHz respectively. The residual solvent signal was used as an internal standard. FT-IR spectroscopy was performed on a Varian 800 FT-IR instrument (Varian inc.). High-resolution mass spectrometry was performed on a Waters LCT Premier mass spectrometer (Waters inc.). pH measurements were made using a Hanna HI 90103 instrument which was calibrated regularly using commercial buffer solutions (Sigma-Aldrich). Aliquots of 1 M or 0.1 M NaOH and HCl were used to increase and lower the pH respectively is all cross-linking reactions. Dynamic light scattering (DLS) was performed on a Malvern HPPS-ET 5002 operating at 25 $^{o}$C fitted with a 633 nm laser module measuring at a detection back scattering angle of 173$^{o}$. Malvern DTS 4.20 software was utilized to analyze and export the data. Gel permeation chromatography (GPC) was conducted on a on a Varian ProStar instrument (Varian Inc.) equipped with a Varian 325 UV-Vis dual wavelength detector with a 254 nm laser, a Dawn Heleos II multi-angle laser light scattering detector (Wyatt Technology Corp.), a Viscotek 3580 differential refractive index detector and two PL gel 5 µm Mixed D 300 × 7.5 mm columns with guard column (Polymer Laboratories Inc.) in series. Chromatogram analysis was performed on Galaxie software (Varian Inc.) and analyzed with the Cirrus software (Varian Inc.) and Astra software (Wyatt Technology Corp.). Near monodisperse poly(methyl methacrylate) standards (Agilent Technologies) were used for calibration. Rheological measurements were performed with a HR-2 Discovery Hybrid Rheometer (TA Instruments) with a standard steel parallel-plate geometry of 20 mm diameter with a 0.5 mm of gap. The strain and the frequency were set to 1% and 1 Hz, respectively.

2,2'-((Disulfanediylbis(4,1-phenylene))bis(azanediyl))bis(N,N,N-triethyl-2-oxoethan-1-aminium) ***(3)***

4-Aminophenyl disulfide (500 mg, 2.01 mmol) was dissolved in $CH_2Cl_2$ (25 mL). Chloroacetyl chloride (450 mg, 3.62 mmol) was added dropwise over 30 min at 0 $^{o}$C. The mixture was allowed to stir at 30 $^{o}$C overnight, and the resulting white precipitate was filtered and the filtrate was evaporated to dryness. The crude solid obtained was dissolved in MeOH (25 mL)

and $Et_3N$ (784.9 mg, 10.5 mmol) was added followed by stirring at 60 $^oC$ for 72 h. The resulting dark brown precipitate was removed by filtration, then $NH_4PF_6$ was added to the filtrate in portions until the solution was saturated. This mixture was stirred at 60 $^oC$ for 16 h, concentrated, and then precipitated into cold water (250 mL). The precipitate was collected by filtration, washed with cold water and dissolved in MeOH. Amberlite® IRA-410 chloride form ion exchange resin beads (2 g) were added and the mixture was stirred at 40 $^oC$ for 18 h. The beads were then filtered and the filtrate evaporated to dryness. The resulting brown solid was dissolved in water (20 mL) and washed with $CH_2Cl_2$ (2 x 50 mL) to remove hydrophobic impurities. Removal of water under reduced pressure yielded disulfide **3** (385 mg, 0.73 mmol, 36 % yield). $^1H$ NMR (300 MHz, $D_2O$): δ = 1.22 (18H, t, J = 7.0 Hz), 3.47 (12H, q, J = 7.0 Hz), 4.01 (4H, s), 7.31 (4H, d, J = 8.5 Hz), 7.41 (4H, d, 8.5 Hz). $^{13}C$ NMR (75 MHz, $D_2O$): δ = 7.0, 54.5, 56.3, 121.7, 129.1, 133.0, 135.9, 162.3. FT-IR (wavenumber, $cm^{-1}$): 3226 (N–H), 3156 (C–H, aromatic), 2971 (C–H, alkyl), 1685 (C=O), 1490 (C=C, aromatic), 1406 (C=C, aromatic). $HRMS^+$ $C_{28}H_{44}N_4O_2S_2$: Theoretical: 266.1531. Actual: 266.1516.

*N-(2-Aminoethyl)-4-(dimethoxymethyl)benzamide (**5**)*

4-Carboxybenzaldehyde (18.3 g, 0.121 mol) was dissolved in MeOH (120 mL) and acidified with concentrated $H_2SO_4$ (10 drops). Methyl orthoformate (37.7 mL, 0.344 mol) was added in one portion and the mixture was refluxed for 48 h with stirring. After this time, the mixture was transferred to a separating funnel with saturated $NaCHO_3$ (100 mL). The aqueous layer was extracted with $CH_2Cl_2$ (3 x 150 ml) and the organic extracts were combined and dried over $MgSO_4$, filtered and evaporated to dryness to afford a yellow oil (22.41 g, 0.11 mol, 88.1 %) which was used without further purification. $^1H$ NMR ($CDCl_3$, 400 MHz): δ 3.30 (s, 6H), 3.90 (s, 3H), 5.42 (s, 1H), 7.52 (d, 2H, J = 8 Hz), 8.03 (d, 2H, J = 8 Hz). $^{13}C$ NMR ($CDCl_3$, 100 MHz) δ 52.1, 52.6, 102.3, 126.8, 129.6, 130.2, 143.0, 166.4. Methyl-4-(dimethoxymethyl)-benzoate (2.5g, 12.0 mmol) was refluxed in ethylenediamine (35 mL) for 18h. Ethylenediamine was removed under pressure to afford a deep brown solid which was purified by column chromatography ($SiO_2$, $CH_2Cl_2$:EtOH:$Et_3N$, 80:15:5 v/v) to furnish intermediate a as a pale white solid (1.3 g, 5.5 mmol, 46 % yield). $^1H$ NMR ($CDCl_3$, 300 MHz): δ 1.75 (s, 2H), 2.89 (t, 2H, J = 5.5 Hz), 3.25 (s, 6H), 3.45 (q, 2H, J = 5.5 Hz), 5.36 (s, 1H), 6.77 (br t, 1H), 7.45 (d, 2H, J = 8.0 Hz), 7.74 (d, 2H, J = 8.0 Hz). FT-IR (wavenumber, cm-1): 3281 (N–H), 2947 (C–H, alkyl), 1634 (C=O), 1593(C=O), 1448 (C=C, aromatic), 1421 (C=C, aromatic).

*2-(4-Formylbenzamido)-N,N,N-trimethylethan-1-aminium (**6**):*

*N*-(2-Aminoethyl)-4- (dimethoxymethyl)benzamide (a) (370 mg, 1.6 mmol) was dissolved in MeOH (8 mL). $K_2CO_3$ (431 mg, 3.12 mmol) was added followed by addition of iodomethane (5.0 g, 35 mmol) in one portion, and this mixture was stirred at 8 h at 55 $^oC$. Residual MeI was removed under reduced pressure and $Et_2O$ (30 mL) was added and the suspension was agitated in a sonic bath for 30 min and filtered to afford a pale brown solid. This solid was dissolved in 1:1 acetone:water (20 mL) and acidified with 5 drops of concentrated HCl. After stirring at room temperature for 2 h the mixture was filtered and the filtrate evaporated to dryness. The resulting brown solid was purified by column chromatography ($SiO_2$, $CH_3CN$:$H_2O$, 8:2 v/v) to afford a pale brown solid (215 mg, 0.91 mmol, 69%) $^1H$ NMR ($CDCl_3$, 300 MHz): δ 3.14 (s, 9H), 3.53 (t, 2H, J = 6.5 Hz), 3.82 (t, 2H, J = 6.5 Hz), 7.82 (d, 2H, J = 8.0 Hz), 7.95 (d, 2H, J = 8.5 Hz), 9.92 (s, 1H). $^{13}C$ NMR ($CDCl_3$, 75MHz) δ 34.3, 53.6, 64.1, 128.0, 130.3, 138.1, 138.4, 169.8, 195.7. FT-IR (wavenumber, $cm^{-1}$): 3391 (N–H), 3001 (C–H, alkyl), 2866 (C-H, CHO), 1659(C=O), 1593(C=O), 1490 (C=C, aromatic), 1455 (C=C, aromatic). $HRMS^+$ $C_{13}H_{19}N_2O_2$: Theoretical: 235.1446. Actual: 235.1506.

*Transition between '4-nodes' (clockwise cycle):*

Node **A** to Node **B**, reduction of disulfide **3**: Aldehyde **6** (7.4 mg, 0.03 mmol), 3-methoxypropylamine (3.0 µL, 0.03 mmol) and disulfide **3** (15.6 mg, 0.03 mmol) were dissolved in $D_2O$ (2 mL) at room temperature. The pH of the mixture was adjusted to pH 6.5 with aliquots of 1 M $D_3PO_4$ (5 µL, in $D_2O$). DL-dithiothreitol (DTT) (4.5 mg, 0.03 mmol) was added in one portion and stirred for 20 min. After this time, the pH of the mixture was re-adjusted to pH 6.5 and the mixture was analysed by $^1H$ NMR spectroscopy. Node **B** to Node **D**, formation of imine **8**: The mixture was raised from pH 6.5 to pH 11.8 with 5 µL aliquots of 1 M NaOH (in $D_2O$). The mixture was analysed by $^1H$ NMR spectroscopy. Node **D** to Node **C**, oxidation of thiol **4** to disulfide **3**: aliquots of $H_2O_2$ (2.5 µL, 0.25 M, in $D_2O$) were added 5 min intervals with stirring and the reaction was monitored by $^1H$ NMR spectroscopy until full oxidation had occurred. The pH was retained between pH 11.6 and pH 11.8 during the oxidation. Node **C** to Node **A**, hydrolysis of imine **8**: The pH of the mixture was decreased from pH 11.8 to pH 6.5 with aliquots of 1 M $D_3PO_4$ (5 µL, in $D_2O$). The mixture was analysed by $^1H$ NMR spectroscopy.

*Transition between '4-nodes' (anticlockwise cycle):*

Node **A** to Node **C**, formation of imine **8**: Aldehyde **6** (7.4 mg, 0.03 mmol), 3-methoxypropylamine (3.0 µL, 0.03 mmol) and disulfide **3** (15.6 mg, 0.03 mmol) were dissolved

in $D_2O$ (2 mL) at room temperature. The mixture was raised from pH 6.5 to pH 11.8 gradually with 5 µL aliquots of 1 M NaOH (in $D_2O$). The mixture was analysed by $^1H$ NMR spectroscopy. Node **C** to Node **D**, reduction of disulfide **3**: DL-dithiothreitol (DTT) (4.5 mg, 0.03 mmol) was added in one portion and stirred for 20 min. After this time, the pH of the mixture was re-adjusted to pH 6.5 with aliquots of 1 M $D_3PO_4$ (5 µL, in D2O) and the mixture was analysed by $^1H$ NMR spectroscopy. Node **D** to Node **B**, hydrolysis of imine **8**: The pH of the mixture was decreased from pH 11.8 to pH 6.5 with aliquots of 1 M $D_3PO_4$ (5 µL, in $D_2O$). The mixture was analysed by $^1H$ NMR spectroscopy. Node **B** to Node **A**, oxidation of thiol **4** to disulfide **3**: aliquots of $H_2O_2$ (2.5 µL, 0.25 M, in $D_2O$) were added at 5 min intervals with stirring and the reaction was monitored by $^1H$ NMR spectroscopy until full oxidation had occurred. The pH was retained between pH 11.6 and pH 11.8 during the oxidation.

# Chapter 3

## *Dynamic Covalent Imine and Disulfide Cross-linked Nanoparticles*

## Table of Contents

## 3.1 Abstract

*Reversible addition-fragmentation polymerization (RAFT) coupled with a post-polymerization modification strategy was utilized to prepare aldehyde-, amine- and thiol- functional random copolymers. Conditions were established under which these pre-formed functional polymer building blocks were shown to undergo stimuli-responsive intermolecular cross-linking in aqueous media yielding redox-sensitive disulfide or pH-imine cross-linked nanoparticles. Imine and disulfide cross-linked nanoparticles were demonstrated to disassemble through controlled modulation of pH and redox-conditions, respectively. The formation of pH-sensitive imine cross-linked nanoparticles was shown to be far more experimentally straightforward than the formation of redox-sensitive disulfide nanoparticles. The product distributions, morphology and size of disulfide cross-linked nanoparticles exhibited a strong dependence on polymer concentration and the rate of hydrogen peroxide addition, highlighting the need for judicious experimental design in the formation of these nanoparticles from the preformed copolymeric pendant-thiol bulding blocks. An initial investigation into the orthogonal utility of imine and disulfide dynamic covalent bonds was then undertaken, wherein, aldehyde and thiol or amine and thiol dual-functional random terpolymers were first prepared and subjected to a range of initial conditions in the interest of encouraging the orthogonal formation and disassembly of imine and disulfide cross-linked nanoparticles. The orthogonality studies revealed that largely uncontrolled and irreversible aggregation phenomena, governed by undesirable intermolecular interactions, proved particularly troublesome in determining conditions for exploiting true orthogonality of imine and disulfide dynamic covalent bonds.*

## 3.2 Introduction

Stimuli-responsive polymeric nanoparticles have been well studied and represent an important class of nanostructured material[80] which have recently been applied in intracellular drug delivery,[81] tissue engineering[82] and multifunctional therapeutics within medical devices.[83] Various strategies have been employed in the construction of stimuli-responsive polymeric nanoparticles including controlled precipitation,[84] chemical cross-linking during polymerization reactions,[85] controlled aggregation and chemical cross-linking of pre-formed macromolecular building blocks[86] to name but a few. Considering the advancing capacity of researchers to construct structurally well-defined, highly functional polymers, a post-polymerization dynamic covalent cross-linking strategy became of particular interest within our group as an approach towards the formation of polymer nanoparticles.

With the aim of developing a polymeric nanoparticle system exhibiting *orthogonal* dual stimuli-responsiveness, the utility of orthogonal dynamic covalent bonds in the formation of intermolecular cross-links between preformed polymeric building blocks was an extremely attractive route. Furthermore, a survey of the current literature revealed an extensive gamut of dynamic covalent chemistries[7a, 18b] had already shown promise in the successful preparation of stimuli-responsive nanoparticles.[12a]

Using the work presented in the model system studied in chapter 2 as a starting point, imines and disulfides were selected as orthogonal dynamic covalent bonding motifs with which to cross-link preformed polymer building blocks into stimuli-responsive nanoparticles. Many systems which utilize dynamic imine[22, 78a, 87] or disulfide[79, 88] bonds in the preparation of polymer cross-linked nanoparticles have been reported. However, endeavours to exploit the orthogonality of these dynamic covalent cross-linking motifs in supramolecular systems are far less common. Additionally, the vast majority of studies on supramolecular systems which exhibit orthogonal dynamic covalent chemistries focus mainly on two or more *orthogonal exchange behaviours*. This work, on the other hand represents progress towards orthogonal *formation* and *disassembly* of two or more contrasting types of dynamic covalent polymeric nanoparticle (Figure 3.1) from the same mixture of functional polymeric precursors, which, to the best of our knowledge, has not yet been reported.

The strategy described herein employs reversible addition-fragmentation chain transfer (RAFT) polymerization to prepare pendant-functional random copolymers capable of forming dynamic covalent imine and disulfide bonds as chemical cross-links in response to changes in pH and redox conditions, respectively. Conditions are established for the formation and cleavage of imine and disulfide cross-linked nanoparticles, and the utility of imine and disulfide bonds

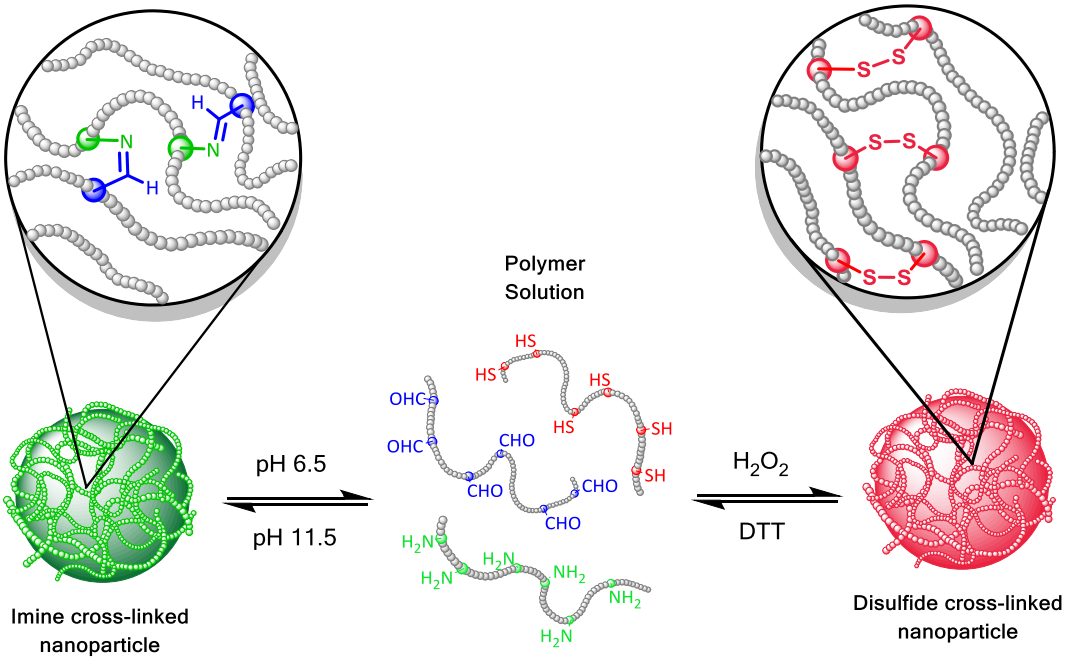


Figure 3.1 Reversible formation of imine and disulfide cross-linked nanoparticles formed by stimuli-responsive formation of intermolecular imine and disulfide bonds.

in the nanoparticle formation processes is compared. Particular attention is paid to the conditions necessary to form disulfide cross-linked nanoparticles wherein the intermolecular disulfide bonds consist of two oxidatively coupled *aromatic* thiols. Whilst many disulfide cross-linked nanoparticles systems which operate in water have been reported,[79, 89] very few systems which exhibit aromatic disulfides are known. Aromatic thiols exhibit vastly different reactivities, pKa's and nucleophilcities to aliphatic thiols and have shown promise in the development of self-healing gel materials with unprecedented properties.[90] Expanding the utility of aromatic disulfides in dynamic polymer systems will broaden the range and versatility of dynamic covalent disulfide-based materials available to researchers in the fields of nanochemistry and functional materials.

## 3.3 Results and Discussion

### 3.3.1 *Synthesis of monomers and preparation of pendant imine polymers by RAFT polymerization*

The imine bond has been well-utilized as a dynamic covalent bond (DCB) to link together polymer precursors into nanoscale architectures.[22] The incorporation of the reaction partners required to form imine bonds—primary amines and aryl aldehydes—as pendant functional groups upon preformed linear polymers provides the appropriate functional groups to cross-link polymeric building block precursors by the formation of intermolecular imines bonds.[91] The equilibrium position of the reaction of an aromatic aldehyde and amine lies to the side of the resulting imine at higher pH (> pH 7), whereas its constituent amine and aldehyde reaction partners are favoured at lower pH (< pH 7).[41] The pH-sensitive nature of this DCB can be exploited to endow a chemical system with stimuli-

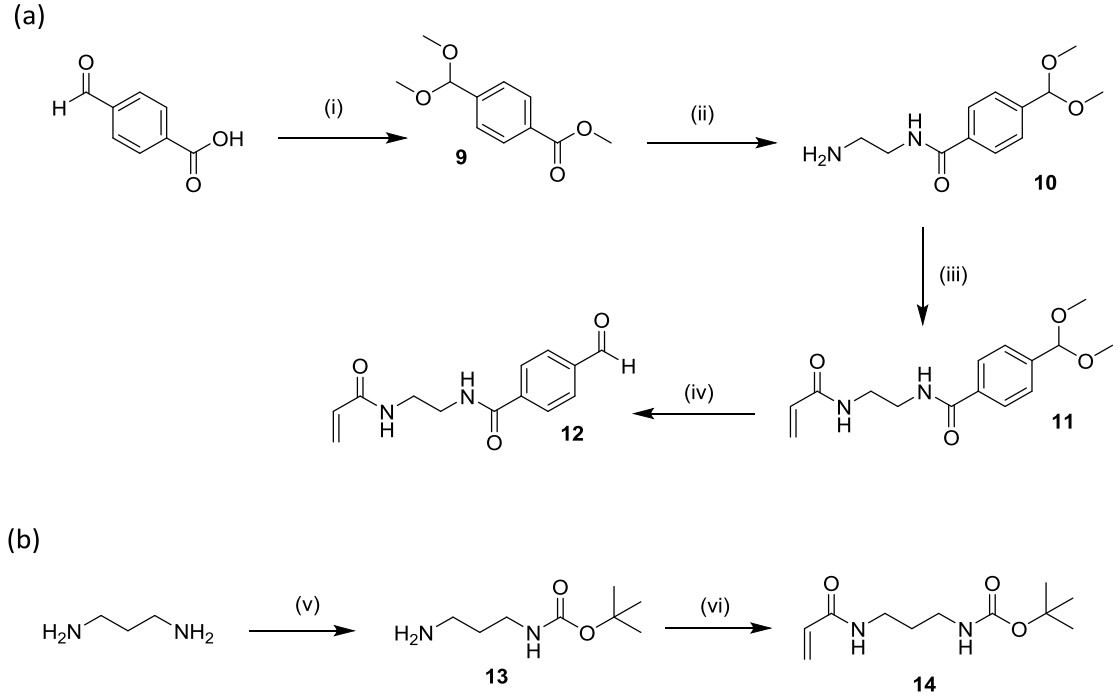


Scheme 3.1 Synthesis of (a) aldehyde and (b) amine-functional monomers **12** and **14**. (i) $CH(OCH_3)_3$, MeOH, $H_2SO_4$, 80 °C, 24 h, 92 %. (ii) 1,2-Diaminoethane, 130 °C, 48 h, 61 %. (iii) Acryloyl chloride, $Et_3N$, $CH_2Cl_2$, 0 °C, 10 h, 46 %. (iv) 1 M HCl (aq), 2 h, 71 %. (b) (v) $Boc_2O$, $CHCl_3$, 0 $^oC$, 18 h, 73 %. (vi) Acryloyl chloride $Et_3N$, $CH_2Cl_2$, 18 h, 79 %.

responsiveness where the stimulus is adjustment of pH and the response is the breaking or forming of intermolecular imine bonds. The imine functional moieties chosen here have been studied and previously reported by the Fulton group.[12a, 78a, 91] Monomers displaying amine or aldehyde functionalities were required for subsequent polymerization to afford polymers presenting these functionalities as pendant groups. Thus, monomer **9** was prepared (Scheme 3.1, a) by refluxing 4-carboxybenzaldehyde with trimethylorthoformate to afford methyl 4-(dimethoxymethyl)benzoate (**9**), which was then refluxed in ethylenediamine to afford amine **10**. Subsequent acylation of **10** with acryloyl chloride at the primary amine afforded acrylamide **11**, whose dimethyl acetal group was hydrolysed in 1 M HCl to afford the aldehyde-containing acrylamide monomer **12**. Monomer **14** was prepared (Scheme 3.1b) by *mono-N-Boc*-protection of 1,3-diaminopropane to afford **13** which was then subsequently acylated with acryloyl chloride to afford *mono-N-Boc* protected acrylamide monomer **14**.

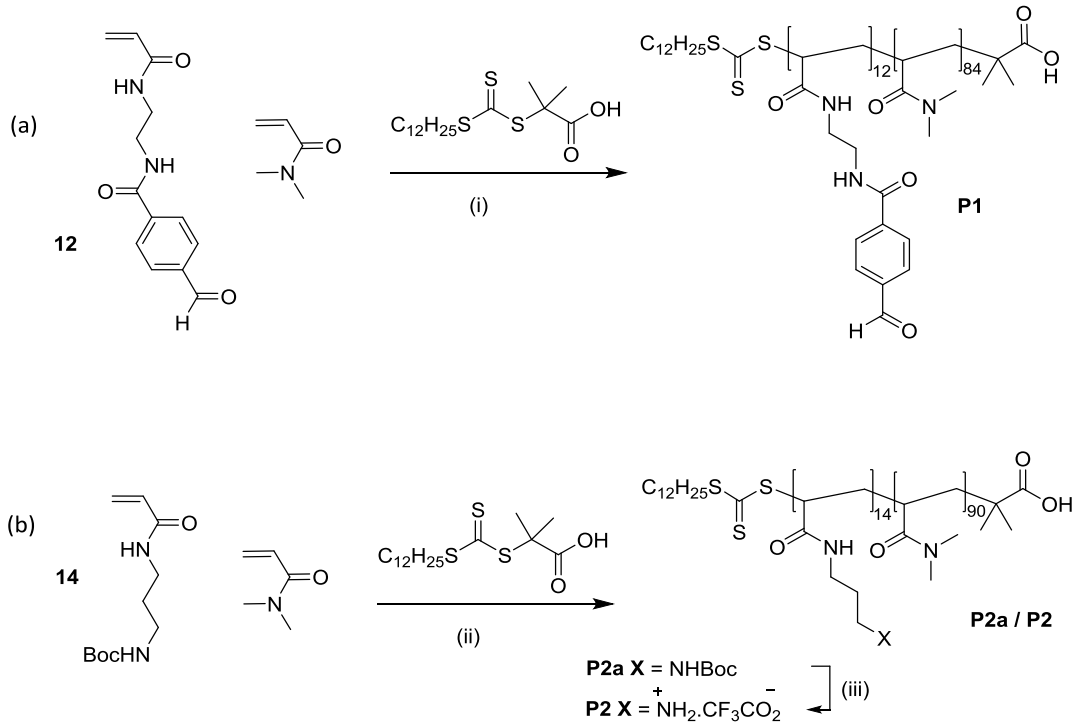


Scheme 3.2 Preparation of copolymers (a) **P1** and (b) **P2** by RAFT polymerization. (i) AIBN, DMF, 70 $^{o}$C, 18 h. (ii) AIBN, DMF, 70 $^{o}$C, 18 h. (iii) $CF_3CO_2H$, $CH_2Cl_2$.

Monomer **12** was copolymerized with dimethyl acrylamide (DMAc) utilizing the RAFT chain transfer agent 2-(dodecylthiocarbonothioylthio)-2-methylpropionic acid (DDMAT) to furnish

polymer **P1** (Scheme 3.2a). The molar feed ratio of monomer **12** to DMA was 1:8 and polymerization was performed at 70 °C in DMF in the presence of the thermal radical initiator AIBN. Copolymer **P1** was collected by precipitation in $Et_2O$ and analysed by $^1H$ NMR spectroscopy (Figure 3.2a) and gel permeation chromatography (GPC) (Figure 3.3c).

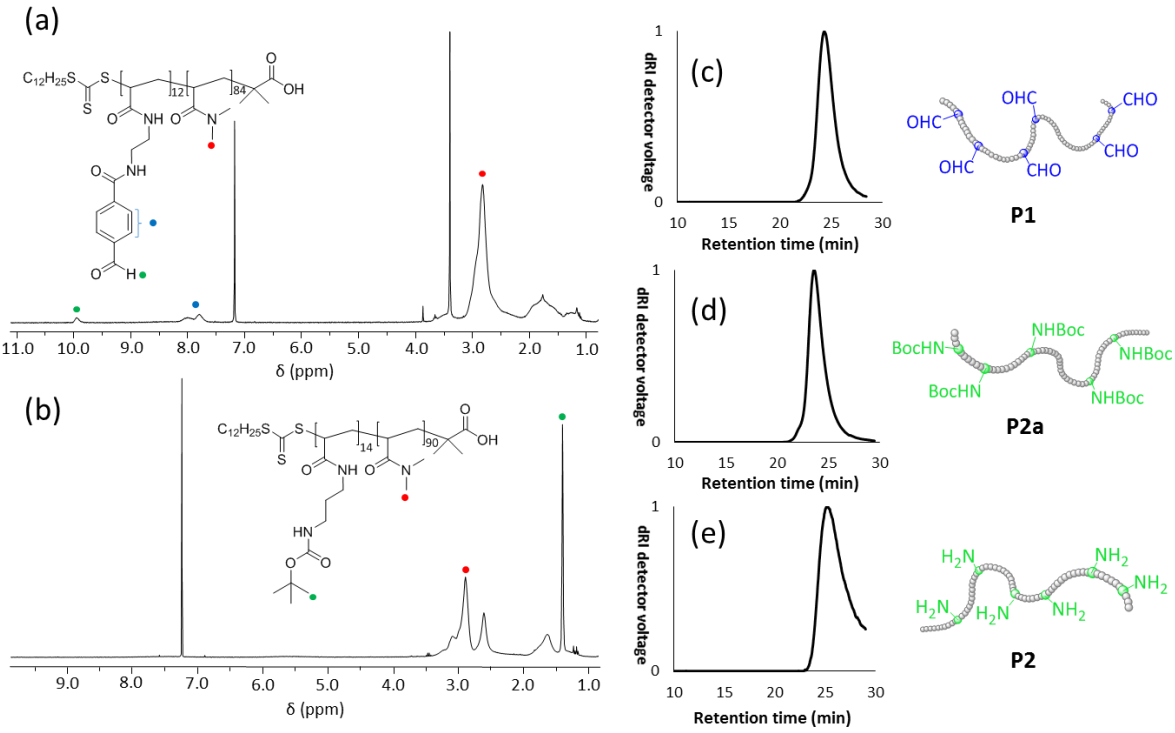


Figure 3.2 $^1H$ NMR spectra (300 MHz, $CDCl_3$) of (a) **P1** and (b) **P2a**. Differential refractive index (dRI) GPC traces of (c) **P1,** (d) **P2a** and (e) **P2** in DMF (0.6 mL/min, DMF with 1 g/L LiBr).

The $^1H$ NMR spectra of **P1** (Figure 3.2a) revealed well-defined signals with characteristic line broadening associated with polymeric species and which are consistent with the desired copolymer structures. The two signals with chemical shifts of δ = 9.9 ppm and δ = 7.7-8.6 ppm, corresponding to the aldehyde and aromatic protons of monomer **12**, respectively and the large singlet with a chemical shift of δ = 2.8 ppm corresponds to the *N*-methyl protons in DMA confirming the successful copolymerization of vinyl monomers **12** and DMA under the described RAFT conditions. This observation indicates the successful copolymerization of monomer **12** with dimethyl acrylamide. The degree of polymerization was calculated by end-group analysis, as described in the experimental section, and the ratio of monomers in the final polymer composition was calculated by comparing the integrals of signals corresponding

to the aromatic proton and aldehyde proton signals with those of the methyl units in DMA. GPC analysis of **P1** (Figure 3.2c) displayed a narrow molecular weight distribution (PDI = 1.21) suggesting successful mediation of the RAFT polymerization process by the CTA. Monomer **14** was copolymerized with DMA (Scheme 3.2b) under identical conditions to afford **P2a** which was then collected by precipitation in $Et_2O$ from THF. $^1$H NMR spectroscopic analysis (Figure 3.2b) revealed the expected line-broadened signals with diagnostic peaks at chemical shift values of δ = 1.4 and δ = 2.8 corresponding to the *N-Boc* methyl protons of **14** and the *N*-methyl protons of DMA, thus, indicating the successful copolymerization of **14** and DMA to afford **P2a**. The degree of polymerization was again calculated by end-group analysis, as described in the experimental section, and the ratio of monomers in the final polymer composition was calculated by comparing the integrals of signals corresponding to the *boc*-group protons signals with those of the methyl units in DMA. GPC analysis of **P2a** (Figure 3.2d) displayed a narrow molecular weight distribution (PDI = 1.26) suggesting good control of polymerization kinetics by the CTA. Copolymer **P2a** was successfully deprotected using a mixture of TFA/$CH_2Cl_2$ (1:1, v/v) to afford the desired amine groups as evidenced by the disappearance of the *t*-butyl signal associated with the *N-Boc* protecting group in the $^1$H NMR spectrum, resulting in **P2** which exhibited the pendant primary amines necessary for the formation of imine bonds. GPC analysis of **P2** (Figure 3.3e) revealed the PDI was considerably higher than that found for **P2a** and there is evidence of broadening/tailing in the GPC trace (Figure 3.2c). However, it can be inferred that the population distribution is unlikely to have changed during the transformation of **P2a** to **P2** and the broadening has likely arisen from interactions between the polymers and the GPC columns on account of enhanced polarity of **P2** compared with **P2a**.

| polymer | $M_n$[a] (g mol$^{-1}$) | $M_n$[b] (g mol$^{-1}$) | $M_w$[b] (g mol$^{-1}$) | PDI[b] ($M_w/M_n$) |
|---|---|---|---|---|
| **P1** | 12,500 | 14,000 | 16,500 | 1.21 |
| **P2a** | 16,000 | 18,000 | 21,500 | 1.26 |
| **P2** | 9,000 | 9,500 | 12,000 | 1.35 |

Table 3.1 Characterization of *(a)* **P1**, *(b)* **P2a** and *(c)* **P2**. [a] As determined by $^1$H NMR (300 MHz, $CDCl_3$) spectroscopy analysis. [b] As determined by GPC in in DMF (0.6 mL/min with 1 g/L LiBr) calibrated against methyl methacrylate standards of very low polydispersity (PDI > 1.08).

Taken together, the spectral and chromatographic characterization data (Table 3.1) presented indicate successful preparation of functional polyaldehyde **P1** and polyamine **P2** by RAFT polymerization of acrylamido comonomers **12** and **14** with dimethylamine.

### 3.3.2 *Synthesis of pendant thiol polymers by aminolysis of poly(pentafluorophenyl acrylate)*

To prepare a suitable pendant thiol-containing polymer building block a postpolymerization modification strategy was followed whereby pendant thiol functionality was grafted under mild conditions onto a preformed reactive polymer scaffold. Poly(pentfluorophenyl acrylate) p(PFPA) has been shown[92] to exhibit near-quantitative reactivity towards primary and secondary amines under a wide range of conditions resulting in well-defined acrylamido copolymers. The facile nature of the aminolysis of p(PFPA) ensures that the feed ratio is mirrored very closely by the final polymer composition providing a high degree of control in the synthesis of functional polymer building blocks.[93]

To prepare the activated ester precursor, pentafluorophenyl acrylate **15** was synthesised by reacting pentafluorophenol with acryloyl chloride (Scheme 3.3).[93] After monomer purification by column chromatography, its RAFT polymerization in 1,4-dioxane mediated by the RAFT chain transfer agent DDMAT in the presence of AIBN yielded

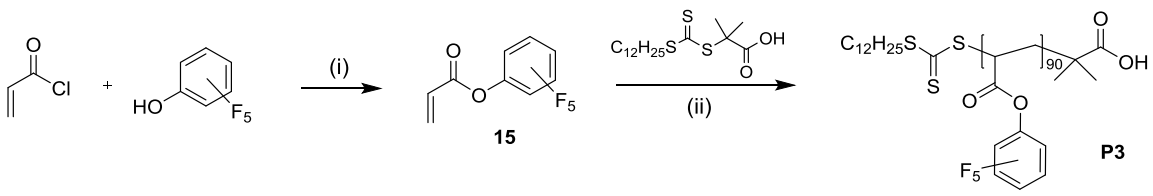


Scheme 3.3 Synthesis of p(PFPA) (i) $Et_3N$, $CH_2Cl_2$, 0 °C, 16 h, 40 %. (ii) AIBN, 1,4-dioxane, 80 °C, 3 h.

poly(pentafluorophenyl acrylate) **P3**. Characterization of **P3** by GPC showed a narrow population distribution (PDI 1.30) and $^1$H NMR spectroscopic analysis displayed all expected

line-broadened signals confirming successful homopolymerization of pentafluorophenyl acrylate. $^1$H NMR Spectroscopic end group analysis also revealed the degree of polymerization and $M_n$ of **P3** to be 90 and 22 kDa, respectively.

Successful preparation of the activated ester backbone **P3** led onto the challenge of designing and synthesizing a thiol-containing compound capable of being grafted onto the preformed p(PFPA) backbone by aminolysis (Scheme 3.4). Compound **19** contains the amine functionality necessary for grafting onto the polymer scaffold and also bears the desired thiol functionality protected as an asymmetrical disulfide. The *t*-butyl protons in compound **19** provided a good handle in establishing polymer composition by $^1$H NMR spectroscopy integral analysis of the resulting polymers formed during aminolysis. 4-Aminophenyl disulfide was reacted with *N-Boc*-β-alanine in the presence of EDC to afford *bis-N-Boc*-terminated disulfide **16** which was cleaved through a thiol-disulfide interchange process in the presence of 10 equivalents of sodium 3-mercapto-1-propanesulfonate to form thiol **17**. Formation of the unsymmetrical disulfide **18** was achieved by coupling with 2-methyl-2-propanethiol using 2,3-dichloro-5,6-dicyano-*p*-benzoquinone (DDQ) as an oxidizing agent. Surprisingly, **18** was formed in a good yield of 65 % despite the potential for competing oxidation products, in particular, the potential symmetrical disulfides formed by the oxidative coupling of each thiol with itself. Finally, **18** was *N-Boc* deprotected by TFA to afford **19**. All steps of the synthesis were high yielding and the synthesis was performed on a multigram scale.

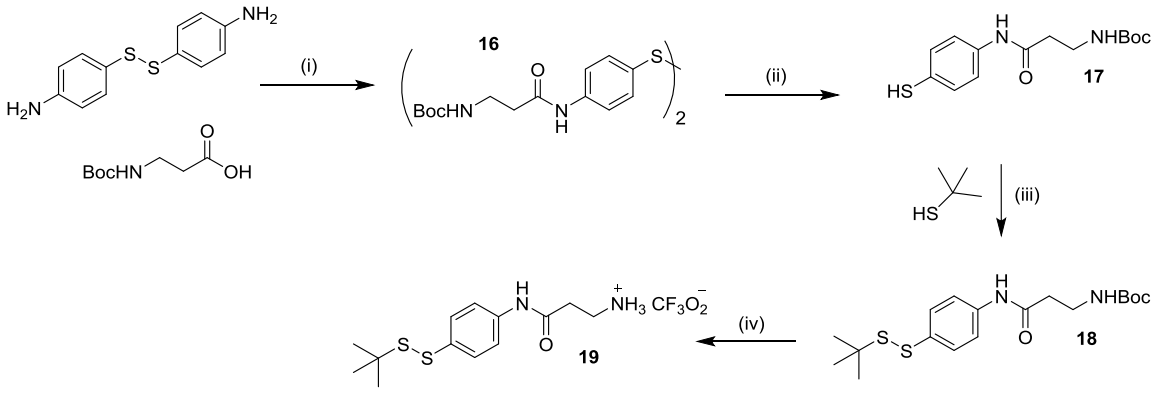


Scheme 3.4 Synthesis of monomer **19**. (i) EDC, $CH_2Cl_2$, 25 °C, 48 h, 86 %. (ii) 3-Mercapto-1-propanesulfonate, NaOH, MeOH, 25 °C, 3 h, 68 %. (iii) DDQ, $CH_2Cl_2$, 0 °C, 5 min, 65 %. (iv) $CF_3O_2H$, MeOH/$CH_2Cl_2$, 25 °C, 3 h, 82 %.

The aminolysis of **P3** with **19** and dimethylamine (Scheme 3.5) was performed in THF at room temperature in the presence of *N,N*-diisopropylethylamine. The compositional target for polythiol **P4** was 15% thiol coverage (where approximately 1 in 7 polymer backbone units contained a thiol functional group) with respect to the total number of pendant thiol units in the furnished polymer composition. It was reasoned that this density of thiols per chain would likely provide a sufficient number of pendant thiol groups for intermolecular disulfide cross-linking whilst inert water-solubilizing lengths of backbone were retained, thus, preserving a degree of chain flexibility upon cross-linking. This target density was achieved by controlling carefully the stoichiometry of the protected thiol-bearing amine **19** with respect to **P3**, adding only enough **19** to displace 15% of the pentafluorophenol units of **P4** to afford **P4a**. The remaining pentafluorophenol units were then displaced in a subsequent step with

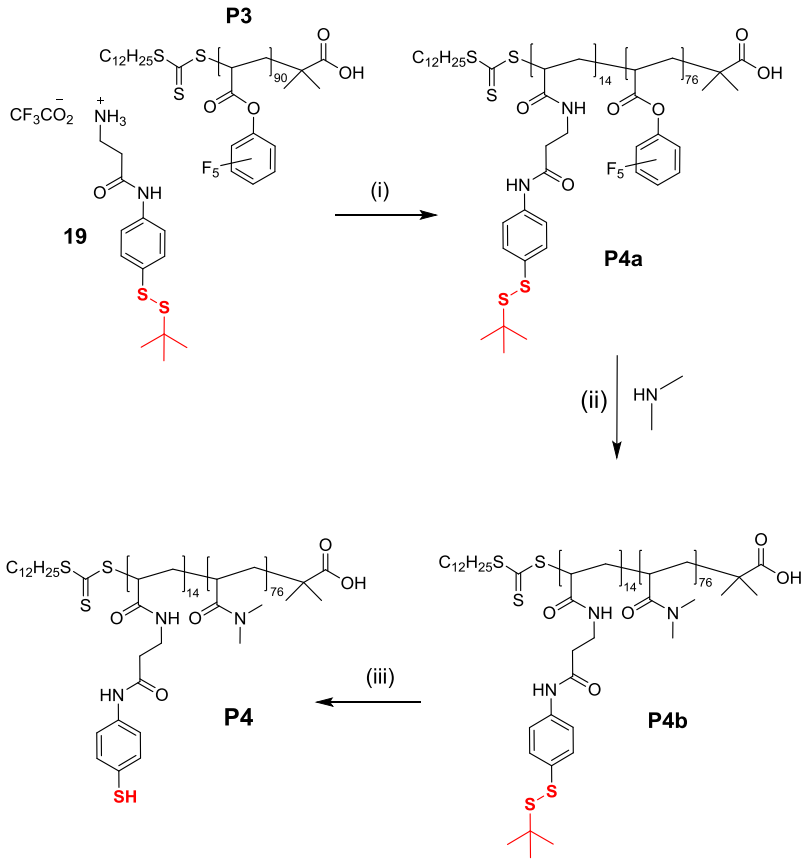


Scheme 3.5 Synthesis of thiolated copolymer **P4**. (i) *N,N*-Diisopropylethylamine, THF, 25 °C, 2 h. (ii) THF, 25 °C, 10 h. (iii) TCEP.HCl, MeOH, 18 h, 25 °C.

dimethylamine to afford random acrylamido copolymer **P4b**. $^{19}$F NMR Spectroscopic analysis provided a useful means of monitoring the displacement of pentafluorophenol as a function

of the addition of **19** (Figure 3.3). Figure 3.5a shows an expanded $^{19}F$ NMR spectrum of **P3** displaying, as expected, three signals corresponding to the aromatic pentafluorophenolate fluorines where characteristic line broadening suggests they are conjugated to the polymer backbone. The addition of 0.15 equivalents of **19** with respect to polymer **P3** resulted in liberation of pentafluorophenolate indicating the primary amine of **19** had reacted with the activated ester. This hypothesis is confirmed by the $^{19}F$ NMR spectrum (Figure 3.3b) which displays a new set of three sharp signals associated with the displaced pentafluorophenolate. A comparison of the integrations of the broad and sharp signals in the $^{19}F$ NMR spectra (Figure 3.3b) revealed a ratio of 6:1, (scaffold-grafted pentafluorophenolate : displaced pentafluorophenolate) namely, $\mathbf{F_a}$:$\mathbf{F_d}$, $\mathbf{F_b}$:$\mathbf{F_e}$ and $\mathbf{F_c}$:$\mathbf{F_f}$ as denoted in the spectrum. This observation suggests that approximately 15% of the pentafluorophenol moieties had been displaced

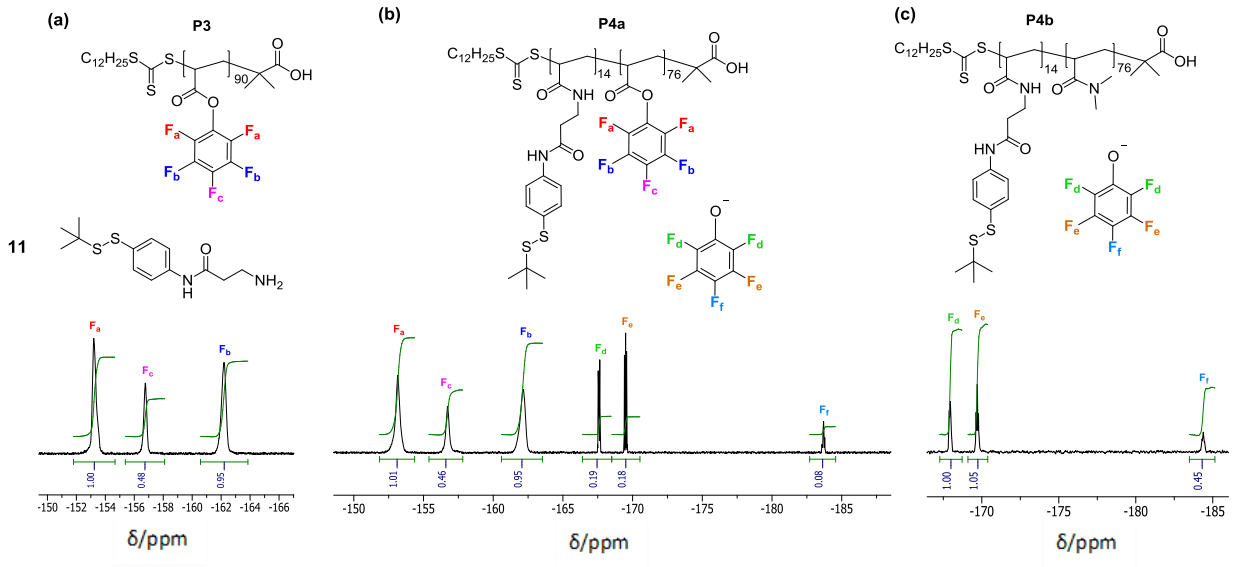


Figure 3.3 $^{19}F$ NMR Spectroscopic analysis (282 MHz, $CDCl_3$) of the aminolysis of **P3** with **19** and dimethylamine. (a) No displacement of pentafluorophenolate had occurred. (b) 15 % of pentafluorophenolate units displaced by amine **19**. (c) Total displacement of pentafluorophenol units by dimethylamine.

as intended, yielding an average of ~14 thiol groups per polymer chain. There is no evidence of carboxylic acid protons in the $^{1}H$ NMR spectrum (not shown) present in the final polymer composition suggesting that there was little or no hydrolysis during the aminolysis process. The addition of excess dimethylamine displaced the remainder of the pentafluorophenol

groups from the backbone. Even though p(PFPA) has been shown to be resistant to hydrolysis on account of its hydrophobic nature and poor solvation in polar solvents there may well be some hydrolysis affording acrylic acids units on the polymer backbone. The presence of a small amount of acrylic acid on the polymer backbone is not expected to cause problems in the orthogonal utility of imine and disulfide bonds. The $^{19}F$ NMR spectrum (Figure 3.3c) of the reaction mixture showed that the broad signals corresponding to the polymer-bound pentafluorophenolates had disappeared, suggesting the aminolysis reaction had gone to completion. After purification by dialysis in MeOH, treatment of **P4b** with TCEP.HCl resulted in cleavage of the protecting disulfide moiety to afford the pendant thiol-bearing polymer building block **P4** (Scheme 3.5). The $^{1}H$ NMR spectra of **P4b** and **P4** (Figure 3.6a, b respectively) is consistent with the successful formation of these polymers. The ratio of DMA : **19** was calculated by integral analysis in the $^{1}H$ NMR spectrum by comparing the integral of the methyl protons in DMA and the t-butyl signals in the asymmetrical boc-disulfide. The cleavage of the protecting disulfide in **P4b** by TCEP was confirmed to have occurred at a yield greater than 95% by the

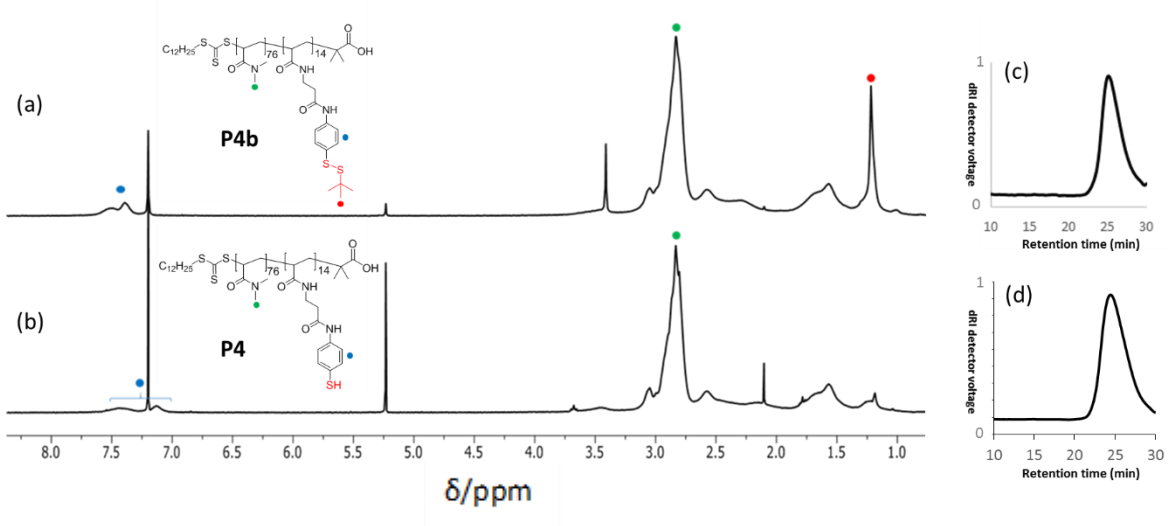


Figure 3.4 Expanded $^{1}H$ NMR spectra (300 MHz, $CDCl_3$) of (a) **P4b**, (b) **P4**. Differential refractive index (dRI) GPC traces of (c) **P4b,** (d) **P4** in DMF (0.6 mL/min, DMF with 1 g/L LiBr).

significant reduction in the intensity of the singlet corresponding to the *t*-butyl protons (δ = 1.21 ppm, Figure 3.4b). Additionally, there is a clear upfield shift in signals corresponding to the aromatic protons (δ = 7.0 – 8.0 ppm) during the transition from **P4b** to **P4** indicating a change in the electronic environment about the aromatic ring. Copolymer **P4** is soluble in $H_2O$ at pH > 6 and is insoluble at pH < 6, values of pH which are close to the value of the p$K_a$ value

of thiophenol (6.6). This observation suggest that at least some of the thiols in **P4** must be deprotonated to impart water solubility and further evidences the presence of pendant thiols. GPC Analysis of **P4b** and **P4** (Figure 3.6c, d) showed narrow population distributions indicating the absence of polymer cross-linking which could have possibly arisen through unwanted thiol oxidation forming disulfide cross-links.

| polymer | $M_n$[a] (g mol$^{-1}$) | $M_n$[b] (g mol$^{-1}$) | $M_w$[b] (g mol$^{-1}$) | PDI ($M_w/M_n$) |
|---|---|---|---|---|
| ***(a)*** **P3** | 22,000 | - | - | 1.30[b,c] |
| ***(b)*** **P4b** | 11,500 | 13,000 | 14,500 | 1.24[b] |
| ***(c)*** **P4** | 10,000 | 11,000 | 11,500 | 1.25[b] |

Table 3.2 Characterization of *(a)* **P3**, *(b)* **P4b** and *(c)* **P4**. [a] As determined by $^1$H NMR (300 MHz, $CDCl_3$) spectroscopic analysis. [b] As determined by GPC in in DMF (0.6 mL/min with 1 g/L LiBr) calibrated against methyl methacrylate standards of very low polydispersity (PDI > 1.08). [c] p(PFPA) was subjected to indirect GPC analysis following a post-polymerization modification by dimethylamine affording p(dimethylacrylamide).

These results indicate a successful post-polymerization methodology for the formation of polythiol **P4** through intermediate preparation of p(PFPA) by RAFT polymerization followed by postpolymerization modification with amine **19** and dimethylamine. A summary of the characterization of polymers **P3**, **P4b** and **P4** is displayed in Table 3.2.

### 3.3.3 Stimuli-Responsive Self Assembly of Polymer Nanoparticles

As described in chapter 2,[75] conditions for the orthogonal formation and cleavage of pH-sensitive imine and redox-sensitive disulfide bonds were established through an investigation of a 'small molecule' model system. The aim now here was to determine the applicability of these model conditions to the formation and cleavage of intermolecular cross-links (Figure 3.5) using **P1**, **P2** and **P4**, and in particular, their scope and utility in the preparation of stimuli-responsive polymeric nanoparticles.

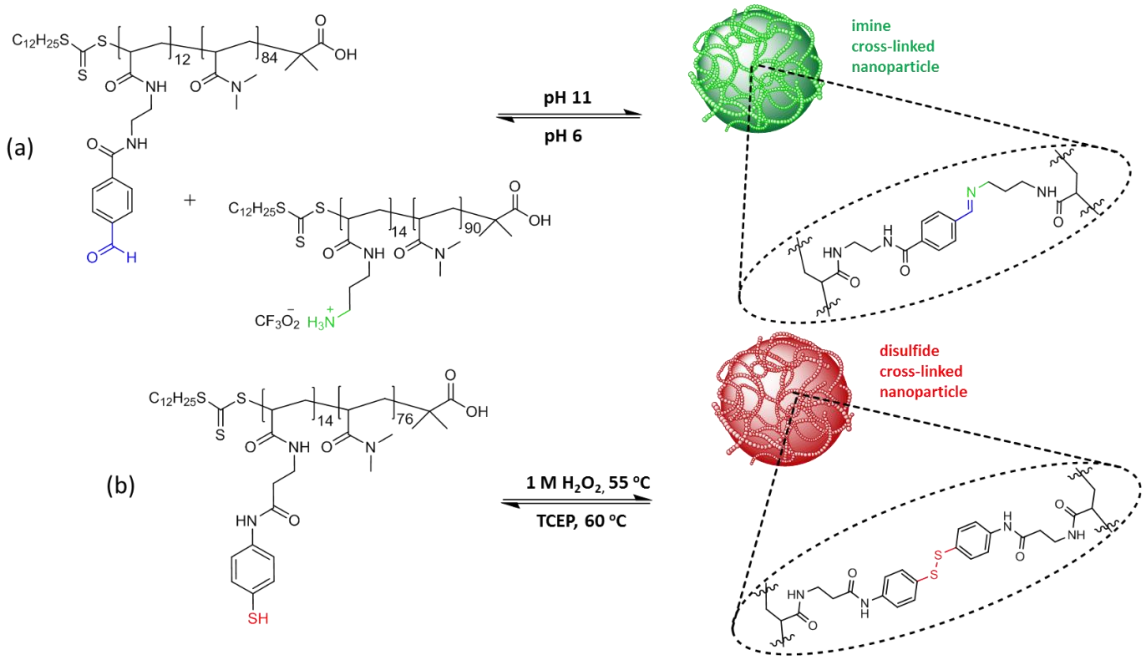


Figure 3.5 Formation of inter-molecular (a) pH-sensitive imine and (b) redox-sensitive disulfide cross-links in the preparation of functional nanoparticles.

Imine cross-linked nanoparticle **NP1** was formed using **P1** and **P2** as building blocks by dissolving an equimolar amount of aldehyde and amine functional groups present as part of **P1** and **P2**, respectively, in $H_2O$ (2% total weight with respect to the total polymer concentration) to form two separate aqueous solutions at pH 7. A small volume of THF was added to aid solubility of **P1**. The two mixtures were then combined rapidly and the pH of the resulting mixture was raised gradually over the course of 6 h to pH 11.0 by slow addition of aliquots of 0.1 M NaOH (5 µL). The mixture was stirred for 18 h at room temperature and an aliquot taken for analysis by GPC (Figure 3.6a). The chromatogram showed a peak at retention time ≈ 18 min indicating the formation of a high molecular weight polymer nanoparticle **NP1** and a second minor peak at retention time ≈ 25 min. It is postulated that the minor peak corresponds to a dimeric product formed between one molecule of **P1** and **P2**, an observation consistent with previous work by Fulton[78b, 91] and Qiao[94] which show convincing evidence for the formation of dimeric polymer species obtained when studying the formation of nanoparticles through the cross-linking of polymer building blocks. Batch dynamic light scattering performed on an aliquot of **NP1** (Figure 3.6c) revealed an $R_h$ of 152 nm and a PDI of 0.182. Disulfide cross-linked nanoparticle **NP2** was prepared by dissolving **P4** in $H_2O$ at pH 7

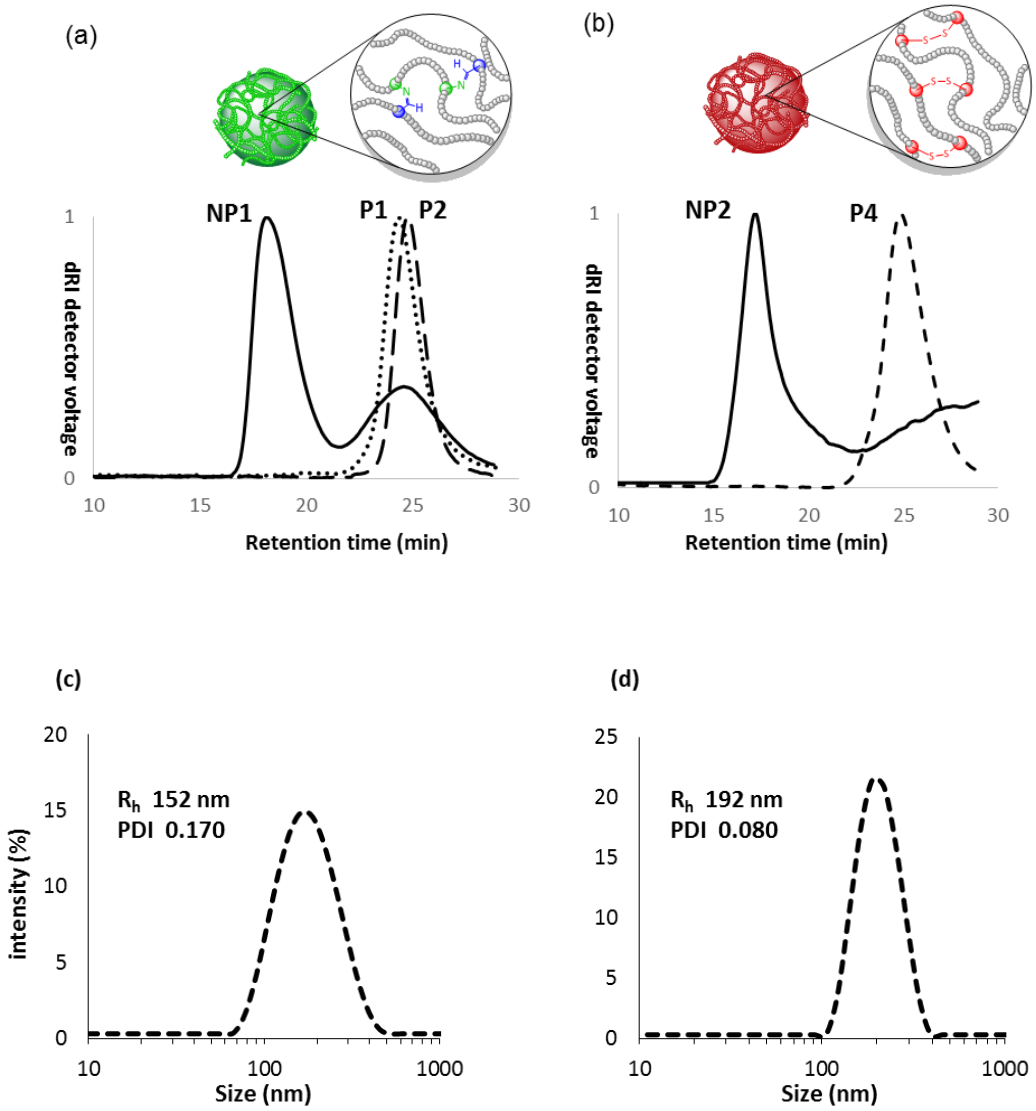


Figure 3.6 GPC traces of nanoparticle assemblies (a) **NP1** formed by cross-linking of **P1** and **P2,** (b) **NP2** formed by cross-linking **P4** in DMF (0.6 mL/min with 1 g/L LiBr). Batch dynamic light scattering of (c) **NP1** and (b) **NP2**.

| nanoparticle | $M_n$[a] (g mol$^{-1}$) | $M_w$[a] (*g mol$^{-1}$*) | PDI[a] ($M_w/M_n$) | Average no. of polymer chains per particle | $R_h$[d] (nm) | PDI[d] |
|---|---|---|---|---|---|---|
| ***NP1*** | 382,000 | 446,000 | 1.17 | 36[b] | 152 | 0.182[d] |
| ***NP2*** | 596,000 | 515,000 | 1.09 | 47[c] | 192 | 0.080[d] |

Table 3.3 Characterization of imine cross-linked polymer nanoparticle **NP1** and disulfide cross-linked nanoparticle **NP2**. [a] As determined by GPC in in DMF (0.6 mL/min with 1 g/L LiBr) calibrated against methyl methacrylate standards of very low polydispersity (PDI > 1.08). [b] Calculated by dividing $M_w$ of **NP2** by the average $M_w$ of **P1** and **P2**. [c] Calculated by dividing $M_w$ of **NP2** by $M_w$ of **P4.** [d] As determined by *in-situ* batch dynamic light scattering in $H_2O$ at 2 wt % with respect to total amount of polymer.

and the mixture was stirred for 14 days at 55 $^{o}$C whilst dilute $H_2O_2$ was added at a rate of 0.25 equivalents per day with respect to the total number of moles of pendant thiols until an upper limit of 4 equivalents of $H_2O_2$ had been reached. GPC analysis (Figure 3.6b) revealed the disappearance of the peak corresponding to **P4** at retention time ≈ 25 min and the emergence of a new signal at retention time at ≈ 17 min, suggesting the formation of high molecular weight nanoparticle **NP2**. There is some evidence in this chromatogram of polymeric material eluting throughout the range of 22 – 30 min, suggesting the presence of a kinetically stable minor species in which thiols are involved in mostly intramolecular disulfide cross-linking and/or dimerization of polymer chains. An aliquot of a solution (2 wt %) of **NP2** was analysed by batch DLS (Figure 3.6d) revealing an $R_h$ of 192 nm and a PDI of 0.080. The formation of imine cross-linked **NP1** was experimentally more simple in comparison to the formation of disulfide cross-linked **NP2**, the former occurring over a considerably shorter timescale at room temperature whereas the latter required extremely slow and careful addition of $H_2O_2$ at elevated temperature to ensure the formation of a well-defined nanoparticle. The characterization data for both experiments is summarized in Table 3.3.

To probe the disassembly of nanoparticles **NP1** and **NP2** back into their constituent building blocks, conditions required for particle disassembly were investigated. The disassembly of **NP1** was performed by lowering the pH of its solution from pH 11 to pH 6 and allowing the mixture to stir for 48 h at 60 $^{o}$C. Successful disassembly of **NP1** was confirmed by GPC and DLS which displayed no evidence for large molecular weight aggregates. **NP2** was disassembled by heating its solution for 72 h in the presence of TCEP. The GPC chromatogram showed the disappearance of peaks corresponding to nanoparticle **NP2** and the re-emergence of peaks corresponding polymer building block **P4**. These experiments strongly suggest the stimuli-responsive reversible self-assembly of **P1** and **P2** into imine- and **P4** into disulfide-crosslinked polymeric nanoparticles possessing a uniform nature.

The time taken for the formation of disulfide cross-linked nanoparticle **NP2** (14 days) was significantly longer than expected based upon observations of disulfide formation with the model system (Chapter 2). Initial experiments revealed that at shorter reaction times the resulting disulfide cross-linked aggregates unfortunately exhibited a broad and ill-defined

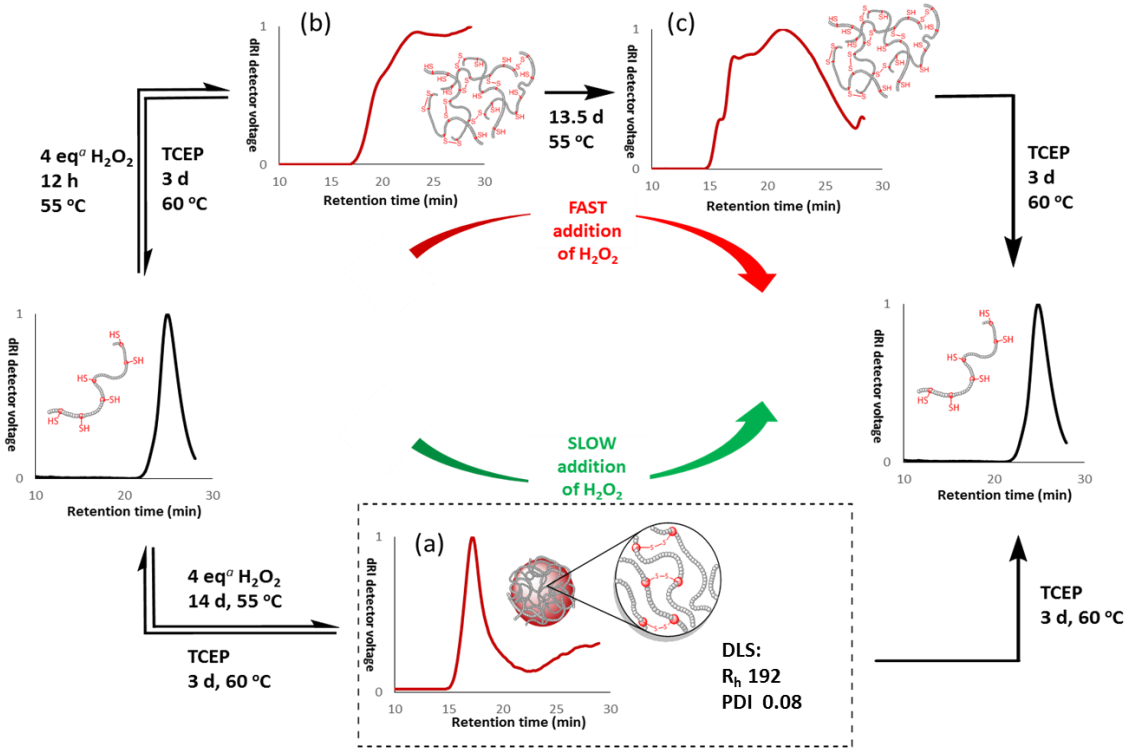


Figure 3.7 GPC analysis in DMF (with 1 g.L$^{-1}$ LiBr, 0.6 mL.min$^{-1}$) of (a) formation of uniform disulfide cross-linked nanoparticle **NP2** over 14 d. (b) Formation of disulfide cross-linked polymer network over 12 h. (c) Re-equilibration over 13.5 d. $^{a}$ 4 equivalents with respect to the total number of thiols in solution.

population distribution. To compare populations of cross-linked aggregates prepared over different reaction times, equimolar amounts of $H_2O_2$ were added to two separate aqueous solutions of **P4** (2 wt. %) over either 12 h (Figure 3.7b) and 14 d (Figure 3.7a) under otherwise identical reaction conditions. Over 12 h, intermolecular oxidative coupling of thiols to form disulfide cross-links had occured as evidenced by a broad, indistinct signal observed at lower elution volumes (retention time 16 – 28 min) in the dRI GPC trace (Figure 3.7b), contrasting with the sharp monomodal signal corresponding to well-defined **NP2** formed over 14 d (Figure 3.7c). After the addition of $H_2O_2$ over 12 h the solution was stirred continuously for a further 13.5 days at 55 °C. The resulting GPC trace (Figure 3.7c) showed a shift in the population distribution towards higher molecular weight, although importantly, these conditions did not result in the formation of uniform nanoparticles. This observation suggests that oxidizing thiols quickly and allowing less time for thiol-disulfide interchange processes to occur in parallel—processes which allow a level of 'error correction' in the assembly process—results

in extremely ill-defined, kinetically fixed disulfide cross-linked polymer networks. The model system investigated[75] in Chapter 2 revealed that oxidative coupling, using $H_2O_2$ as an oxidant, of thiol containing moieities chemically similar to those in **P4** was a fast (< 10 min) process. The lack of structural definition observed thus may arise on account of restricted chain mobility as molecules of **P4** become rapidly cross-linked by intermolecular disulfide bond formation, in turn encumbering thiol-disulfide interchange leading to a diminished capacity for thermodynamic reorganization of polymer chains on the nanoscale. Considering the p$K_a$ of the thiols in **P4**, at pH 7-8, greater than 90% are deprotonated and so in principal the system should undergo exchange when considered on a molecular level as thiol disulfide interchange is first order with respect to thiolate and disulfide concentration.[95] Another possible factor in the necessity for long time scales in the formation of uniform disulfide cross-linked nanoparticles is that negatively charged thiolates, which are not involved in bonding, are allowed sufficient time to position themselves on the periphery of the forming particle imparting improved particle stability in aqueous solution. It is well known that stratification-like behaviour of surfactant moieties has significant influence on particle morphology.[96] Therefore, increasing the time over which $H_2O_2$ is added would increase possibilities for stratification of thiolates to the particle surface whilst the growing particles exhibit a diffuse, loosely packed nature for longer in the formation process. To eliminate the possibility of auto-oxidation of thiols to disulfides by air dissolved in $H_2O$, a control experiment was performed in which a sample of **P4** was dissolved at 2 wt. % in water and maintained at 55 $^oC$ for 7 d. There was no evidence for the formation of high molecular weight aggregates by GPC and the $^1H$ NMR spectrum in $D_2O$ remained unchanged in the absence of $H_2O_2$ at pH 7-8. This observation suggests that intermolecular disulfide cross-links do not form to an extent detectable by these methods without the presence of chemical oxidizing agents such as $H_2O_2$.

### 3.3.4 *Probing concentration effects in disulfide cross-linked polymer nanoparticle formation*

A series of experiments was designed to establish whether there is a concentration dependence in the formation of higher molecular weight aggregates when cross-linking **P4** by the formation of intermolecular disulfide bonds. To investigate the effect of total polymer concentration on the population distribution during the formation of disulfide cross-linked polymeric nanoparticles, **P4** was dissolved in $H_2O$ at four concentrations, 1, 2, 3 and 5 weight % with respect to the total amount of polymer. The formation of disulfide cross-links was

achieved by slow addition of $H_2O_2$ (2 equivalents with respect to the total number of thiols in solution) over the course of 7 d at 55 °C. The four mixtures were analysed by GPC (Figure 3.8a) and DLS (Figure 3.8b). At each of the four concentrations investigated, the GPC trace shows two

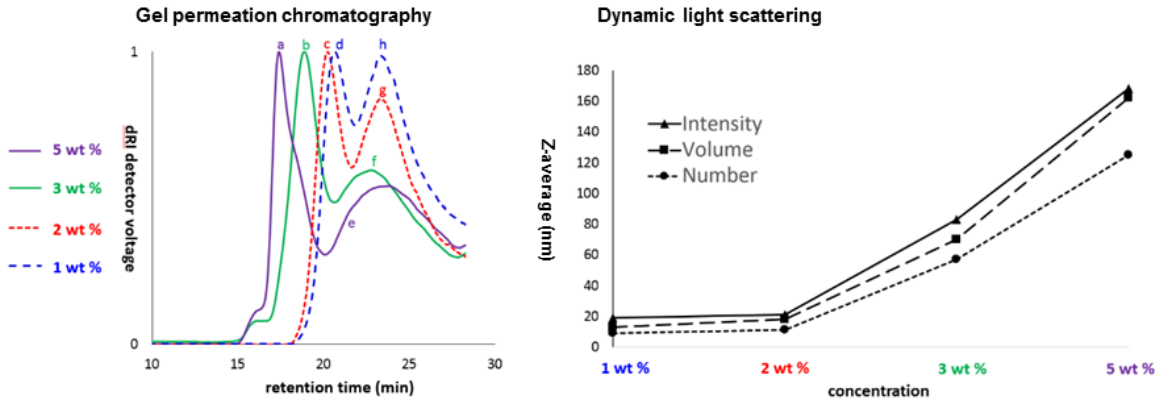


Figure 3.8 Variable concentration disulfide nanoparticle formation experiments at 1, 2, 3 and 5 wt % in $H_2O$ at pH 7 over 7 d . (a) Differential refractive index (dRI) GPC traces conducted in DMF with 1 g/L LiBr (0.6 mL/min). (b) Intensity, volume and number batch DLS analysis performed after 7 d at each concentration.

distinct populations indicated by two peaks, **a-d** and **e-h**. The peak corresponding to the preformed linear polymer in solution at retention time ~ 25 min was absent at all concentrations, indicating the consumption of all polymer in the formation of higher molecular weight aggregates **a-d** and **e-h**. At higher concentration the retention time of the peak corresponding to the larger nanoparticle (**a-d**) was observed to decrease as the total polymer concentration increases. This observation suggests a relationship between molecular weight and concentration for the larger molecular weight population of species (**a-d**). In contrast, the retention time of the peak corresponding to the smaller particle (**e-h**) is similar at all four concentrations suggesting the presence of particles which are smaller and similar in size at all four concentrations. Furthermore,

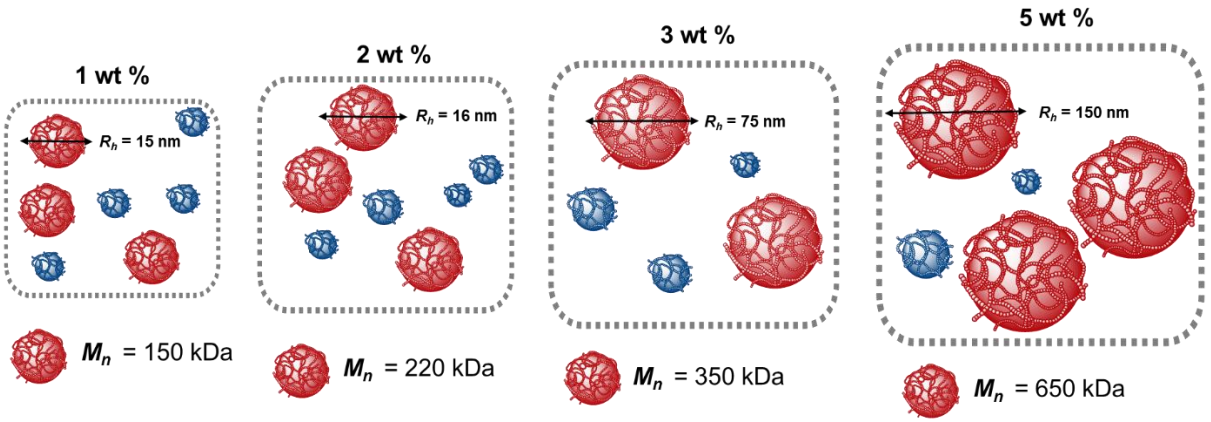


Figure 3.9 Cartoon representation of disulfide cross-linked nanoparticle size distributions in concentration dependent studies. Two nanoparticles populations were observed (red and blue) at each concentration, the nanoparticle coloured red increased in size as the total polymer concentration was increased whereas the nanoparticle coloured blue remained constant throughout all investigated concentrations with a size of < 10 nm. Values of $R_h$ displayed here were calculated here by DLS (Figure 3.8b).

at higher concentration the breadth of the peak corresponding to **e**-**h** increases indicating a larger polydispersity. At 5 wt % and 3 wt % there is the suggestion of a third species of very high molecular weight as evidenced by a small shoulder at retention time ~ 16 min, and interestingly, these species do not feature at 2 wt. % or 1 wt. %. These species are likely to be eluted at the exclusion volume of the GPC system on account of their molecular weight being too large to be approximated by GPC analysis. These large species did not appear in DLS measurements (Figure 3.8b) suggesting their removal by filtration through a 0.2 µm filter prior to measurement. The GPC (Figure 3.8a) and DLS (Figure 3.8b) measurements were in good agreement with respect to nanoparticles **a**-**d**, however, particles **e**-**h** in the GPC were not detected by DLS, presumably on account of their poorer ability to scatter light compared to particles **a**-**d**. This is a limitation of these detection methods when investigating systems which are no monomodal in nature such as the dual populations observed in both imine and disufide described herein.

Taken together these observations demonstrate the concentration dependency on the size and nature of disulfide cross-linked nanoparticles prepared from copolymer **P4**.

### 3.3.5 *Investigation into the orthogonality of imine and disulfide cross-links*

To investigate the orthogonality of imine and disulfide inter-molecular cross-links an equal mass of **P1**, **P2** and **P4** were dissolved in $H_2O$ to afford three separate polymer solutions each at a total polymer concentration of 2 wt %. The pH of each solution was maintained at pH 6.5 by addition of small aliquots (5 – 10 µL) of 1 M HCl and 1 M NaOH. The three polymer solutions were rapidly combined which resulted immediately in a white precipitate which was isolated by filtration and was completely insoluble in a wide range of common solvents suggesting the formation of a cross-linked aggregate. The pH of the mixture remained between pH 6 and pH 7 after mixing of the three polymer solutions and it can be inferred from the model studies presented in chapter 2 that no intermolecular imine bonds should have formed as the pH was too low. Furthermore it was demonstrated that adjusting the pH of the suspension to pH 12 or pH 2 did not result in redissolution of the observed aggregate suggesting that pH-sensitive inter-molecular imine bond formation is unlikely to be the cause of the observed aggregation. To further investigate the source of the observed precipitation, control experiments were performed wherein one of the polymer building blocks (**P1**, **P2** and **P4**) was omitted from the mixture. Firstly, **P2** and **P4** were dissolved in $H_2O$ to form two separate solutions at a concentration of 2 wt % with respect to the total polymer concentration and the pH of both solutions was adjusted to pH 6.5. The solutions of **P2** and **P4** were combined rapidly and stirred for 1 h and no precipitation was observed. Analysis of the mixture of **P2** and **P4** by GPC showed the absence of supramolecular aggregates suggesting no interaction between **P2** and **P4**. Solutions containing **P1** and **P4** were then prepared at concentrations of 2 wt % with respect to the total mass of polymer. The pH of both solutions was adjusted to pH 6.5 and then rapidly combined, with precipitation observed immediately. This observation suggested an interaction between copolymers **P1** and **P4** which had resulted in the irreversible formation of an insoluble aggregate. Based on these observations it was concluded that the formation of this species was pH independent, forming at both pH 12 and pH 2. The observed aggregation of **P1** and **P4** had likely arisen on account of the formation of intermolecular

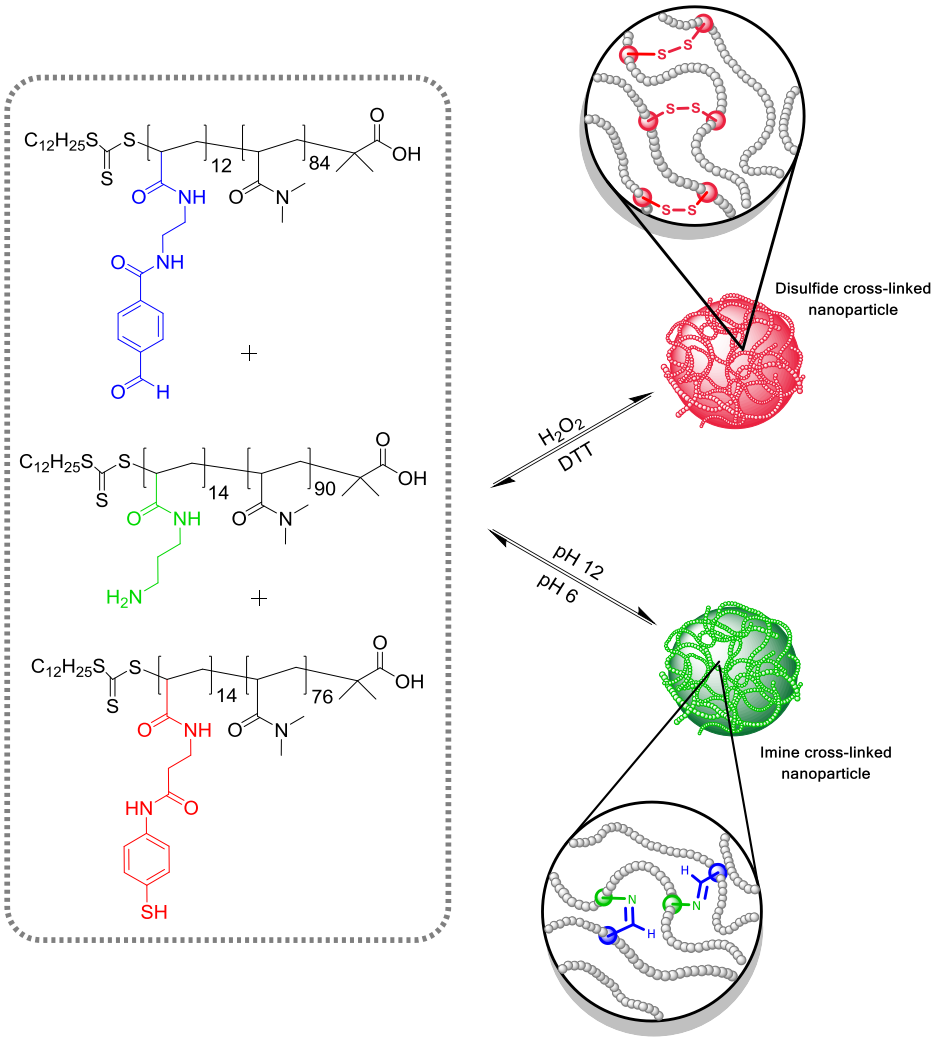


Figure 3.10 Stimuli-responsive reversible formation of imine *or* disulfide nanoparticles from a mixture of **P1**, **P2** and **P4**.

hemithioacetal bonds between the pendant aldehyde groups of **P1** and pendant thiol groups of **P4** – a process which was shown to exhibit pH-independency. Whilst the hemithioacetal bond is widely regarded as being labile in nature[28, 97] the formation of multiple short-lived intermolecular hemithioacetal bonds between **P1** and **P4** along their polymer backbones may stabilise hemithioacetal based aggregates through a multivalence phenomenon where the sum of multiple weak interactions affords an overall strong interaction. The formation of hemithioacetal was not prevalent in the small molecule model system, however, when the same functionality (electron poor, aromatic aldehyde and aromatic thiol) this affect seems to be a serious limitation. The experiment was repeated wherein mixtures of **P1** and **P4** were combined rapidly resulting in solutions of 1.5 wt % and 1 wt % with respect to the total polymer concentration and precipitation was observed in both cases.

These observations taken together highlight the experimental difficulties of introducing polymer-bound aldehyde and thiol functional groups within the same aqueous system, an outcome which was difficult to predict based on the understanding of the 'model' small molecular system described in Chapter 2.

### 3.3.6 *Preparation of dual-functional random terpolymers*

An alternative strategy for the dual-incorporation of imine and disulfide dynamic covalent bonding motifs into a single dynamic polymer system was investigated. Two random terpolymers, **P5** and **P8**, were designed (Scheme 3.6). It was hypothesized that polymers **P5** and **P8**, when deprotected to form **P7** and **P10**, could undergo cross-linking through the formation of imine and/or disulfide DCBs on between amine *or* aldehyde and thiol pendant functional groups, respectively. Terpolymers **P5** and **P8** were prepared using a similar strategy

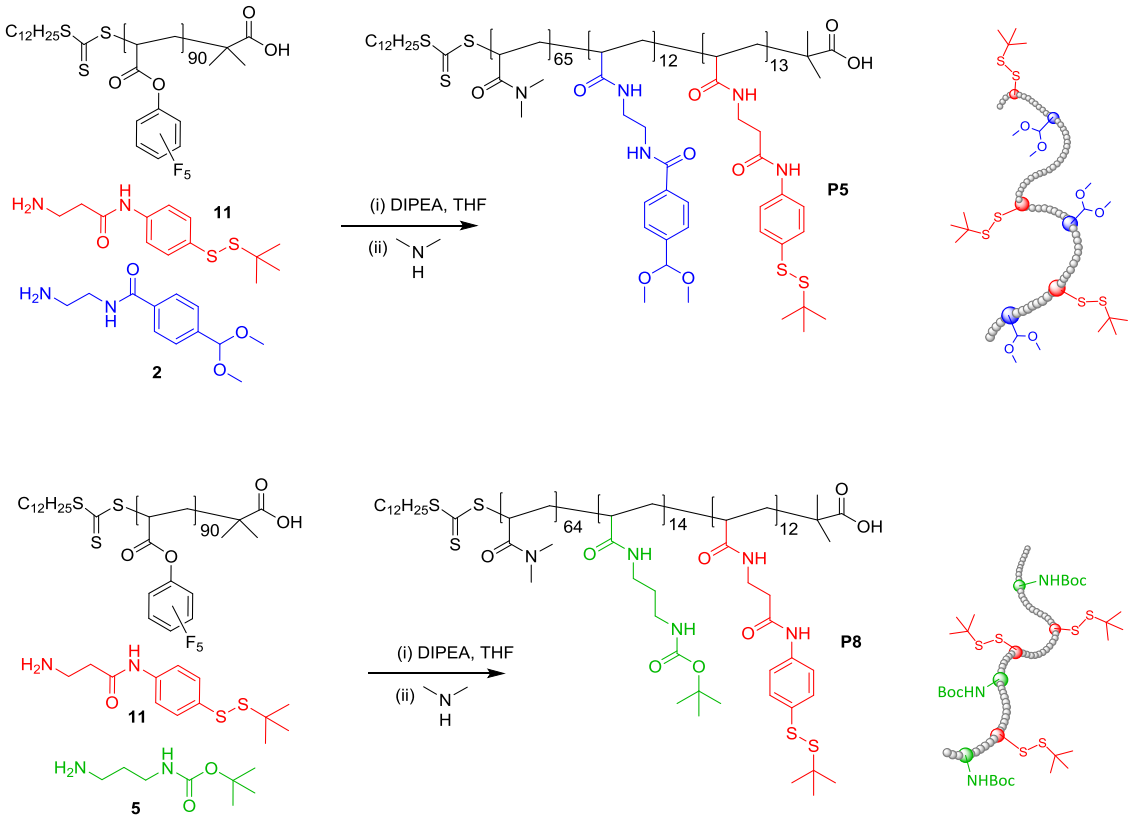


Scheme 3.6 Synthesis of dual-functional random terpolymers **P5** and **P8** using an aminolysis strategy with a variety of functional amines and p(PFPA).

to that reported earlier in this chapter where p(PFPA) was utilized as an activated precursor polymeric scaffold onto which functionality was grafted through an aminolysis reaction with functional amines **10**, **13** and **19**. Copolymers **P5** and **P8** were isolated as protected dual-functional random terpolymers. The aminolysis reactions were monitored by $^{19}F$ NMR spectroscopy analysis, **P5** and **P8** were characterized by GPC and $^{1}H$ NMR spectroscopic

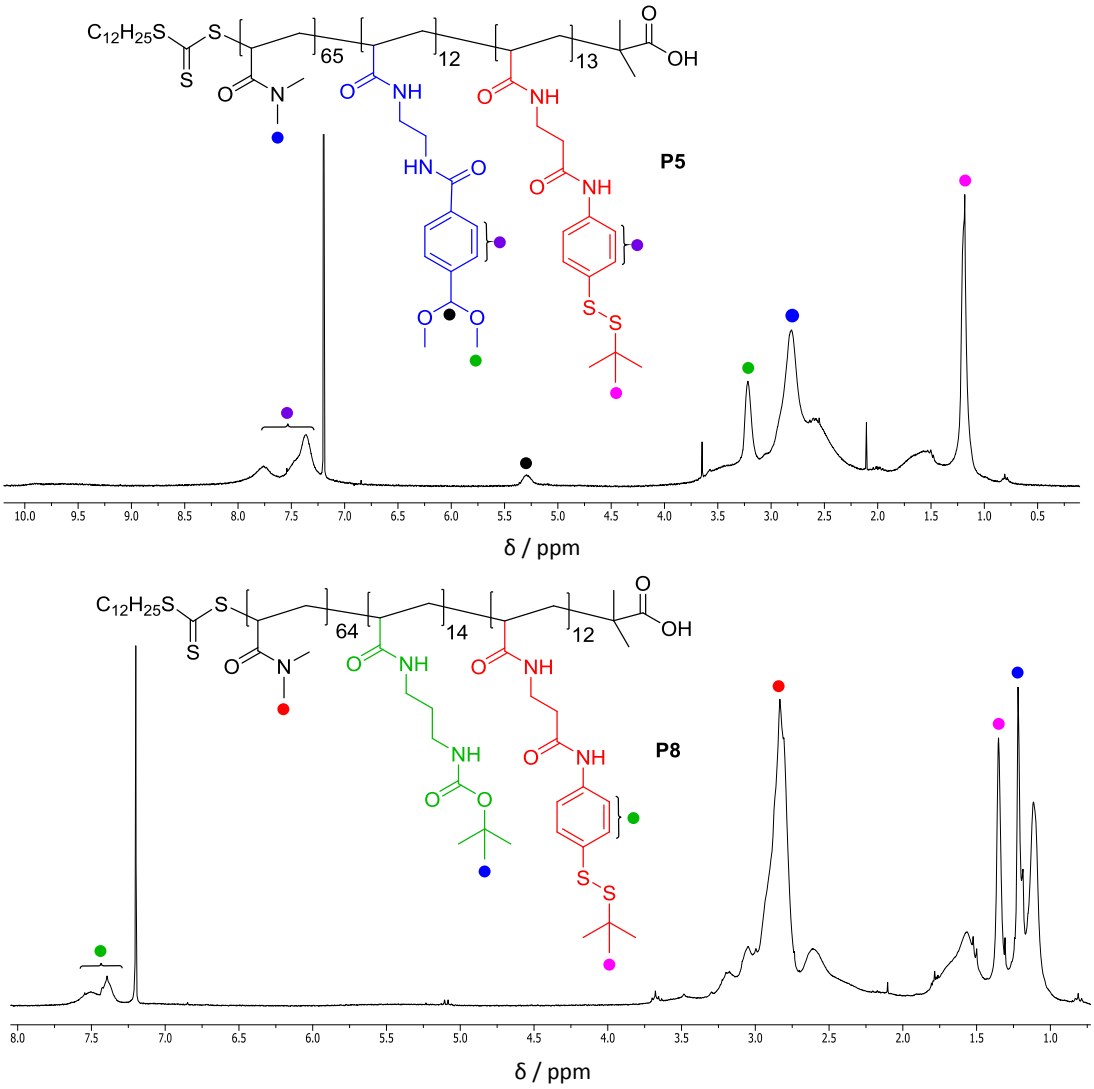


Figure 3.11 $^{1}H$ NMR Spectroscopic analysis (300 MHz, $CDCl_3$) of 'protected' dual-functional random terpolymers **P5** and **P8**.

analysis (Figure 3.12). Upon successful preparation of copolymers **P5** and **P8** a sequential deprotection strategy was developed (Figure 3.11) to reveal amine, aldehyde and thiol pendant functional groups, thus endowing the corresponding deprotected polymer building

blocks **P7** and **P10** with the capability to undergo stimuli-responsive cross-linking through the formation of imine and disulfide dynamic covalent bonds. Firstly, a solution of **P5** was prepared in a 1:1 (v/v) solution of 1 M HCl and THF and aldehyde bearing terpolymer **P6** was collected by precipitaton in ice-cold $Et_2O$. Methyl-3-mercaptopropionate was used in large excess in basic MeOH to cleave the pendant disulfide groups of **P6** yielding pendant thiols via a thiol-disulfide interchange mechanism.

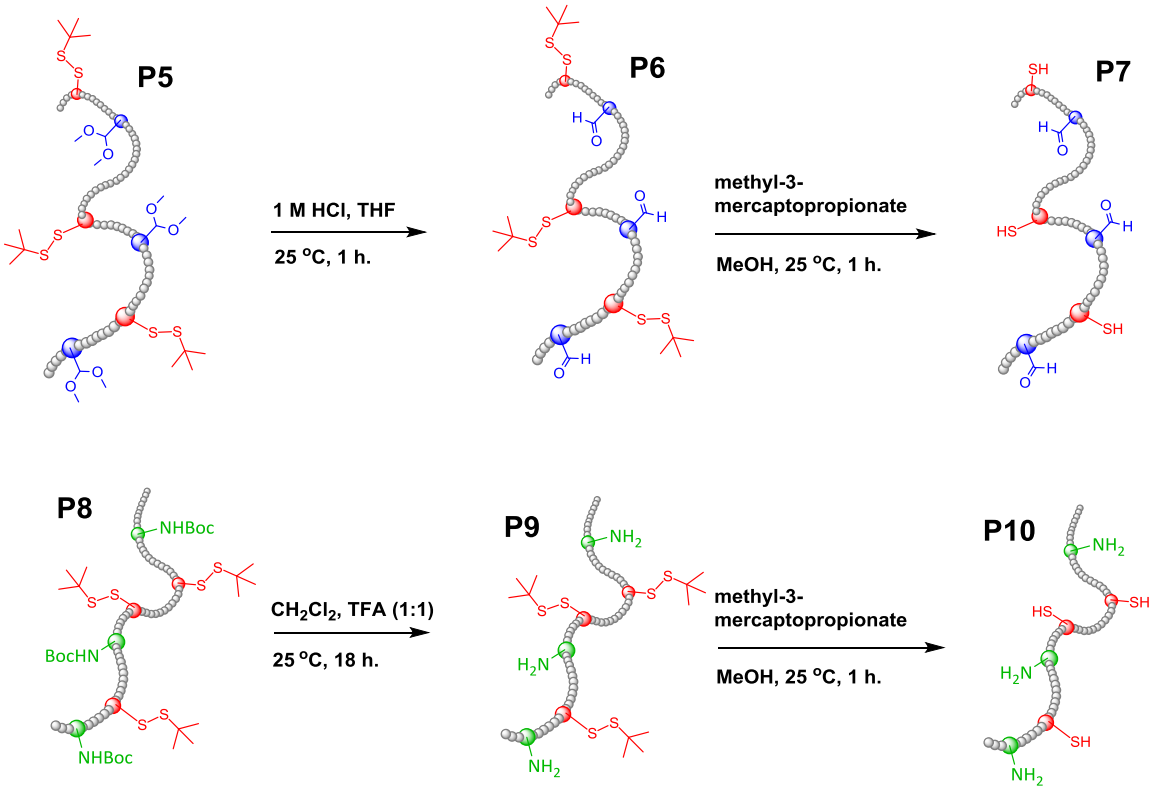


Figure 3.12 Schematic representation of the sequential deprotection strategy adopted for the preparation of aldehyde and thiol bearing copolymer **P7** and amine and thiol copolymer **P10**.

The resulting copolymer **P7** was precipitated in ice-cold $Et_2O$ yielding a waxy solid. $^1$H NMR Spectroscopic analysis revealed that > 95 % of the disulfide bonds in **P6** had been cleaved. The $^1$H NMR spectrum of **P7** displays the absence of the aldehyde signal which was present in **P6**. The furnished dual-functional copolymer, **P7**, was extremely difficult to handle and became increasingly insoluble in all solvents over time perhaps indicating the formation of insoluble aggregates during the cleavage of the pendant disulfide bonds of **P6**. On account of the observed insolubility, no further analysis was performed.

Copolymer **P8** was deprotected using 1:2 TFA : DCM (v/v) furnishing **P9** which was collected by precipitation in $Et_2O$. Cleavage of the disulfide groups of **P9** was conducted using methyl-3-mercaptopropionate in basic MeOH and **P10** was collected by dialysis to yield a waxy solid. The isolated material was insoluble in all tested solvents therefore characterization was unobtainable using GPC or $^1$H NMR spectroscopy. The insolubility of **P7** and **P10**, formed by cleavage of the pendant 'protecting' disulfides in **P6** and **P9**, respectively, suggests a macroscopic cross-linking of the polymers was occuring. With respect to aldehyde- and thiol-copolymer **P7** the observed aggregation may arise on account of intra- and intermolecular hemithioacetal formation between aldehyde and thiol moieties, in contrast, **P10** cannot undergo hemithioacetal formation on account of the absence of the aldehyde functionality. To further investigate the post-disulfide reduction precipitation, various disulfide cleavage protocols were then investigated including the use of TCEP, propanethiol and mercaptoethanol. Deprotection of **P6** and **P9** with these reagents did not yield soluble materials which could be analysed. It was reasoned that the poor solubility is on account of unwanted aggregation of polymer chains on account of the cleavage of the protecting disulfide bonds yielding pendant thiol functional groups. No further analysis was performed on random terpolymers **P7** and **P10** and a different strategy will be adopted in future work be to furnish dual-functional random copolymers.

Confining thiol and aldehyde *or* amine functional on a single polymer backbone proved experimentally very difficult and therefore no experiments were performed to investigate the orthogonality of polymeric building blocks **P7** and **P10**.

### 3.3 Conclusion

RAFT polymerization was utilized to prepare amine-, aldehyde- and thiol- bearing random copolymers possessing the capacity to form intermolecular dynamic covalent imine and disulfide cross-links. Conditions were established for successful formation of imine and disulfide cross-linked nanoparticles from the pre-prepared polymeric building blocks. Furthermore, it was demonstrated that stimuli-responsive nanoparticle disassembly could be achieved, recovering the polymeric precursors. The formation of disulfide cross-linked nanoparticles was shown to proceed over a much greater time-scale compared with the

formation of imine cross-linked nanoparticles. Perhaps, employing the use of diblock copolymers wherein one block exhibits pendant thiol functional groups and a second block is comprised of inert, hydrophilic units, a system with a greater predisposition for the structural organization of polymer chains into disulfide cross-linked nanoparticles may be achieved. Furthermore, it was demonstrated that great care was necessary with respect to the addition of $H_2O_2$ on account of the propensity for over-oxidation of pendant thiol groups. Taken together these studies highlight potential difficulties in transposing a small molecule model system onto a polymeric supramolecular framework. Whilst true orthogonality was observed in the small molecule system, in the polymeric system, unwanted aggregation phenomena on the macromolecular regime led to intractable precipitates. It is hypothesized that a further expansion of this work will yield a truly orthogonal system wherein either imine and/or disulfide cross-linked nanoparticles can be formed through independent pathways in the absence of cross-talk.

### 3.5 Experimental

*Methyl-4-(dimethoxymethyl)benzoate (**9**)*[12a]

A solution of 4-carboxybenzaldehyde (15.4 g, 102.6 mmol), trimethylorthoformate (32.7 g, 307.8 mmol) and conc. $H_2SO_4$ (8 drops) in MeOH (100 mL) was heated under reflux conditions for 24 h. The reaction mixture was transferred to a separating funnel with saturated $NaHCO_3$ ($_{aq}$) (100 mL). The aqueous layer was extracted with $CH_2Cl_2$ (3 × 150 mL). The organic extracts were combined and dried over $MgSO_4$, filtered and evaporated to dryness to afford a crude liquid which was purified by vacuum distillation to afford the title product as a colourless liquid (19.8 g, 92 %). $^1$H NMR ($CDCl_3$, 300 MHz): δ 3.30 (s, 6H, $CH(OCH_3)_2$), 3.89 (s, 3H, $OCH_3$), 5.42 (s, 1H, $CH(OCH_3)_2$), 7.51 (d, 2H, Ar, J = 8.1 Hz), 8.02 (d, 2H, Ar, J = 8.1 Hz). $^{13}$C NMR ($CDCl_3$): δ 52.2, 53.0, 103.0, 127.1, 129.8, 130.8, 143.8, 167.1. FT-IR (wavenumber, $cm^{-1}$): 2947 (C–H), 2905 (C–H), 2834 (C–H), 1724 (C=O), 1452 (C=C), 1436 (C=C), 1410 (C=C).

*N-(2-aminoethyl)-4-(dimethoxymethyl)benzamide (**10**)*[12a]

A solution of *methyl-4-(dimethoxymethyl)benzoate (**9**)*, 6.0 g, 28.5 mmol) in 1,2-diaminoethane (100 mL) was heated under reflux for 24 h then evaporated to dryness. The viscous yellow oil obtained was purified by column chromatography [$SiO_2$, $CH_2Cl_2$-EtOH-$Et_3N$

(80:15:5)] to afford a pale yellow waxy solid (3.3 g, 61 %). $^1$H NMR ($CDCl_3$): δ 2.91 (t, 2H, $CH_2$, 3.22 (s, 6H, $OCH_3$), 3.46 (q, 2H, $CH_2$), 3.61 (br s, 2H, $NH_2$), 5.30 (s, 3H, $CH(OCH_3)_2$), 7.33 (t, 1H, NH), 7.38 (d, 2H, Ar, J = 9.0 Hz), 7.73 (d, 2H, Ar, J = 9.0 Hz). ($CDCl_3$, 100 MHz): δ 52.1, 52.6, 102.3, 126.8, 129.6, 130.2, 143.0, 166.4. HRMS$^+$ $C_{12}H_{18}N_2O_3$: Theoretical: 238.1317. Actual: 238.1320

*N-ethylacrylamide-2-(4-(dimethoxymethyl)benzamide (**11**)*[12a]

N-(2-Aminoethyl)-4-(dimethoxymethyl)benzamide (**10**) was dissolved in $CH_2Cl_2$ (70 mL) and $Et_3N$ (3.9 g, 38.2 mmol) in a round bottom flask which was submersed in an ice bath. Acryloyl chloride (1.8 g, 19.3 mmol) in $CH_2Cl_2$ (40 mL) was added dropwise over 30 min. The reaction was stirred overnight at room temperature then added to a separating funnel with saturated $NaHCO_3$ ($_{aq}$) (100 mL). The aqueous layer was extracted with $CH_2Cl_2$ (3 × 100 mL), and the organic extracts were combined and dried over $MgSO_4$, filtered and evaporated to dryness to afford a off-white solid which was purified by column chromatography [$SiO_2$, EtOAc-$Et_3N$ (95:5)] to afford the title product as a white solid (2.6 g, 46 %). $^1$H NMR ($CDCl_3$): δ 3.28 (s, 6H, $CH(OCH_3)_2$), 3.52 (m, 4H, $(CH_2)_2$), 5.37 (s, 1H, $CH(OCH_3)_2$), 5.58 (dd, 1H, J = 1.8 Hz, J = 9.9 Hz), 6.14 (dd, 1H, J = 9.9 Hz, J = 17.0 Hz), 6.23 (dd, 1H, J = 1.8 Hz, J = 17.0 Hz), 7.37 (s, 1H, NH), 7.45 (d, 2H, Ar, J = 8.1 Hz), 7.79 (d, 2H, Ar, J = 8.1 Hz), 7.84 (s, 1H, NH). $^{13}$C NMR ($CDCl_3$): δ 41.3, 53.1, 103.1, 127.3, 128.2, 130.0, 131.3, 134.6, 142.1, 167.5, 168.6. FT-IR (wavenumber, cm$^{-1}$): 3290 (N–H), 3096 (C–H, alkene), 2947 (C–H, alkyl), 1634 (C=O), 1593 (C=O), 1448 (C=C, aromatic), 1413 (C=C, aromatic). HRMS$^+$ $C_{15}H_{21}N_2O_4$: Theoretical: 293.1501. Actual: 293.1503.

*N-Ethylacrylamide-2-(4-formylbenzamide) (**12**)*[12a]

A solution of N-ethylacrylamide-2-(4-(dimethoxymethyl)benzamide) (**11**), 1.8 g, 6.2 mmol) in 1 M HCl(aq) (25 mL) was stirred at room temperature for 2 h then neutralized with saturated $NaHCO_3$($_{aq}$) (100 mL). The aqueous layer was extracted with EtOAc (3 × 200 mL), and the organic extracts were combined and dried over $MgSO_4$, filtered and evaporated to dryness to afford the title product as a white solid (1.1 g, 71 %). $^1$H NMR (DMSO-$d_6$): δ 3.72 (m, 4H, $(CH_2)_2$), 5.59 (dd, 1H, J = 2.5 Hz, J = 9.8 Hz), 6.09 (dd, 1H, J = 2.5 Hz, J = 17.1 Hz), 6.23 (dd, 1H, J = 9.8 Hz, J = 17.1 Hz), 7.99 (d, 2H, Ar, J = 8.4 Hz), 8.03 (d, 2H, Ar, J = 8.4 Hz), 8.23 (s, 1H, NH), 8.79 (s, 1H, NH), 10.07 (s, 1H, CHO). $^{13}$C NMR (75 MHz, DMSO-$d_6$): δ 39.9, 125.7, 128.3, 129.8, 132.2, 139.1, 140.3, 164.9, 166.1, 192.9. FT-IR (wavenumber, cm$^{-1}$): 3264 (N–H), 3091 (C–H, alkene),

2943 (C–H, alkyl), 1699 (C=O, aldehyde), 1627 (C=O, amide), 1549 (C=O, amide), 1447 (C=C, aromatic), 1414 (C=C, aromatic). HRMS$^+$ $C_{13}H_{15}N_2O_3$: Theoretical: 247.1083. Actual: 247.1085.

*N-(Tert-butoxycarbonyl)-1,3-diaminopropane (**13**)*[12a]

A solution of 1,3-diaminopropane (25.0 g, 337 mmol) in $CHCl_3$ (200 mL) was cooled to 0 ˚C in an ice bath. A solution of di-*tert*-butyl dicarbonate (10.5 g, 48 mmol) in $CHCl_3$ (100 mL) was added dropwise over 30 min and the reaction mixture was stirred overnight at room temperature, then filtered and the filtrate evaporated to dryness to afford a clear oil. Saturated NaCl ($_{aq}$) (150 mL) was added to the clear oil and the solution was filtered to remove the *bis*-protected product and transferred into a separating funnel with diethyl ether (150 mL). The aqueous layer was extracted with diethyl ether (2 × 150 mL). The organic extracts were combined and dried over $Na_2SO_4$, filtered and evaporated to dryness to afford the title product as a colourless liquid (6.1 g, 73 %). $^1$H NMR ($CDCl_3$, 400 MHz): δ 1.40 (s, 9H, $C(CH_3)_3$), 1.49 (s, 2H, N-H), 1.57 (m, 2H, $C(CH_2)3$), 2.72 (m, 2H, $CH_2N$), 3.16 (m, 2H, $CH_2N$), 4.95 (s, 1H, N-H). $^{13}$C NMR ($CDCl_3$): δ 28.8, 31.5, 33.9, 40.0, 79.4, 156.5. HRMS (ES$^+$) $C_8H_{19}N_2O_2$: Theoretical: 175.1447. Actual: 175.1449.

*N-(Tert-butoxycarbonyl)-propylaminoacrylamide (**14**)*[12a]

A solution of *N*-(*tert*-butoxycarbonyl)-l,3-diaminopropane (4, 3.1 g, 17.8 mmol) and $Et_3N$ (2.2 g, 21.4 mmol) in $CH_2Cl_2$ (75 mL) was cooled to 0 ˚C in an ice bath. Acryloyl chloride (1.6 g, 17.8 mmol) in $CH_2Cl_2$ (50 mL) was added dropwise over 30 min, and the reaction was stirred overnight at room temperature, then transferred to a separating funnel with saturated $NaHCO_3$($_{aq}$) (150 mL). The aqueous layer was extracted with $CH_2Cl_2$ (2 × 150 mL) and the organic extracts were combined and dried over $Na_2SO_4$, filtered and evaporated to dryness to afford a crude solid which was purified by column chromatography [$SiO_2$, Hexane-EtOAc (1:1)] to afford the title product as a white solid (3.2 g, 79 %). $^1$H NMR ($CDCl_3$, 400 MHz): δ 1.42 (s, 9H, $C(CH_3)_3$), 1.62 (m, 2H, $CH_2$-$CH_2$-$CH_2$), 3.16 (m, 2H, $CH_2N$), 3.35 (m, 2H, $CH_2N$), 4.96 (br. s, 1H, N-H), 5.61 (dd, 1H, J = 1.4 Hz, J = 10.2 Hz), 6.11 (dd, 1H, J = 10.0 Hz, J = 16.8 Hz), 6.26 (dd, 1H, J = 1.6 Hz, J = 17.2 Hz), 6.52 (br. s, 1H, N-H). $^{13}$C NMR ($CDCl_3$, 100 MHz): δ 27.4, 30.1, 36.2, 37.3, 78.9, 125.4, 131.1, 156.5, 166.1. HRMS (ES$^+$) $C_{11}H_{20}N_2O_3Na$: Theoretical: 251.1372. Actual: 251.1374.

*Aldehyde functionalized Copolymer (**P1**)*[12a]

2-(Dodecylthiocarbonothioylthio)-2-methylpropionic acid (DDMAT), (34.2 mg, 0.094 mmol, 1 eq) and AIBN (3.08 mg, 19 µmol, 0.2 eq) were added to a small schlenk tube. *N,N*-Dimethylacrylamide (DMA) (0.745 g, 7.52 mmol, 80 eq) and *N*-ethylacrylamide-2-(4-formylbenzamide) (**12**, 0.463 g, 1.88 mmol, 20 eq) were then added followed by DMF (3 mL). The reaction mixture was degassed through five freeze-pump-thaw cycles before the vessel was backfilled with $N_2$, purged with $N_2$, and allowed to warm to room temperature. The reaction mixture was then placed in an oil bath at 70 ˚C, and the polymerization was quenched after 22 h. The reaction mixture was dissolved in a minimal amount of THF-acetone and added dropwise to a large excess of ice-cold diethyl ether. The polymer precipitate was then isolated by filtration and the precipitation was repeated before drying under high vacuum. Polymer **P1** was obtained as a pale yellow solid (1.05 g). $^1$H NMR (300 MHz, $CDCl_3$): 1.4 – 1.8 (br, CHC*H*$_2$, polymer backbone), 2.2 – 2.7 (br, C*H*CH$_2$, polymer backbone), 2.88 (br, N(C*H*$_3$)$_2$), 3.4 – 3.6 (br, (C*H*$_2$)$_2$), 7.88 (br, Ar), 8.07 (br, Ar), 8.59 (br, N*H*), 10.04 (br, Ar). The composition of **P1** was determined by comparing the integration of the aldehyde protons of **12** with the integration of the N(C*H*$_3$)$_2$ protons of DMA, showing the monomer composition to be 5 : 1 DMA : **12**.

*Boc-amine Functionalized Copolymer (**P2a**)*

DDMAT (24.0 mg, 66 µmol, 1 eq) and AIBN (2.16 mg, 13.2 µmol, 0.2 eq) were added to a small schlenk tube. *N,N'*-Dimethylacrylamide (1.05 g, 10.56 mmol, 160 eq) and *N*-(tert-butoxycarbonyl)- propylaminoacrylamide, **14**, (0.30 g, 1.32 mmol, 20 eq) followed by DMF (4 mL). The reaction mixture was degassed five times, and then the vessel was backfilled with $N_2$ and allowed to warm to room temperature. The reaction mixture was then placed in an oil bath at 70 ˚C and the polymerization was quenched after 21 h. The reaction mixture was dissolved in a minimal amount of THF and added dropwise to a large excess of ice-cold diethyl ether. The polymer precipitate was then isolated by filtration and the precipitation was repeated before drying under high vacuum. Polymer **P2a** was obtained as a pale yellow solid (1.28 g). $^1$H NMR ($CDCl_3$): δ 1.45 (9H, br s, C(CH$_3$)$_3$), 1.50-1.90 (br, CHC*H*$_2$), 2.61 (br, C*H*CH$_2$), 2.87 (br, N(CH$_3$)$_2$), 3.45 (br, (CH$_2$)$_3$). The composition of **P2a** can be determined by comparing the integration of the *boc* protons of the *boc* group of **14** with the integration of the N(CH$_3$)$_2$ protons of DMA. The monomer composition was determined to be 1:6 (*boc*-amine:DMA) which differs to the feed ratio (1:5), presumably due to the difference in reactivity between DMA and the mono-substituted N-alkylacrylamide monomer **14**. GPC analysis in DMF + 1 g.L$^-$

[1] LiBr (0.6 mL $min^{-1}$) revealed an $M_n$ of 16 kDa and a PDI of 1.26 when analysed a set of near-monodisperse poly(methyl methacrylate) standards.

*Amine Functionalized Copolymer (**P2**)*

Copolymer **P2a** (1.07 g) was dissolved in $CHCl_3$ (5 mL) and TFA (5 mL) was added then the reaction mixture was left to stir for 4 h. After this time the solvent and excess TFA were removed on a rotary evaporator and the oil obtained was dissolved in a minimal amount of $CHCl_3$ and added dropwise to a large excess of diethyl ether. The polymer precipitate was then isolated by filtration and dried under high vacuum. The polymer precipitate was then isolated by filtration and the precipitation was repeated before drying under high vacuum. Copolymer **P2b** was obtained as a pale yellow solid (0.92 g). $^1$H NMR ($CDCl_3$): δ 0.86 (br, $CH_2CH_3$, of the chain terminus), 1.71 (br, $CHCH_2$), 2.44 (br, $CHCH_2$), 2.87 (br, $N(CH_3)_2$.

*Pentafluorophenyl Acrylate (**15**)*

Pentfluorophenol (9.80 g, 53.24 mmol) and triethylamine (5.66 g, 55.90 mmol) were dissolved in $CH_2Cl_2$ and cooled to 0 $^oC$. Acryloyl chloride (5.66 g, 55.90 mmol) was added dropwise over 2 h and the mixture was stirred at 25 $^oC$ for 16 h. A salt precipitate was removed by filtration and the filtrate washed with 1 M HCl (150 mL) and deionized $H_2O$ (150 mL) and dried over $MgSO_4$. The solvent was removed *in vacuo* and the resultant faint yellow solution was purified by column chromatography [$SiO_2$, petroleum ether] to afford the title product as a clear viscous liquid. (3.3 g, 40 %). $^1$H NMR ($CDCl_3$): δ 6.20 (d, 1H), 6.39 (dd, 1H), 6.75 (dd, 1H). $^{13}$C NMR ($CDCl_3$): δ 125.1, 134.9, 136.0, 137.8, 139.3, 141.1, 142.8, 161.5. $^{19}$F NMR ($CDCl_3$) δ -162.6 (d, Ar, 2F), -158.0 (t, Ar, 1F), -162.4 (m, Ar, 2F). FT-IR (wavenumber, $cm^{-1}$): 1771 (C=O, ester), 1516 (C=C, Ar).

*Poly(pentafluorophenyl acrylate) (**P3**)*

In a typical RAFT polymerization a mixture of PFPA (3.5 g, 14.70 mmol), DDMAT (53.53 mg, 0.147 mmol, 1 eq) and AIBN (12.07 mg, 0.073 mmol, 0.5 eq) were dissolved in 1,4-dioxane (3.5 mL). The reaction mixture was degassed by five freeze-pump-thaw cycles, then the vessel was backfilled with $N_2$ and allowed to warm to room temperature. The reaction mixture was then placed in an oil bath at 80 ˚C, and the polymerization was quenched after 3 h by rapid freezing. The polymer was collected as a pale yellow solid by precipitation in MeOH twice. $^1$H NMR

($CDCl_3$, 300 MHz): δ 3.01 (br s), 2.42 (br s), 2.05 (br s). $^{19}F$ NMR ($CDCl_3$): δ -153.56 (br s), -156.72 (br s), -162.28 (br s). The composition of **P3** was determined by comparing the integral value of the CH and $CH_2$ protons on the polymer backbone with the integral value of the $CH_3$ protons of the CTA at the chain terminus. GPC Analysis of **P3** was performed indirectly following its conversion to p(DMA) by aminolysis revealing an $M_n$ of 10.5 kDa and a PDI of 1.28.

*di-tert-butyl(((disulfanediylbis(4,1-phenylene))bis(azanediyl))bis(3-oxopropane-3,1-diyl))dicarbamate (**16**)*

4-Aminophenyl disulfide (3.25 g, 13.08 mmol), 1-ethyl-3-(3-dimethylaminopropyl) carbodiimide (EDC) (7.52 g, 39.24 mmol) and boc-β-alanine-OH (6.19 g, 32.71 mmol) were dissolved in $CH_2Cl_2$ (100 ml) and the mixture was stirred at room temperature for 24 h. After this time a pale yellow precipitate had formed and was collected by filtration and washed with $CH_2Cl_2$ (4 x 50 ml) and $H_2O$ (3 x 50 ml). The product was dried *in vacuo* for 24 h (6.65g, 11.27 mmol, 86 %). $^1H$ NMR (DMSO-$d_6$, 300 MHz): δ 1.37 (s, 9H, $CH_3$), 2.47 (t, 2H, $CH_2$), 3.22 (m, 2H, $CH_2$), 6.86 (br t, 1H, NH), 7.43 (d, 2H, Ar, J = 9 Hz), 7.62 (d, 2H, J = 9 Hz), 10.01 (s, 1H, NH). $^{13}C$ NMR ($CDCl_3$, 75 MHz): δ 28.4, 36.6, 37.6, 78.9, 119.7, 129.4, 130.1, 139.5, 168.5. $HRMS^+$ $C_{28}H_{38}N_4O_6S$: Theoretical: 590.2233. Actual: 590.2239.

*tert-butyl (3-((4-mercaptophenyl)amino)-3-oxopropyl)carbamate (**17**)*

Compound **16** (6.35 g, 10.76 mmol) was added to a stirring suspension of sodium-3-mercapto-1-propanesulfonate (19.17 g, 107.6 mmol) and NaOH (3.43 g, 85.75 mmol) in MeOH (330 ml), stirring was continued at room temperature for 24 h. After this time the suspended solid was filtered off and MeOH was removed *in vacuo* and the residual amorphous solid redissolved in $H_2O$ (150 ml). The pH of the mixture was adjusted to pH 4.5 forming a white precipitate which was collected by filtration and washed with $H_2O$ (2 x 150), this was repeated once before collecting the product as a white amorphous solid (4.33 g, 14.50 mmol, 68 %).$^1H$ NMR (DMSO-$d_6$, 300 MHz): δ 1.38 (s, 9H, $CH_3$), 2.45 (t, 2H, $CH_2$), 3.19 (m, 2H, $CH_2$), 6.85 (br t, 1H NH), 7.22 (d, 2H, Ar J = 8.7), 7.49 (d, 2H, Ar J = 8.7), 9.90 (s, 1H NH). $^{13}C$ NMR ($CDCl_3$, 75 MHz): δ 28.4, 36.6, 37.6, 78.9, 120.6, 125.2, 130.6, 136.2, 156.5, 169.8. $HRMS^+$ $C_{14}H_{20}N_2O_3S$: Theoretical: 296.1195. Actual: 296.1194.

*tert-butyl (3-((4-(tert-butyldisulfanyl)phenyl)amino)-3-oxopropyl)carbamate (**18**)*

Compund **17** (4.15 g, 13.91 mmol) was dissolved in $CH_2Cl_2$ (130 ml) at 0 $^oC$ with stirring. 2-Methyl-2-propanethiol (1.57 ml/1.26 g, 13.91 mmol) was added in one portion followed quickly by one portion addition of 2,3-Dichloro-5,6-dicyano-1,4-benzoquinone (DDQ) (3.31 g, 14.60 mmol). After 20 min a deep green colour was observed. $CH_2Cl_2$ was removed *in vacuo* and the crude solid was finely suspended in a mixture of $CH_2Cl_2$:MeOH (95:5 v/v, 80 mL) and filtered. The filtrate was then followed by purification by column chromatography [$SiO_2$, $CH_2Cl_2$:MeOH (95:5, v/v)] to afford the title product as a brown amorphous solid (2.64 g, 6.89 mmol, 65 %).$^1$H NMR (DMSO-$d_6$, 300 MHz): δ 1.26 (s, 9H, $CH_3$), 1.37 (s, 9H, $CH_3$), 2.47 (t, 2H, $CH_2$), 3.20 (m, 2H, $CH_2$), 6.87 (br t, 1H NH), 7.48 (d, 2H, Ar J = 9.0), 7.60 (d, 2H, Ar J = 9.0), 10.01 (s, 1H, NH). $^{13}$C NMR ($CDCl_3$, 75 MHz): δ 28.2, 29.5, 36.5, 49.1, 77.6, 119.6, 128.3, 131.1, 138.3, 155.5, 169.5. HRMS$^+$ $C_{18}H_{28}N_2O_3S_2$: Theoretical: 384.1541. Actual: 384.1544

*3-amino-N-(4-(tert-butyldisulfanyl)phenyl)propanamide (**19**)*

Compound **18** (2.0 g, 5.22 mmol) was added to a 1:2 (v/v) mixture of TFA:$CH_2Cl_2$ (9 ml) with stirring. After 3 hours the solvent was removed *in vacuo* and repeated co-evaporation with MeOH (8 x 50 ml) removed residual acid. The product was collected as a brown oil (1.71 g, 4.28 mmol, 82 %). $^1$H NMR (DMSO-$d_6$, 300 MHz): δ 1.26 (s, 9H, $CH_3$), 2.42 (t, 2H, $CH_2$), 2.86 (m, 2H, $CH_2$), 7.48 (d, 2H, Ar J = 9.0), 7.60 (d, 2H, Ar J = 9.0), 10.01 (s, 1H, NH). $^{13}$C NMR ($CDCl_3$, 75 MHz): 48.6, 81.0, 119.6, 128.3, 131.1, 138.3, 169.5. HRMS$^+$ $C_{13}H_{20}N_2O_1S_2$: Theoretical: 284.1017. Actual: 284.1019

*Thiol-Functionalized Copolymer **P4***

Poly(pentafluorophenyl acrylate) **P3** (1.0 g, 46 µmol) was dissolved in THF (5 mL) and stirred for 5 min. Hünig's Base (50 mg, 0.39 mmol) was added in one portion followed by the addition of **19** (280 mg, 0.75 mmol). The mixture was stirred at 40 $^oC$ for 1 h after which time a large excess of dimethylamine (DMA) solution (5 ml, 2.0 M in THF) was added. After stirring for 3 h at 40 $^oC$, the white precipitate was filtered and the filtrate evaporated to dryness to remove THF and residual dimethylamine. The crude brown material was redissolved in THF (5 mL) and precipitated by dropwise addition into ice-cold $Et_2O$ (300 mL). The pale brown precipitate was collected by filtration and precipitated twice more in $Et_2O$ (300 mL) from THF (5 mL). Pendant disulfide copolymer **P4b** was collected and dried under high vacuum affording an amorphous pale brown solid (360 mg, 31 µmol, 67 %). $^1$H NMR ($CDCl_3$, 300 MHz): δ 1.24 (9H, br s, $C(CH_3)_3$),

1.48-1.75 (2H, br, CHC*H*$_2$, polymer backbone), 2.55 (1H, br, C*H*CH$_2$, polymer backbone), 2.75-2.98 (6H, br s, NCH$_3$) 7.30-7.55 (4H, br, Ar). The composition of **P4b** was determined to be 1:5 (thiol:DMA) by comparing the integral value of the C(CH$_3$) *t*- butyl group and aromatic protons with the integral value of the CH$_3$ protons of the CTA at the chain terminus. GPC Analysis in DMF + 1 g.L$^{-1}$ LiBr (0.6 mL min$^{-1}$) revealed an $M_n$ of 11.5 kDa and a PDI of 1.24 when analysed against a set of near-monodisperse poly(methyl methacrylate) standards. Copolymer **P4b** (300 mg, 26.1 µmol) was dissolved in MeOH and TCEP.HCl (25 mg, 87.1 umol) was added in one portion. The solution was stirred at room temperature for 18 h, after this time thiol-functionalized copolymer **P4** was purified by dialysis for 2 d in a 1:1 (v/v) MeOH:CH$_2$Cl$_2$ mixture. Copolymer **P4** was collected by removal of the dialysate *in vacuo* to afford a pale brown, slightly crystalline solid (140 mg, 14 µmol, 53 %). $^1$H NMR (CDCl$_3$, 300 MHz): δ 1.48-1.75 (2H, br, CHC*H*$_2$, polymer backbone), 2.55 (1H, br, C*H*CH$_2$, polymer backbone), 2.75-2.98 (6H, br s, NCH$_3$) 7.05-7.5 (4H, br, Ar). The composition of **P4** could be inferred from the composition of **P4b** to be 1:5 (thiol:DMA) as it was extremely unlikely that C-C bonds within the polymer backbone were broken under the reaction conditions. GPC Analysis in DMF + 1 g.L$^{-1}$ LiBr (0.6 mL min$^{-1}$) revealed an $M_n$ of 11 kDa and a PDI of 1.25 when analysed a set of near-monodisperse poly(methyl methacrylate) standards.

*Preparation of Imine Cross-Linked Nanoparticle **NP1***

Copolymer **P1** (20.1 mg, 1.6 umol) was dissolved in H$_2$O (1 mL) and 100 µL of THF added to aid solubiity. A separate solution of **P2** (20. 0 mg, 2.2 umol) was then prepared in H$_2$O (1 mL). The pH of both solutions was adjusted to pH 7 by the addition of 5 µL aliquots of 0.1 M HCl until the pH remained stable for 10 min. The solutions were mixed rapidly with stirring and the pH was adjusted slowly to pH 11.0 with 5 µL aliquots of 0.1 M NaOH over 6 h. After 6 h and when the solutions pH had stabilised at pH 11, the solution was stirred vigorously for a further 18 h at room temperature open to the atmosphere to aid the evaporation of THF. After this time aliquots (2 x 300 µL) of the reaction mixture were taken for analysis by GPC by direct aqueous injection and online batch DLS measurements.

*Preparation of Disulfide Cross-Linked Nanoparticle **NP2***

Copolymer **P4** (40.5 mg, 4.1 umol) was dissolved in H$_2$O (2 mL) and 1.0 M NaOH added to raise the pH of the solution to pH 7. After **P4** had dissolved and the pH of the solution stabilised between 7.0 and 7.5 for at least 15 min, the reaction vessel was tightly sealed and the

temperature was slowly raised to 55 °C after which the solution was stirred vigorously for 3 h. An aliquot of 1 M $H_2O_2$ (15 µL) was added each day for 14 days whilst stirring was continued at this temperature. Care was taken to ensure the pH did not fall below pH 7.0, with 0.1 M NaOH was added in small quantities (< 5 µL) as necessary. After 14 d the reaction mixture was analysed by GPC by direct aqueous injection and online batch DLS.

*Disassembly of Imine Cross-linked **NP1***

To an aqueous solution of **NP1** (2 wt %, 1 mL total volume) at pH 11, 1.0 M HCl was added in 20 µL aliquots with vigorous stirring until the pH was stable between pH 5.5 and pH 6. The mixture was stirred at 60 °C for 48 h after which time 300 µL aliquots were taken for analysis by GPC and DLS.

*Disassembly of Disulfide Cross-linked **NP2***

To an aqueous solution of **NP2** (2 wt %, 1 mL total volume) at pH 7, an excess of TCEP.HCl (50 mg, 0.172 mmol) was added and the temperature of the solution raised to 60 °C. Stirring was continued at this temperature for 72 h after which time a 300 µL aliquot was taken for analysis by GPC and DLS.

*Probing the Concentration Dependence of Disulfide Nanoparticle Formation*

In a typical experiment, **P4** was dissolved in $H_2O$ and the pH of the solution was adjusted to pH 7.0 – 7.2 with 1.0 M NaOH. The solution was stirred at 55 °C and 1 M $H_2O_2$ was added slowly using a syringe pump over the course of 7 d until a maximum of 2 equivalent with respect to the total number of pendant thiols in solution had been added. The solution was analysed by direct aqueous injection GPC analysis and online batch DLS. The above protocol was repeated at four concentrations: 1, 2, 3 and 5 wt % with respect to the total amount of polymer **P4** in solution.

*'Dual-protected' Disulfide and Acetal Terpolymer **P5***

Poly(pentafluorophenyl acrylate) **P3** (1.0 g, 46 µmol) was dissolved in THF (5 mL) and stirred for 5 min. Hünig's Base (40 mg, 0.31 mmol) was added in one portion followed by the addition of **19** (260 mg, 0.70 mmol) and **10** (164 mg, 0.69 mmol) with stirring. The mixture was stirred at 35 °C for 1.5 h after which time dimethylamine (DMA) solution (2.0 M in THF) was added in excess (4 mL). After stirring for 3 h at 35 °C, the white precipitate was filtered and the filtrate

evaporated to dryness to remove THF and residual dimethylamine. The crude brown material was dissolved in $CH_2Cl_2$ (15 mL) and dialysed in $CH_2Cl_2$ for 3 d. The dialysate was removed *in vacuo* and pendant disulfide and acetal copolymer **P5** was collected and dried under high vacuum affording an amorphous pale brown solid (248 mg, 21 µmol, 46 %). $^1$H NMR ($CDCl_3$, 300 MHz): δ 1.20 (9H, br, C(C*H*$_3$)$_3$), 1.45-1.8 (2H, br, CHC*H*$_2$, polymer backbone), 2.62-2.93 (6H, br s, $NCH_3$), 3.18-3.29 ($OCH_3$), 5.25-5.37 (C*H*($OCH_3$)$_2$), 7.25-7.8 (8H, br, Ar).

*'Dual-protected' Disulfide and Boc-amine Terpolymer **P8***

Poly(pentafluorophenyl acrylate), **P3** (1.0 g, 46 µmol), was dissolved in THF (5 mL) and stirred for 5 min. Hünig's Base (40 mg, 0.31 mmol) was added in one portion followed by the addition of disulfide containing amine **19** (260 mg, 0.70 mmol) and *boc*-protected amine **5** (142 mg, 0.81 mmol) with stirring. The mixture was stirred at 35 $^o$C for 1.5 h after which time DMA solution (2.0 M in THF) was added in excess (4 mL). After stirring for 3 h at 35 $^o$C, the white precipitate was filtered and the filtrate evaporated to dryness to remove THF and residual dimethylamine. The crude brown material was dissolved in $CH_2Cl_2$ (15 mL) and dialysed in $CH_2Cl_2$ for 3 d. The dialysate was removed *in vacuo* and pendant disulfide and acetal copolymer **P5** was collected and dried under high vacuum affording an amorphous pale brown solid (312 mg, 25 µmol, 54 %). $^1$H NMR ($CDCl_3$, 300 MHz): δ 1.15 (br s), 1.21 (9H, br, C(C*H*$_3$)$_3$), 1.32 (9H, br, C(C*H*$_3$)$_3$) 1.50-1.76 (2H, br, CHC*H*$_2$, polymer backbone), 2.64-2.90 (6H, br s, $NCH_3$), 7.30-7.65 (4H, br, Ar).

# Chapter 4

## *Dynamic Covalent Imine and Disulfide Cross-linked Hydrogels*

# Table of Contents

## 4.1 Abstract

*Water soluble amine-, aldehyde- or thiol-bearing random copolymers were prepared using reversible addition-fragmentation chain transfer (RAFT) polymerization coupled with post-polymerization modification. Conditions were successfully established for the stimuli-responsive formation of imine or disulfide cross-linked hydrogel materials from the preformed polymeric building blocks and the mechanical properties of the hydrogels were probed using rheological analysis. It was demonstrated that the mechanical properties of imine and disulfide cross-linked hydrogels depended strongly on the structural nature and total concentration of the polymeric building blocks utilized. The formation of an imine and disulfide dual cross-linked interpenetrating network was achieved which was shown to exhibit a higher storage modulus (G') compared with the G' values for the imine or disulfide 'single' networks. An initial investigation into the orthogonal cleavage of imine and disulfide dynamic covalent bonds within the interpenetrating network structure yielded intractable precipitates rather than the expected disulfide or imine cross-linked semi-interpenetrating network.*

## 4.2 Introduction

Significant progress has been made in the development of stimuli-responsive chemically cross-linked hydrogels— a class of covalently cross-linked material wherein $H_2O$ is used as the swelling agent— which, in their swollen gel state, are capable of responding to external stimuli such as changes in pH,[98] temperature,[99] ionic strength,[100] light,[101] electric field[102] and magnetic field.[103] The utility of dynamic covalent chemistry (DCC) has been a key driver in the increasing ability of researchers to impart covalently cross-linked gels with stimuli-responsive properties. The capacity for dynamic covalent bonds such as disulfides, hydrazones and boronic acids to undergo component exchange processes under specific conditions provides a molecular-level mechanism through which gels can adjust their volume and mechanical properties on the macroscale, adopting macroscopic flow and stress-relaxation characteristics classically associated with physical gels. This feature has led to a broad range of stimuli-responsive gels exhibiting vastly different mechanical properties designed to serve a multitude of functions. Examples include self-healing gels,[68, 104] gel-based sensors,[18c, 105] controlled release in drug delivery,[106] tissue engineering[107] and nanomedicine.[108]

Recent progress in the field of stimuli-responsive hydrogels has highlighted the demand for more sophisticated systems which are capable of more complex, multi-faceted stimuli-responsive behaviors. This has drawn attention to the implementation of

orthogonality within responsive gel systems, that is to say, gels which can respond in multiple ways to more than one contrasting external stimuli. Careful selection of multiple orthogonal DCBs provides an opportunity to pre-programme covalent adaptable networks with orthogonal stimuli-responsive behaviors. The utility of orthogonal dynamic covalent bonds has been exploited in several recently reported studies,[23, 68] however, there still remains an extensive amount of work to do to increase the complexity of 'smart' gel-based systems.

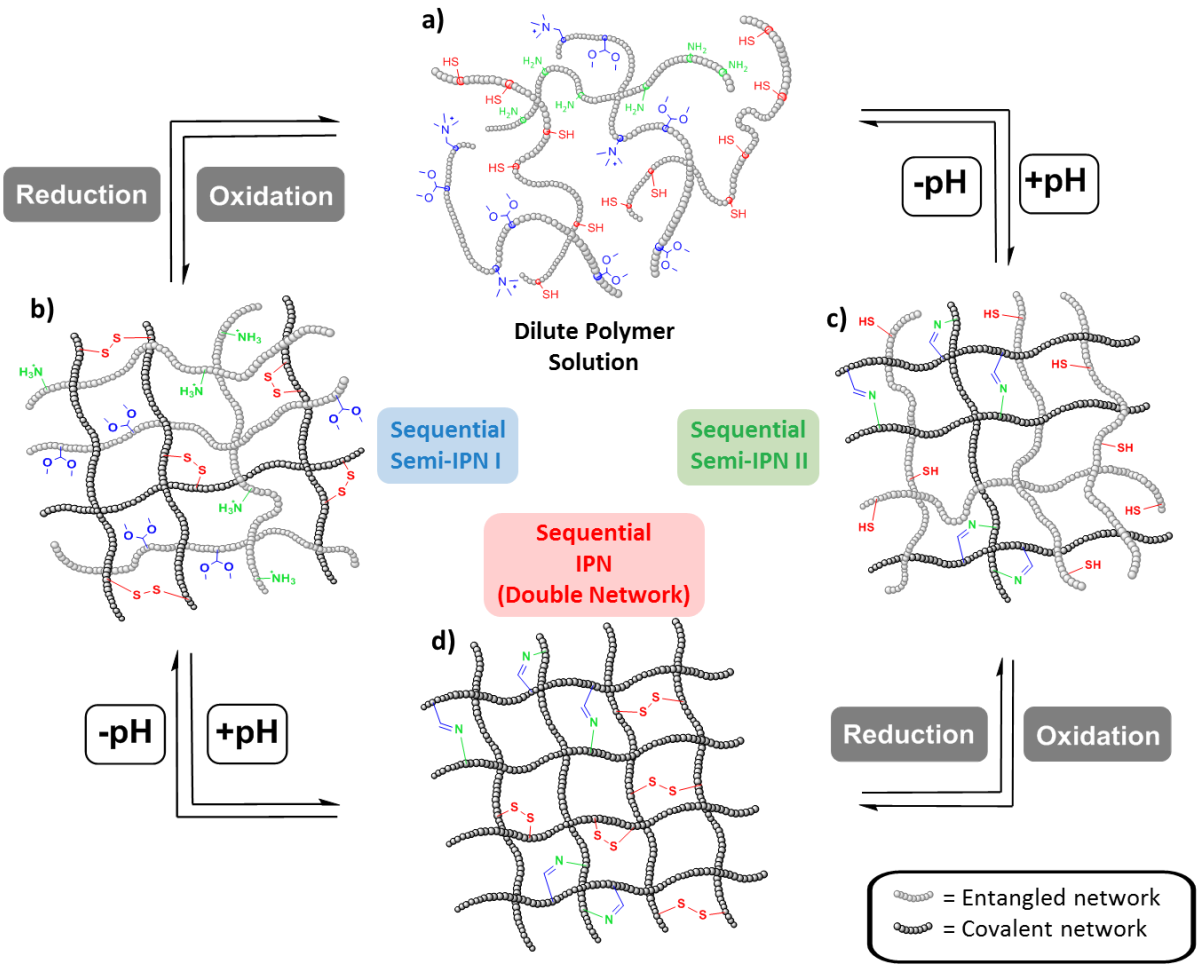


Figure 4.1 Schematic representation of '4-node network'. Considering only situations in which imine and disulfide DCBs are in either ''broken'' or ''formed'' states, there are four distinct scenarios which can be mapped onto a four-node network. a) Dilute polymer solutions consisting of random terpolymers. b) Disulfide cross-linked semi-interpenetrating network. c) Imine cross-linked semi-interpenetrating network. d) Imine and disulfide dual cross-linked double network.

In this work a system was designed consisting of functional polymeric building blocks which were cross-linked by the formation of disulfide and/or imine dynamic covalent bonds

to form a hydrogel (Figure 4.1). It was hypothesized that the presence of two orthogonal and reversible dynamic covalent bonds—disulfide (redox-sensitive) and imine (pH sensitive)—would give rise to a stimuli-responsive behavior which can be mapped onto a '4-node network'. Within the boundaries of the four node network, and considering only situations in which DCBs are in either ''broken'' or ''formed'' states, the system can interconvert between four distinct states (Figure 4.1, a-d) depending on the order in which orthogonal stimuli are applied. From a dilute solution of preformed functional polymers (Figure 4.1, a) intermolecular imine bonds would be formed in response to an increase in pH or disulfide bonds in the presence of suitable chemical oxidizing agents forming *either* an imine *or* disulfide cross-linked semi-interpenetrating network, **semi-IPN I** or **II**, respectively (Figure 4.1 b, c). Interconversion of imine cross-linked **semi-IPN I** to a dual-cross linked (imine and disulfide) interpenetrating network (**IPN**) (Figure 4.1 d) would be achieved by the introduction of chemical oxidizing agents which encourages the formation intermolecular disulfide bonds. Disulfide cross-linked **semi-IPN II** would then be converted to the corresponding **IPN** in response to an increase in pH which drives the formation of intermolecular imine bonds.

## 4.3 Results and Discussion

### 4.3.1 *Imine cross-linked hydrogels*

The first objective was to prepare water-soluble polymer building blocks capable of forming imine dynamic covalent cross-links. A new set of suitable copolymers were developed which were structurally similar to those described in the previous chapter. The new set of target polymers were designed to exhibit greater polarity and a higher density of fuctional groups. This would allow for the formation of more cross-links which was reasoned to increase the chance of forming gels at lower total polymer concentrations. Copolymer **P12** was prepared using a post-polymerization modification strategy similar to that described in Chapter 3, wherein, p(PFPA) (**P3**) was prepared by RAFT polymerization of pentafluorophenyl acrylate affording an activated ester scaffold onto which amine **10** was grafted by aminolysis followed by subsequent reaction with dimethylamine to furnish copolymer **P11**. It was intended to maintain the dimethyl acetal functionality in the final composition of copolymer **P12** to prove an additional protection against hemithioacetal formation. Prior to dimethyl acetal hydrolysis there is no electron-deficient aldehyde to engage in undesirable hemithioacetal formation

with polythiols. Girard's reagent T (**20**) was added in acidic MeOH to afford target copolymer **P12** whose poly-cationic nature imparts improved water-solubility. It was chosen to introduce cationic charge in this manner as it provided a facile way of introducing a small amount of solubilizing charge, it was simply not suitable to use aldehyde containing copolymers from the previous chapter on account of their inherently low solubility. Initial experiments demonstrated that significantly higher polymer concentrations were needed to form hydrogels than was possible to obtain. Pendant-amine bearing copolymer **P14** was prepared by aminolysis of **P3** with commercially available *N*-Boc-1,3-propanediamine (**13**) followed by reaction with excess dimethylamine to afford copolymer **P13**. Reaction of **P13** with TFA in $CH_2Cl_2$ resulted in cleavage of its *N*-boc moieties followed by precipitation in $Et_2O$ to furnish amine-bearing copolymer **P14**.

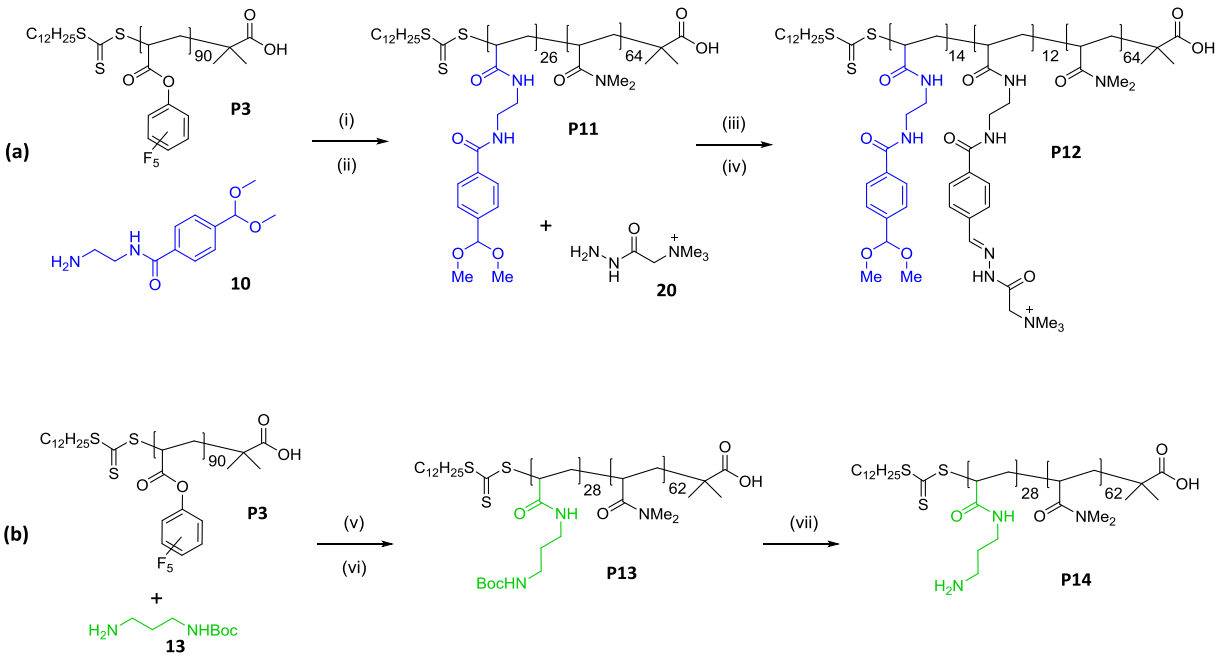


Scheme 4.1 Synthetic route to (a) aldehyde- and (b) amine-functional acrylamido copolymers **P12** and **P14**. (i) DIPEA, THF, 25 °C 2 h. (ii) DMA, THF, 25 °C 1 h. (iii) Girard's reagent T (**20**), MeOH, 6 h, 35 °C. (iv) HCl, MeOH, 25 °C, 1 h. (v) DIPEA, THF, 25 °C, 2 h. (vi) DMA, THF, 25 °C 1 h. (vii) TFA/$CH_2Cl_2$ (1:1, v/v), 3 h.

Upon successful preparation of polymer building blocks **P12** and **P14**, their capacities to form imine cross-linked hydrogels was investigated. A series of five cross-linking experiments at a range of copolymer concentrations were performed to establish an approximate critical gelation concentration of an aqueous solution of **P12** and **P14**. The copolymer stoichiometries

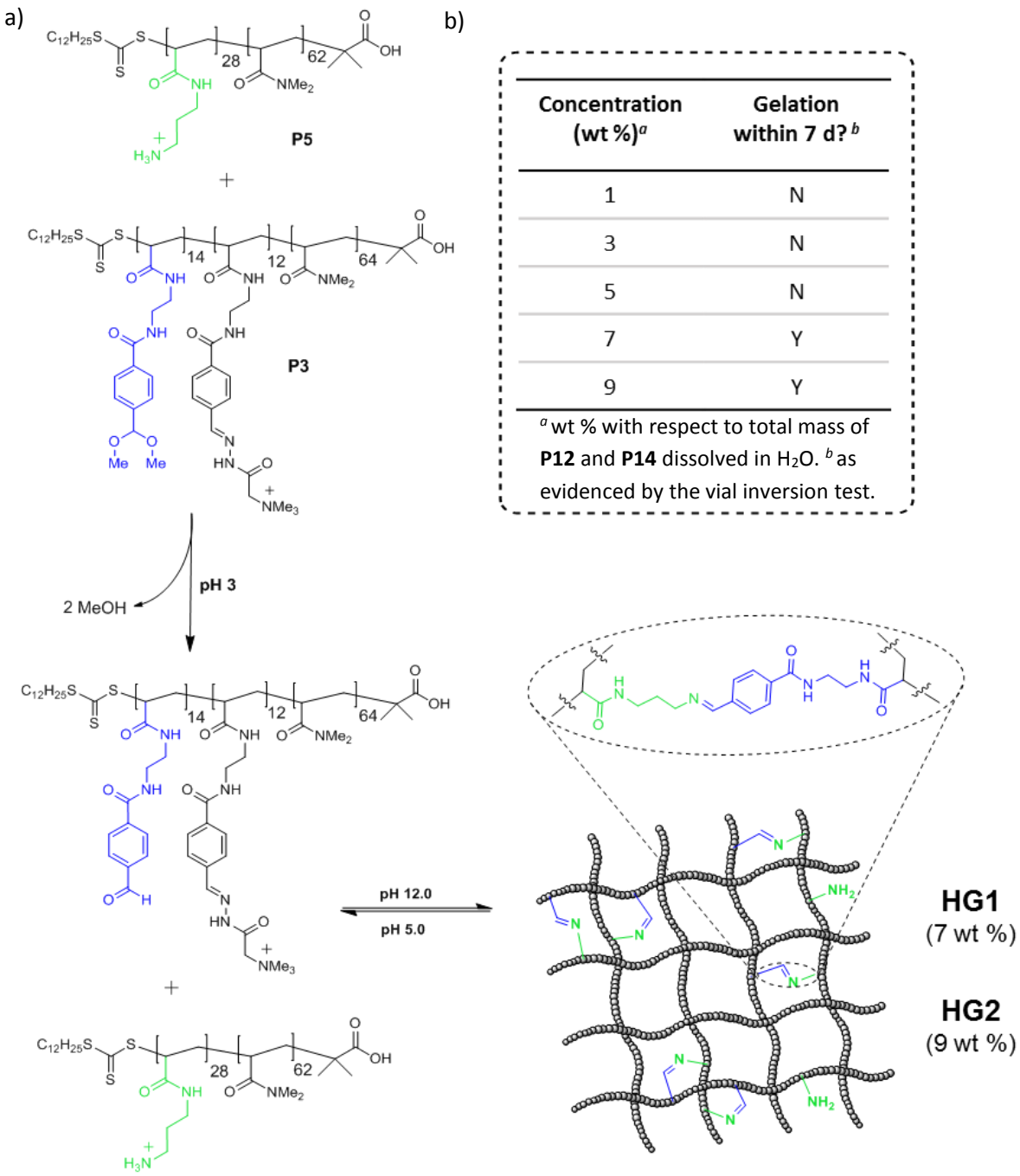


| Concentration (wt %)[a] | Gelation within 7 d? [b] |
|---|---|
| 1 | N |
| 3 | N |
| 5 | N |
| 7 | Y |
| 9 | Y |

[a] wt % with respect to total mass of **P12** and **P14** dissolved in $H_2O$. [b] as evidenced by the vial inversion test.

Figure 4.2 a) Preparation of imine cross-linked hydrogel **HG1** and **HG2** from pre-formed polymeric building blocks **P14** and **P12**. b) Concentration dependant initial gelation studies of **P12** and **P14**.

were set to equimolar concentrations of amine and dimethyl acetal functionalities in each solution. Solutions were prepared in acidic $H_2O$ (pH 3) at concentrations of 1, 3, 5, 7 and 9 wt % with respect to the total mass of copolymers (**P12** + **P14**). With the aid of sonic agitation polymers **P12** and **P14** dissolved rapidly at all five concentrations. At pH 3, rapid *in-situ* hydrolysis of the dimethyl acetal moieites in **P12** occurred liberating its corresponding aldehyde which is then capable of participating in the formation of imine cross-links with the

pendant amines of **P14** (Figure 4.2). To drive imine formation, the pH of each solution was rapidly adjusted to pH 12.0 with aliquots of 1.0 M NaOH. The solutions were allowed to stand for up to 7 d at 25 $^{o}$C and pH was carefully maintained between pH 11.8 and pH 12.0. No gelation was observed at concentrations of 1, 3 and 5 wt %, however, at 7 and 9 wt % the formation of a macroscopic imine cross-linked polymer networks (**HG1** and **HG2**, respectively) had occurred as evidenced by the vial-inversion test. This observation suggests the critical gelation concentration for an aqueous solution of **P12** and **P14** at pH 12 is between 5 and 7 wt %. As observed by vial-inversion, the formation of **HG1** occurred over approximately 3 h whereas the formation of **HG2** occurred within 10 min following addition of 1.0 M NaOH.

The mechanical properties of **HG1** and **HG2** were investigated using oscillatory shear rheology. Initially, a time-sweep measurement was performed on both hydrogels to determine the values of the storage modulus (G') and the loss modulus (G") for hydrogels **HG1** and **HG2**. The value of G' is an indication of the ability of a hydrogel to store elastic energy upon the application of an oscillatory shear deformation.[109] The value of G" is an indication

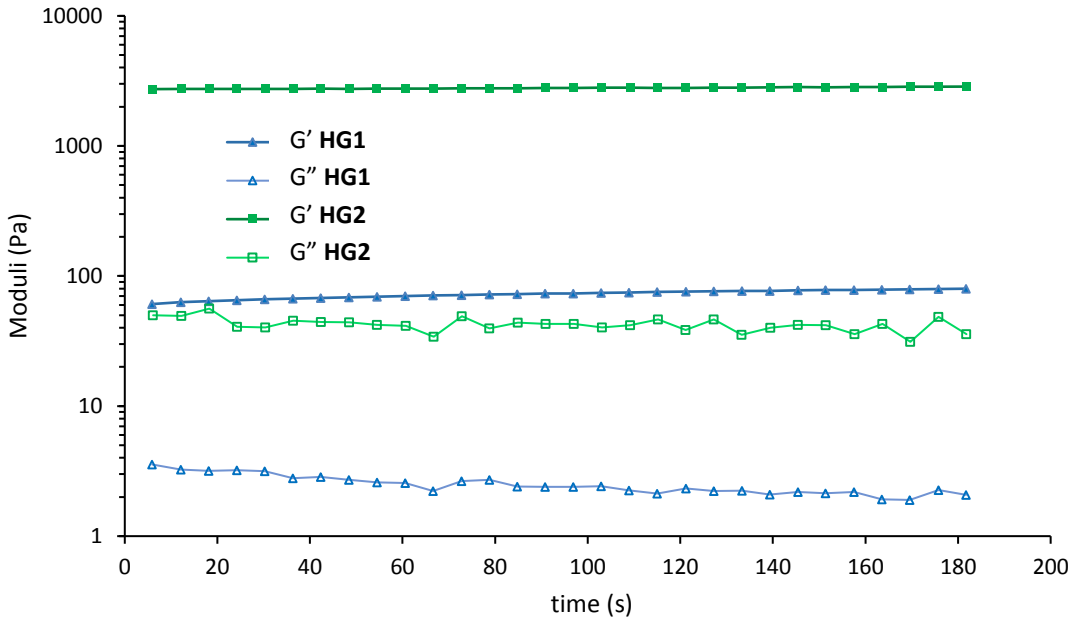


Figure 4.3 Time-sweep oscillatory rheological analysis of imine hydrogels **HG1** and **HG2**.

of a material's capacity to dissipate energy as heat and represents its viscous properties. The measurements were taken 24 h after gelation to ensure the gelation processes were complete. The time-sweep experiment was conducted over a time-scale of 200 s at a fixed

frequency 1 Hz and a percentage strain of 1%. As evidenced by the rheological data (Figure 4.3), G' was larger than G" for both **HG1** and **HG2** an observation suggesting these materials exhibit a viscoelastic nature. Values of G' for **HG1** and **HG2** were measured to be 70 Paand 2800 Pa, respectively, indicating **HG2** is a considerably stronger hydrogel exhibiting greater mechanical rigidity than **HG1**. This difference is most likely on account of a greater number of imine cross-links present in **HG2** compared with **HG1**, as the magnitude of G' is linked to a hydrogel's cross-link density by rubber elasticity theory.[110] Furthermore, there is most likely a larger contribution to the structural stability of **HG2** from hydrogen bonding interactions on account of a higher total polymer concentration. The values of G' and G" remain more or less constant for both **HG1** and **HG2** across the 200 s time-scale measured suggesting they undergo no structural change over the time-scale measured. It is known[107c, 111] that 'grip-slip'—a phenomena caused by $H_2O$ expulsion from the hydrogel during application of shear stress—may be reflected in G" resulting in an erratic nature in the value of G" as observed in Figure 4.3. It is worth noting that erratic here does not imply a significant trend, simply non-uniform oscillation about a mean value of G".

A strain-sweep analysis was undertaken in which **HG1** and **HG2** were subjected to an increasing oscillatory shear stress at constant frequency of 1 Hz. Such analysis provides insights into the effect of increasing strain amplitude on values of G' and G" which provides

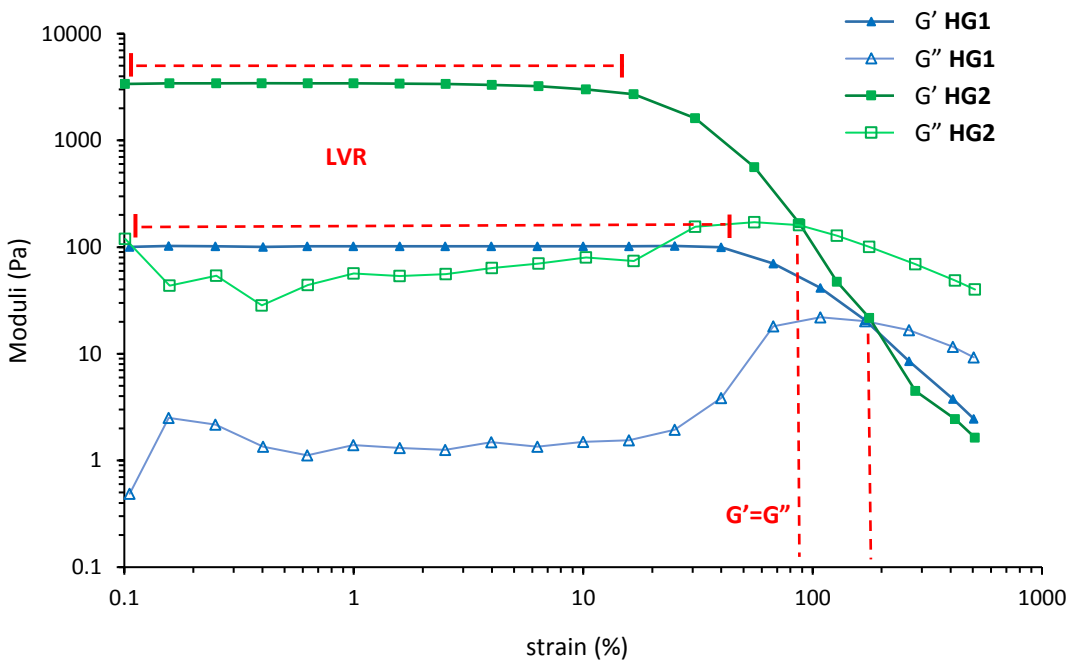


Figure 4.4 Strain-sweep oscillatory rheological analysis of imine hydrogels **HG1** and **HG2**.

an opportunity to probe flexibility and strength in viscoelastic material. As observed in the strain-sweep plot (Figure 4.4) both **HG1** and **HG2** display linear regions where G' is independent of strain amplitude. The range of % strain under which the hydrogel material exhibits this linear behaviour is known as the linear viscoelastic region (LVR). Within the LVR, the microstructure of **HG1** and **HG2** remain intact irrespective of the magnitude of the applied strain, therefore, to ensure compliancy with the principle of small deformation rheology,[109] it is necessary that hydrogel materials are analyzed within the LVR with respect to applied shear stress. The respective LVR values for **HG1** and **HG2** were determined to be 40 and 16 % strain, respectively, suggesting **HG1** undergoes structural breakdown at a larger critical strain value than **HG2**. This observation indicates that **HG1** is more flexible than **HG2** as it retains its structural integrity up to higher values of % strain. Furthermore, the greater flexibility of **HG1** compared with **HG2** is reflected in the G'=G" 'cross-over point'—considered as the value of % strain necessary to induce a gel-sol transition, beyond which, structural breakdown occurs, viscoelasticity is lost and viscous properties dominate with the values of G">G'. For **HG1** and **HG2**, G'=G" at 170 % and 130 % strain, respectively.

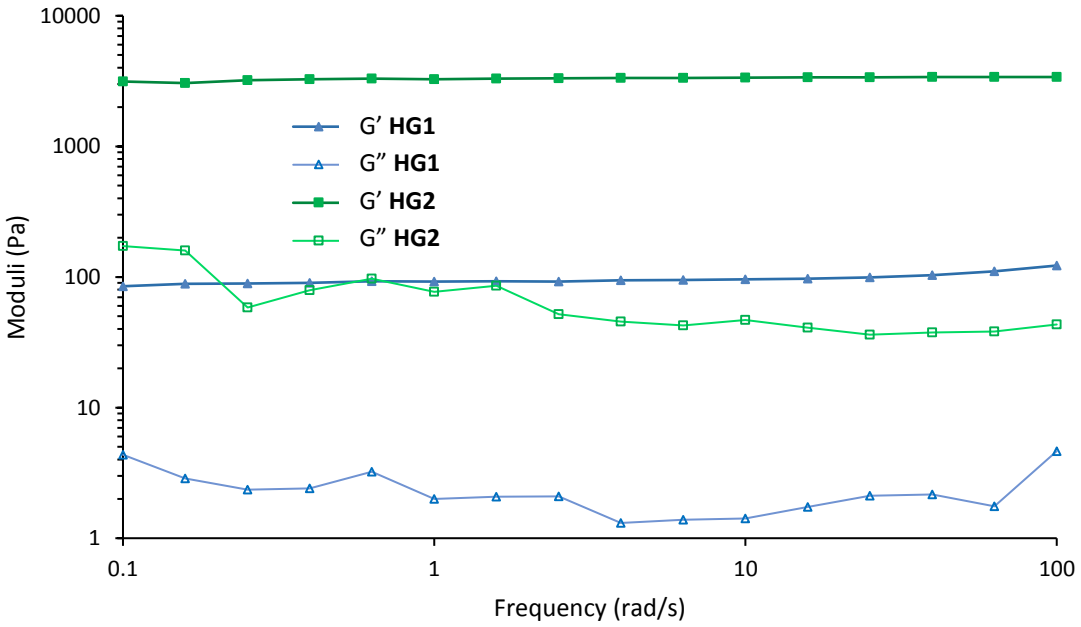


Figure 4.5 Frequency-sweep oscillatory rheological analysis of imine hydrogels **HG1** and **HG2**.

Frequency-sweep oscillatory rheology was performed to further understand the stability and nature of macroscopic covalently cross-linked polymer networks by probing the material's response to repeated deformation at different time-scales[109]. In response to

imposed oscillatory strain at sufficiently high frequencies, viscoelastic materials will exhibit an inability to relax between oscillations, aside from the very fastest of its relaxation processes (e.g. polymer side-group bond rotation), between increasingly rapid oscillations. This feature manifests as an increase in the value of G' tending towards higher frequencies—diagnostic of an increase in solid-like character— as the material 'stiffens-up' through failure to relax. As the frequency of imposed oscillatory strain is reduced, longer length-scale relaxation processes, relating to curvilinear diffusion of large segments of the polymer matrix throughout the hydrogel's macrostructure or adjacent chain slippage/disentanglement, are allowed sufficient time to occur. Thus, the value of G' remains constant on account of the time-scales of these processes being shorter than the time-scales of imposed mechanical motion–the hydrogel matrix fully relaxes between imposed oscillations. By performing frequency-sweep measurements to gauge the relationship between G' and angular frequency, information can be brought to light relating to the microstructural nature of covalently cross-linked hydrogels. Thus, frequency-sweep measurements were performed on **HG1** and **HG2** (Figure 4.5) at a fixed percentage strain of 1% and over a frequency range of 0.1 – 100 rad/s (near the upper limit of the rheometer upon which measurements were conducted). As observed in the rheological data, the values of G' for **HG1** and **HG2** do not exhibit frequency dependency. This observation indicates that **HG1** and **HG2** are well formed hydrogels whose structure does not permit adjacent polymer chains to slip past each other or segmental diffusion of large regions of aggregated polymer (longer time-scale relaxation processes), which is characteristic of densely cross-linked polymer matrices. It was reasoned that the large number of imine cross-links present in **HG1** and **HG2** result in stable linkages between all polymer chains and thus longer time-scale relaxation phenomena cannot occur.

The reversibility of the formation of **HG1** and **HG2** was investigated. The pH of the **HG1** and **HG2** was reduced to pH 5 by addition of 1 M HCl and the mixture was heated at 40 $^{o}$C. Under these conditions dissolution of both **HG1** and **HG2** occurred over 6 h as confirmed by the vial-inversion test. This observation suggests that the pH-sensitive formation of **HG1** and **HG2** by cross-linking **P12** and **P14** is a reversible process.

### 4.3.2 *Disulfide cross-linked hydrogels*

The protocol for the preparation of pendant thiol containing polymers was adopted from that described in Chapter 3. Homopolymer p(PFPA) (**P1**) was reacted with disulfide-containing

amine **3** (Scheme 4.2) followed by the addition of excess dimethylamine to afford copolymer **P6**. The pendant disulfide containing moieties in **P6** were cleaved using TCEP to furnish pendant thiol copolymer **P7**. An acrylic acid-based structural analogue of **P7** was prepared (Scheme 4.2) in which amine **3** was reacted with **P1** followed by refluxing in basic $H_2O$ (pH 11.0) for 48 h to afford polymer **P8**. Pendant thiol-containing **P9** was achieved using TCEP.

To investigate the formation of disulfide cross-linked hydrogels (Figure 4.6), copolymer **P7** was dissolved in $H_2O$ at pH 8.0 at 1, 3, 5, 7 and 9 wt %. To drive cross-linking, $H_2O_2$ (1 M) was added

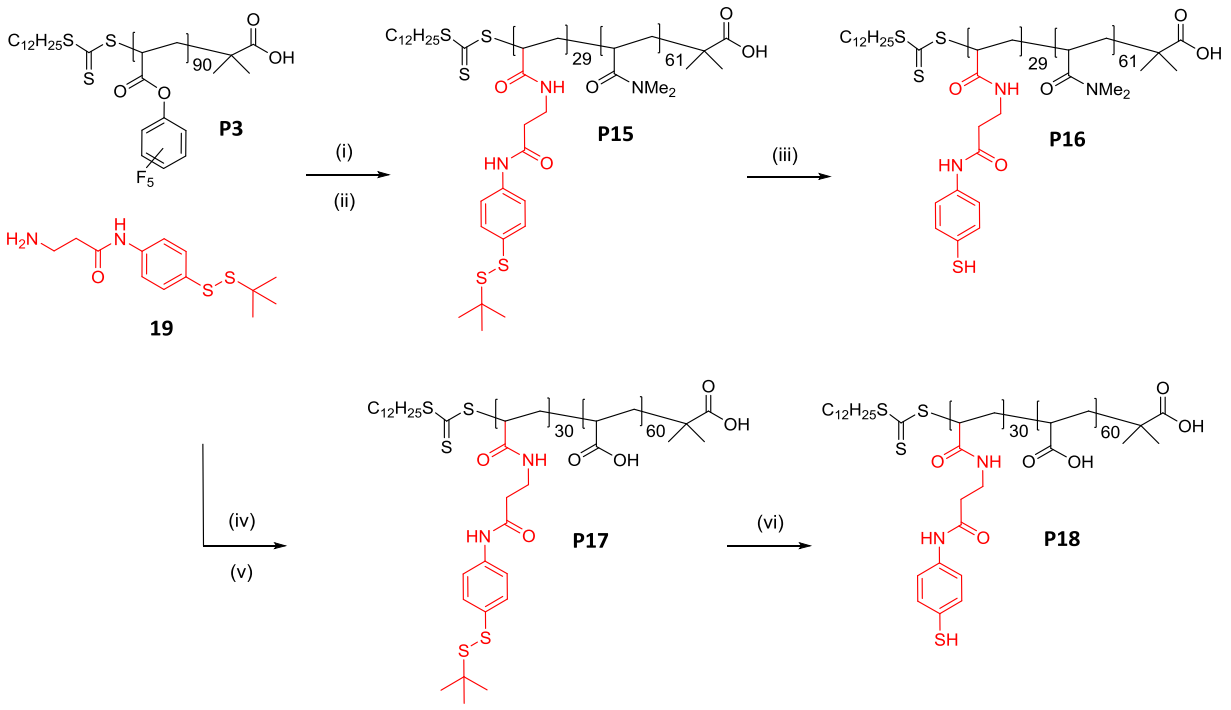


Scheme 4.2 Synthesis of thiol-functional copolymers **P16** and **P18**. (i) DIPEA, THF, 25 °C, 3 h. (ii) DMA, THF, 25 °C. (iii) TCEP, MeOH, 35 °C, 6 h. (iv) DIPEA, THF, 25 °C, 3 h. (v) NaOH, $H_2O$, THF, 25 °C, 48 h. (vi) TCEP, MeOH, 35 °C, 8 h.

in one portion (2 equivalents with respect to the total number of thiols in each solution) and the solutions were gently agitated and then allowed to stand for up to 7 d at room temperature. After this time the solutions at concentrations of 1, 3, 5 and 7 wt % afforded no visible gels, as evidenced by the vial inversion test. At a concentration of 9 wt % a gel-like material had formed within 7 d, and these results suggest that the critical gelation concentration of an aqueous solution of **P16** at pH 8 is therefore between 7 and 9 wt %.

To investigate the capacity for copolymer **P18** to form disulfide cross-linked hydrogels, solutions of **P18** were prepared in $H_2O$ at pH 8 at copolymer concentrations of 1, 3, 5, 7 and 9 wt %. $H_2O_2$ (1 M) was added and the solutions stood for 7 d. No gelation was observed at concentrations of 1, 3, and 5 wt % after 7 d, however, solutions at 7 and 9 wt % yielded gel-

like materials, suggesting that the critical gelation concentration of a solution of **P18** is between 5 and 7 wt %, slightly lower than the critical gelation concentration determined for copolymer **P16.** These results suggest acrylic acid copolymer **P18** is a more effective gelator than acrylamido copolymer **P16** in aqueous solutions using $H_2O_2$ as the oxidizing agent. To determine values of

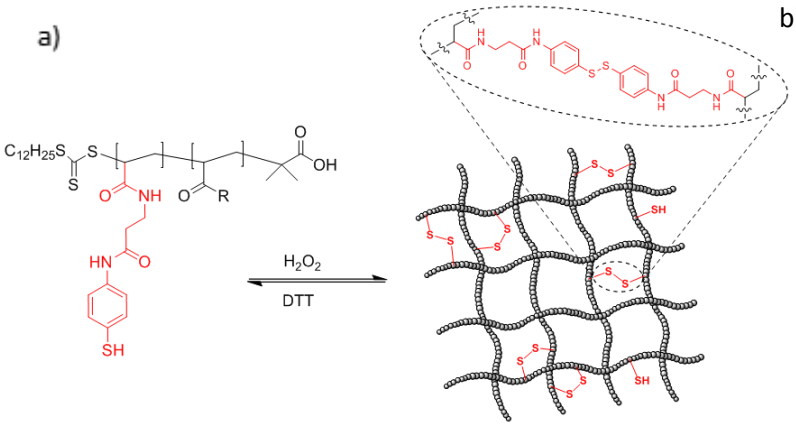


b)

| | P16 | P18 |
|---|---|---|
| Concentration (wt %)[a] | Gelation within 7 d?[b] | Gelation within 7 d?[b] |
| 1 | N | N |
| 3 | N | N |
| 5 | N | N |
| 7 | N | Y |
| 9 | Y | Y |

[a] wt % with respect to total mass of **P16** and **P18** dissolved in $H_2O$. [b] as evidenced by the vial inversion test.

Figure 4.6 Formation of disulfide hydrogels **HG3** and **HG4** from pre-formed polymeric building blocks **P16** and **P18**, respectively.

G' for **HG3** and **HG4**, time-sweep oscillatory rheology was performed on hydrogels formed at 9 wt % for both **P16** (**HG3**) and **P18** (**HG4**) (Figure 4.7). The rheogram shows that G' for both **HG3** and **HG4** are higher than their respective G" and there is no change in G', suggesting that both **HG3** and **HG4** exhibit viscoelasticity and they are structurally stable over the time-scale measured. The values of G' for **HG3** and **HG4** was 53 Pa and 2300 Pa, respectively, suggesting that **HG4** is considerably stronger than **HG3**. Given that **P16** and **P18** are very similar in size and exhibit equal densities of pendant thiol functionalities per chain, it was reasoned that the enhanced mechanical stability of **HG4** compared with **HG3** arises on account of the presence of the acrylic acid monomer units in **P18**. The nature of a polymeric hydrogel is influenced by the polarity of the polymeric gelators which comprise it, and importantly, at pH 8, the acrylic acid units within **P18** exist in their anionic form imparting extensively enhanced polarity compared with acrylamide-based **P16** on account of its poly-anionic nature.

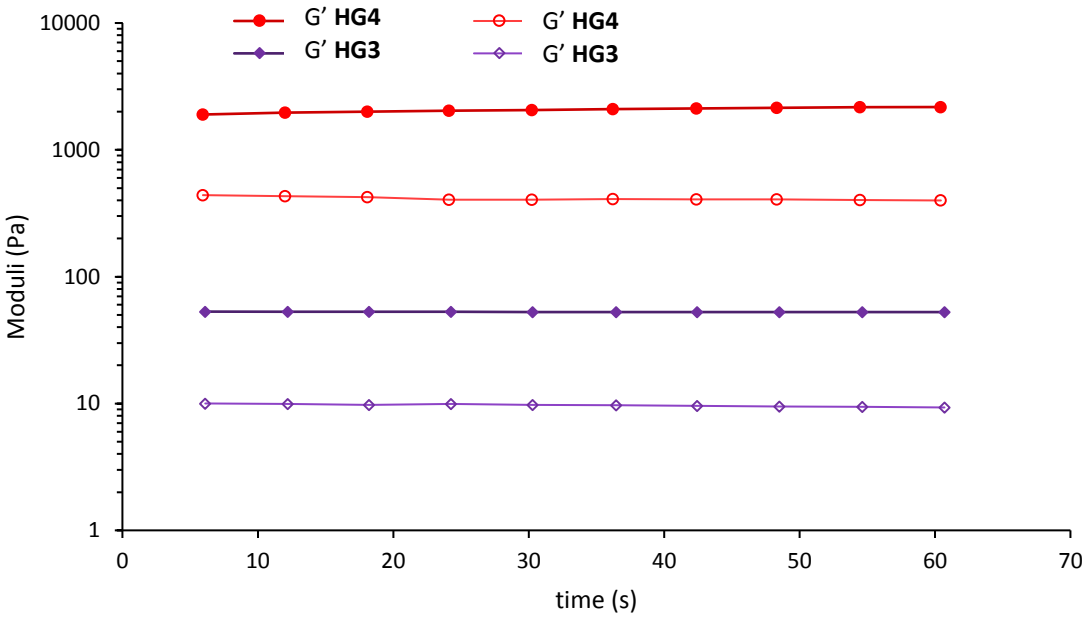


Figure 4.7 Time-sweep oscillatory rheological analysis of disulfide hydrogel **HG3** and **HG4**.

Strain-sweep oscillatory rheology measurements were performed on hydrogels **HG3** and **HG4** (Figure 4.8) to determine their respective LVRs and G'=G" cross-over points. The LVR for **HG3** and **HG4** was determined to be 16 % and 64 %, respectively, indicating that **HG4** undergoes

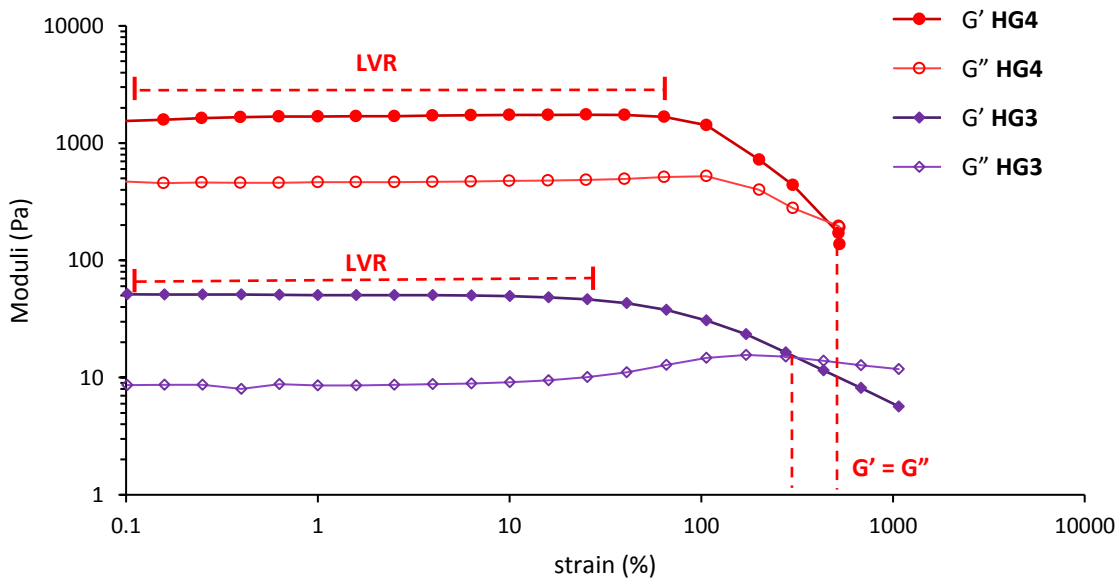


Figure 4.8 Strain-sweep oscillatory rheological analysis of disulfide hydrogels **HG3** and **HG4**.

structural breakdown at higher % strain values and is therefore more flexible than **HG3**. The greater flexibility of **HG4** compared with **HG3** is reflected in the G'=G" cross-over point, where the G'=G" point occurs at 300 % strain for **HG3** and at 460 % strain for **HG4**. Frequency-sweep oscillatory rheological analysis was performed to further probe the structural attributes of **HG3** and **HG4** (Figure 4.9). The measurement shows G' > G" for both **HG3** and **HG4** over the frequency range measured, suggesting they both exhibit viscoelasticity and hydrogel structure is retained. The rheogram (Figure 4.9) shows that both **HG3** and **HG4** exhibit frequency dependency with respect to both shear moduli, G' and G". The value of G' increases as a function of frequency for both **HG3** and **HG4** indicating an increase in solid-like character as

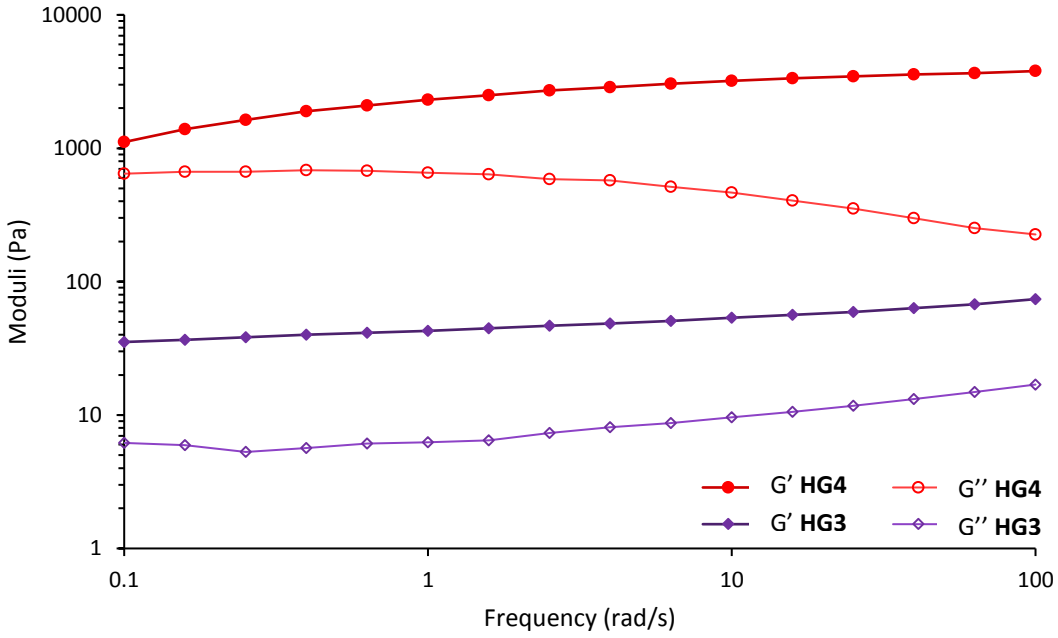


Figure 4.9 Frequency-sweep oscillatory rheological analysis of disulfide hydrogels **HG3** and **HG4**.

both hydrogels are not given sufficient time to undergo stress-relaxation even at lower measured frequencies. This observation suggests 'imperfections' with regard to the cross-linked microstructures of **HG3** and **HG4**. It was reasoned that **HG3** and **HG4** exhibit a more sparsely cross-linked nature in comparison to **HG1** and **HG2**, neither of which exhibited frequency dependency over the same range of measured frequencies.

| hydrogel | DCB | wt % | G' (Pa) | LVR (%strain) | G'=G" |
|---|---|---|---|---|---|
| **HG1** | imine | 7 | 70 | 40 | 170 |
| **HG2** | imine | 9 | 2800 | 16 | 90 |
| **HG3** | disulfide | 9 | 53 | 16 | 300 |
| **HG4** | disulfide | 9 | 2200 | 64 | 460 |

Table 4.1 Characterization of hydrogels **HG1**, **HG2**, **HG3** and **HG4**.

The characterization for all hydrogels (**HG1**, **HG2**, **HG3** and **HG4**) is summarized in Table 4.1. Interestingly, disulfide hydrogels **HG3** and **HG4** exhibit significantly larger G'=G" cross-over point (gel-sol transition) values than imine cross-linked hydrogels **HG1** and **HG2,** even where the value of G' is similar, namely in the comparison between **HG2** and **HG4**. The G' of **HG2** and **HG4** was determined to be 1900 and 2200 Pa, however, their G'=G" cross-over points were 130 % and 460 % strain, respectively. This difference in G'=G" may arise on account of a greater capacity for chemical exchange processes in **HG4** (thiol-disulfide interchange) compared with **HG2** (imine exchange), perhaps on account of a greater number of non-bonding pendant thiolate groups in **HG4** compared to non-bonding amines in **HG2**, thus, allowing more scope for network rearrangement dynamics as the network undergoes

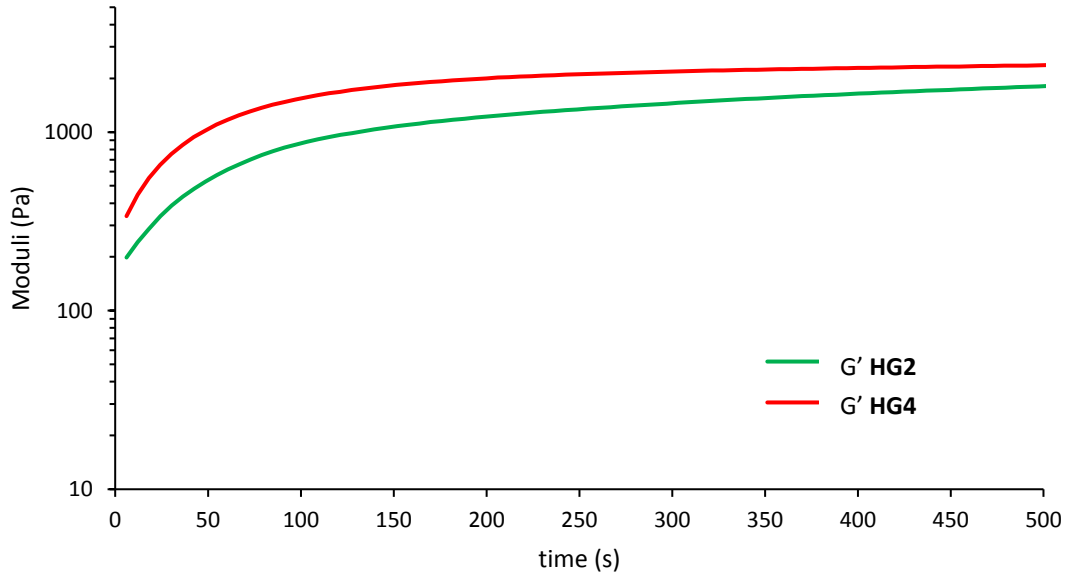


Figure 4.10 Time-sweep oscillatory rheological analysis of the gelation kinetics of **HG2** and **HG4**.

stress relaxation upon application of oscillatory shear stress of increasing amplitude. Imine cross-linked hydrogel **HG2** and disulfide cross-linked hydrogel **HG4** were selected as candidates for implementation in a '4-node network' on account of their greater mechanical stabilities and fast gelation kinetics compared to **HG1** and **HG3**. Furthermore, **HG2** and **HG4** were stable over the full range of frequencies tested.

Time-sweep oscillatory rheology was performed on **HG2** and **HG4** in order to establish the time-resolved gelation point (Figure 4.10) at a fixed frequency 1 Hz and applied percentage strain of 1%. In both cases the gelation process was initiated in a small glass vial followed by rapid transfer of the gelating solution onto the Peltier plate of the rheometer, and time-sweep measurements were started within 5 s of gelation initiation. Both **HG2** and **HG4** formed too quickly to observe the G'=G" cross-over point–the point at which the material begins to exhibit viscoelasticity. Thus, it was inferred the gelation point for **HG2** and **HG4** is < 10 s. Furthermore the value of G' for both **HG2** and **HG4** reach a plateau at times close to their respective G' as derived from the initial time sweeps (Figure 4.3 and 4.7, respectively).

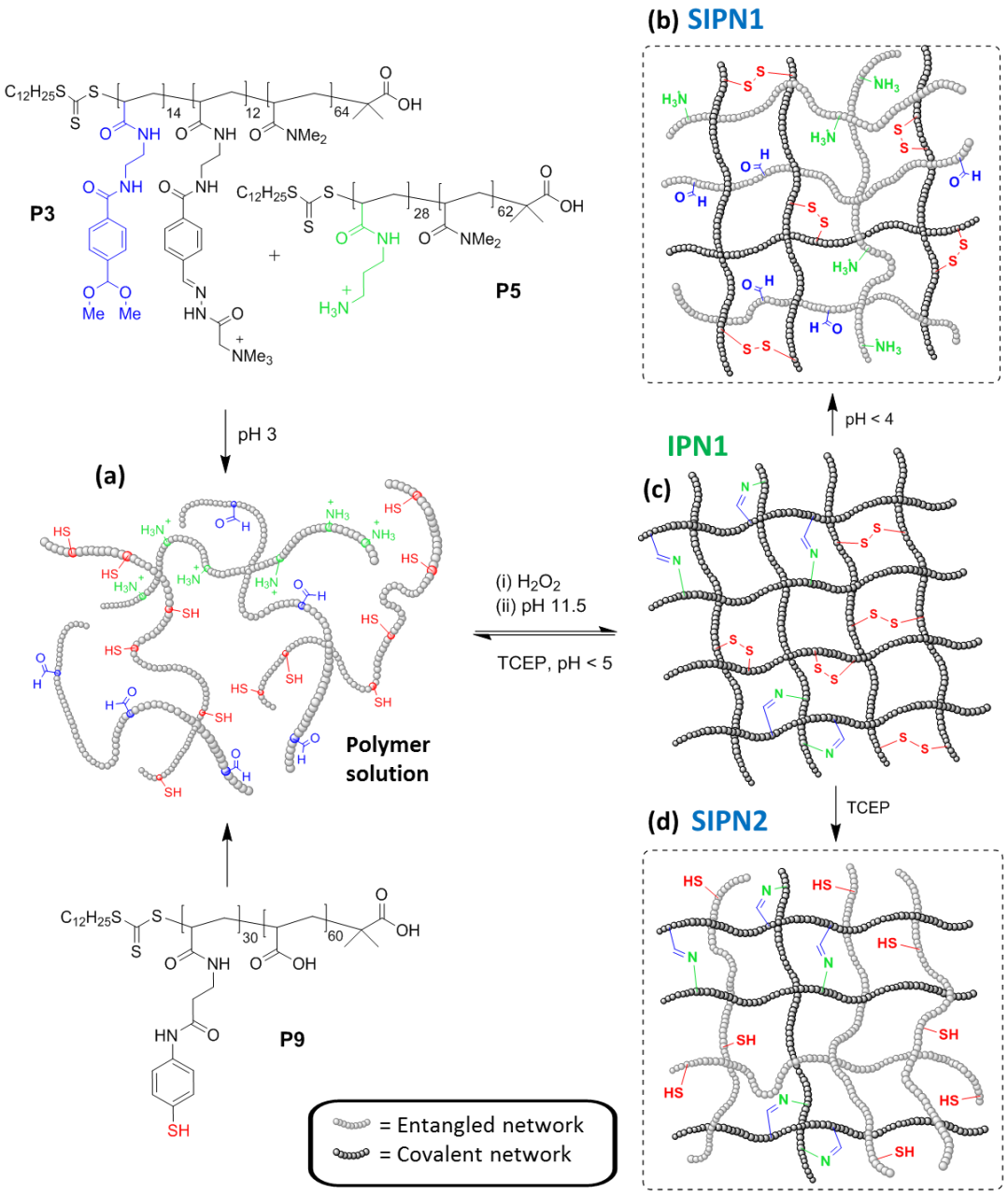


Figure 4.11 Schematic route for preparation of imine and disulfide dual-crosslinked, interpenetrating network (**IPN1**) and subsequent orthogonal bond-breaking processes leading to semi-interpenetrating networks, **SIPN1** and **SIPN2**. (a) Aqueous solution of preformed building blocks **P12**, **P14** and **P18**. (b) Disulfide cross-linked semi-interpenetrating network **SIPN1**. (c) Dual cross-linked interpenetrating network **IPN1**. (d) Imine-crosslinked semi-interpenetrating network **SIPN2**.

### 4.3.3 *Imine and disulfide dual cross-linked interpenetrating network*

The next challenge was to investigate the orthogonality of imine and disulfide DCBs by dual-incorporation of copolymers **P12**, **P14** and **P18** within a single hydrogel matrix, moving closer towards the development of a pH-redox sensitive *4-node* hydrogel network as detailed in Figure 4.1. An experiment was designed (Figure 4.11) in which **P12**, **P14** and **P18** were each dissolved in aqueous solution (pH 4.5) at a total copolymer concentration of 14 wt % to afford a free-flowing polymer solution (Figure 4.11a). 1 M $H_2O_2$ was then added and after 5 min the pH of the copolymer solution was immediately adjusted to pH 11.5 with an injection of 4 M NaOH followed by vigorous swirling. Rapid gelation occurred affording a homogenous macroscopic polymer network, **IPN1** (Figure 4.11b), as confirmed by the vial-inversion test.

Time-sweep rheological analysis was performed on **IPN1** (Figure 4.12a). The rheogram displays that the value of G' > G" and that both the value of G' and G" are independent of time. These observations indicate that **IPN1** is viscoelastic in nature and undergoes no noticeable structural changes over 200 s under these conditions. The value of

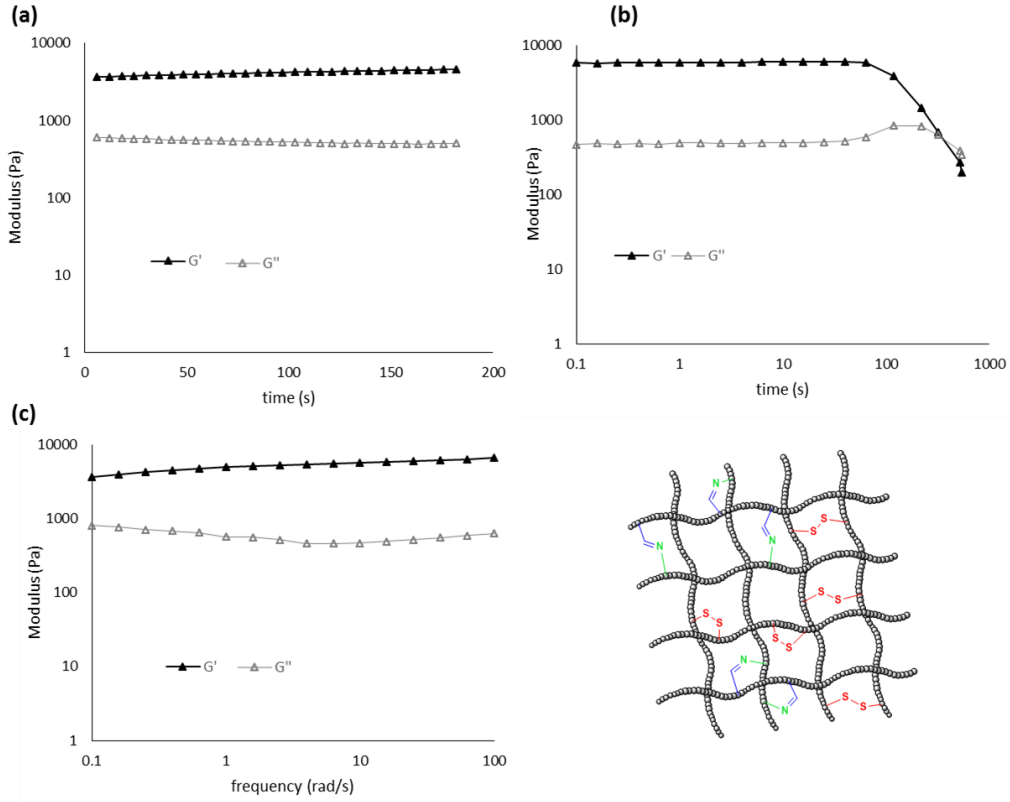


Figure 4.12 Oscillatory rheological analysis of dual cross-linked interpenetrating network **IPN1**. (a) Time-sweep measurement. (b) Strain-sweep measurement. (c) Frequency-sweep measurements.

G’ of **IPN1** was found to be 4600 Pa under these conditions, significantly higher than the G’ values for **HG1**-**HG4**. It should be noted that with respect to **IPN1**, there is likely a greater contribution from physical effects such as ionic interactions, Van der Waals interactions and polymer entanglement when compared to **HG1**-**HG4** on account of the higher total polymer concentration and the presence of both positive and negative charges of **P12** and **P18**, respectively.

Strain-sweep oscillatory rheological analysis was performed on **IPN1** (Figure 4.12b), the LVR and G’=G” cross-over value of **IPN1** was determined to be 64 % strain and 350 % strain, respectively.

Frequency-sweep oscillatory rheology was performed on **IPN1** (Figure 4.12c). The value of G’ > G” over the range of measured frequencies suggesting **IPN1** retains its structural integrity and thus its viscoelastic nature. The rheogram of **IPN1** shows that, similar to the case of **HG4** (Figure 4.9), there is a small dependency of G’ on oscillation frequency. This suggests that, similar to **HG4**, **IPN1** exhibits regions of mechanically entangled polymer within a less-uniform, more sparsely cross-linked microstructure unlike **HG2** which exhibited no frequency dependency (Figure 4.5). The dependency of G’ on frequency in **IPN1** is more similar to the dependence observed with respect to **HG4**.

Unfortunately, successful orthogonal cleavage of imine and disulfide cross-links in **IPN1** to yield **SIPN1** (Figure 4.11b) and **SIPN2** (Figure 4.11d) was not achieved. A major obstacle in the formation of homogenous interpenetrating and semi-interpenetrating networks is phase separation of polymeric components. Under all of the conditions studied, manipulations on **IPN1** yield heterogeneous mixtures which were not analyzable by rheological methods. Even complete and ‘simultaneous’ cleavage of imine and disulfide bonds in **IPN1** - i.e. the reverse reaction to its formation, yielding the polymer solution of **P12**, **P14** and **P18** displayed in Figure 4.11a – was unsuccessful. These limitations have had dramatic consequences on the capacity of the system described to exhibit orthogonality with respect to imine and disulfide DCBs. To investigate orthogonality in the context of this ‘4-node network’, structure-property relationships must be established for the disulfide cross-linked (**SIPN1**), imine cross-linked (**SIPN2**), and dual cross-linked (**IPN1**) hydrogels described. pH, redox conditions, polymer concentration, the rate of stimulus application, electrostatic interaction and bulk polarity all affect the mechanical properties of **IPN1** and **SIPN1**/**SIPN2** and, importantly, not only because they influence the formation/breaking of the desired

cross-links but because they will have a significant impact on the resultant gel architecture which in turn greatly affects mechanical stability.

### 4.4 Conclusion

RAFT polymerization was utilized to prepare a well-defined polymeric scaffold with a high degree of control which displayed pendant activated ester groups along its backbone. This polymeric precursor was then reacted with a variety of functional amines, followed by post-polymerization modification, to yield a range of suitable thiol-, amine- and aldehyde-containing random copolymers. Conditions were successfully determined for the pH-sensitive formation of imine cross-linked hydrogels using the preformed pendant aldehyde and pendant amine copolymers. Redox-sensitive formation of disulfide cross-linked hydrogels using a preformed pendant thiol copolymer was also demonstrated. Rheological characterization was performed on all hydrogel materials which proved to be a very powerful technique for investigating their mechanical properties. It was demonstrated that varying polymer concentration and the polarity of the polymeric precursor used in hydrogel formation resulted in significant variation in mechanical strength and flexibility, reflected in the values of G' and the G'=G" cross-over point, respectively. An investigation into the formation of an imine- and disulfide-based interpenetrating network was undertaken. The formation of a strong, macroscopically homogenous hydrogel was achieved, however, subsequent breaking of imine or disulfide bonds within the interpenetrating network structure yielded macroscopically heterogeneous mixtures which could not be subjected to further chemical modification or rheological analysis. We speculate that, prior to the formation of imine and disulfide covalent bonds, extensive polymer chain entanglement arises upon mixing of polymeric precursors and is likely encouraged by electrostatic interaction. This entanglement predisposes the mixture to form an interpenetrating network upon rapid, near-simultaneous formation of imine and disulfide bonds. When either disulfide or imine bonds are broken, phase separation is observed and the covalent network 'ejects' the entangled network. Rationally redesigning the polymeric precursors to negate this ejection effect may derive a system capable of existing as a thermodynamically stable semi-interpenetrating network. Only when each of the '4 nodes' as depicted in the '4-node' network have been accessed, analyzed by rheology and cross-compared, can a conclusion relating to the orthogonal utility of imine and disulfide dynamic covalent bonds within the context of hydrogel materials be reached.

## 4.4 **Experimental**

*Acetal-functionalized Copolymer **P11***

Poly(pentafluorophenyl acrylate), **P3** (1.0 g, 46 µmol), was dissolved in THF (5 mL) and stirred for 5 min. Hünig's Base (40 mg, 0.31 mmol) was added in one portion followed by the addition of *N*-(2-aminoethyl)-4-(dimethoxymethyl)benzamide (**10**) (536 mg, 1.94 mmol) and with stirring. The mixture was stirred at 35 $^{o}$C for 1 h after which time dimethylamine (DMA) solution (2.0 M in THF) was added in excess (5 mL). After stirring for 3 h at 35 $^{o}$C, the white precipitate was filtered and the filtrate evaporated to dryness to remove THF and residual dimethylamine. The crude brown material was dissolved in THF (15 mL) and precipitated dropwise into ice-cold $Et_2O$ (300 mL). The pale yellow amorphous solid was collected by filtration, redissolved in THF (15 mL) and precipitated twice in $Et_2O$ (300 mL). Acetal-functionalized copolymer **P11** was collected by filtration (334 mg, 26 µmol, 59 %). $^{1}$H NMR ($CDCl_3$, 300 MHz): δ 1.39-1.76 (br, CHC$H_2$, polymer backbone), 2.18-2.65 (br, C$H$C$H_2$, polymer backbone), 2.68-2.95 (br, N(C$H_3$)$_2$), 3.18-3.26 ($OCH_3$), 5.24-5.37 (C$H$($OCH_3$)$_2$), 7.25-7.8 (4H, br, Ar). The composition of **P11** can be determined by comparing the integration of the dimethyl acetal protons of **10** with the integration of the N(C$H_3$)$_2$ protons of DMA, showing the monomer composition to be 2 : 1 DMA : **10**. GPC analysis in DMF + 1 g.L$^{-1}$ LiBr (0.6 mL min-1) revealed an $M_n$ of 12.5 kDa and a PDI of 1.25 when analysed against a set of near-monodisperse poly(methyl methacrylate) standards.

*Polycationic Acetal-Functionalized Copolymer **P12***

Acetal-functionalized copolymer **P11** (370 mg, 0.03 mmol) was dissolved in MeOH (3 mL) with stirring. Girard's Reagent T (**20**) (28 mg, 0.17 mmol) was dissolved in a separate solution of MeOH (5 mL) and added quickly to the solution of **P11** and the mixture was stirred at 65 $^{o}$C for 3 h. After this time the solvent was removed in vacuo and the polymer was redissolved in MeOH (3 mL) and precipitated into $Et_2O$ (200 mL). Polycationic acetal-functionalized copolymer **P12** was collected by filtration and dried under high vacuum for 6 h. $^{1}$H NMR ($CDCl_3$, 300 MHz): δ 1.43-1.81 (br, CHC$H_2$, polymer backbone), 2.24-2.71 (br, C$H$C$H_2$, polymer backbone), 2.59-2.78 (br, N(C$H_3$)$_2$), 3.21-3.33 ($OCH_3$), 3.38 C(C$H_3$)$_3$, 4.28 (C$H_2$) 5.31- 5.44 (C$H$(OCH3)2), 7.52-8.05 (br, Ar). The composition of **P12** can be determined by comparing the

integration of the dimethyl acetal protons of **10** with the integration of the N(C*H*3)2 protons of DMA and the *N*-methyl protons of Girard's reagent T (**20**), showing the monomer composition to be 4 : 1 : 1, DMA : **10** : **20**.

*Boc-protected Amine-functionalized Copolymer **P13***

Poly(pentafluorophenyl acrylate), **P3** (1.0 g, 46 µmol), was dissolved in THF (5 mL) and stirred for 5 min. Hünig's Base (40 mg, 0.31 mmol) was added in one portion followed by the addition of **3** (313 mg, 1.80 mmol) with stirring. The mixture was stirred at 35 $^{o}$C for 1 h after which time dimethylamine (DMA) solution (2.0 M in THF) was added in excess (4 mL). The mixture was stirred for 2h at 35 $^{o}$C after which the white precipitate was filtered off and the filtrate dried *in vacuo*. The crude material was dissolved in THF (10 mL) and precipitated dropwise into ice-cold $Et_2O$ (250 mL). *Boc*-protected amine-functionalized Copolymer **P13** was collected by filtration and redissolved in THF (10 mL) before precipitating again into $Et_2O$ and the precipitate was collected by filtration and dried under high vacuum for 3 h. (295 mg, 26 µmol, 57 %). $^{1}$H NMR ($CDCl_3$, 300 MHz): δ 1.41 (9H, br s, $C(CH_3)_3$), 1.32-1.83 (br, $CHCH_2$), 2.55 (br, $CHCH_2$), 2.61-2.98 (br, $N(CH_3)_2$), 3.40 (br, $(CH_2)_3$). The composition of **P13** can be determined by comparing the integration of the *boc* protons of **13** with the integration of the $N(CH_3)_2$ protons of DMA. GPC analysis in DMF + 1 g.L$^{-1}$ LiBr (0.6 mL min$^{-1}$) revealed an $M_n$ of 11.5 kDa and a PDI of 1.27 when analysed against a set of near-monodisperse poly(methyl methacrylate) standards.

*Amine-functionalized Copolymer **P14***

**P13** (300 mg, 27 µmol) was dissolved in $CHCl_3$ (6 mL) and TFA (6 mL) was added, the reaction mixture was left to stir for 4 h. After this time the solvent and excess TFA were removed on the rotary evaporator and the oil obtained was dissolved in a minimal amount of $CHCl_3$ and added dropwise to a large excess of $Et_2O$ (300 mL). The precipitate was then isolated by filtration and dried under high vacuum for 6 h. The polymer precipitate was then isolated by filtration and the precipitation was repeated before drying under high vacuum. Polymer **P14** was obtained as a pale yellow solid (0.241 mg, 23.0 µmol, 85 % ). 1H NMR ($CDCl_3$): δ 0.88 (br, $CH_2CH_3$, RAFT chain terminus), 1.51-1.68 (2H, br, $CHCH_2$), 2.44 (1H, br, $CHCH_2$), 2.72-2.94 (6H, br, $N(CH_3)_2$). The composition of **P14** could be inferred from the composition of **P13** to be 1 :

2, **13** : DMA as it is extremely unlikely that C-C bonds within the polymer backbone were broken under the aforementioned conditions. GPC analysis in DMF + 1 $g.L^{-1}$ LiBr (0.6 mL $min^{-1}$) revealed an $M_n$ of 11.5 kDa and a PDI of 1.30 when analysed against a set of near-monodisperse poly(methyl methacrylate) standards.

*Imine Cross-linked Hydrogel* ***HG1***

**P12** (80 mg, 6.4 µmol) was dissolved in THF (240 µL) and $H_2O$ (1.6 mL) was added. The pH of the solution was adjusted to pH 3.0 ± 0.5 with aliquots of 1.0 M HCl. The mixture was gently agitated for 5 min and left to stand for 1 h. Copolymer **P14** (40 mg, 3.5 µmol) was added in one portion with gentle agitation to encourage full dissolution of **P14**. After this time the pH was rapidly increased to pH 12 using aliquots of 1.0 M NaOH. The mixture was left to stand for 3 d at 25 $^oC$.

*Imine Cross-linked Hydrogel* ***HG2***

**P12** (81 mg, 6.4 µmol) was dissolved in THF (240 µL) and $H_2O$ (1.2 mL) was added. The pH of the solution was adjusted to pH 3.0 ± 0.5 with aliquots of 1.0 M HCl. The mixture was gently agitated for 5 min and left to stand for 1 h. Copolymer **P14** (40 mg, 3.5 µmol) was added in one portion with gentle agitation to encourage full dissolution of **P14**. After this time the pH was rapidly increased to pH 12 using aliquots of 1.0 M NaOH. The mixture was left to stand for 3 d at 25 $^oC$.

*Disulfide-protected Acrylamide Copolymer* ***P15***

Poly(pentafluorophenyl acrylate), **P3** (1.0 g, 46 µmol), was dissolved in THF (5 mL) and stirred for 5 min. Hünig's Base (50 mg, 0.39 mmol) was added in one portion followed by the addition of **19** (545 mg, 1.45 mmol). The mixture was stirred at 25 $^oC$ for 1 h after which time dimethylamine (DMA) solution (2.0 M in THF) was added in large excess (5 ml). After stirring for 3 h at 40 $^oC$, the white precipitate was filtered and the filtrate evaporated to dryness to remove THF and residual dimethylamine. The crude brown material was redissolved in THF (5 mL) and precipitated by dropwise addition into ice-cold $Et_2O$ (300 mL). The pale brown precipitate was collected by filtration and precipitated twice more in $Et_2O$ (300 mL) from THF

(5 mL). Pendant disulfide copolymer **P15** was collected and dried under high vacuum affording an amorphous pale brown solid (401 mg, 28 µmol, 61 %). 1H NMR ($CDCl_3$, 300 MHz): δ 1.21 (9H, br s, $C(CH_3)_3$), 1.52-1.75 (2H, br, $CHCH_2$, polymer backbone), 2.57 (1H, br, $CHCH_2$, polymer backbone), 2.70-2.98 (6H, br s, $NCH_3$) 7.30-7.58 (4H, br, Ar). The composition of **P15** was determined to be 1 : 2, **19** : DMA by comparing the integral value of the $C(CH_3)$ *t*-butyl group and aromatic protons with the integral value of the CH3 protons of the CTA at the chain terminus. GPC analysis in DMF + 1 $g.L^{-1}$ LiBr (0.6 mL $min^{-1}$) revealed an Mn of 14.5 kDa and a PDI of 1.29 when analysed against a set of near-monodisperse poly(methyl methacrylate) standards.

*Thiol-functionalized Acrylamide Copolymer **P16***

Copolymer **P16** (350 mg, 25.0 µmol) was dissolved in MeOH and TCEP.HCl (30 mg, 104.1 µmol) was added in one portion. The solution was stirred at room temperature for 18 h, after this time thiol-functionalized copolymer **P16** was purified by dialysis for 3 d in a 1:1 (v/v) MeOH:$CH_2Cl_2$ mixture. Copolymer **P13** was collected by removal of the dialysate *in vacuo* to afford a brown, crystalline solid (140 mg, 14 µmol, 53 %). 1H NMR ($CDCl_3$, 300 MHz): δ 1.48-1.69 (2H, br, $CHCH_2$, polymer backbone), 2.51 (1H, br, $CHCH_2$, polymer backbone), 2.75-2.98 (6H, br s, $NCH_3$) 7.05-7.5 (4H, br, Ar). The composition of **P16** could be inferred from the composition of **P15** to be 1 : 2, **19** : DMA as it was extremely unlikely that C-C bonds within the polymer backbone were broken under the aforementioned conditions. GPC analysis in DMF + 1 $g.L^{-1}$ LiBr (0.6 mL $min^{-1}$) revealed an Mn of 14 kDa and a PDI of 1.28 when analysed a set of near-monodisperse poly(methyl methacrylate) standards.

*Disulfide-protected Acrylic Acid Copolymer **P17***

p(PFPA) (1.3 g, 57 µmol) was dissolved in THF (10 mL) with stirring, **19** (600 mg, 1.6 mmol) was added in one portion followed quickly by Hünig's Base (0.1 mL). This mixture was stirred at 25 $^oC$ for 2 h, after this time $H_2O$ (4 mL) was added and the mixture was heated at 75 $^oC$. for 48 h after which the mixture was precipitated into Et2O and collected by filtration. This precipitation was repeated twice to furnish acrylic acid-based copolymer **P17** (270 mg, 21.6 µmol, 37.9 %). $^1H$ NMR ($D_2O$, 300 MHz): δ 1.15 (9H, br s, $C(CH_3)_3$), 1.31-1.69 (2H, br, $CHCH_2$, polymer backbone), 1.89-2.20 (1H, br, $CHCH_2$, polymer backbone), 7.12-7.45 (4H, br, Ar).

*Thiol-functionalized Acrylic Acid Copolymer **P18***

**P17** (700 mg, 56 µmol) was dissolved in MeOH (10 mL) and $H_2O$ (3 mL) with stirring at 25 $^oC$. TCEP.HCl (500 mg, 1.72 mmol) was added in one portion and the mixture was stirred for 48 h at 65 $^oC$. The solvent was removed *in vacuo* and the resulting deep brown crude solid was redissolved in a 1:1 mixture of $H_2O$:MeOH (15 mL). Dialysis was performed against a 1:1 mixture of $H_2O$:MeOH for 3 d. The final copolymer **P18** (570 mg, 47.5 µmol, 85 %) was collected by removing the residual MeOH:$H_2O$ *in vacuo*. $^1H$ NMR ($D_2O$, 300 MHz): δ 1.28-1.69 (2H, br, CHC*H*$_2$, polymer backbone), 1.75-2.10 (1H, br, C*H*$CH_2$, polymer backbone), 6.85-7.45 (4H, br, Ar).

*Disulfide Cross-linked Hydrogel **HG3***

**P16** (61 mg, 4 µmol) was dissolved in THF (150 µL) and $H_2O$ (50 µL) was added and the mixture was agitated vigorously. 1 M NaOH (330 µL) was added and upon full dissolution of copolymer **P16** the pH of the solution was adjusted to pH 8.0 ± 0.5 with aliquots of 1.0 M NaOH. 1 M $H_2O_2$ (240 µL) was added in one portion with vigorous swirling. The mixture was allowed to stand for 7 d at room temperature.

*Disulfide Cross-linked Hydrogel **HG4***

**P18** (60 mg, 4 µmol) was dissolved in H2O (160 µL) was added and the mixture was agitated vigorously. 1 M NaOH (220 µL) was added and upon full dissolution of copolymer **P16** the pH of the solution was adjusted to pH 8.0 ± 0.5 with aliquots of 1.0 M NaOH. 1 M $H_2O_2$ (240 µL) was added in one portion with vigorous swirling. The mixture was allowed to stand for 7 d at room temperature.

*Disulfide and Imine Cross-linked Interpenetrating Network **IPN1***

**P12** (45 mg, 3.6 μmol) was dissolved in 1 M HCl (120 μL) and THF (30 μL) and the mixture was left to stand for 1 h. To this mixture **P14** (23 mg, 2 μL) in THF (180 μL) was added in one portion with swirling. The pH of the solution was adjusted to pH 6 – 7 with aliquots of 0.1 M NaOH. A separate solution of **P18** (90 mg, 6 μL) was prepared in $H_2O$ (500 μL) with the addition of aliquots (10 μL) 1 M NaOH to afford a solution whose pH was pH 6 - 7. The two solutions were combined with gentle agitation and 1 M $H_2O_2$ (400 μL) was added in one
portion followed immediately by the addition of aliquots of 4 M NaOH (5 μL) with rapid swirling affording an increase in the solutions pH to pH 11.5 ± 0.5.

## 4.5 References


[1] L Chen, R Wang, X Zhang, *Biomolecular Networks: Methods and Applications in Systems Biology*, *Wiley*, *New Jersey*, *2009*.

[2] U. Alon, *An Introduction to Systems Biology: Design Principles of Biological Circuits; CRC Press: Florida, 2006*

[3] R. Pepperkok, J. Ellenberg, *Nat Rev Mol Cell Biol* **2006**, *7*, 690-696.

[4] aG. Ashkenasy, T. M. Hermans, S. Otto, A. F. Taylor, *Chemical Society Reviews* **2017**, *46*, 2543-2554; bR. F. Ludlow, S. Otto, *Chemical Society Reviews* **2008**, *37*, 101-108.

[5] G. Barany, R. B. Merrifield, *Journal of the American Chemical Society* **1977**, *99*, 7363-7365.

[6] M. L. Saha, S. De, S. Pramanik, M. Schmittel, *Chemical Society Reviews* **2013**, *42*, 6860-6909.

[7] aP. T. Corbett, J. Leclaire, L. Vial, K. R. West, J.-L. Wietor, J. K. M. Sanders, S. Otto, *Chemical Reviews* **2006**, *106*, 3652-3711; bJ.-M. Lehn, A. V. Eliseev, *Science* **2001**, *291*, 2331; cJ. Li, P. Nowak, S. Otto, *Journal of the American Chemical Society* **2013**, *135*, 9222-9239.

[8] aJ.-M. Lehn, *Science* **2002**, *295*, 2400; bM. Schmittel, K. Mahata, *Chemical Communications* **2010**, *46*, 4163-4165.

[9] N. V. Tsarevsky, B. S. Sumerlin, **2013**.

[10] aY. K. Chong, G. Moad, E. Rizzardo, M. A. Skidmore, S. H. Thang, *Macromolecules* **2007**, *40*, 9262-9271; bY. K. Chong, G. Moad, E. Rizzardo, S. H. Thang, *Macromolecules* **2007**, *40*, 4446-4455; cG. Moad, E. Rizzardo, S. H. Thang, *Accounts of Chemical Research* **2008**, *41*, 1133-1142; dG. Moad, E. Rizzardo, S. H. Thang, *Australian Journal of Chemistry* **2005**, *58*, 379-410; eG. Moad, E. Rizzardo, S. H.

Thang, *Australian Journal of Chemistry* **2006**, *59*, 669-692; fG. Moad, E. Rizzardo, S. H. Thang, *Australian Journal of Chemistry* **2009**, *62*, 1402-1472; gJ. Chiefari, Y. K. Chong, F. Ercole, J. Krstina, J. Jeffery, T. P. T. Le, R. T. A. Mayadunne, G. F. Meijs, C. L. Moad, G. Moad, E. Rizzardo, S. H. Thang, *Macromolecules* **1998**, *31*, 5559-5562.

[11] aB. Yu, J. W. Chan, C. E. Hoyle, A. B. Lowe, *Journal of Polymer Science Part A: Polymer Chemistry* **2009**, *47*, 3544-3557; bG. Gody, C. Rossner, J. Moraes, P. Vana, T. Maschmeyer, S. Perrier, *Journal of the American Chemical Society* **2012**, *134*, 12596-12603; cV. Vázquez-Dorbatt, Z. P. Tolstyka, H. D. Maynard, *Macromolecules* **2009**, *42*, 7650-7656.

[12] aA. W. Jackson, D. A. Fulton, *Polymer Chemistry* **2013**, *4*, 31-45; bG. Moad, M. Chen, M. Haussler, A. Postma, E. Rizzardo, S. H. Thang, *Polymer Chemistry* **2011**, *2*, 492-519.

[13] aJ. Jennings, G. He, S. M. Howdle, P. B. Zetterlund, *Chemical Society Reviews* **2016**, *45*, 5055-5084; bD. J. Keddie, *Chemical Society Reviews* **2014**, *43*, 496-505; cA. J. Convertine, B. S. Lokitz, Y. Vasileva, L. J. Myrick, C. W. Scales, A. B. Lowe, C. L. McCormick, *Macromolecules* **2006**, *39*, 1724-1730; dC. L. McCormick, B. S. Sumerlin, B. S. Lokitz, J. E. Stempka, *Soft Matter* **2008**, *4*, 1760-1773; eG. Zhou, I. I. Harruna, *Macromolecules* **2005**, *38*, 4114-4123.

[14] aR. Barbey, L. Lavanant, D. Paripovic, N. Schüwer, C. Sugnaux, S. Tugulu, H.-A. Klok, *Chemical Reviews* **2009**, *109*, 5437-5527; bM. Baum, W. J. Brittain, *Macromolecules* **2002**, *35*, 610-615; cM. H. Stenzel, L. Zhang, W. T. S. Huck, *Macromolecular rapid communications* **2006**, *27*, 1121-1126.

[15] aT. Haino, *Polym J* **2013**, *45*, 363-383; bA. C. Kamps, T. Magbitang, A. Nelson, *Chemical Communications* **2007**, 954-956; cS. Chen, B.-D. Lechner, A. Meister, W. H. Binder, *Nano Letters* **2016**, *16*, 1491-1496; dD. Montarnal, N. Delbosc, C. Chamignon, M.-A. Virolleaud, Y. Luo, C. J. Hawker, E. Drockenmuller, J. Bernard, *Angewandte Chemie International Edition* **2015**, *54*, 11117-11121.

[16] aA. Vanderkooy, P. Pfefferkorn, M. S. Taylor, *Macromolecules* **2017**, *50*, 3807-3817; bL. C. Gilday, S. W. Robinson, T. A. Barendt, M. J. Langton, B. R. Mullaney, P. D. Beer, *Chemical Reviews* **2015**, *115*, 7118-7195.

[17] aQ.-L. Li, W.-X. Gu, H. Gao, Y.-W. Yang, *Chemical Communications* **2014**, *50*, 13201-13215; bI. Insua, A. Wilkinson, F. Fernandez-Trillo, *European Polymer Journal* **2016**, *81*, 198-215.

[18] aY. Jin, C. Yu, R. J. Denman, W. Zhang, *Chemical Society Reviews* **2013**, *42*, 6634-6654; bS. J. Rowan, S. J. Cantrill, G. R. L. Cousins, J. K. M. Sanders, J. F. Stoddart, *Angewandte Chemie International Edition* **2002**, *41*, 898-952; cS. D. Bull, M. G. Davidson, J. M. H. van den Elsen, J. S. Fossey, A. T. A. Jenkins, Y.-B. Jiang, Y. Kubo, F. Marken, K. Sakurai, J. Zhao, T. D. James, *Accounts of Chemical Research* **2013**, *46*, 312-326; dY. Jin, Q. Wang, P. Taynton, W. Zhang, *Accounts of Chemical Research* **2014**, *47*, 1575-1586; eR. J. Wojtecki, M. A. Meador, S. J. Rowan, *Nat Mater* **2011**, *10*, 14-27.

[19] S. P. Black, J. K. Sanders, A. R. Stefankiewicz, *Chem Soc Rev* **2014**, *43*, 1861-1872.

[20] W. L. A. Brooks, B. S. Sumerlin, *Chemical Reviews* **2016**, *116*, 1375-1397.

[21] aY. Shi, C. F. van Nostrum, W. E. Hennink, *ACS Biomaterials Science & Engineering* **2015**, *1*, 393-404; bR. Tong, N. P. Gabrielson, T. M. Fan, J. Cheng, *Current opinion in solid state & materials science* **2012**, *16*, 323-332.

[22] M. E. Belowich, J. F. Stoddart, *Chemical Society Reviews* **2012**, *41*, 2003-2024.

[23] J. Collins, M. Nadgorny, Z. Xiao, L. A. Connal, *Macromolecular rapid communications* **2017**, *38*.

[24] R. Caraballo, H. Dong, J. P. Ribeiro, J. Jimenez-Barbero, O. Ramstrom, *Angewandte Chemie (International ed. in English)* **2010**, *49*, 589-593.

[25] G. Joshi, E. V. Anslyn, *Organic Letters* **2012**, *14*, 4714-4717.

[26] aD. A. Hudson, S. A. Gannon, C. Thorpe, *Free Radical Biology and Medicine* **2015**, *80*, 171-182; bB. P. Tu, J. S. Weissman, *The Journal of cell biology* **2004**, *164*, 341-346.
[27] P. D. Kiser, M. Golczak, K. Palczewski, *Chemical Reviews* **2014**, *114*, 194-232.
[28] S. Patai, *Ed. The Chemistry of Thiols: Volume 2; Interscience: London* **1968**.
[29] J. P. Danehy, M. Y. Oester, *The Journal of Organic Chemistry* **1967**, *32*, 1491-1495.
[30] J. A. Burns, J. C. Butler, J. Moran, G. M. Whitesides, *The Journal of Organic Chemistry* **1991**, *56*, 2648-2650.
[31] A. Kraj, H.-J. Brouwer, N. Reinhoud, J.-P. Chervet, *Analytical and Bioanalytical Chemistry* **2013**, *405*, 9311-9320.
[32] L. Li, W. Feng, A. Welle, P. A. Levkin, *Angewandte Chemie International Edition* **2016**, *55*, 13765-13769.
[33] R. Singh, G. M. Whitesides, in *Sulphur-Containing Functional Groups (1993)*, John Wiley & Sons, Inc., **2010**, pp. 633-658.
[34] L. Wang, L. Li, X. Wang, D. Huang, F. Yang, H. Shen, Z. Li, D. Wu, *Polymer Chemistry* **2016**, *7*, 1429-1438.
[35] U. F. Fritze, M. von Delius, *Chemical Communications* **2016**, *52*, 6363-6366.
[36] S. Otto, R. L. Furlan, J. K. Sanders, *Science* **2002**, *297*, 590-593.
[37] N. Ponnuswamy, F. B. L. Cougnon, J. M. Clough, G. D. Pantoş, J. K. M. Sanders, *Science* **2012**, *338*, 783.
[38] aJ. M. A. Carnall, C. A. Waudby, A. M. Belenguer, M. C. A. Stuart, J. J. P. Peyralans, S. Otto, *Science* **2010**, *327*, 1502; bM. Malakoutikhah, J. J. P. Peyralans, M. Colomb-Delsuc, H. Fanlo-Virgós, M. C. A. Stuart, S. Otto, *Journal of the American Chemical Society* **2013**, *135*, 18406-18417.
[39] J. Li, J. M. A. Carnall, M. C. A. Stuart, S. Otto, *Angewandte Chemie International Edition* **2011**, *50*, 8384-8386.
[40] R. W. Layer, *Chemical Reviews* **1963**, *63*, 489-510.
[41] C. Godoy-Alcántar, A. K. Yatsimirsky, J. M. Lehn, *Journal of Physical Organic Chemistry* **2005**, *18*, 979-985.
[42] aV. Saggiomo, U. Luning, *Chemical Communications* **2009**, 3711-3713; bV. Saggiomo, C. Goeschen, R. Herges, R. Quesada, U. Lüning, *European Journal of Organic Chemistry* **2010**, *2010*, 2337-2343.
[43] K. S. Chichak, S. J. Cantrill, A. R. Pease, S.-H. Chiu, G. W. V. Cave, J. L. Atwood, J. F. Stoddart, *Science* **2004**, *304*, 1308.
[44] aG. T. Wang, J. B. Lin, X. K. Jiang, Z. T. Li, *Langmuir* **2009**, *25*, 8414-8418; bY.-G. Jia, X. X. Zhu, *Chemistry of Materials* **2015**, *27*, 387-393.
[45] J. J. Armao, J.-M. Lehn, *Angewandte Chemie International Edition* **2016**, *55*, 13450-13454.
[46] H. Hu, R. G. Larson, *The Journal of Physical Chemistry B* **2002**, *106*, 1334-1344.
[47] J. P. Lorand, J. O. Edwards, *The Journal of Organic Chemistry* **1959**, *24*, 769-774.
[48] aA. E. Ivanov, H. A. Panahi, M. V. Kuzimenkova, L. Nilsson, B. Bergenstahl, H. S. Waqif, M. Jahanshahi, I. Y. Galaev, B. Mattiasson, *Chemistry (Weinheim an der Bergstrasse, Germany)* **2006**, *12*, 7204-7214; bF. Kuralay, S. Sattayasamitsathit, W. Gao, A. Uygun, A. Katzenberg, J. Wang, *Journal of the American Chemical Society* **2012**, *134*, 15217-15220.
[49] aA. E. Ivanov, N. Solodukhina, M. Wahlgren, L. Nilsson, A. A. Vikhrov, M. P. Nikitin, A. V. Orlov, P. I. Nikitin, M. V. Kuzimenkova, V. P. Zubov, *Macromolecular bioscience* **2011**, *11*, 275-284; bA. E. Ivanov, N. M. Solodukhina, L. Nilsson, M. P. Nikitin, P. I. Nikitin, V. P. Zubov, A. A. Vikhrov, *Polymer Science Series A* **2012**, *54*, 1-10.
[50] J. N. Cambre, D. Roy, S. R. Gondi, B. S. Sumerlin, *Journal of the American Chemical Society* **2007**, *129*, 10348-10349.

[51] C. C. Deng, W. L. A. Brooks, K. A. Abboud, B. S. Sumerlin, *ACS Macro Letters* **2015**, *4*, 220-224.
[52] aZ. Tang, Y. Guan, Y. Zhang, *Polymer Chemistry* **2014**, *5*, 1782-1790; bC. Zhang, M. D. Losego, P. V. Braun, *Chemistry of Materials* **2013**, *25*, 3239-3250; cY. Zhang, Y. Guan, S. Zhou, *Biomacromolecules* **2007**, *8*, 3842-3847; dY. Zhang, Y. Guan, S. Zhou, *Biomacromolecules* **2006**, *7*, 3196-3201.
[53] J. Cao, S. Liu, Y. Chen, L. Shi, Z. Zhang, *Polymer Chemistry* **2014**, *5*, 5029-5036.
[54] J. F. Teichert, D. Mazunin, J. W. Bode, *Journal of the American Chemical Society* **2013**, *135*, 11314-11321.
[55] M. J. S. Dewar, W. W. Schoeller, *Journal of the American Chemical Society* **1971**, *93*, 1481-1482.
[56] H. Liu, Y. Li, K. Sun, J. Fan, P. Zhang, J. Meng, S. Wang, L. Jiang, *Journal of the American Chemical Society* **2013**, *135*, 7603-7609.
[57] J. I. Jay, S. Shukair, K. Langheinrich, M. C. Hanson, G. C. Cianci, T. J. Johnson, M. R. Clark, T. J. Hope, P. F. Kiser, *Advanced Functional Materials* **2009**, *19*, 2969-2977.
[58] M. L. Stolowitz, C. Ahlem, K. A. Hughes, R. J. Kaiser, E. A. Kesicki, G. Li, K. P. Lund, S. M. Torkelson, J. P. Wiley, *Bioconjugate Chemistry* **2001**, *12*, 229-239.
[59] Y. Pérez-Fuertes, A. M. Kelly, A. L. Johnson, S. Arimori, S. D. Bull, T. D. James, *Organic Letters* **2006**, *8*, 609-612.
[60] A. M. Kelly, Y. Pérez-Fuertes, S. Arimori, S. D. Bull, T. D. James, *Organic Letters* **2006**, *8*, 1971-1974.
[61] M. von Delius, E. M. Geertsema, D. A. Leigh, A. M. Z. Slawin, *Organic & Biomolecular Chemistry* **2010**, *8*, 4617-4624.
[62] aM. Hutin, G. Bernardinelli, J. R. Nitschke, *Chemistry – A European Journal* **2008**, *14*, 4585-4593; bR. J. Sarma, S. Otto, J. R. Nitschke, *Chemistry – A European Journal* **2007**, *13*, 9542-9546.
[63] S. Hagihara, H. Tanaka, S. Matile, *Journal of the American Chemical Society* **2008**, *130*, 5656-5657.
[64] A. Wilson, G. Gasparini, S. Matile, *Chemical Society Reviews* **2014**, *43*, 1948-1962.
[65] aS. Otto, R. L. E. Furlan, J. K. M. Sanders, *Journal of the American Chemical Society* **2000**, *122*, 12063-12064; bS. Otto, R. L. E. Furlan, J. K. M. Sanders, *Science* **2002**, *297*, 590; cS. L. Roberts, R. L. E. Furlan, S. Otto, J. K. M. Sanders, *Organic & Biomolecular Chemistry* **2003**, *1*, 1625-1633.
[66] M. von Delius, E. M. Geertsema, D. A. Leigh, *Nat Chem* **2010**, *2*, 96-101.
[67] M. J. Barrell, A. G. Campaña, M. von Delius, E. M. Geertsema, D. A. Leigh, *Angewandte Chemie International Edition* **2011**, *50*, 285-290.
[68] G. Deng, F. Li, H. Yu, F. Liu, C. Liu, W. Sun, H. Jiang, Y. Chen, *ACS Macro Letters* **2012**, *1*, 275-279.
[69] N. Sakai, S. Matile, *Journal of the American Chemical Society* **2011**, *133*, 18542-18545.
[70] Q. Yan, Z. Luo, K. Cai, Y. Ma, D. Zhao, *Chemical Society Reviews* **2014**, *43*, 4199-4221.
[71] G. Sforazzini, E. Orentas, A. Bolag, N. Sakai, S. Matile, *Journal of the American Chemical Society* **2013**, *135*, 12082-12090.
[72] H. M. Seifert, K. Ramirez Trejo, E. V. Anslyn, *Journal of the American Chemical Society* **2016**, *138*, 10916-10924.
[73] E. Mattia, S. Otto, *Nat Nano* **2015**, *10*, 111-119.
[74] M. A. Aleman Garcia, N. Bampos, *Organic & Biomolecular Chemistry* **2013**, *11*, 27-30.
[75] M. E. Bracchi, D. A. Fulton, *Chemical Communications* **2015**, *51*, 11052-11055.
[76] J. M. Spruell, C. J. Hawker, *Chemical Science* **2011**, *2*, 18-26.
[77] aY. Zhang, M. Barboiu, *Chemical Reviews* **2016**, *116*, 809-834; bZ. Rodriguez-Docampo, S. Otto, *Chemical Communications* **2008**, 5301-5303.

[78] aA. W. Jackson, D. A. Fulton, *Macromolecules* **2012**, *45*, 2699-2708; bA. W. Jackson, D. A. Fulton, *Chemical Communications* **2010**, *46*, 6051-6053.
[79] B. T. Tuten, D. Chao, C. K. Lyon, E. B. Berda, *Polymer Chemistry* **2012**, *3*, 3068-3071.
[80] X. Liu, Y. Yang, M. W. Urban, *Macromolecular rapid communications* **2017**, *38*.
[81] aE. Q. Fleige, Mohiuddin; Haag; Rainer, *Advanced Drug Delivery Reviews* **2012**, *64*, 866-884; bS. Mura, J. Nicolas, P. Couvreur, *Nat Mater* **2013**, *12*, 991-1003.
[82] S. Rose, A. Prevoteau, P. Elziere, D. Hourdet, A. Marcellan, L. Leibler, *Nature* **2014**, *505*, 382-385.
[83] aC. I. Crucho, *ChemMedChem* **2015**, *10*, 24-38; bW. Lin, *Chemical Reviews* **2015**, *115*, 10407-10409.
[84] S. Hornig, T. Heinze, C. R. Becer, U. S. Schubert, *Journal of Materials Chemistry* **2009**, *19*, 3838-3840.
[85] L. Tan, B. Tan, *Chem Soc Rev* **2017**, *46*, 3481.
[86] M. Elsabahy, K. L. Wooley, *Chem Soc Rev* **2012**, *41*, 2545-2561.
[87] aJ. Gu, W.-P. Cheng, J. Liu, S.-Y. Lo, D. Smith, X. Qu, Z. Yang, *Biomacromolecules* **2008**, *9*, 255-262; bR. Deng, M. J. Derry, C. J. Mable, Y. Ning, S. P. Armes, *Journal of the American Chemical Society* **2017**, *139*, 7616-7623.
[88] aE. G. Kelley, J. N. L. Albert, M. O. Sullivan, I. I. I. T. H. Epps, *Chemical Society Reviews* **2013**, *42*, 7057-7071; bY. Li, B. S. Lokitz, S. P. Armes, C. L. McCormick, *Macromolecules* **2006**, *39*, 2726-2728; cJ.-H. Ryu, R. T. Chacko, S. Jiwpanich, S. Bickerton, R. P. Babu, S. Thayumanavan, *Journal of the American Chemical Society* **2010**, *132*, 17227-17235.
[89] aY. Yang, Y. Li, Q. Lin, C. Bao, L. Zhu, *ACS Macro Letters* **2016**, *5*, 301-305; bA. N. Zelikin, J. F. Quinn, F. Caruso, *Biomacromolecules* **2006**, *7*, 27-30.
[90] I. Azcune, I. Odriozola, *European Polymer Journal* **2016**, *84*, 147-160.
[91] A. W. Jackson, C. Stakes, D. A. Fulton, *Polymer Chemistry* **2011**, *2*, 2500-2511.
[92] P. A. Woodfield, Y. Zhu, Y. Pei, P. J. Roth, *Macromolecules* **2014**, *47*, 750-762.
[93] B. L. Moore, R. K. O'Reilly, *Journal of Polymer Science Part A: Polymer Chemistry* **2012**, *50*, 3567-3574.
[94] M. Spiniello, A. Blencowe, G. G. Qiao, *Journal of Polymer Science Part A: Polymer Chemistry* **2008**, *46*, 2422-2432.
[95] aP. Nagy, *Antioxidants & Redox Signaling* **2013**, *18*, 1623-1641; bA. Fava, A. Iliceto, E. Camera, *Journal of the American Chemical Society* **1957**, *79*, 833-838.
[96] aD. J. Lestage, M. W. Urban, *Langmuir* **2004**, *20*, 6443-6449; bY. Zhao, M. W. Urban, *Macromolecules* **2000**, *33*, 2184-2191.
[97] M. E. Peach, in *The Thiol Group (1974)*, John Wiley & Sons, Ltd., **2010**, pp. 721-784.
[98] aW. S. Shim, J. S. Yoo, Y. H. Bae, D. S. Lee, *Biomacromolecules* **2005**, *6*, 2930-2934; bD. Wang, T. Liu, J. Yin, S. Liu, *Macromolecules* **2011**, *44*, 2282-2290; cY. Guan, Y. Zhang, *Chemical Society Reviews* **2013**, *42*, 8106-8121; dY. Zhang, F. Wu, M. Li, E. Wang, *Polymer* **2005**, *46*, 7695-7700.
[99] aN. Morimoto, T. Ohki, K. Kurita, K. Akiyoshi, *Macromolecular rapid communications* **2008**, *29*, 672-676; bD. Roy, W. L. A. Brooks, B. S. Sumerlin, *Chemical Society Reviews* **2013**, *42*, 7214-7243; cL. A. Lyon, Z. Meng, N. Singh, C. D. Sorrell, A. St. John, *Chemical Society Reviews* **2009**, *38*, 865-874.
[100] aZ. Hua, Z. Chen, Y. Li, M. Zhao, *Langmuir* **2008**, *24*, 5773-5780; bN. Rasool, T. Yasin, J. Y. Y. Heng, Z. Akhter, *Polymer* **2010**, *51*, 1687-1693.
[101] aB. D. Fairbanks, S. P. Singh, C. N. Bowman, K. S. Anseth, *Macromolecules* **2011**, *44*, 2444-2450; bM. E. Harmon, D. Kuckling, C. W. Frank, *Macromolecules* **2003**, *36*, 162-172; cZ. Li, Z. Wei, F. Xu, Y. H. Li, T. J. Lu, Y. M. Chen, G. J. Zhou, *Macromolecular rapid communications* **2012**, *33*, 1191-1196.
[102] J. Lin, Q. Tang, D. Hu, X. Sun, Q. Li, J. Wu, *Colloids and Surfaces A: Physicochemical and Engineering Aspects* **2009**, *346*, 177-183.

[103] aF. Xu, C.-a. M. Wu, V. Rengarajan, T. D. Finley, H. O. Keles, Y. Sung, B. Li, U. A. Gurkan, U. Demirci, *Advanced Materials* **2011**, *23*, 4254-4260; bC.-H. Chen, A. R. Abate, D. Lee, E. M. Terentjev, D. A. Weitz, *Advanced Materials* **2009**, *21*, 3201-3204; cX. Q. Wang, S. Yang, C. F. Wang, L. Chen, S. Chen, *Macromolecular rapid communications* **2016**, *37*, 759-768.

[104] aZ. Wei, J. H. Yang, J. Zhou, F. Xu, M. Zrinyi, P. H. Dussault, Y. Osada, Y. M. Chen, *Chemical Society Reviews* **2014**, *43*, 8114-8131; bY. Yang, M. W. Urban, *Chemical Society Reviews* **2013**, *42*, 7446-7467; cP. Casuso, I. Odriozola, A. Pérez-San Vicente, I. Loinaz, G. Cabañero, H.-J. Grande, D. Dupin, *Biomacromolecules* **2015**, *16*, 3552-3561; dR. Chang, X. Wang, X. Li, H. An, J. Qin, *ACS Applied Materials & Interfaces* **2016**, *8*, 25544-25551; eA. Pérez-San Vicente, M. Peroglio, M. Ernst, P. Casuso, I. Loinaz, H.-J. Grande, M. Alini, D. Eglin, D. Dupin, *Biomacromolecules* **2017**; fJ. A. Yoon, J. Kamada, K. Koynov, J. Mohin, R. Nicolaÿ, Y. Zhang, A. C. Balazs, T. Kowalewski, K. Matyjaszewski, *Macromolecules* **2012**, *45*, 142-149.

[105] aW. Luo, Y. Zhu, J. Zhang, J. He, Z. Chi, P. W. Miller, L. Chen, C.-Y. Su, *Chemical Communications* **2014**, *50*, 11942-11945; bT. Yang, R. Ji, X.-X. Deng, F.-S. Du, Z.-C. Li, *Soft Matter* **2014**, *10*, 2671-2678.

[106] J. J. Roberts, P. Naudiyal, L. Jugé, L. E. Bilston, A. M. Granville, P. J. Martens, *ACS Biomaterials Science & Engineering* **2015**, *1*, 1267-1277.

[107] aH. Wang, S. C. Heilshorn, *Advanced materials (Deerfield Beach, Fla.)* **2015**, *27*, 3717-3736; bJ. A. Burdick, G. D. Prestwich, *Adv Mater* **2011**, *23*, H41-56; cK. Ghosh, X. Z. Shu, R. Mou, J. Lombardi, G. D. Prestwich, M. H. Rafailovich, R. A. F. Clark, *Biomacromolecules* **2005**, *6*, 2857-2865.

[108] aR. Tong, L. Tang, L. Ma, C. Tu, R. Baumgartner, J. Cheng, *Chemical Society Reviews* **2014**, *43*, 6982-7012; bM. Molina, M. Asadian-Birjand, J. Balach, J. Bergueiro, E. Miceli, M. Calderon, *Chemical Society Reviews* **2015**, *44*, 6161-6186.

[109] J Goodwin, R. Hughes, in *Rheology for Chemists: An Introduction (2)*, The Royal Society of Chemistry, **2008**, pp. 194-257.

[110] C. J. Kloxin, C. N. Bowman, *Chemical Society Reviews* **2013**, *42*, 7161-7173.

[111] E. Hachet, H. Van Den Berghe, E. Bayma, M. R. Block, R. Auzély-Velty, *Biomacromolecules* **2012**, *13*, 1818-1827.

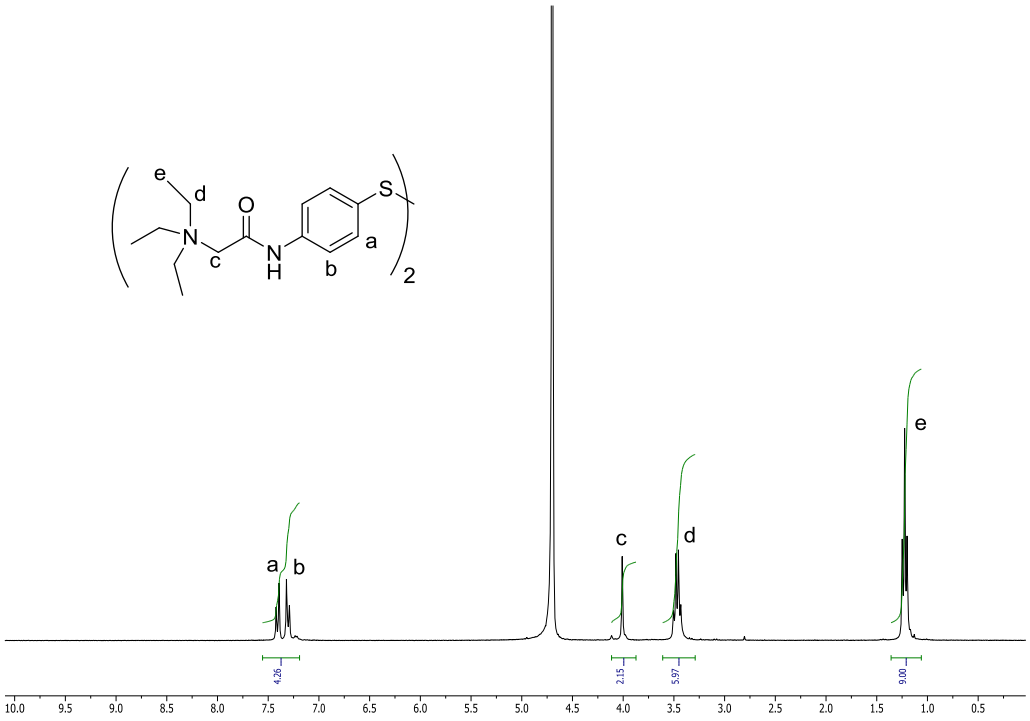


**Figure 1** $^{1}$H NMR spectrum (300 MHz, $D_2O$) of compound **3.**

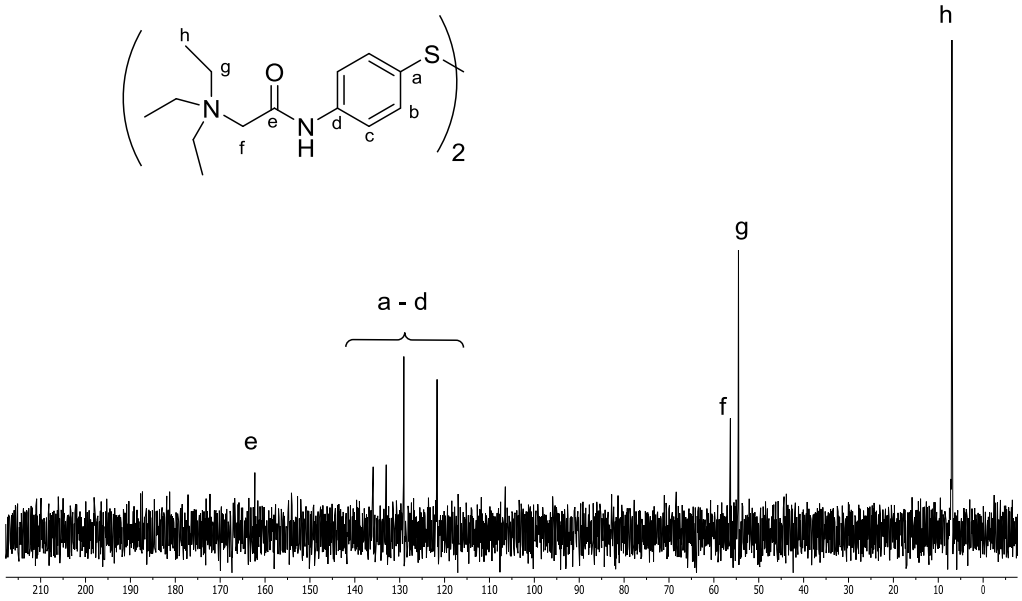


**Figure 2** $^{13}$C NMR spectrum (75 MHz, $D_2O$) of disulfide **3.**

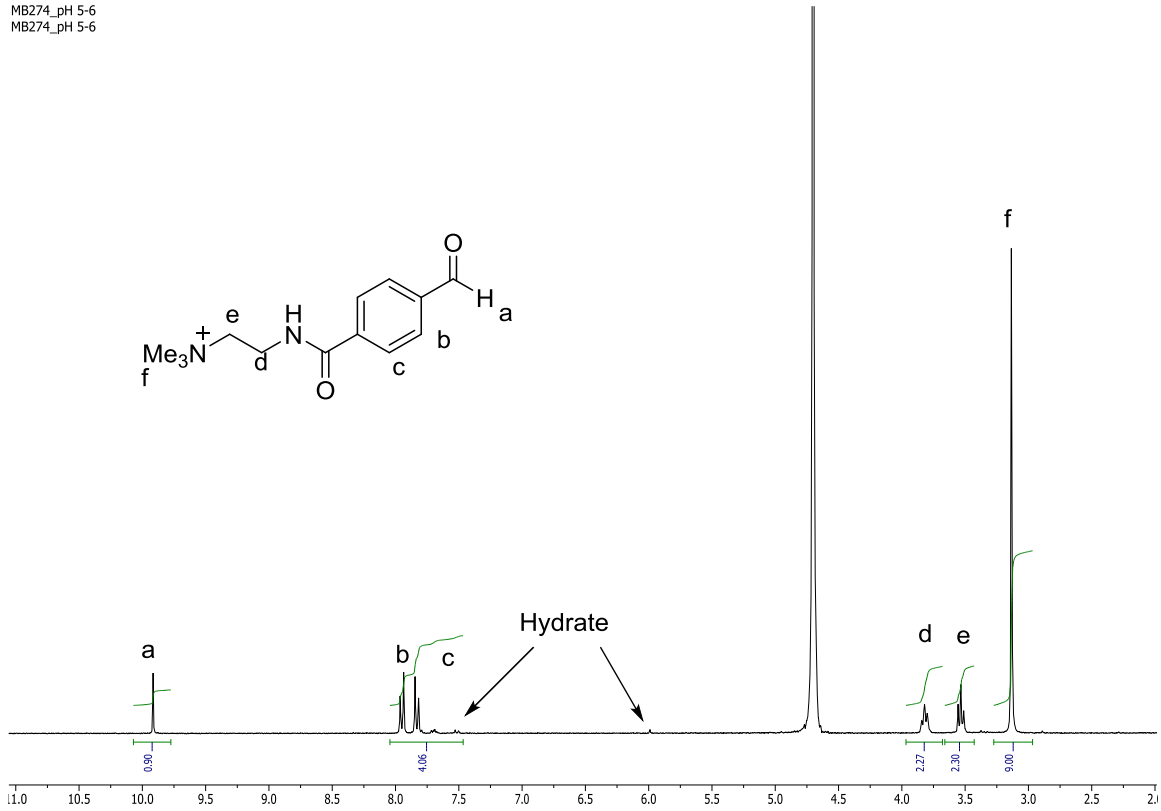


**Figure 3** $^{1}$H NMR spectrum (300 MHz, $D_2O$) of aldehyde **6**.

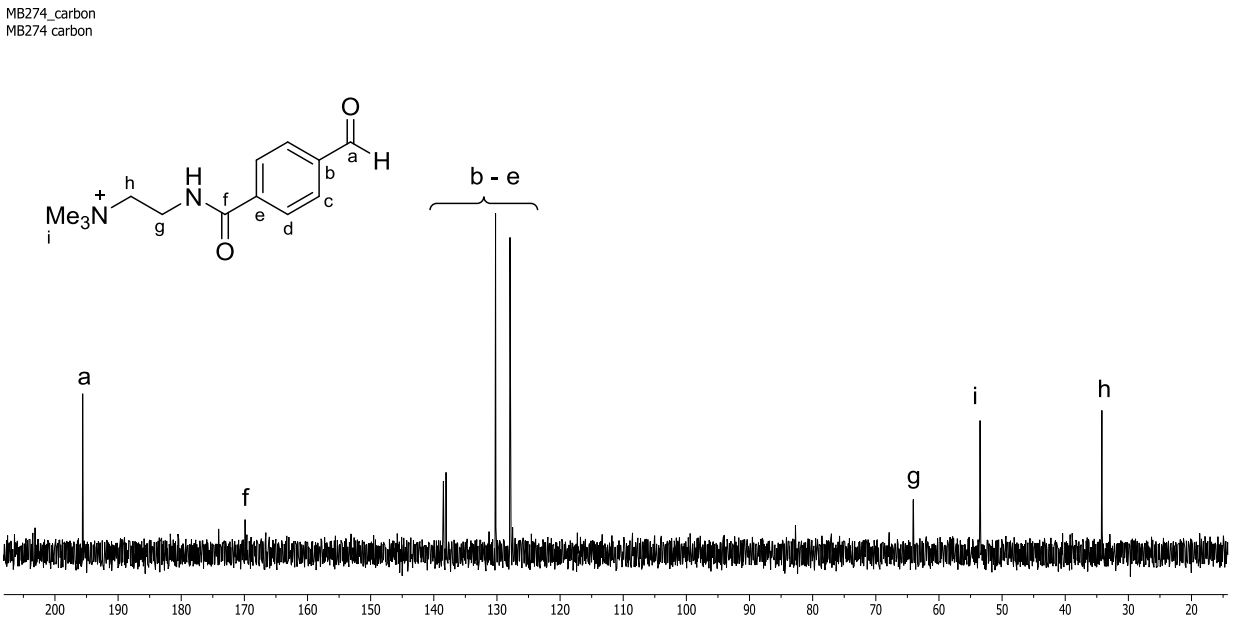


**Figure 4** $^{13}$C NMR spectrum (75 MHz, $D_2O$) of aldehyde **6**.

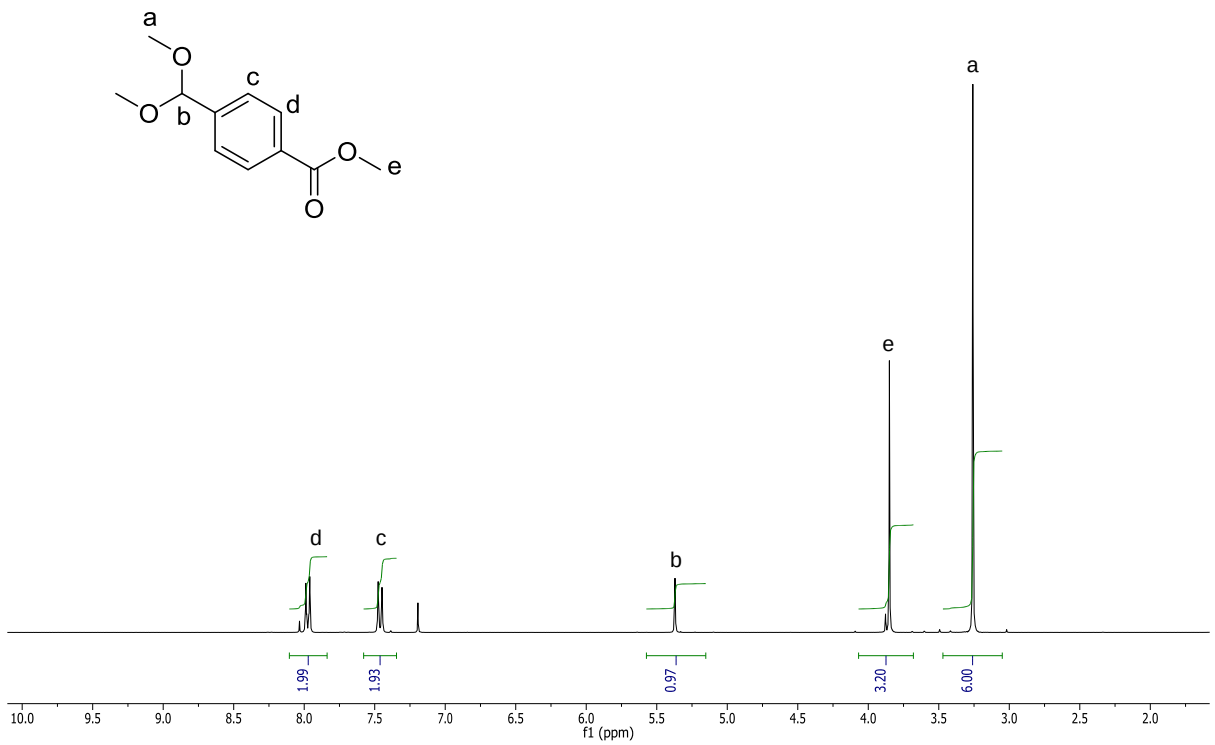


**Figure 5** $^{1}$H NMR spectrum (300 MHz, $CDCl_3$) of compound **9**.

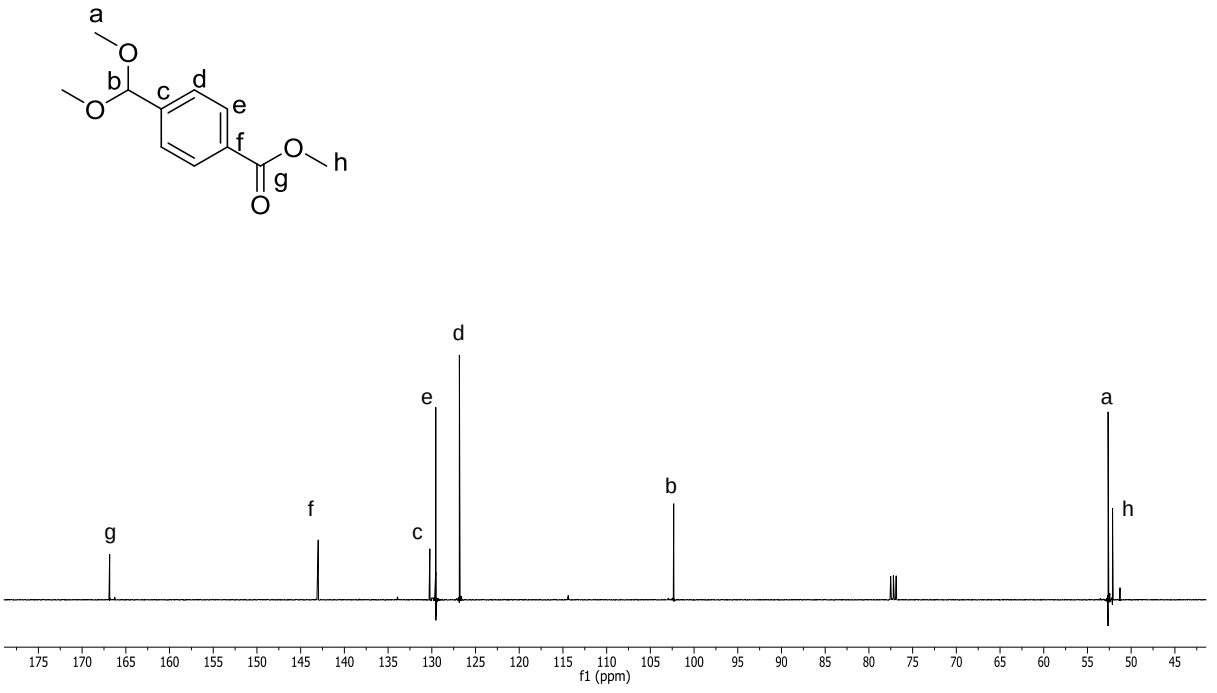


**Figure 6** $^{13}$C NMR spectrum (75 MHz, $CDCl_3$) of compound **9**.

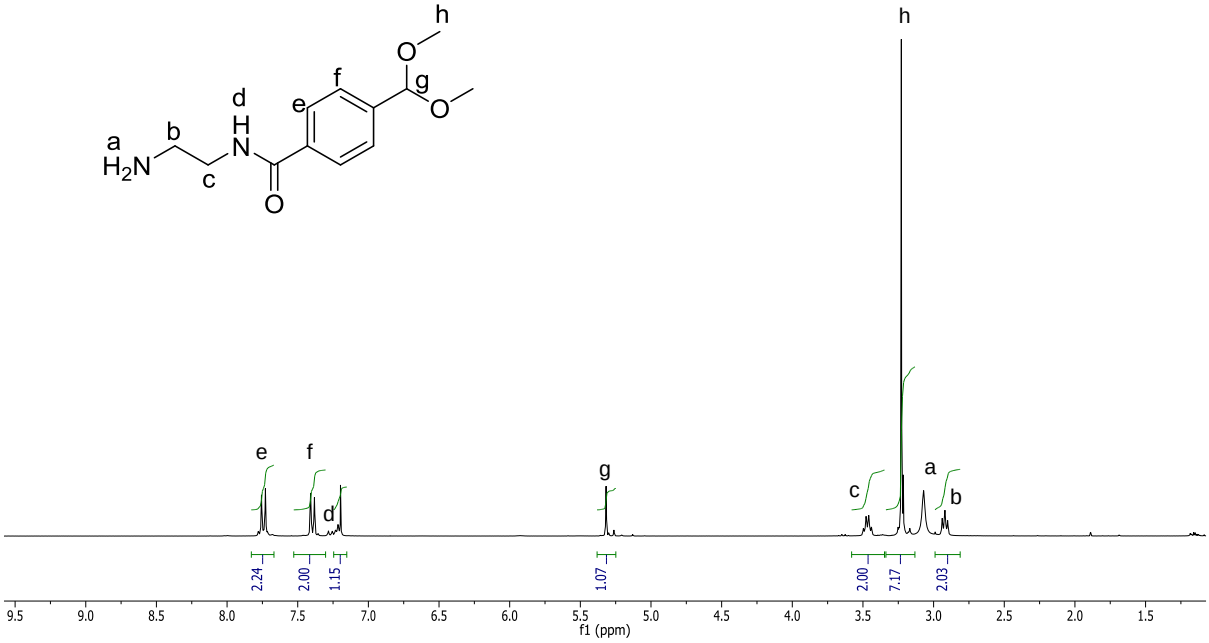


**Figure 7** $^{1}$H NMR spectrum (300 MHz, $CDCl_3$) of compound **10**.

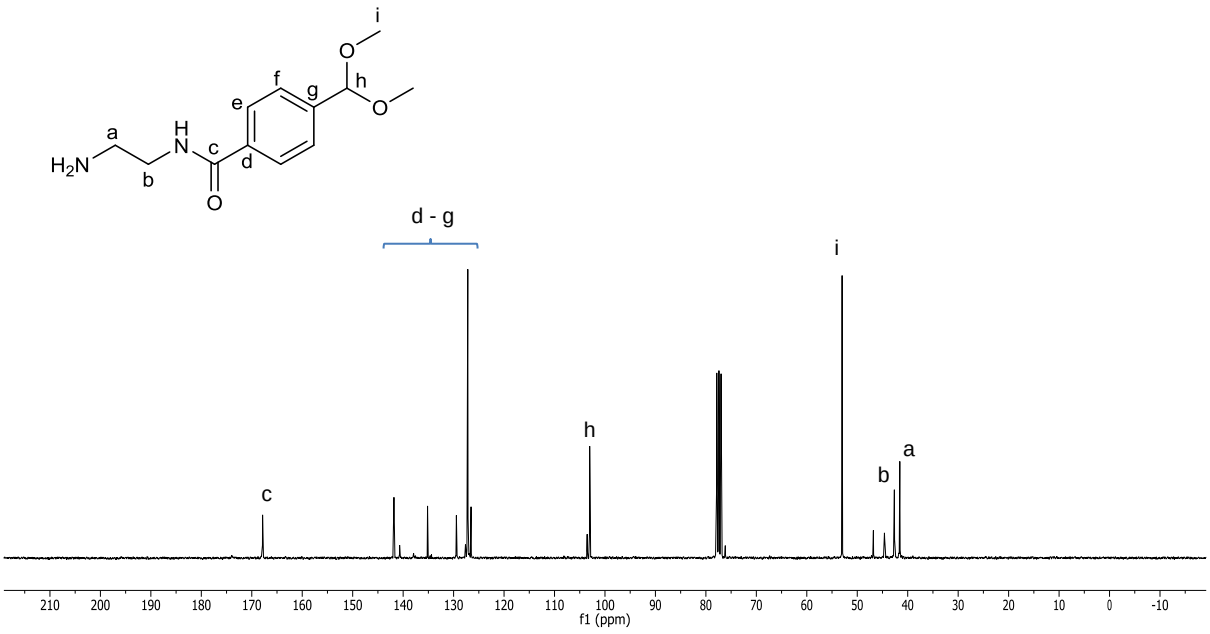


**Figure 8** $^{13}$C NMR spectrum (75 MHz, $CDCl_3$) of compound **10**.

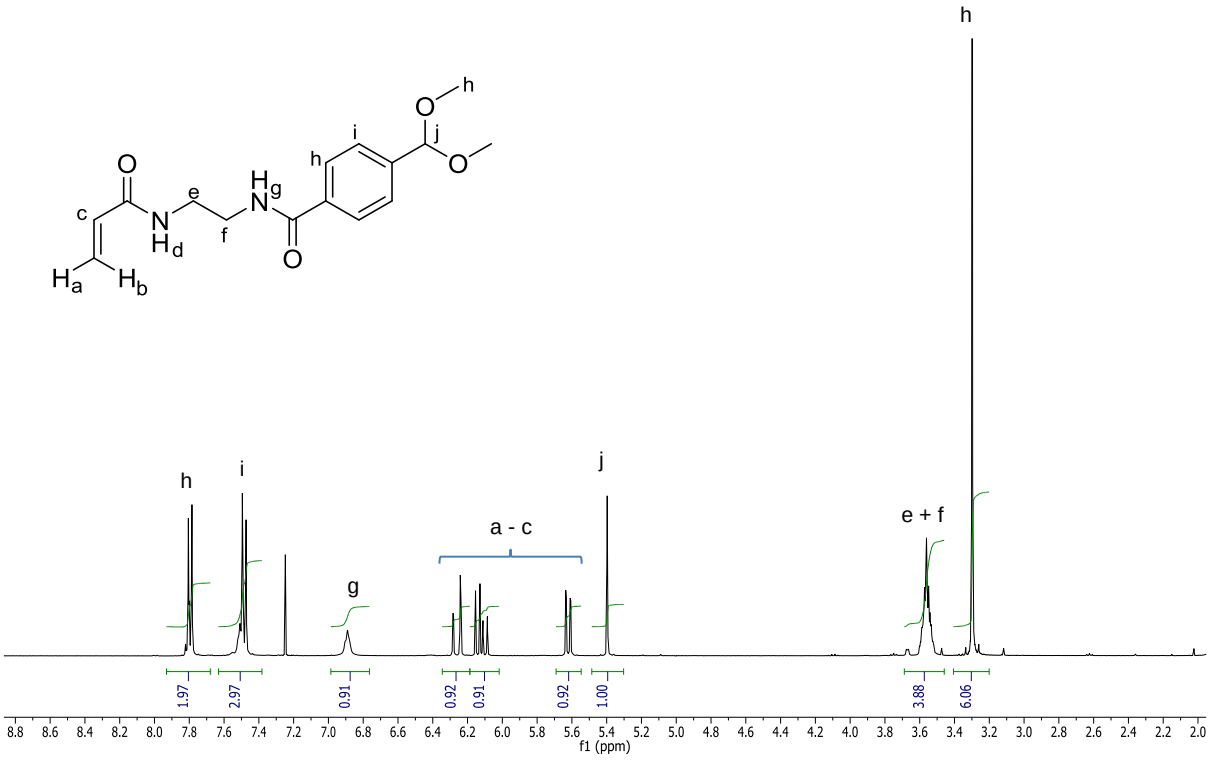


**Figure 9** $^{1}$H NMR spectrum (300 MHz, $CDCl_3$) of compound **11**.

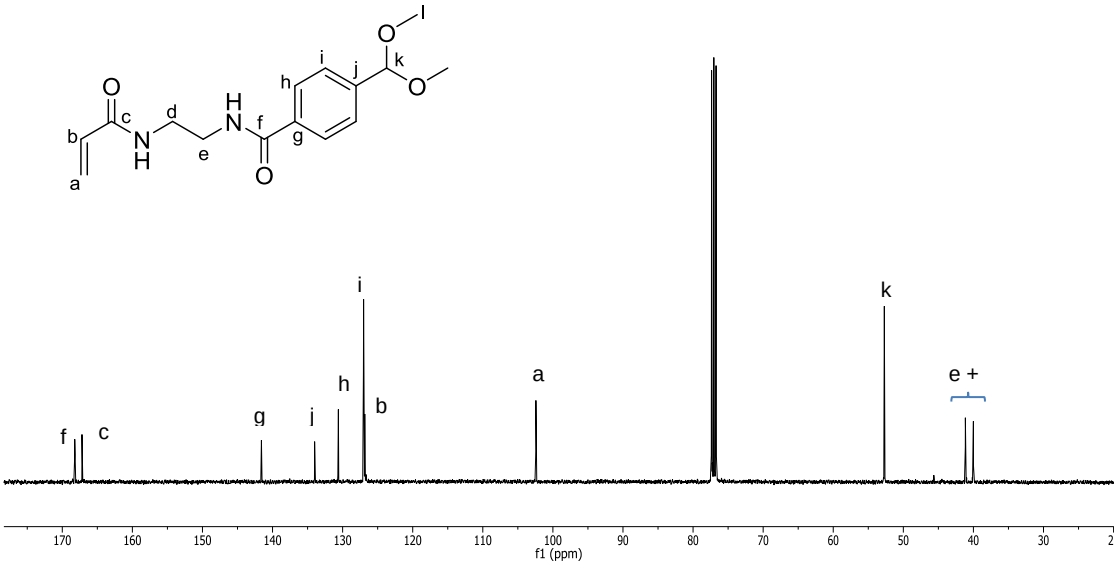


**Figure 10** $^{13}$C NMR spectrum (75 MHz, $CDCl_3$) of compound **11**.

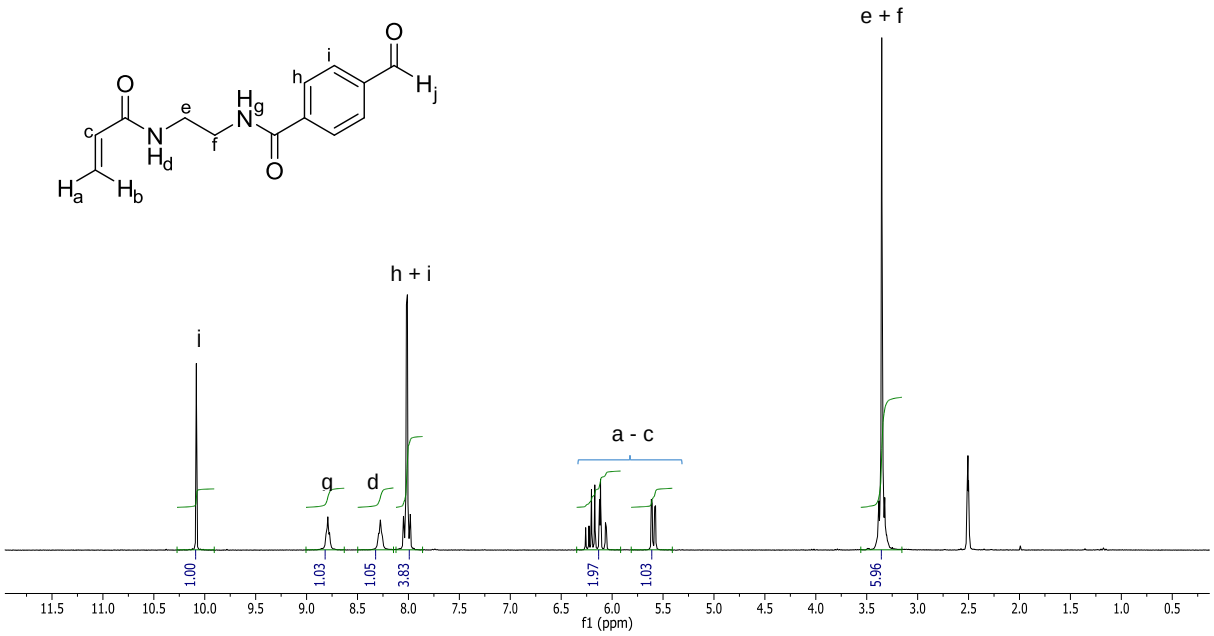


**Figure 11** $^{1}$H NMR spectrum (300 MHz, $CDCl_3$) of compound **12**.

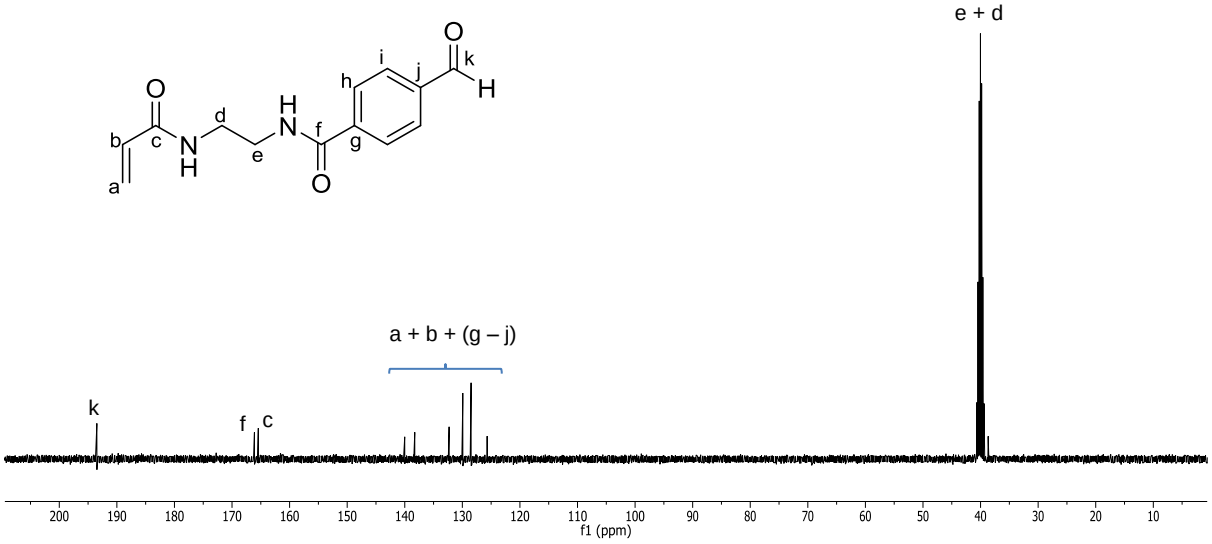


**Figure 12** $^{13}$C NMR spectrum (75 MHz, $CDCl_3$) of compound **12**.

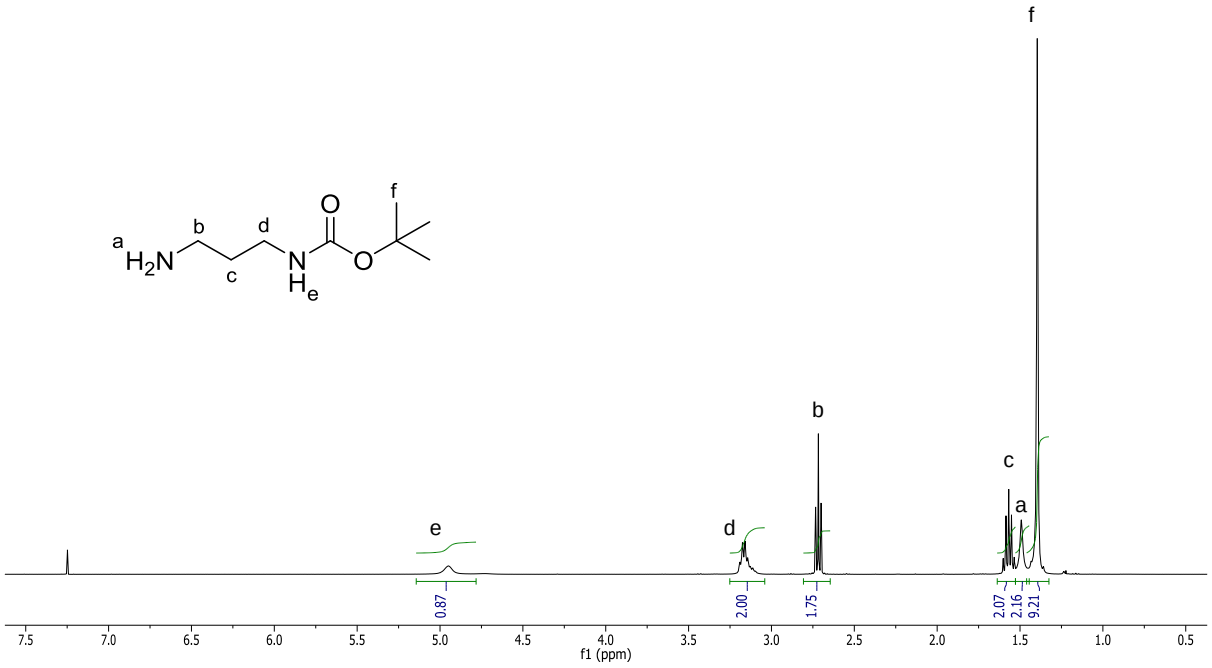


**Figure 13** $^{1}$H NMR spectrum (300 MHz, $CDCl_3$) of compound **13**.

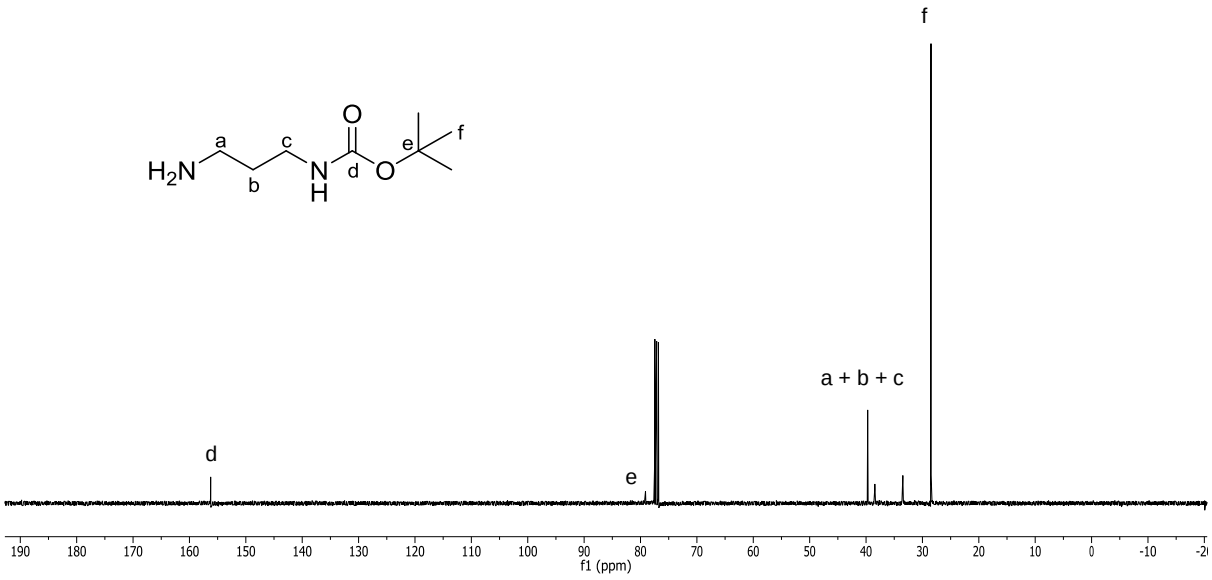


**Figure 14** $^{13}$C NMR spectrum (75 MHz, $CDCl_3$) of compound **13**.

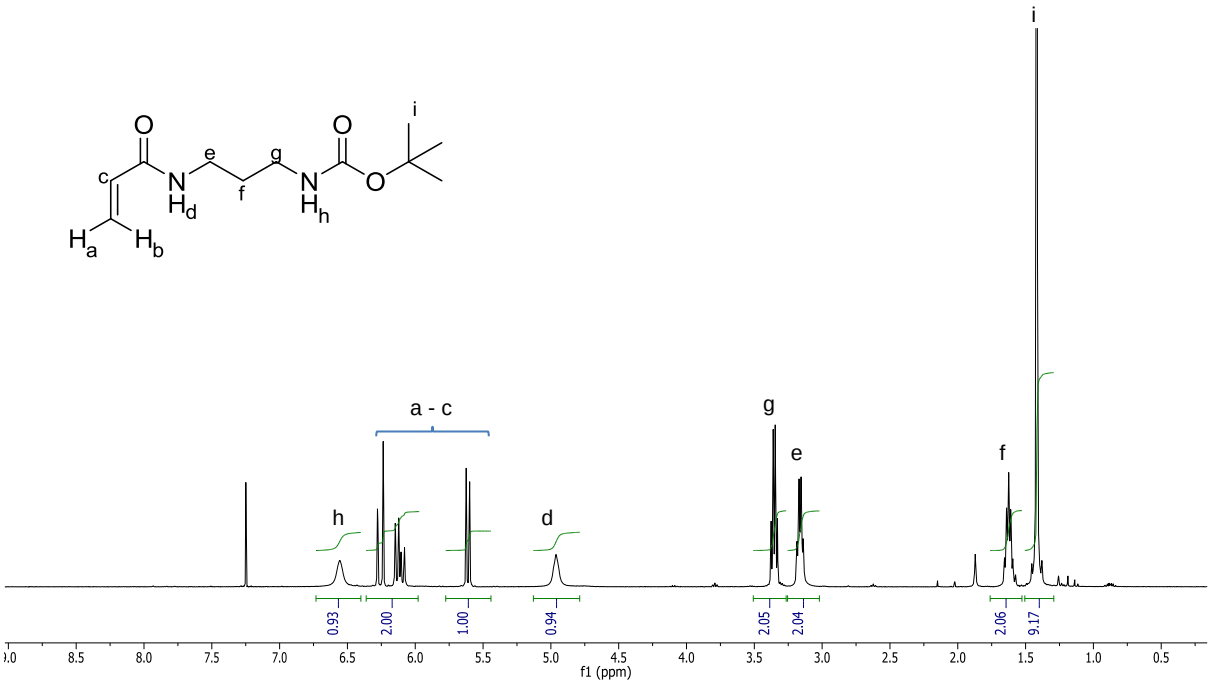


**Figure 15** $^{1}$H NMR spectrum (300 MHz, $CDCl_3$) of compound **14**.

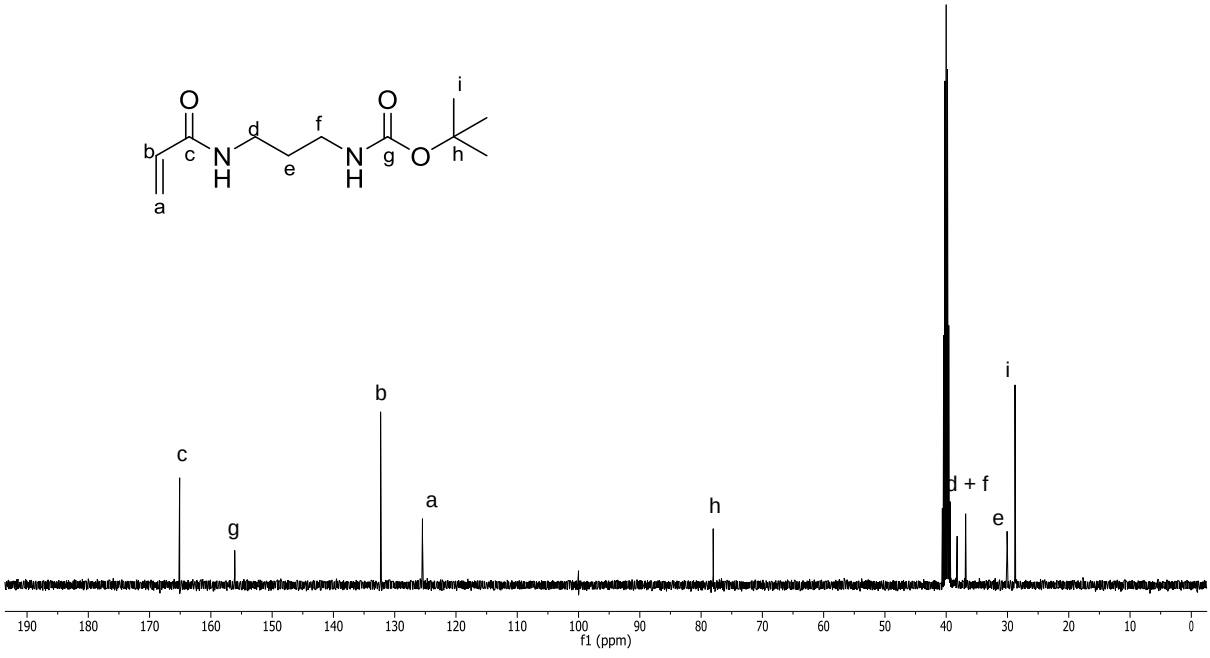


**Figure 16** $^{13}$C NMR spectrum (75 MHz, $CDCl_3$) of compound **14**.

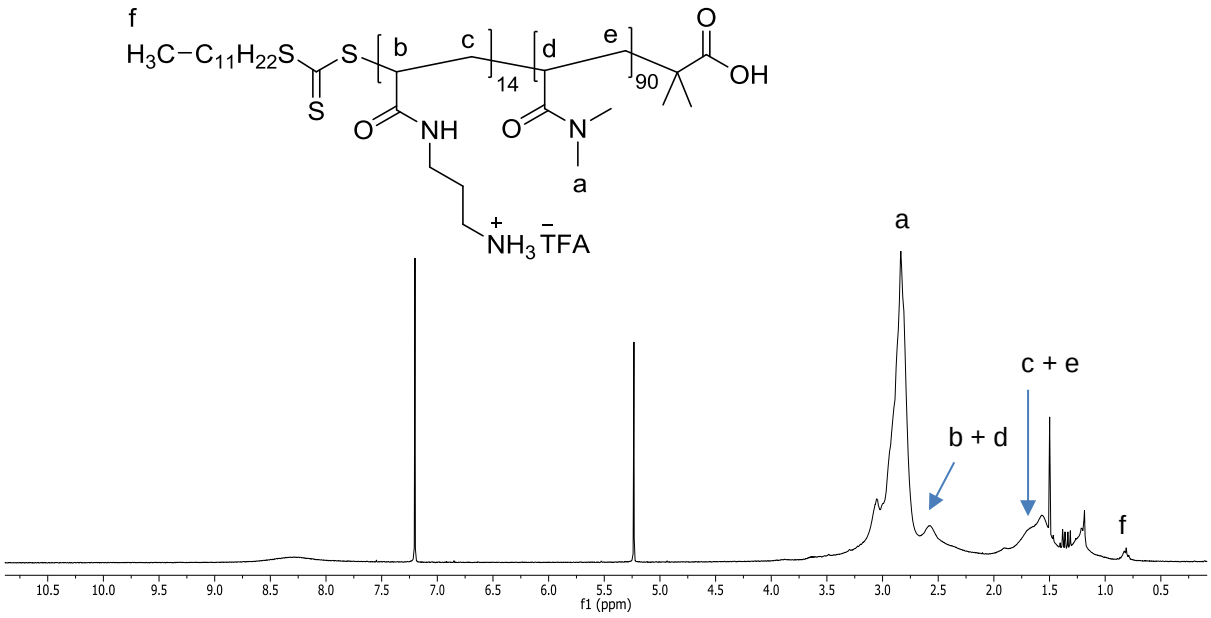


**Figure 17** $^{1}$H NMR spectrum (300 MHz, $CDCl_3$) of copolymer **P2**.

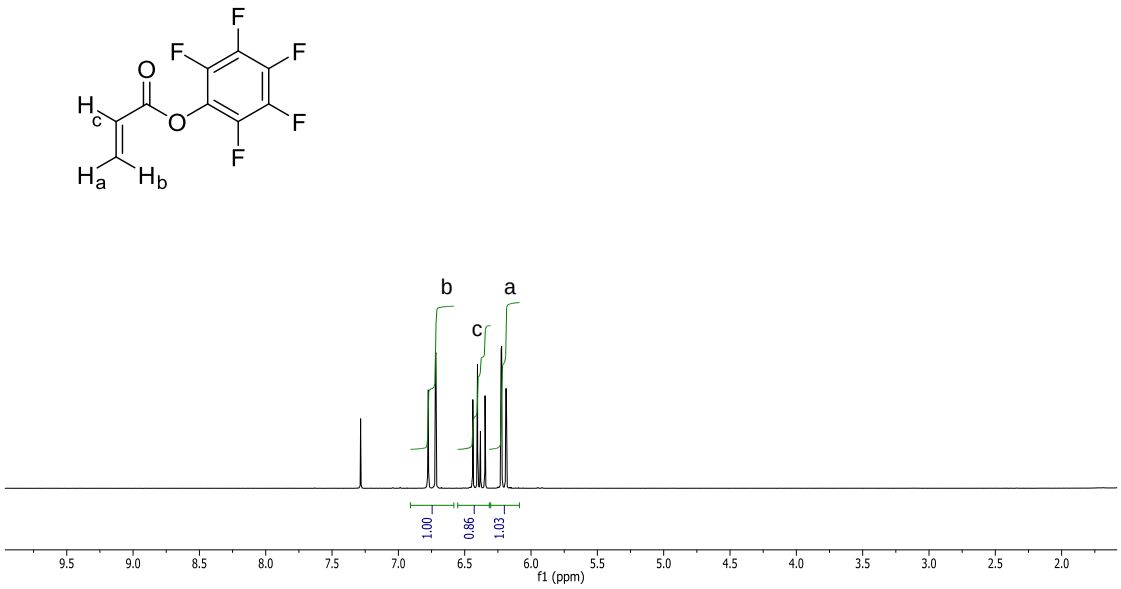


**Figure 18** $^{1}$H NMR spectrum (300 MHz, $CDCl_3$) of compound **15**.

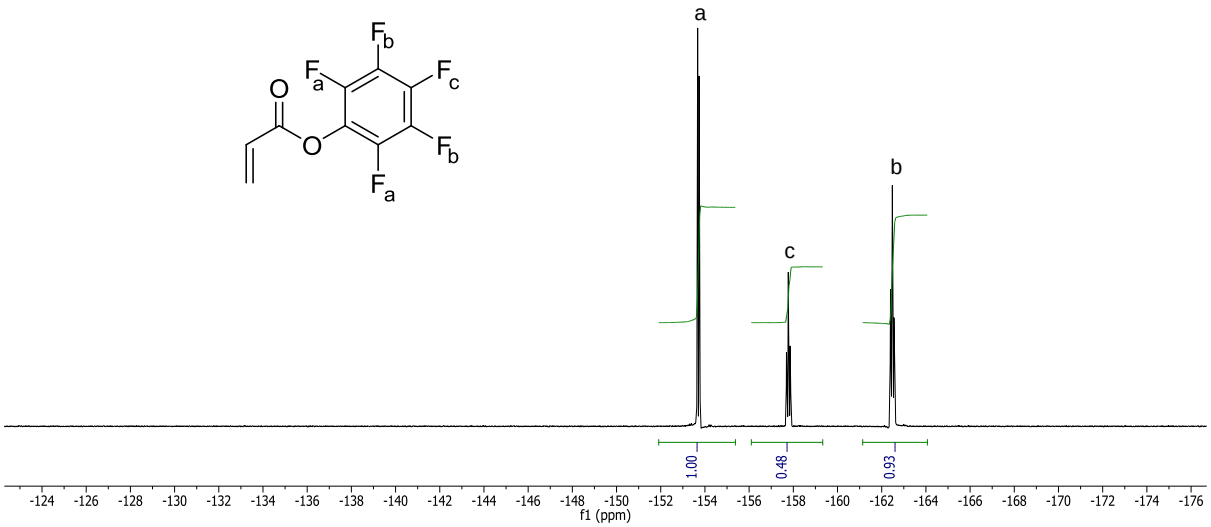


**Figure 19** $^{19}F$ NMR spectrum (282 MHz, $CDCl_3$) of compound **15**.

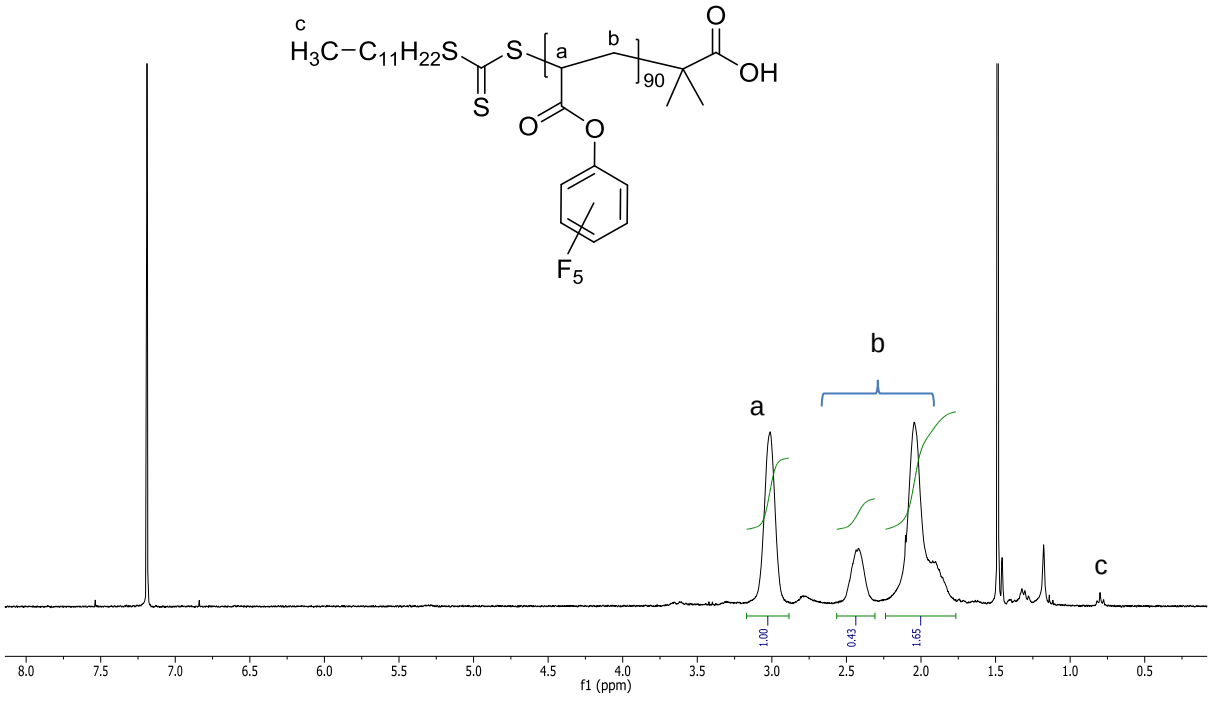


**Figure 20** $^{1}H$ NMR spectrum (300 MHz, $CDCl_3$) of p(PFPA) (**P3**).

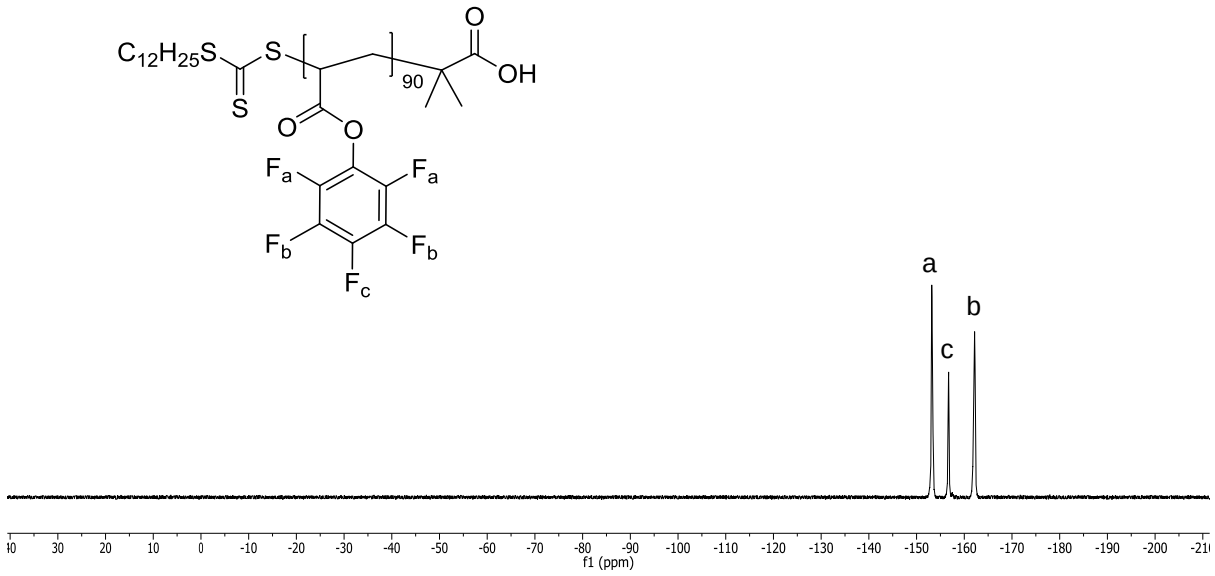


**Figure 21** $^{19}F$ NMR spectrum (282 MHz, $CDCl_3$) of p(PFPA) (**P3**).

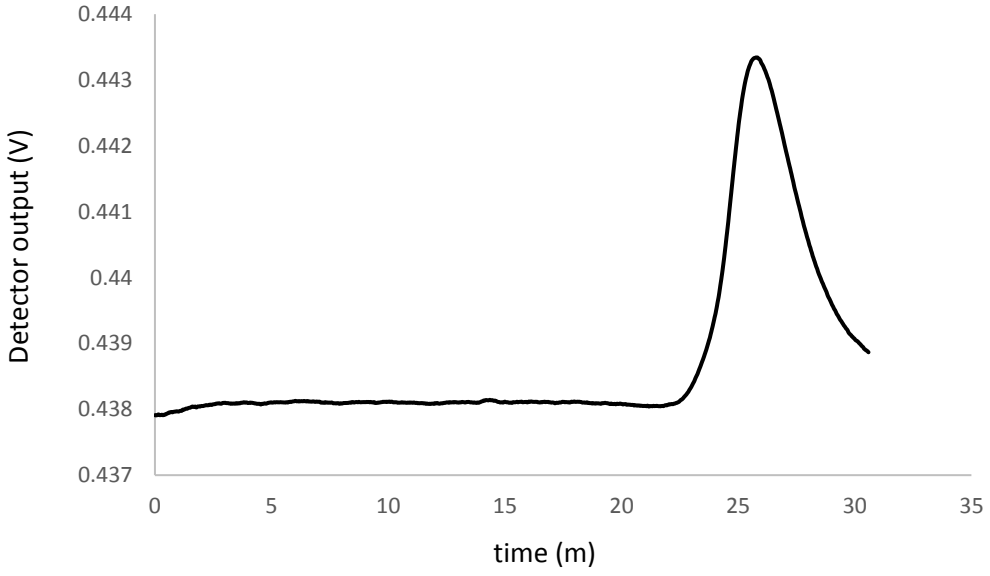


**Figure 22** Differential refractive index (dRI) trace of **P3** after conversion to p(DMA) by aminolysis with DMA.

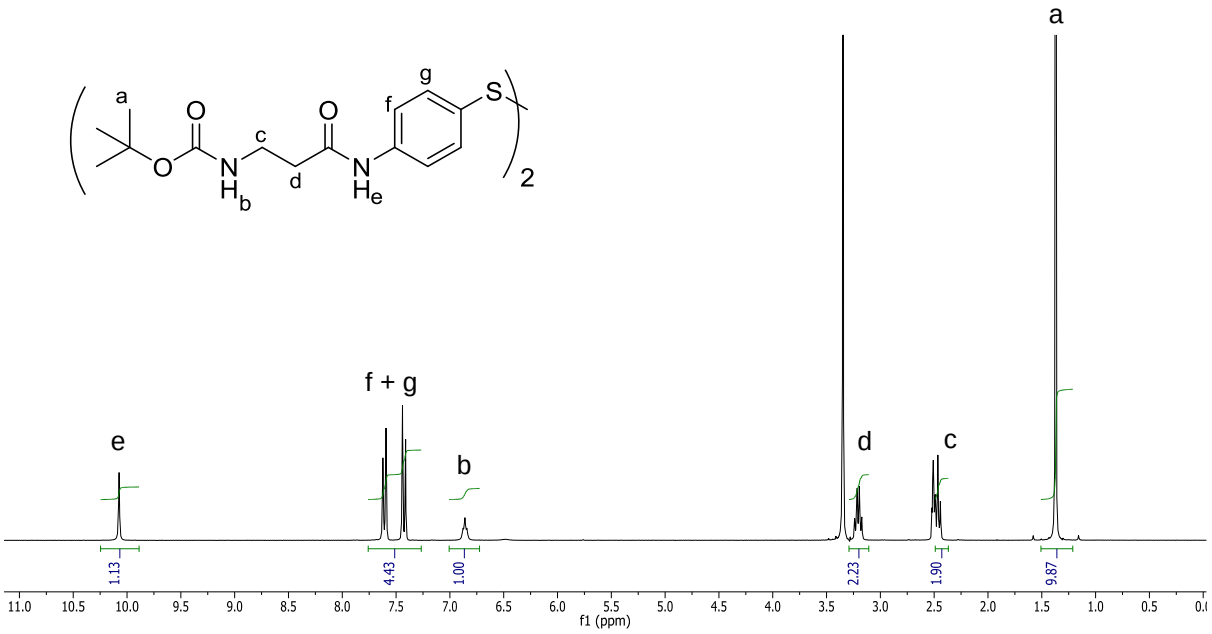


**Figure 23** $^{1}$H NMR spectrum (300 MHz, dmso-$d_6$) of compound **16**.

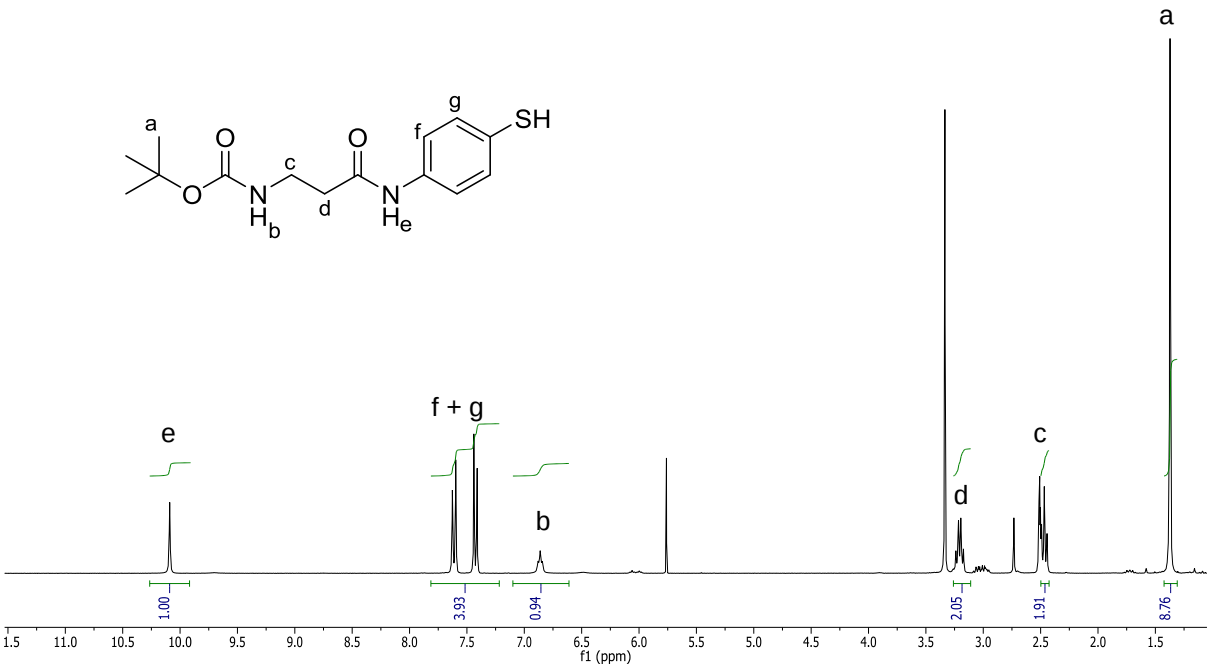


**Figure 24** $^{1}$H NMR spectrum (300 MHz, dmso-$d_6$) of compound **17**.

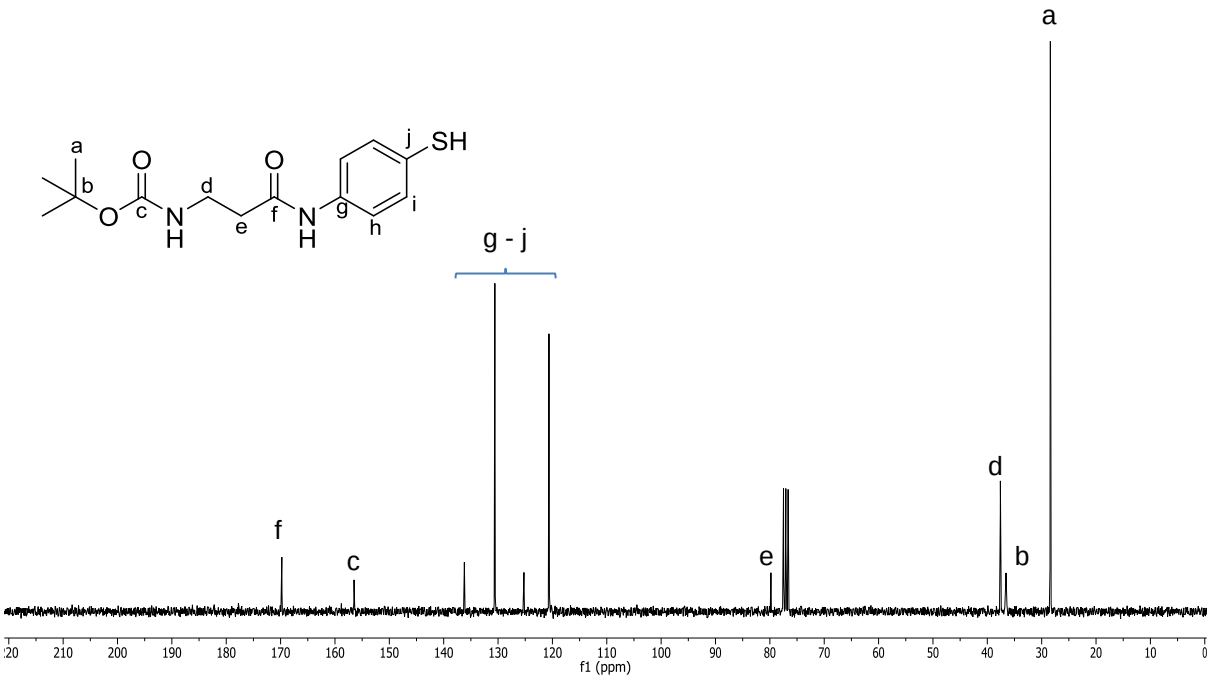


**Figure 25** $^{13}$C NMR spectrum (75 MHz, dmso-$d_6$) of compound **17**.

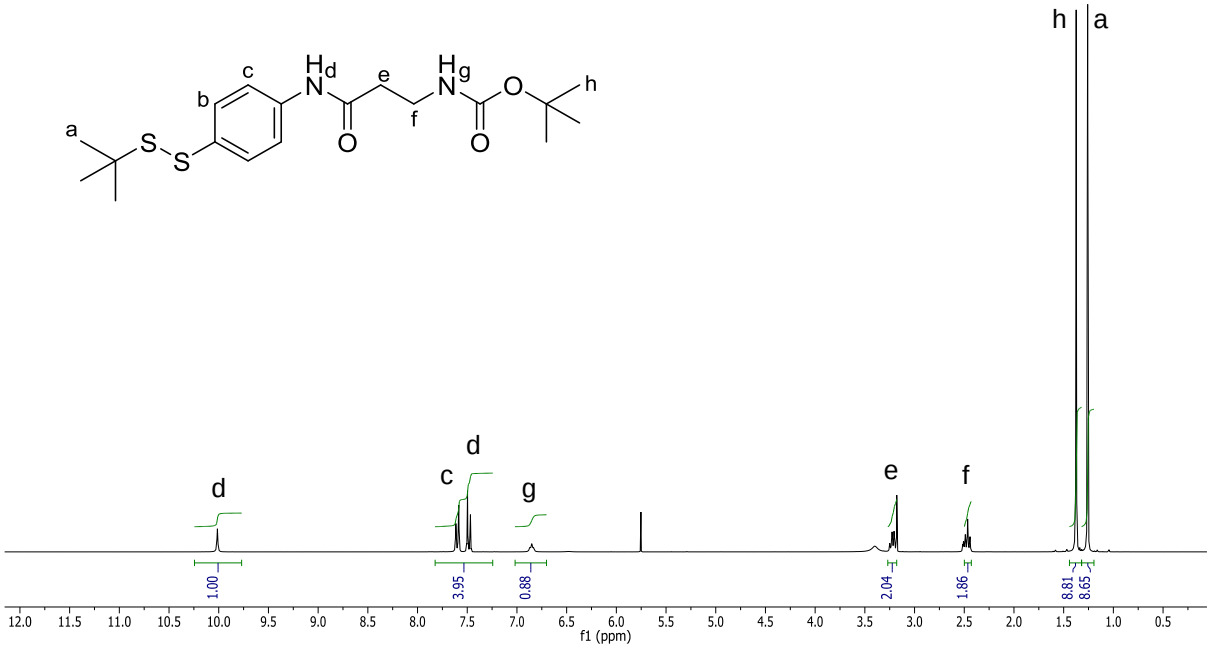


**Figure 26** $^{1}$H NMR spectrum (300 MHz, dmso-$d_6$) of compound **18**.

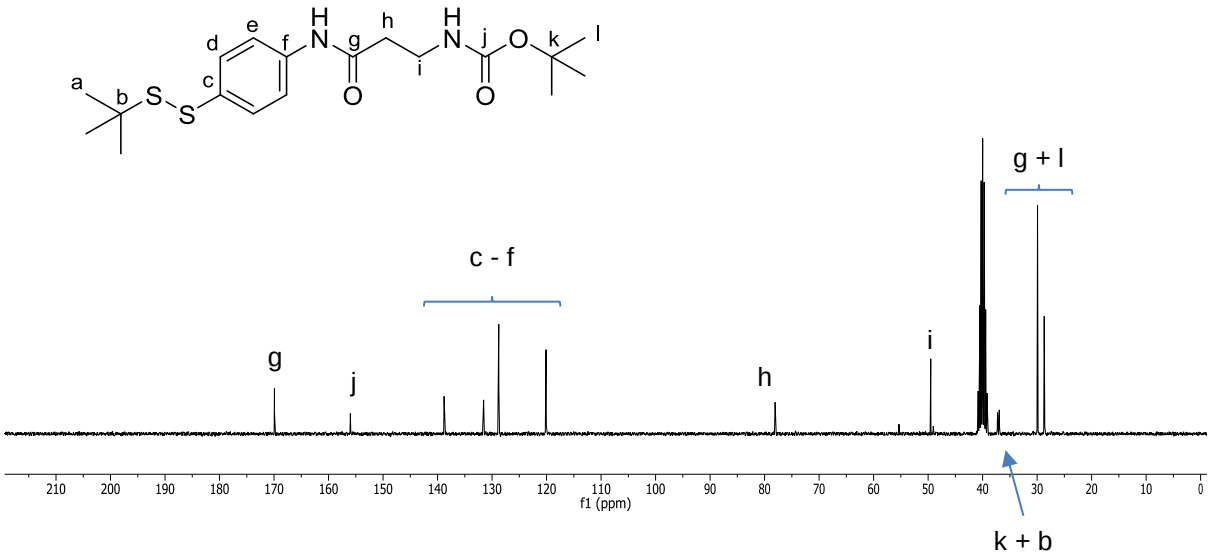


**Figure 27** $^{13}$C NMR spectrum (75 MHz, dmso-$d_6$) of compound **18**.

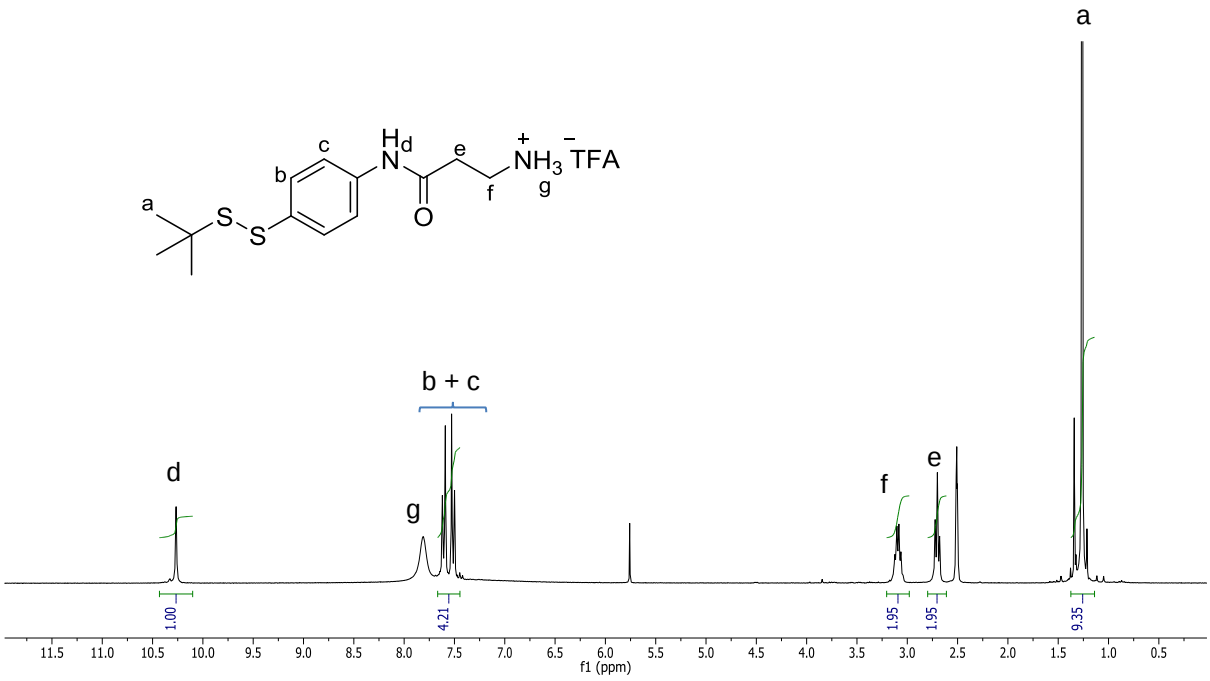


**Figure 28** $^{1}$H NMR spectrum (300 MHz, dmso-$d_6$) of compound **19**.

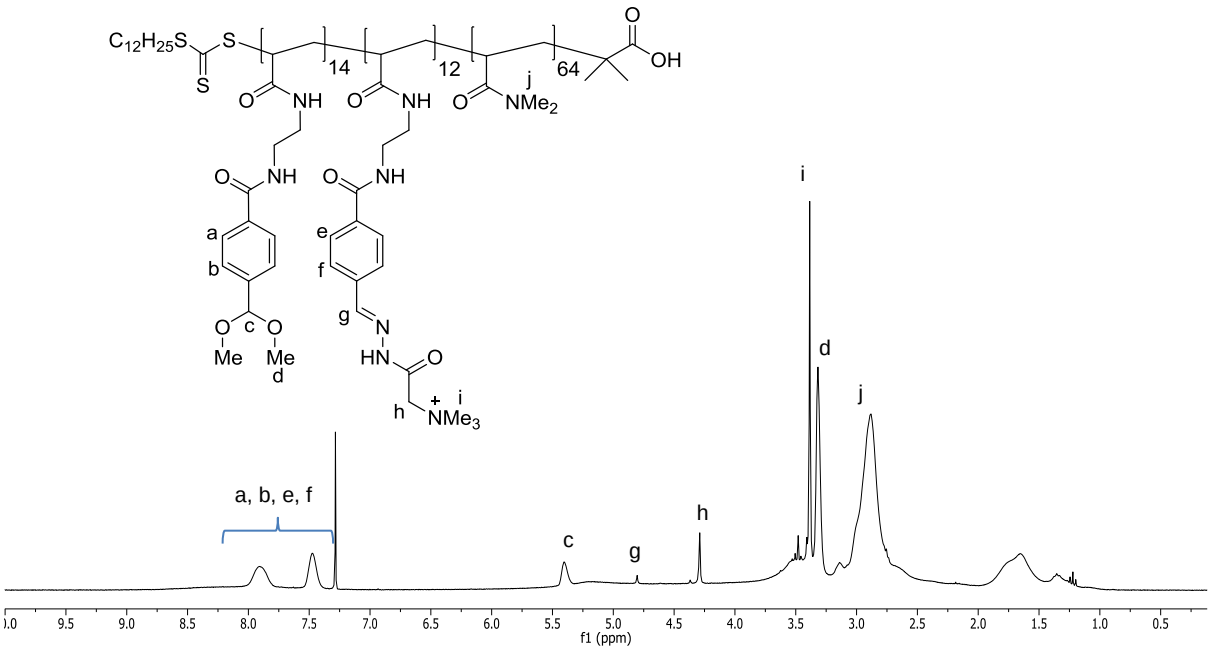


**Figure 29** $^{1}$H NMR spectrum (300 MHz, $CDCl_3$) of copolymer **P12**.

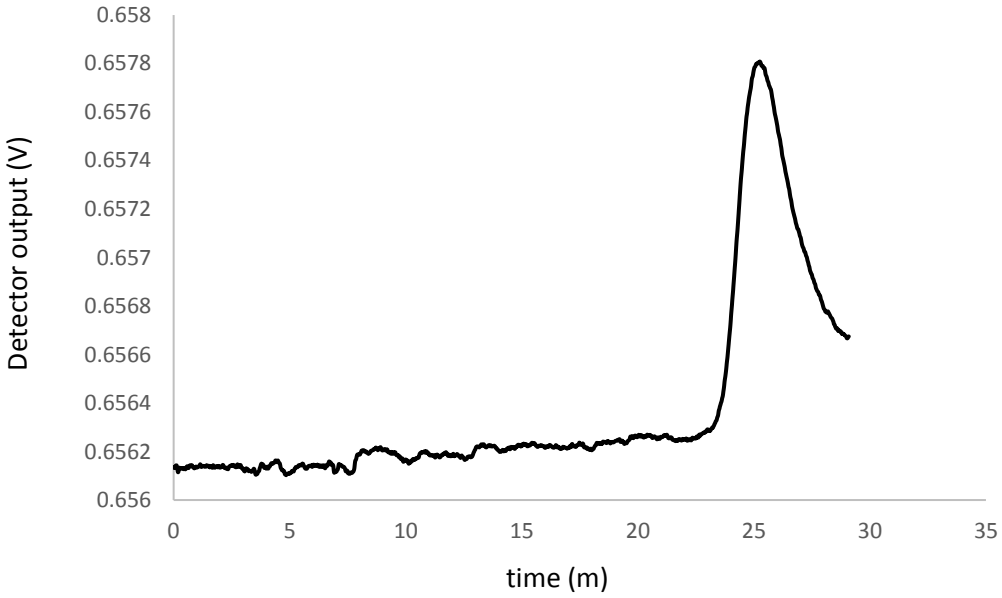


**Figure 30** Differential refractive index (dRI) trace of copolymer **P12.**

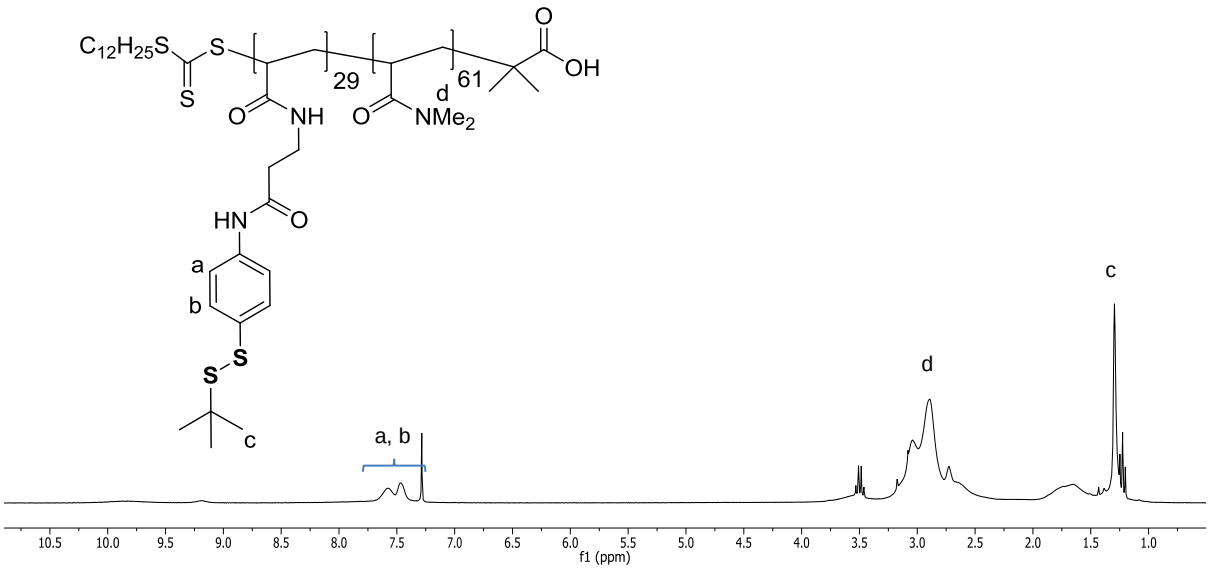


**Figure 31** $^{1}$H NMR spectrum (300 MHz, $CDCl_3$) of copolymer **P15**.

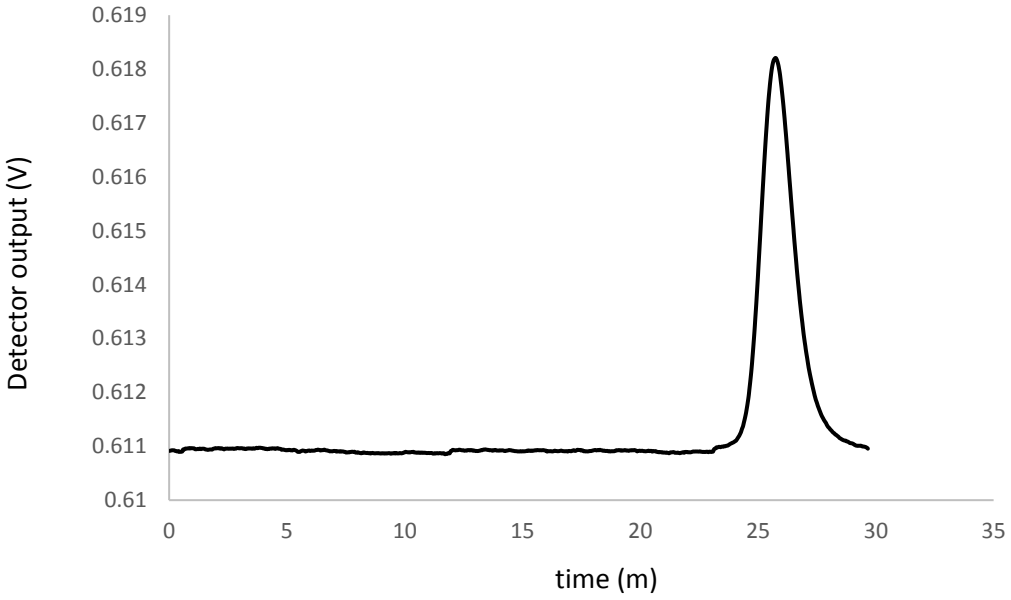


**Figure 32** Differential refractive index (dRI) trace of copolymer **P15.**

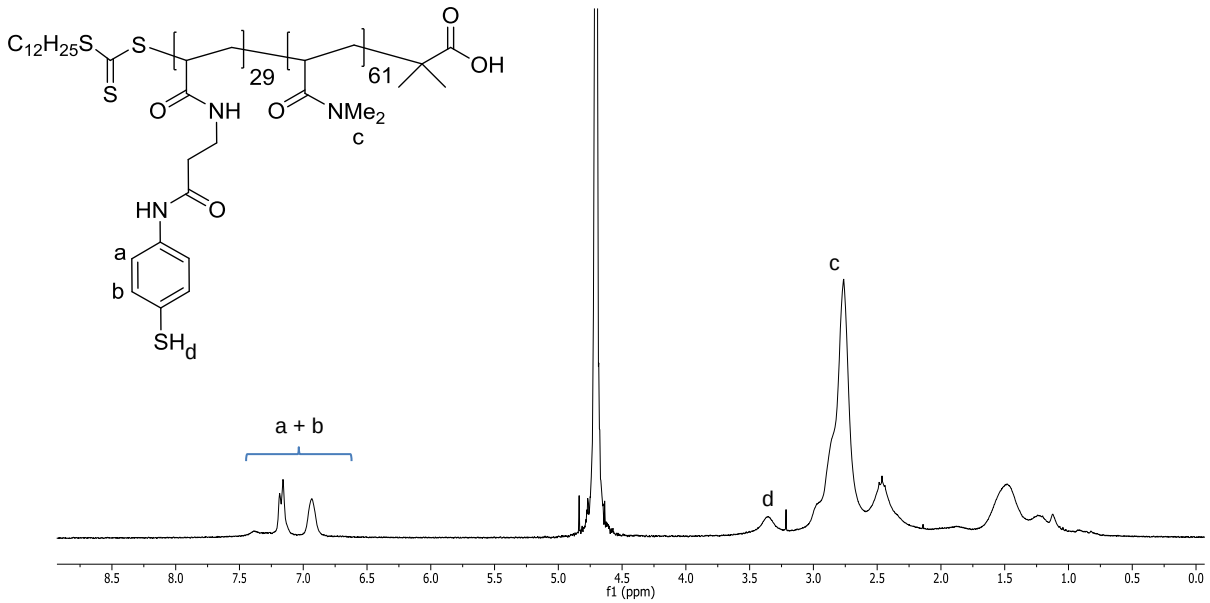


**Figure 33** $^{1}$H NMR spectrum (300 MHz, $CDCl_3$) of copolymer **P16**.

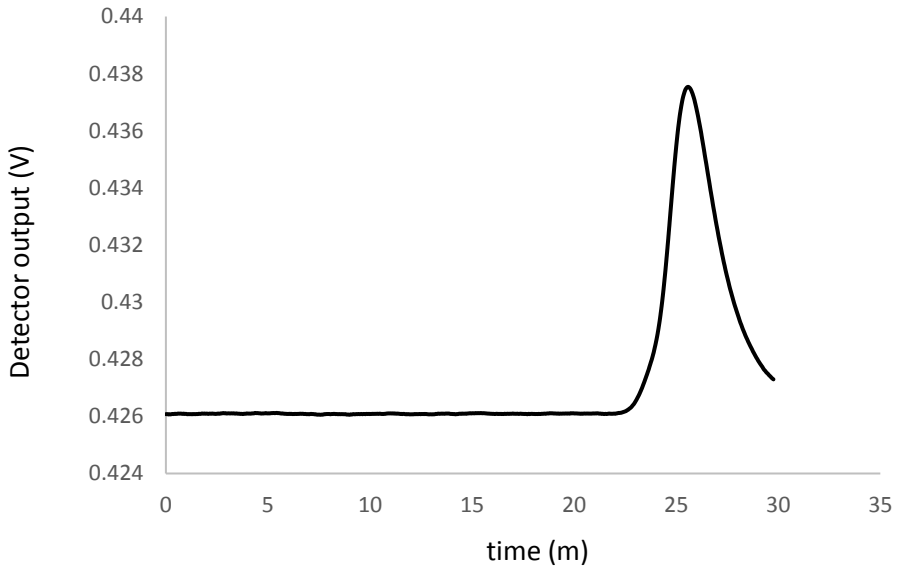


**Figure 34** Differential refractive index (dRI) trace of copolymer **P16.**

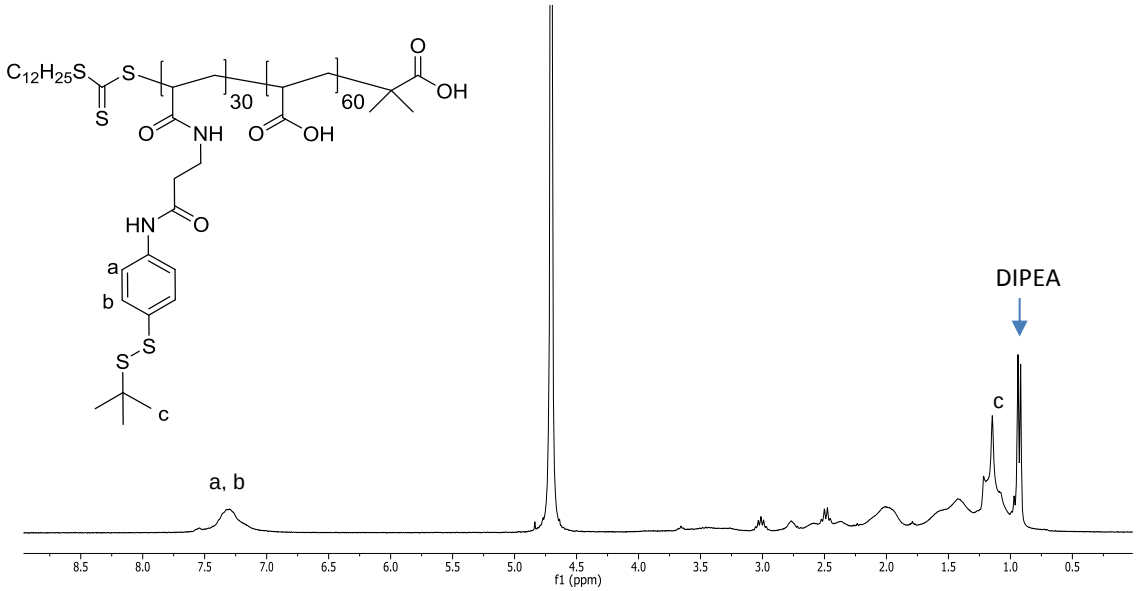


**Figure 35** $^{1}$H NMR spectrum (300 MHz, $CDCl_3$) of copolymer **P17**.

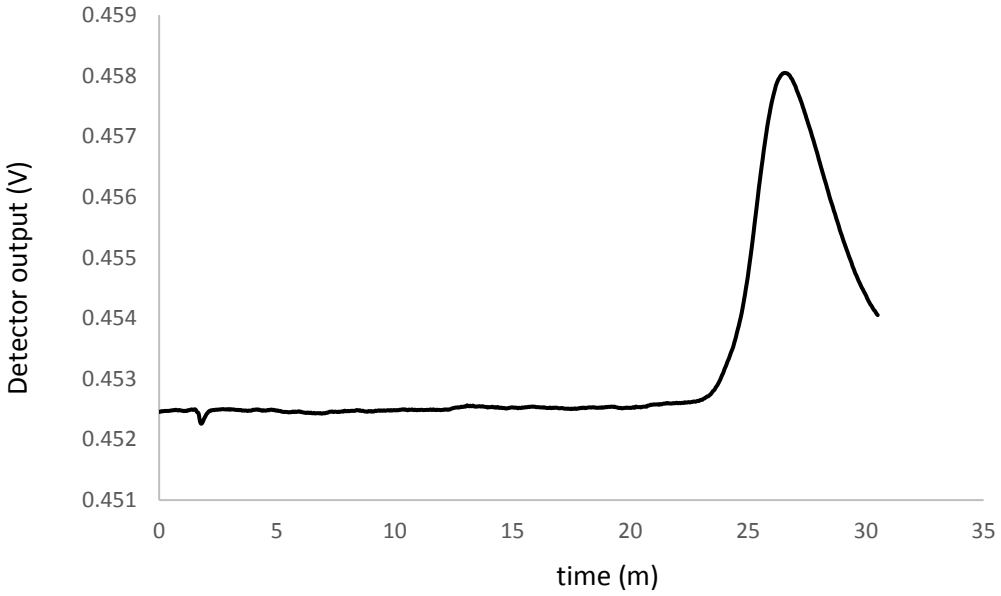


**Figure 36** Differential refractive index (dRI) trace of copolymer **P17.**

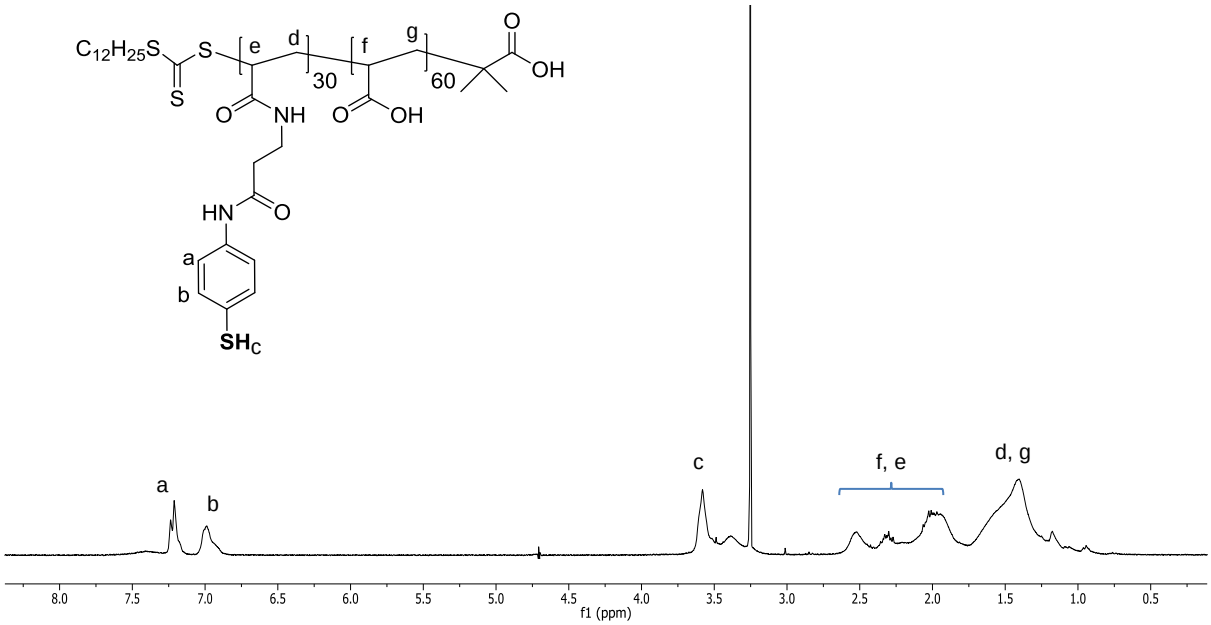


**Figure 37** $^{1}$H NMR spectrum (300 MHz, $CDCl_3$) of copolymer **P18**.

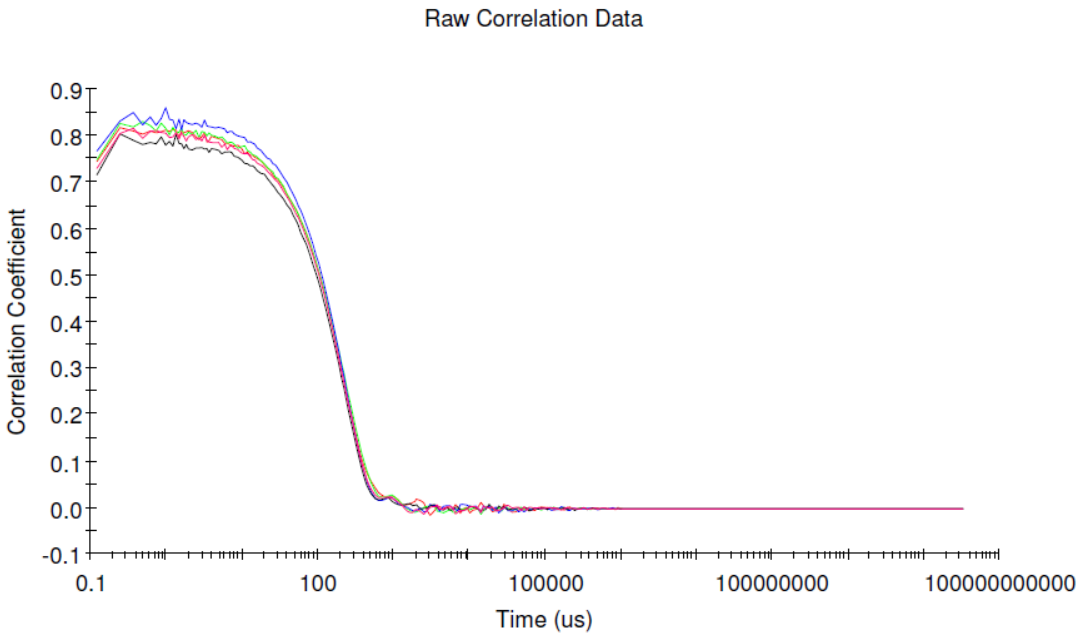


**Figure 38** DLS Autocorrelation function for disulfide cross-linked nanoparticle **NP2.** (Data for 5 consecutive runs in a typical experiment performed at a concentration of 20 mg.mL).

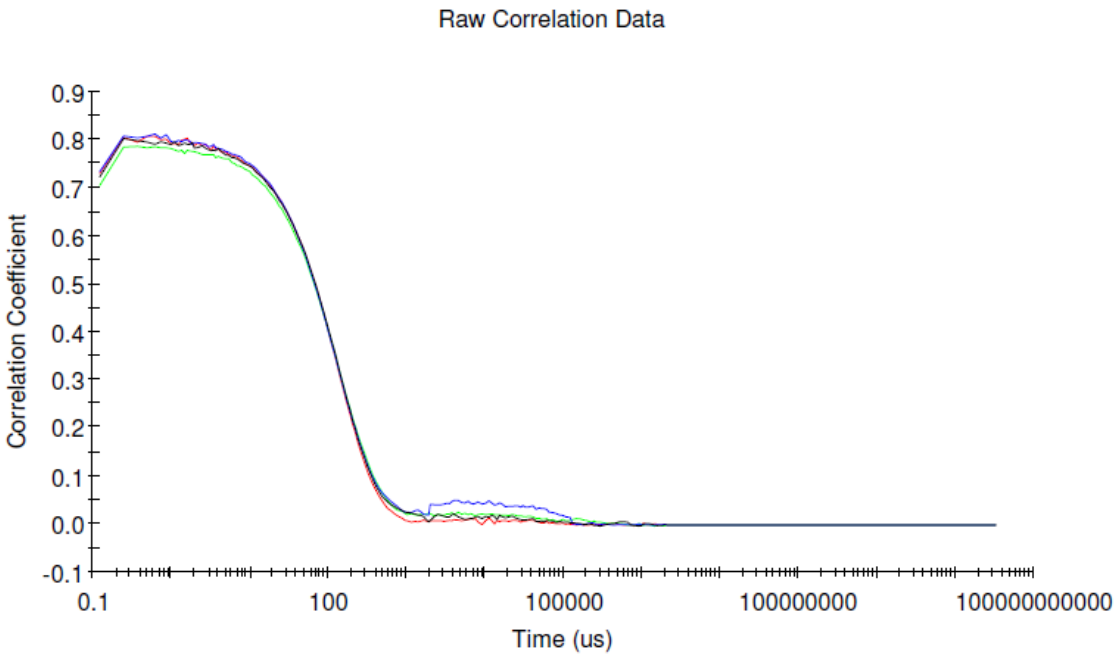


**Figure 39** DLS Autocorrelation function for imine cross-linked nanoparticle **NP1.** (Data for 5 consecutive runs in a typical experiment performed at a concentration of 20 mg.mL).